



*technical and clinical analysis of safety*

M.N.G.J.A. Braat

# Radioembolization: technical and clinical analysis of safety

Maria Nicole Gerardine Johanna Aleida Braat

**Radioembolization: technical and clinical analysis of safety**

PhD thesis, Utrecht University, the Netherlands

© M.N.G.J.A. Braat, Utrecht, 2023

mngjabraat@gmail.com

All rights reserved. No part of this publication may be reproduced, stored in a retrieval system, or transmitted, in any form or by any means, without the permission in writing from the author. The copyright of the articles that have been published or have been accepted for publication has been transferred to the respective journals.

ISBN: 978-94-6473-298-6

Cover design: M.N.G.J.A. Braat, R. Sanders

Lay-out: R. Sanders

Printing: Ipskamp Printing B.V.

# Radioembolization: technical and clinical analysis of safety

Radioembolisatie:  
Technische en klinische analyse van de veiligheid  
(met een samenvatting in het Nederlands)

Proefschrift

ter verkrijging van de graad van doctor aan de Universiteit Utrecht op gezag van de rector magnificus, prof.dr. H.R.B.M. Kummeling, in gevolge het besluit van het college voor promoties in het openbaar te verdedigen op donderdag 14 december 2023 des middags te 4.15 uur

door

Maria Nicole Gerardine Johanna Aleida Braat  
geboren op 13 november 1982 te Breda

**Promotoren**

Prof. dr. M.G.E.H. Lam

Prof. dr. M.A.A.J. van den Bosch

**Copromotor**

Dr. J. de Bruijne



## Table of Contents

Chapter 1	General introduction and outline of this thesis	9
<b>Part I Clinical perspectives on radioembolization</b>		<b>27</b>
Chapter 2	Radioembolization-induced liver disease: a systemic review	29
Chapter 3	Toxicity comparison of yttrium-90 resin and glass microspheres radioembolization	57
Chapter 4	Prophylactic Medication During Radioembolization in Metastatic Liver Disease, is it Really Necessary? A Retrospective Cohort Study and Review of Literature	81
<b>Part II Nuclear medicine perspectives on radioembolization</b>		<b>107</b>
Chapter 5	Hepatobiliary scintigraphy may improve radioembolization treatment planning in HCC patients	109
Chapter 6	A pilot study on hepatobiliary scintigraphy to monitor regional liver function in <sup>90</sup> Y radioembolization	127
Chapter 7	Radioembolization-induced changes in hepatic [ <sup>18</sup> F]FDG metabolism in non-tumorous liver parenchyma	147
<b>Part III Radiological perspectives on radioembolization</b>		<b>169</b>
Chapter 8	The caudate lobe: The blind spot in radioembolization or an overlooked opportunity?	171
Chapter 9	Liver CT for vascular mapping during radioembolization workup: comparison of an early and late arterial phase protocol	189
Chapter 10	The value of a dual arterial phase CT protocol in the preparation of radioembolization in neuroendocrine liver metastases	209

Chapter 11	General discussion	227
Chapter 12	Summary	267
Chapter 13	Nederlandse samenvatting	273
	List of publications	277
	Curriculum vitae auctoris	285
	Postscriptum	289







CHAPTER  
ONE

General introduction  
and outline of this thesis

Over the years, radioembolization or selective internal radiation therapy (SIRT) has become an established treatment strategy for patients with primary and secondary hepatic malignancy. Hepatic tumors and metastases are primarily vascularized by the hepatic artery, contrary to the non-tumorous liver parenchyma that receives most of its nutrients and oxygen from the portal vein (1-3). This preferential arterial flow enables targeting of the hepatic tumors by the injection of radio-active microspheres into the hepatic or tumor supplying arteries, resulting in selective radiation of these tumors.

The work-up for a radioembolization treatment consists of: 1) a clinical and biochemical status; 2) a pre-treatment computed tomography (CT) to assess the arterial anatomy and tumor load; 3) a simulation treatment, including a hepatic angiography and administration of technetium-99m-macroaggregated albumin ( $^{99m}\text{Tc}$ -MAA) or a scout dose of  $^{166}\text{Ho}$  microspheres, to exclude extrahepatic depositions and assess the intrahepatic distribution of the microspheres; 4) treatment planning and calculation of the optimal absorbed dose to the tumor and/or non-tumorous liver (**Figure 1**). Afterwards, the dose distribution is evaluated by use of a  $^{90}\text{Y}$  positron emission tomography/CT ( $^{90}\text{Y}$ -PET/CT) or a single photon emission computed tomography ( $^{166}\text{Ho}$ -SPECT) (**Table 1**).

**Table 1.** Characteristics of  $^{90}\text{Y}$  and  $^{166}\text{Ho}$  microspheres

Microsphere characteristics	SIR-spheres®	TheraSphere®	QuiremSpheres®
Matrix	Resin	Glass	Poly-L-lactid acid
Diameter (mean, range)	32 $\mu\text{m}$ (30-60 $\mu\text{m}$ )	25 $\mu\text{m}$ (20-30 $\mu\text{m}$ )	30 $\mu\text{m}$ (15-60 $\mu\text{m}$ )
Density	1.6 g/ml	3.3 g/ml	1.4 g/ml
Isotope	$^{90}\text{Y}$	$^{90}\text{Y}$	$^{166}\text{Ho}$
$\beta$ -energy	2.28 MeV	2.28 MeV	1.81 MeV
$\gamma$ -energy	-	-	81 keV (6.7%)
Half-life	64.1 h	64.1 h	26.8 h
Number of microspheres for 3 GBq	40-50 million	1-8 million	9-10 million
Activity per microsphere	50 Bq	1250-2500 Bq	340 Bq
Imaging technique	Bremsstrahlung SPECT/ PET	Bremsstrahlung SPECT/ PET	SPECT/MRI
Surrogate/Scout	$^{99m}\text{Tc}$ -MAA	$^{99m}\text{Tc}$ -MAA	$^{166}\text{Ho}$ (or $^{99m}\text{Tc}$ -MAA)

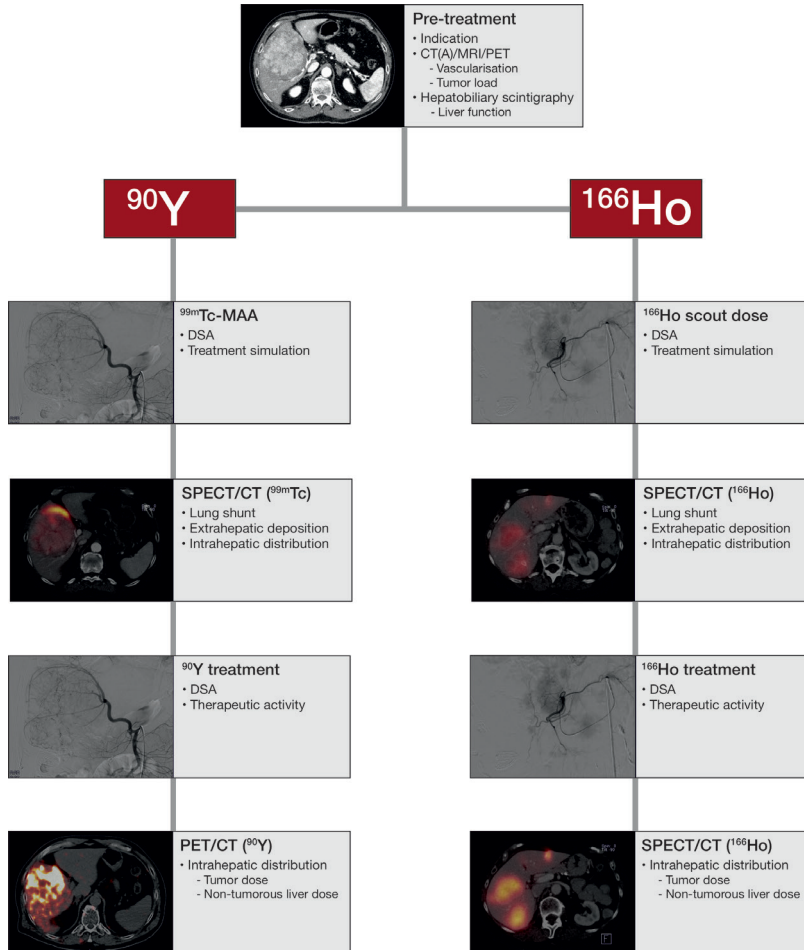


**Figure 1.** Flowchart of the standard workup for radioembolization treatment with <sup>90</sup>Yttrium and <sup>166</sup>Holmium.

In this thesis important clinical, nuclear medicine and radiologic perspectives will be examined with a focus on the hepatotoxicity of radioembolization treatment.

Until recently, radioembolization was primarily performed as a salvage treatment, yet the qualities of radioembolization (including selective tumor targeting, the lack of heat-sink effect near the great vessels and the induction of hypertrophy in non-embolized lobes) make its use in the curative setting, as an adjunct to surgery or bridge to liver transplantation for example, more and more accepted. In the updated ESMO guidelines for HCC, radioembolization is now also considered as an alternative treatment option in Barcelona Clinic Liver Cancer (BCLC) categories 0-A, next to BCLC B and C (4). Also, in the ENETS guidelines for neuro-endocrine tumors with liver-only, unresectable disease, radioembolization is one of the adopted strategies (5). And in a recent consensus paper on radioembolization in liver-dominant metastatic colorectal cancer (the most common hepatic metastases), radioembolization can be used to downstage patients with borderline resectable disease, as a chemotherapy-sparing and time-delaying strategy in selected patients with resectable disease or as a salvage treatment for unresectable disease (6). In the light of this paradigm shift to a curative treatment intent and prolonged survival, (long-term) hepatotoxicity becomes more relevant.

In 2008, Sangro et al. were the first to describe the clinical picture of hepatotoxicity after radioembolization, called radioembolization-induced liver disease (REILD). In earlier large patient series - analyzing  $^{90}\text{Y}$  resin treatments of HCC and colorectal metastases - fatal REILD occurred in up to 5% of patients, and in patients with CTCAE grade 3 bilirubin toxicities in up to 19% (7-10). In the more recent studies, such as the SARAH trial ( $^{90}\text{Y}$  resin SIRT vs. sorafenib in HCC patients (Child Pugh score <7)) radioembolization related deaths were reported in 13/174, of which 6/13 due to cirrhosis and its complications and 3/13 due to hepatic failure, but no REILD was reported (11). The other deaths were attributed to sepsis (n=2), progressive disease (n=1), radiation pneumonitis (n=1) and unknown cause (n=1). Grade 3 liver dysfunction occurred in 11% in the radioembolization group (vs. 13% in the sorafenib group). In the study by Wasan et al., combining the data of the SIRFLOX,

FOXFIRE and FOXFIRE global data (FOLFOX +/- <sup>90</sup>Y resin radioembolization), fatal REILD (i.e. grade 5) was present in 3/507 patients with an additional 1/507 patients with hepatic failure. Grade 3 hepatotoxicity occurred in three patients (grade 3 hepatic failure in 1/507 and REILD grade 3 in 2/507) (12). A similar study on <sup>90</sup>Y glass radioembolization +/- second line oxaliplatin or irinotecan-based chemotherapy reported 4% fatal radioembolization-related hepatotoxicity, whereas another registry study on <sup>90</sup>Y resin treatments of colorectal liver metastases reported 8.3% grade 3 or 4 bilirubin toxicity and 3.7% grade 3 albumin toxicity (13, 14). Even now, in these large randomized controlled trials inconsistency exists in the reporting of radioembolization-related hepatotoxicity (i.e. REILD, hepatic failure, complications of cirrhosis, etc.), complicating the comparison of toxicity between studies and especially between the microspheres used. In **CHAPTER 2** we performed a systematic review of the literature to explore the inconsistencies in the definition of REILD and its reporting. Based on the outcome a suggestion is made for a definition and timeline for REILD, with a five-point severity scale, similar to the Common Terminology Criteria for Adverse Events (CTCAE) grading system.

Currently, three types of microspheres are commercially available: <sup>90</sup>Y glass microspheres (TheraSphere®, Boston Scientific), <sup>90</sup>Y resin microspheres (SIR-Spheres®, SIRTEX) and <sup>166</sup>Ho poly (L-lactic acid) microspheres (QuiremSpheres®, Terumo). Of these, the <sup>90</sup>Y loaded microspheres are most commonly used, as QuiremSpheres are not available in the United States and Canada. Several important differences exist between these microspheres (**Table 1**). These differences result in different embolic effects and different dose-effect relationships (15-18), potentially leading to other toxicity profiles (**CHAPTER 3**).

Almost all patients experience some form of hepatotoxicity after radioembolization - mainly (transient) alanine aminotransferase (ALT), aspartate aminotransferase (AST) and alkaline phosphatase elevation - due to radiation damage to the non-tumorous parenchyma (8, 19-21). However, as illustrated in the previous paragraph, clinically evident serious toxicity is limited. Nonetheless, several authors have focused on the prevention of toxicity (20, 22). Based on the previous work of Gil-Alzugaray et al. a combination of ursodeoxycholic acid and prednisolone is widely used as medical prophylaxis (20). Yet, in this study not only prophylaxis was used, but a significant dose reduction (10-20% for whole liver treatments)

was introduced as part of the new protocol. Seidensticker et al. compared this prophylactic regimen to a more extensive regimen of pentoxifylline, ursodeoxycholic acid and low-molecular weight heparin (22), without a significant decrease in radiation-induced toxicity (based on bilirubin levels and/or the presence of ascites) in a patient population with breast cancer liver metastases treated with  $^{90}\text{Y}$  resin. To date, no studies have compared the prophylactic combination of ursodeoxycholic acid and prednisolone to a control group without prophylaxis (**CHAPTER 4**).

Overall liver function encompasses multiple subfunctions, including synthetic, excretory and detoxifying functions. Several tests are used to assess total liver or future liver remnant function, though none are able to weigh the entire spectrum of different liver functions. Some tests are based on biochemical and clinical findings and primarily used in cirrhosis, such as the Child-Pugh score and MELD score (**Table 2**). More recently, the ALBI score was

**Table 2.** Calculation methods for the Child Pugh, MELD and ALBI score

Clinical scoring system	Equation
Child-Pugh-(Turcotte) score	= sum of allocated scores for bilirubin, albumin, INR, ascites and encephalopathy in which bilirubin: <2 mg/dL = +1, 2-3 mg/dL = +2, >3 mg/dL = +3 albumin: >3.5 g/dL = +1, 2.8-2.5 g/dL = +2, <2.8 g/dL = +3 INR: <1.7 = +1, 1.7-2.3 = +2, >2.3 = +3 ascites: absent = +1, slight = +2, moderate = +3 encephalopathy: no = +1, grade 1-2 = +2, grade 3-4 = +3
MELD score	= $3.78 \times \ln(\text{bilirubin (in mg/dL)}) + 1.2 \times \ln(\text{INR}) + 9.57 \times \ln(\text{creatinine (in mg/dL)}) + 6.43$
ALBI score	= $(\log_{10} \text{bilirubin (in } \mu\text{mol/L)} \times 0.66) + (\text{albumin (in g/L)} \times 0.085)$ in which grade 1 = $\leq -2.60$ ; grade 2 = $> -2.60$ to $\leq -1.39$ and grade 3 = $> -1.39$

INR = international normalized ratio

Bilirubin conversion factor (mg/dL to  $\mu\text{mol/L}$ ) = 17.1

introduced, resolving the subjectivity and dependency of some of the variables in the Child Pugh score (23).

The ALBI score has shown the ability to subdivide cirrhotic patients with a Child Pugh score of 5 into two distinctly different prognostic groups, not only in case of uncomplicated cirrhosis, but also in patients with HCC and prior to radioembolization (23, 24). Although used as a surrogate for liver function in some trials, its value in the prediction of clinically relevant hepatotoxicity/REILD needs to be further researched (22, 25).

Currently, non-invasive assessment of liver function, using nuclear imaging techniques (hepatobiliary scintigraphy) is gaining ground. Two liver-specific radiopharmaceuticals are commonly used:  $^{99m}\text{Tc}$ -iminodiacetic acid ( $^{99m}\text{Tc}$ -IDA) and  $^{99m}\text{Tc}$ -galactosylneoglycoalbumin ( $^{99m}\text{Tc}$ -GSA) (not available in Europe and the United States) (26, 27).  $^{99m}\text{Tc}$ -IDA is processed by hepatocytes by the same organic anion-transporting polypeptides (OATP 1B1 and 1B3) and multidrug resistance protein (MDR2) as bilirubin and indocyanine green (ICG) (28, 29). Thus, hepatic uptake of IDA analogs is influenced by hyperbilirubinemia, while  $^{99m}\text{Tc}$ -GSA uptake generally is not (26).  $^{99m}\text{Tc}$  mebrofenin is the most used IDA analog, because it has the strongest resistance to displacement by bilirubin and highest hepatic extraction fraction.

Several hepatobiliary scintigraphy studies have shown that there is a decreased hepatic uptake rate in patients with parenchymal disease and that there is little to no correlation between hepatic uptake and liver volume (especially in compromised livers) (26, 28, 30, 31). Additionally, a strong association exists between the preoperatively determined future liver remnant (FLR) function and the actual liver remnant function one day after surgery as measured by hepatobiliary scintigraphy ( $r = 0.95$ ,  $p < 0.001$ ). And hepatobiliary scintigraphy is more accurate in the prediction of postoperative liver failure than CT volumetry (30, 31), with a cut-off value of  $>2.69\%/ \text{min}/\text{m}^2$  body surface area corrected  $^{99m}\text{Tc}$  mebrofenin uptake rate (cMUR) for safe resection (3% liver failure chance). Furthermore, inhomogeneous liver function distribution is quite common, especially in cirrhotic livers, in case of a hilar cholangiocarcinoma and after portal vein embolization (PVE) (26, 27). In contrast to CT and MRI volumetry, hepatobiliary scintigraphy can image regional and segmental differences in liver function, especially when combined with SPECT/CT (26, 32). Another advantage



of hepatobiliary scintigraphy in combination with SPECT/CT is the better delineation of the separate segments and thus the FLR, when compared to the planar two-dimensional images (26). Interestingly, few authors have reported on hepatobiliary scintigraphy after PVE (32, 33), with consistent results of a larger increase in FLR function than in FLR volume in both normal and compromised livers. This faster functional increase argues for a shorter interval between PVE and surgery, even when volumetric hypertrophy is not yet up to par.

Even fewer authors have reported on hepatobiliary scintigraphy in radioembolization. Bennink et al. was the first to report on two cases with multifocal HCC undergoing  $^{99m}\text{Tc}$ -mebrofenin hepatobiliary scintigraphy both prior to and six weeks after radioembolization (34). After radioembolization both patients had a reduced total liver function (reduced cMUR) due to an decrease in uptake in the treated lobe(s). One patient underwent two whole liver treatments in six months, resulting in a reduction in BSA corrected cMUR<sub>total liver</sub> from 7.4 to 6.1%/min/m<sup>2</sup> after the first treatment and from 4.8 to 2.2%/min/m<sup>2</sup> after the second treatment. This patient was thereafter diagnosed with REILD. In **CHAPTER 5** and **CHAPTER 6** we report our experiences with  $^{99m}\text{Tc}$ -mebrofenin hepatobiliary scintigraphy in patients undergoing radioembolization.

Though hepatobiliary scintigraphy is gaining ground, most centers still adhere to volumetric measurements for the FLR. A FLR is considered sufficient if it comprises >20% (of the initial total liver volume (TLV)) in non-exposed livers, >30% after heavy chemotherapeutic pre-treatment and >40% in cirrhotic livers (26, 35). Extensive resections are often in conflict with an adequate FLR. In these cases PVE, portal vein ligation (PVL), in situ liver splitting techniques and SIRT can be applied to overcome this problem and increase the FLR (36, 37). FLR increase is more pronounced in small FLR and, as can be expected, less pronounced in cirrhotic livers (36, 38, 39). Also, contralateral hypertrophy after radioembolization seems to develop at a slower pace and to a lesser extent than in case of PVE/PVL with FLR increases of ca. 23% within 1-3 months after treatment (40-42). Even so, hypertrophy continues with FLR increases of 31-34% and 40-45% after six and twelve months, respectively (40, 41). Conversely, radioembolization has the advantage of its anti-tumoral effect, permitting a biologic test of time, especially in the non-treated parts (up to 9% of patients will become ineligible for surgery after PVE due to new lesions in the designated FLR) (43-46). Factors

associated with diminished contralateral hypertrophy after radioembolization in HCC patients are higher Child Pugh score, higher splenic volume and ascites at baseline (i.e. (decompensated) cirrhosis) and higher patient age (41, 42, 47).

Thus, follow-up imaging plays a key role in FLR measurements (if hepatobiliary scintigraphy is not available) and guiding of subsequent surgical planning, in addition to assessing response and determining the success of downstaging. Unfortunately, response assessment after radioembolization can be complicated on CT and magnetic resonance imaging (MRI). Firstly, there is a discordance between radiologic and pathologic complete response, for all response criteria; i.e. the World Health Organization (WHO) criteria, Response Evaluation Criteria in Solid Tumor (RECIST), modified RECIST (mRECIST), and the European Association of the Study of the Liver (EASL) criteria (used in HCC) (41, 48). Secondly, size-only based response criteria (RECIST and WHO) are not useful in the first month(s) due to the delay in size decrease - and sometimes even initial increase in size - for both HCC and metastases (49, 50). Additional signs of response are useful in this time-frame, such as necrosis, increase in apparent diffusion coefficient (ADC) and decrease in attenuation on CT (49, 51, 52). Thirdly, radiation-induced changes in the surrounding non-tumorous liver parenchyma can hamper the size assessment and detection of new lesions, especially on CT (**Figure 2 and 3**). Positron emission tomography using  $^{18}\text{F}$ -fluorodeoxyglucose ( $^{18}\text{F}$ FDG PET/CT) is able to detect more and earlier treatment responses in (colorectal) liver metastases than CT or MRI (50, 53, 54). Furthermore, response on  $^{18}\text{F}$ FDG PET/CT is correlated with tumor markers, progression-free survival and overall survival in colorectal liver metastases (18, 54-56). Yet, little is known on the potential radiation-induced changes in the non-tumorous liver parenchyma as seen on  $^{18}\text{F}$ FDG PET/CT after radioembolization (**CHAPTER 7**).

In recent years research has focused more on the dose-response relationships in radioembolization. Several studies, using all three different commercially available microspheres and analyzing various tumor types, have shown that tumor response is associated with tumor absorbed dose (18, 57-60). Not surprisingly, hepatotoxicity is also correlated with the absorbed dose in the total non-tumorous liver volume (including the non-treated parts) (18, 57, 59). So ideally, a tumoricidal dose is combined with an as low as reasonably achievable absorbed dose in the non-tumorous liver parenchyma.

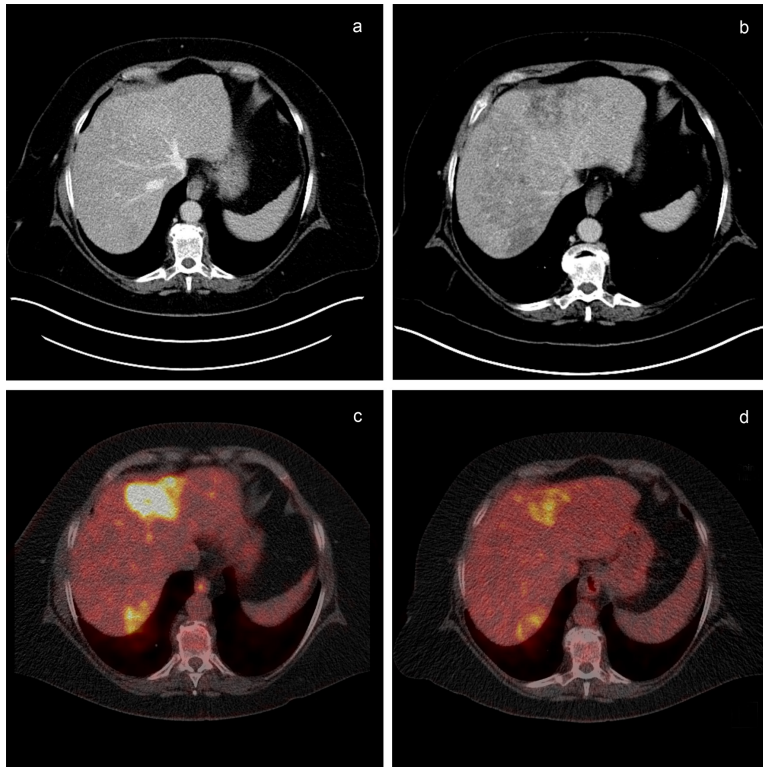


**Figure 2.** 66-years-old female with liver metastases of an uveal melanoma, who underwent a whole liver treatment with  $^{90}\text{Y}$  glass microspheres. On the portal venous CT (a) prior to radioembolization treatment the liver metastases are difficult to discern. On the corresponding fused image of the pre-treatment  $^{18}\text{F}$ FDG PET/CT (c) focally increased activity concentration is present in segment 4A and segment seven, consistent with two metastases. On post-treatment portal venous CT (b) patchy hypodense areas are visible in the liver parenchyma, obscuring the hypodense change of the liver metastases. The corresponding fused image of the post-treatment  $^{18}\text{F}$ FDG PET/CT (d) shows an evident decrease in the  $^{18}\text{F}$ FDG activity concentration in the metastases.

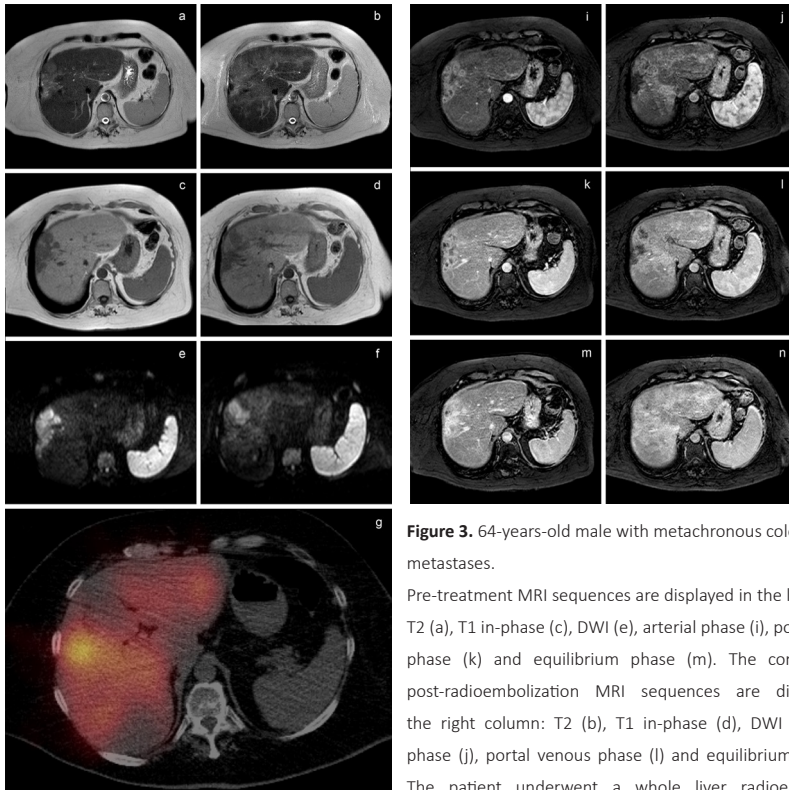


**Figure 3.** 64-years-old male with metachronous colorectal liver metastases.

Pre-treatment MRI sequences are displayed in the left column: T2 (a), T1 in-phase (c), DWI (e), arterial phase (i), portal venous phase (k) and equilibrium phase (m). The corresponding post-radioembolization MRI sequences are displayed in the right column: T2 (b), T1 in-phase (d), DWI (f), arterial phase (j), portal venous phase (l) and equilibrium phase (n). The patient underwent a whole liver radioembolization

treatment with  $^{90}\text{Y}$  resin microspheres. The  $^{99\text{m}}\text{Tc}$ -MAA scintigraphy of the simulation procedure (g) showed adequate targeting of the subcapsular metastasis in segment eight. Non-target embolization is present centrally in segment two and three, as well as in the medial part of segment eight. In the post-treatment images the pattern of the activity distribution (as seen on the  $^{99\text{m}}\text{Tc}$ -MAA scintigraphy (g)) is matched by a corresponding pattern of T2 hyperintensity (b), T1 hypointensity (d), higher signal on the B1000 (f) and early arterial enhancement with persistent enhancement in the portal and equilibrium phase (j, l, m).

This insight has triggered many treatment improvements, especially regarding dosimetry methods. These have evolved from the empirical method to semi-empirical methods (BSA method and MIRD method) to the partition model and voxel-based dosimetry (Table 3) (61).

**Table 3.** Dosimetric calculation methods

Method	Activity calculation equation
Empirical method for whole liver delivery	Tumor load $\leq$ 25% = 2.0 GBq Tumor load 25-50% = 2.5 GBq Tumor load $\geq$ 50% = 3.0 GBq
BSA-based method for $^{90}\text{Y}$ resin	$A(\text{GBq}) = (\text{BSA} - 0.2) + \left[ \frac{\text{tumor volume}}{\text{tumor volume} + \text{liver volume}} \right]$  $\text{BSA} = 0.20247 \times \text{height}(\text{m})^{0.725} \times \text{weight}(\text{kg})^{0.425}$
Mono-compartment method for $^{90}\text{Y}$ glass	$A(\text{GBq}) = \frac{\text{desired dose (Gy)} \times M_{\text{target}}(\text{kg})}{50 \text{ (J/GBq)}}$ in which the estimated total activity shunting to the lungs should not exceed 610 MBq (which corresponds to approximately 30 Gy in 1 kg lung tissue)
Mono-compartment method for $^{166}\text{Ho}$	$A(\text{GBq}) = \frac{\text{desired dose (Gy)} \times M_{\text{target}}(\text{kg})}{15.9 \text{ (J/GBq)}}$
Multi-compartment method	$A(\text{GBq}) = D_{\text{liver}}(\text{Gy}) \frac{\text{TN} \times (M_{\text{tumor}}(\text{kg}) + M_{\text{liver}}(\text{kg}))}{50 \text{ (J-GBq)} \times (1-\text{LSF})}$  Tumor-to-non-tumor ratio (TN) = $\frac{A_{\text{tumor}}(\text{MBq}) / M_{\text{tumor}}(\text{kg})}{A_{\text{liver}}(\text{MBq}) / M_{\text{liver}}(\text{kg})}$ in which liver = non-tumorous liver

A = activity, BSA = body surface area, LSF = lung shunt fraction, M = mass

The BSA method is currently most used in planning  $^{90}\text{Y}$  resin treatments, while the MIRD method is used for  $^{90}\text{Y}$  glass and  $^{166}\text{Ho}$  microspheres. Yet, each model has its limitations. The BSA method is based on the correlation between BSA and liver volume in healthy individuals (62); an assumption that is not true for patients with liver tumors (63, 64),

leading to over- and underdosing. The MIRD model takes the mass of the perfused liver into account, but does not account for any tumor-to-non-tumor ratio (T/N ratio). Furthermore, both models assume a homogeneous distribution of the microspheres in the perfused volume. The partition model takes all this into account by using the  $^{99m}\text{Tc}$  MAA simulation as a proxy for the T/N ratio (65, 66), yet mediating the T/N ratios of all tumors within the same perfused volume (potentially resulting in underdosing of a specific lesion) (66). In line with this limitation,  $^{99m}\text{Tc}$  MAA scintigraphy has shown to be accurate in its prediction of the absorbed dose to the non-tumorous liver parenchyma, but less accurate in its prediction of the tumor absorbed dose (67, 68). Treatment simulation using a  $^{166}\text{Ho}$  scout dose outperforms  $^{99m}\text{Tc}$  MAA with regard to the tumor absorbed dose prediction, yet is comparable in the non-tumorous liver absorbed dose prediction (69). Yet, in the DOSISPHERE-01 trial – comparing personalized (partition model) and standard dosimetry in HCC treatments with  $^{90}\text{Y}$  glass microspheres – a better objective response and significant survival benefit was observed in the personalized dosimetry group (70).

Another strategy, also used in the DOSISPHERE-01 trial, was to reduce the absorbed dose to the non-tumorous liver volume by ensuring >30% hepatic reserve; i.e. untreated, a strategy similar to the earlier described volumetry criteria in hepatic resections. It is recognized that personalized treatment involves dosimetry-based treatment planning, but also involves dosimetry-focused angiography techniques. The interventional radiologist should carefully assess catheter positioning, flow dynamics (e.g. spasm, preferential flow) and number of injection positions in order to spare as much non-tumorous liver volume as possible. In **CHAPTER 8** we focus on the caudate lobe as a separate lobe; either to treat or to spare as part of the hepatic reserve.

Prior to the angiography and treatment simulation using  $^{99m}\text{Tc}$  MAA or a  $^{166}\text{Ho}$  scout dose, an extensive non-invasive work-up is performed, including clinical status, hematological and biochemical status (including Child Pugh scores in cirrhosis) and anatomic assessment using CT or MRI (71). This allows for exclusion of unsuitable patients, for example due to too high tumor load or insufficient liver reserve (based on the clinical parameters). Furthermore, within the multiphase CT protocol an arterial phase is acquired to map the hepatic vascular anatomy. This helps guide the treatment by visualizing aberrant arteries and thus helps define the need for additional injection positions prior to angiography.

In **CHAPTER 9** and **CHAPTER 10** we focus on the value of the arterial phase CT in patient selection.

Finally, in **CHAPTER 11** this thesis is discussed and a summary is provided in **CHAPTER 12**.

## References

1. Vollmar B, Menger MD. The hepatic microcirculation: mechanistic contributions and therapeutic targets in liver injury and repair. *Physiol Rev*. 2009;89(4):1269-339.
2. Ackerman NB. The blood supply of experimental liver metastases. IV. Changes in vascularity with increasing tumor growth. *Surgery*. 1974;75(4):589-96.
3. Breedis C, Young G. The blood supply of neoplasms in the liver. *Am J Pathol*. 1954;30(5):969-77.
4. Vogel A, Martinelli E, clinicalguidelines@esmo.org EGCEa, Committee EG. Updated treatment recommendations for hepatocellular carcinoma (HCC) from the ESMO Clinical Practice Guidelines. *Ann Oncol*. 2021;32(6):801-5.
5. Pavel M, O'Toole D, Costa F, Capdevila J, Gross D, Kianmanesh R, et al. ENETS Consensus Guidelines Update for the Management of Distant Metastatic Disease of Intestinal, Pancreatic, Bronchial Neuroendocrine Neoplasms (NEN) and NEN of Unknown Primary Site. *Neuroendocrinology*. 2016;103(2):172-85.
6. Jeyarajah DR, Doyle MBM, Espat NJ, Hansen PD, Iannitti DA, Kim J, et al. Role of yttrium-90 selective internal radiation therapy in the treatment of liver-dominant metastatic colorectal cancer: an evidence-based expert consensus algorithm. *J Gastrointest Oncol*. 2020;11(2):443-60.
7. Bester L, Feitelson S, Milner B, Chua TC, Morris DL. Impact of prior hepatectomy on the safety and efficacy of radioembolization with yttrium-90 microspheres for patients with unresectable liver tumors. *Am J Clin Oncol*. 2014;37(5):454-60.
8. Kennedy AS, McNeillie P, Dezarn WA, Nutting C, Sangro B, Wertman D, et al. Treatment parameters and outcome in 680 treatments of internal radiation with resin 90Y-microspheres for unresectable hepatic tumors. *Int J Radiat Oncol Biol Phys*. 2009;74(5):1494-500.
9. Golfieri R, Bilbao JJ, Carpanese L, Cianni R, Gasparini D, Ezziddin S, et al. Comparison of the survival and tolerability of radioembolization in elderly vs. younger patients with unresectable hepatocellular carcinoma. *J Hepatol*. 2013;59(4):753-61.
10. Lam MG, Abdelmaksoud MH, Chang DT, Eclow NC, Chung MP, Koong AC, et al. Safety of 90Y radioembolization in patients who have undergone previous external beam radiation therapy. *Int J Radiat Oncol Biol Phys*. 2013;87(2):323-9.
11. Vilgrain V, Pereira H, Assenat E, Guiu B, Ilonca AD, Pageaux GP, et al. Efficacy and safety of selective internal radiotherapy versus chemotherapy alone in patients with liver metastases from colorectal cancer (FOXFIRE, SIRFLOX, and FOXFIRE-Global): an open-label randomised controlled phase 3 trial. *Lancet Oncol*. 2017;18(12):1624-36.
12. Wasan HS, Gibbs P, Sharma NK, Taieb J, Heinemann V, Ricke J, et al. First-line selective internal radiotherapy plus chemotherapy versus chemotherapy alone in patients with liver metastases from colorectal cancer (FOXFIRE, SIRFLOX, and FOXFIRE-Global): a combined analysis of three multicentre, randomised, phase 3 trials. *Lancet Oncol*. 2017;18(9):1159-71.
13. Mulcahy MF, Mahvash A, Pracht M, Montazeri AH, Bandula S, Martin RCG, et al. Radioembolization With Chemotherapy versus chemotherapy alone in patients with liver metastases: A Randomized, Open-Label, International, Multicenter, Phase III Trial. *J Clin Oncol*. 2021;39(35):3897-907.
14. Emmons EC, Bishay S, Du L, Krebs H, Gandhi RT, Collins ZS, et al. Survival and Toxicities after. *Radiology*. 2022;305(1):228-36.



15. Strigari L, Sciuto R, Rea S, Carpanese L, Pizzi G, Soriani A, et al. Efficacy and toxicity related to treatment of hepatocellular carcinoma with 90Y-SIR spheres: radiobiologic considerations. *J Nucl Med.* 51. United States 2010. p. 1377-85.
16. Chiesa C, Mira M, Maccauro M, Spreafico C, Romito R, Morosi C, et al. Radioembolization of hepatocarcinoma with (90)Y glass microspheres: development of an individualized treatment planning strategy based on dosimetry and radiobiology. *Eur J Nucl Med Mol Imaging.* 2015;42(11):1718-38.
17. Westcott MA, Coldwell DM, Liu DM, Zikria JF. The development, commercialization, and clinical context of yttrium-90 radiolabeled resin and glass microspheres. *Adv Radiat Oncol.* 2016;1(4):351-64.
18. van Roelck C, Bastiaannet R, Smits MLJ, Bruijnen RC, Braat AJAT, de Jong HWAM, et al. Dose-effect relationships of holmium-166 radioembolization in colorectal cancer. *J Nucl Med.* 2020.
19. Piana PM, Gonsalves CF, Sato T, Anne PR, McCann JW, Bar Ad V, et al. Toxicities after radioembolization with yttrium-90 SIR-spheres: incidence and contributing risk factors at a single center. *J Vasc Interv Radiol.* 2011;22(10):1373-9.
20. Gil-Alzugaray B, Chopitea A, Inarrairaegui M, Bilbao JI, Rodriguez-Fraile M, Rodriguez J, et al. Prognostic factors and prevention of radioembolization-induced liver disease. *Hepatology.* 2013;57(3):1078-87.
21. Sangro B, Gil-Alzugaray B, Rodriguez J, Sola I, Martinez-Cuesta A, Viudez A, et al. Liver disease induced by radioembolization of liver tumors: description and possible risk factors. *Cancer.* 2008;112(7):1538-46.
22. Seidensticker M, Fabritius MP, Beller J, Seidensticker R, Todica A, Ilhan H, et al. Impact of Pharmaceutical Prophylaxis on Radiation-Induced Liver Disease Following Radioembolization. *Cancers (Basel).* 2021;13(9).
23. Johnson PJ, Berhane S, Kagebayashi C, Satomura S, Teng M, Reeves HL, et al. Assessment of liver function in patients with hepatocellular carcinoma: a new evidence-based approach-the ALBI grade. *J Clin Oncol.* 2015;33(6):550-8.
24. Lescurc C, Estrade F, Pedrono M, Campillo-Gimenez B, Le Sourd S, Pracht M, et al. ALBI Score Is a Strong Predictor of Toxicity Following SIRT for Hepatocellular Carcinoma. *Cancers (Basel).* 2021;13(15).
25. Ricke J, Schinner R, Seidensticker M, Gasbarrini A, van Delden OM, Amthauer H, et al. Liver function after combined selective internal radiation therapy or sorafenib monotherapy in advanced hepatocellular carcinoma. *J Hepatol.* 2021;75(6):1387-96.
26. de Graaf W, van Lienden KP, van Gulik TM, Bennink RJ. (99m)Tc-mebrofenin hepatobiliary scintigraphy with SPECT for the assessment of hepatic function and liver functional volume before partial hepatectomy. *J Nucl Med.* 2010;51(2):229-36.
27. Geisel D, Lüdemann L, Hamm B, Denecke T. Imaging-Based Liver Function Tests--Past, Present and Future. *Rofo.* 2015;187(10):863-71.
28. Nanashima A, Yamaguchi H, Shibasaki S, Morino S, Ide N, Takeshita H, et al. Relationship between indocyanine green test and technetium-99m galactosyl serum albumin scintigraphy in patients scheduled for hepatectomy: Clinical evaluation and patient outcome. *Hepatol Res.* 2004;28(4):184-90.
29. Krishnamurthy GT, Krishnamurthy S. Cholescintigraphic measurement of liver function: how is it different from other methods? *Eur J Nucl Med Mol Imaging.* 2006;33(10):1103-6.
30. Bennink RJ, Dinant S, Erdogan D, Heijnen BH, Straatsburg IH, van Vliet AK, et al. Preoperative assessment of postoperative remnant liver function using hepatobiliary scintigraphy. *J Nucl Med.* 2004;45(6):965-71.

31. Dinant S, de Graaf W, Verwer BJ, Bennink RJ, van Lienden KP, Gouma DJ, et al. Risk assessment of posthepatectomy liver failure using hepatobiliary scintigraphy and CT volumetry. *J Nucl Med.* 2007;48(5):685-92.
32. de Graaf W, van Lienden KP, van den Esschert JW, Bennink RJ, van Gulik TM. Increase in future remnant liver function after preoperative portal vein embolization. *Br J Surg.* 2011;98(6):825-34.
33. Kanamura T, Murakami G, Ko S, Hirai I, Hata F, Nakajima Y. Evaluating the hilar bifurcation territory in the human liver caudate lobe to obtain critical information for delimiting reliable margins during caudate lobe surgery: anatomic study of livers with and without the external caudate notch. *World J Surg.* 2003;27(3):284-8.
34. Bennink RJ, Cieslak KP, van Delden OM, van Lienden KP, Klumpen HJ, Jansen PL, et al. Monitoring of Total and Regional Liver Function after SIRT. *Front Oncol.* 2014;4:152.
35. Abdalla EK, Adam R, Bilchik AJ, Jaeck D, Vauthey JN, Mahvi D. Improving resectability of hepatic colorectal metastases: expert consensus statement. *Ann Surg Oncol.* 2006;13(10):1271-80.
36. Denys A, Prior J, Bize P, Duran R, De Baere T, Halkic N, et al. Portal vein embolization: what do we know? *Cardiovasc Intervent Radiol.* 2012;35(5):999-1008.
37. Garlipp B, Gibbs P, Van Hazel GA, Jeyarajah R, Martin RCG, Bruns CJ, et al. Secondary technical resectability of colorectal cancer liver metastases after chemotherapy with or without selective internal radiotherapy in the randomized SIRFLOX trial. *Br J Surg.* 2019;106(13):1837-46.
38. Farges O, Belghiti J, Kianmanesh R, Regimbeau JM, Santoro R, Vilgrain V, et al. Portal vein embolization before right hepatectomy: prospective clinical trial. *Ann Surg.* 2003;237(2):208-17.
39. Kokudo N, Tada K, Seki M, Ohta H, Azekura K, Ueno M, et al. Proliferative activity of intrahepatic colorectal metastases after preoperative hemihepatic portal vein embolization. *Hepatology.* 2001;34(2):267-72.
40. Theysohn JM, Ertle J, Muller S, Schlaak JF, Nensa F, Sipilae S, et al. Hepatic volume changes after lobar selective internal radiation therapy (SIRT) of hepatocellular carcinoma. *Clin Radiol.* 2014;69(2):172-8.
41. Vouche M, Lewandowski RJ, Atassi R, Memon K, Gates VL, Ryu RK, et al. Radiation lobectomy: time-dependent analysis of future liver remnant volume in unresectable liver cancer as a bridge to resection. *J Hepatol.* 2013;59(5):1029-36.
42. Edeline J, Lenoir L, Boudjema K, Rolland Y, Boulic A, Le Du F, et al. Volumetric changes after (90)Y radioembolization for hepatocellular carcinoma in cirrhosis: an option to portal vein embolization in a preoperative setting? *Ann Surg Oncol.* 2013;20(8):2518-25.
43. Garlipp B, de Baere T, Damm R, Irmischer R, van Buskirk M, Stubs P, et al. Left-liver hypertrophy after therapeutic right-liver radioembolization is substantial but less than after portal vein embolization. *Hepatology.* 2014;59(5):1864-73.
44. Al-Sharif E, Simoneau E, Hassanain M. Portal vein embolization effect on colorectal cancer liver metastasis progression: Lessons learned. *World J Clin Oncol.* 2015;6(5):142-6.
45. de Baere T, Terriethau C, Deschamps F, Catherine L, Rao P, Hakime A, et al. Predictive factors for hypertrophy of the future remnant liver after selective portal vein embolization. *Ann Surg Oncol.* 2010;17(8):2081-9.
46. Simoneau E, Aljiffry M, Salman A, Abualhassan N, Cabrera T, Valenti D, et al. Portal vein embolization stimulates tumour growth in patients with colorectal cancer liver metastases. *HPB (Oxford).* 2012;14(7):461-8.

47. Goebel J, Sulke M, Lazik-Palm A, Goebel T, Dechêne A, Bellendorf A, et al. Factors associated with contralateral liver hypertrophy after unilateral radioembolization for hepatocellular carcinoma. *PLoS One*. 2017;12(7):e0181488.
48. Labgaa I, Tabrizian P, Titano J, Kim E, Thung SN, Florman S, et al. Feasibility and safety of liver transplantation or resection after transarterial radioembolization with Yttrium-90 for unresectable hepatocellular carcinoma. *HPB (Oxford)*. 2019;21(11):1497-504.
49. Keppke AL, Salem R, Reddy D, Huang J, Jin J, Larson AC, et al. Imaging of hepatocellular carcinoma after treatment with yttrium-90 microspheres. *AJR Am J Roentgenol*. 2007;188(3):768-75.
50. Miller FH, Keppke AL, Reddy D, Huang J, Jin J, Mulcahy MF, et al. Response of liver metastases after treatment with yttrium-90 microspheres: role of size, necrosis, and PET. *AJR Am J Roentgenol*. 2007;188(3):776-83.
51. Spina JC, Hume I, Pelaez A, Peralta O, Quadrelli M, Garcia Monaco R. Expected and Unexpected Imaging Findings after. *Radiographics*. 2019;39(2):578-95.
52. oo I, Kim HC, Kim GM, Paeng JC. Imaging Evaluation Following. *Korean J Radiol*. 2018;19(2):209-22.
53. Bienert M, McCook B, Carr BI, Geller DA, Sheetz M, Tutor C, et al. 90Y microsphere treatment of unresectable liver metastases: changes in 18F-FDG uptake and tumour size on PET/CT. *Eur J Nucl Med Mol Imaging*. 2005;32(7):778-87.
54. Zerizer I, Al-Nahhas A, Towey D, Tait P, Ariff B, Wasan H, et al. The role of early <sup>18</sup>F-FDG PET/CT in prediction of progression-free survival after <sup>90</sup>Y radioembolization: comparison with RECIST and tumour density criteria. *Eur J Nucl Med Mol Imaging*. 2012;39(9):1391-9.
55. Fendler WP, Philippe Tiega DB, Ilhan H, Paprottka PM, Heinemann V, Jakobs TF, et al. Validation of several SUV-based parameters derived from 18F-FDG PET for prediction of survival after SIRT of hepatic metastases from colorectal cancer. *J Nucl Med*. 2013;54(8):1202-8.
56. Jongen JMJ, Rosenbaum CENM, Braat MNGJ, van den Bosch MAAJ, Sze DY, Kranenburg O, et al. Anatomic versus Metabolic Tumor Response Assessment after Radioembolization Treatment. *J Vasc Interv Radiol*. 2018;29(2):244-53.e2.
57. Alsultan AA, van Roekel C, Barentsz MW, Smits MLJ, Kunnen B, Koopman M, et al. Dose-response and dose-toxicity relationships for yttrium-90 glass radioembolization in patients with colorectal cancer liver metastases. *J Nucl Med*. 2021.
58. Hermann AL, Dieudonné A, Ronot M, Sanchez M, Pereira H, Chatellier G, et al. Relationship of Tumor Radiation-absorbed Dose to Survival and Response in Hepatocellular Carcinoma Treated with Transarterial Radioembolization with. *Radiology*. 2020;296(3):673-84.
59. Chiesa C, Mira M, Bhoori S, Bormolini G, Maccauro M, Spreafico C, et al. Radioembolization of hepatocarcinoma with. *Eur J Nucl Med Mol Imaging*. 2020;47(13):3018-32.
60. Eaton BR, Kim HS, Schreiber E, Schuster DM, Galt JR, Barron B, et al. Quantitative dosimetry for yttrium-90 radionuclide therapy: tumor dose predicts fluorodeoxyglucose positron emission tomography response in hepatic metastatic melanoma. *J Vasc Interv Radiol*. 2014;25(2):288-95.
61. Ho S, Lau WY, Leung TW, Chan M, Ngar YK, Johnson PJ, et al. Partition model for estimating radiation doses from yttrium-90 microspheres in treating hepatic tumours. *Eur J Nucl Med*. 1996;23(8):947-52.
62. Vauthey JN, Abdalla EK, Doherty DA, Gertsch P, Fenstermacher MJ, Loyer EM, et al. Body surface area and body weight predict total liver volume in Western adults. *Liver Transpl*. 2002;8(3):233-40.

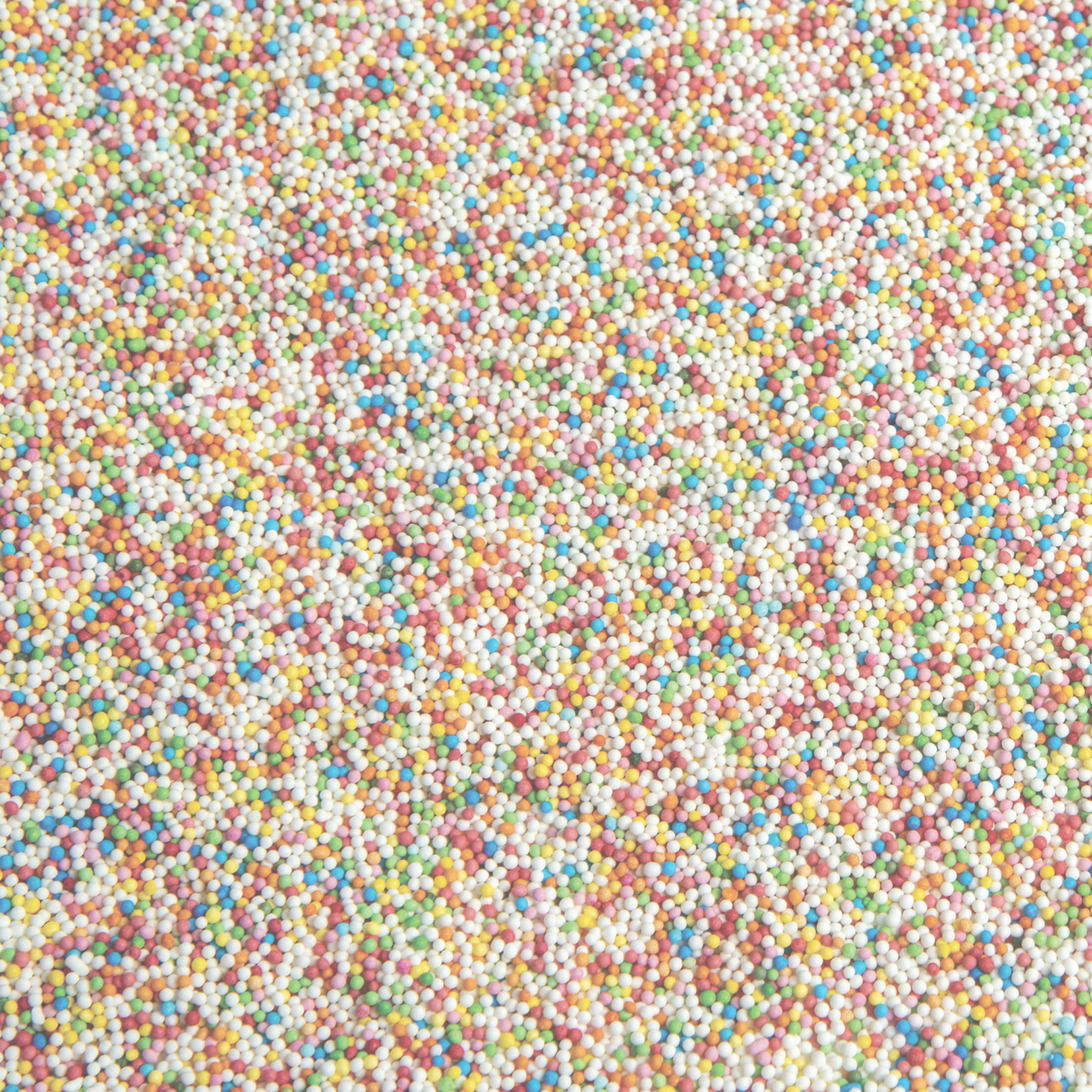
63. Lam MG, Louie JD, Abdelmaksoud MH, Fisher GA, Cho-Phan CD, Sze DY. Limitations of body surface area-based activity calculation for radioembolization of hepatic metastases in colorectal cancer. *J Vasc Interv Radiol.* 2014;25(7):1085-93.
64. Kao YH, Tan EH, Ng CE, Goh SW. Clinical implications of the body surface area method versus partition model dosimetry for yttrium-90 radioembolization using resin microspheres: a technical review. *Ann Nucl Med.* 2011;25(7):455-61.
65. Giammarile F, Bodei L, Chiesa C, Flux G, Forrer F, Kraeber-Bodere F, et al. EANM procedure guideline for the treatment of liver cancer and liver metastases with intra-arterial radioactive compounds. *Eur J Nucl Med Mol Imaging.* 2011;38(7):1393-406.
66. Bastiaannet R, Kappadath SC, Kunnen B, Braat AJAT, Lam MGEH, de Jong HWAM. The physics of radioembolization. *EJNMMI Phys.* 2018;5(1):22.
67. Jadoul A, Bernard C, Lovinfosse P, Gérard L, Lilet H, Cornet O, et al. Comparative dosimetry between. *Eur J Nucl Med Mol Imaging.* 2020;47(4):828-37.
68. Gnesin S, Canetti L, Adib S, Cherbuin N, Silva Monteiro M, Bize P, et al. Partition Model-Based <sup>99m</sup>Tc-MAA SPECT/CT Predictive Dosimetry Compared with <sup>90Y</sup> TOF PET/CT Posttreatment Dosimetry in Radioembolization of Hepatocellular Carcinoma: A Quantitative Agreement Comparison. *J Nucl Med.* 2016;57(11):1672-8.
69. Smits MLJ, Dassen MG, Prince JF, Braat A, Beijst C, Bruijnen RCG, et al. The superior predictive value of (166)Ho-scout compared with (99m)Tc-macroaggregated albumin prior to (166)Ho-microspheres radioembolization in patients with liver metastases. *Eur J Nucl Med Mol Imaging.* 2020;47(4):798-806.
70. Garin E, Tselikas L, Guiu B, Chalaye J, Edeline J, de Baere T, et al. Personalised versus standard dosimetry approach of selective internal radiation therapy in patients with locally advanced hepatocellular carcinoma (DOSISPHERE-01): a randomised, multicentre, open-label phase 2 trial. *Lancet Gastroenterol Hepatol.* 2021;6(1):17-29.
71. Weber M, Lam M, Chiesa C, Konijnenberg M, Cremonesi M, Flamen P, et al. EANM procedure guideline for the treatment of liver cancer and liver metastases with intra-arterial radioactive compounds. *Eur J Nucl Med Mol Imaging.* 2022;49(5):1682-99.





# Part I

Clinical perspectives on  
radioembolization





CHAPTER  
TWO

**Radioembolization Induced Liver Disease:  
a systematic review**

Manon N. Braat, Karel J. van Erpecum, Bernard A. Zonnenberg,  
Maurice A. van den Bosch, Marnix G. Lam

*European Journal Gastroenterology & Hepatology* 2017 Feb;29(2):144-152.



## **Abstract**

### **Background**

Radioembolization (RE) is a relatively novel treatment modality for primary and secondary hepatic malignancies. Microspheres embedded with a beta-emitting radio-isotope are injected into the hepatic artery, resulting in microsphere deposition in the tumor arterioles and normal portal triads. Microsphere deposition in non-tumorous parenchyma can result in radiation induced liver injury, with lethal radioembolization induced liver disease (REILD) at the outer end of the spectrum. The primary aim of this study was to evaluate RE-related hepatotoxicity and give an overview of the currently applied definitions and clinically relevant characteristics of REILD.

### **Methods**

A systematic literature search on REILD was conducted. Studies after the introduction of the term REILD (2008) were screened for definitions of REILD. Hepatotoxicity and applied definitions of REILD were compared.

### **Results**

Liver biochemistry test abnormalities occur in up to 100% of patients after RE, mostly self-limiting. The incidence of symptomatic REILD varied between 0-31%, although in most reports the incidence was 0-8% with a lethal outcome in 0-5%. With the exception of bilirubin, the presentation of hepatotoxicity and REILD were similar for cirrhotic and non-cirrhotic patients. No uniform definition of REILD was established in current literature. We here propose a unifying definition and grading system for REILD.

### **Conclusion**

RE-related hepatotoxicity is a common phenomenon, symptomatic REILD however is rare. Currently, reporting of REILD is highly variable, precluding reliable comparison between studies, identification of risk factors and treatment developments.

## Introduction

Radioembolization (RE) is a relatively novel treatment modality for primary and secondary hepatic malignancies. This form of selective radiation therapy uses intra-arterially delivered microspheres embedded with a beta- emitting radio-isotope (most commonly yttrium-90 ( $^{90}\text{Y}$ )). Both primary and secondary hepatic tumors are thought to be preferentially vascularized by the arterial system, as opposed to the portal venous preference of liver parenchyma, provided that the tumor size is  $>2$  mm (1). Therefore, microspheres will preferentially accumulate in the tumors, resulting in a higher toxic dose in the tumors and relative sparing of the liver parenchyma.

In patients with hepatocellular carcinoma (HCC), RE was associated with a longer overall survival and longer time to progression than transarterial chemoembolization (TACE), while having the benefit of shorter hospitalization, less postembolization syndrome, fewer treatment sessions and a similar toxicity profile (2). Moreover, RE is a well-recognized treatment option in cases with portal vein thrombosis, contrary to TACE (2, 3). Also, in patients with colorectal liver metastases, RE seems a promising option to increase overall survival, although evidence from large randomized controlled trials is still awaited (4).

Various complications have been described after or during the RE procedure. These are caused either by the angiographic procedure itself (eg. arterial dissection), the embolic effect (i.e. post-embolization syndrome) or by the delivery of a radiation absorbed dose to normal liver parenchyma or to extrahepatic sites, such as the gastro-intestinal system (eg. gastroduodenal ulceration, radiation gastritis, cholecystitis or pancreatitis), the abdominal wall (i.e. radiation dermatitis) and the lungs (i.e. radiation pneumonitis) (5, 6).

In general, liver disease due to radiation is a long-known complication after external beam radiation therapy (EBRT) (7, 8). The low tolerance of normal liver parenchyma is the most important limiting factor in terms of dose and volume for EBRT, making the clinical value of EBRT in liver malignancies very limited (9). In contrast, RE has the potential to selectively deliver an effective dose to the tumors, by means of their supplying arteries. Nevertheless, radiation dose distribution in RE is more heterogeneous than in EBRT (10-13), complicating the accurate calculation of an effective, yet safe dose for the individual patient. Histology

after RE has shown large inter- and intra-patient variation in microsphere distribution with tumor to normal tissue radiation dose ratios (T/N ratio) ranging from only 0.4 to 45 (median 5), corresponding to tissue doses of 9-75 Gy (10).

In 2008 Sangro et al. (14) were the first to use the term RE-induced liver disease (REILD). They described the clinical syndrome of REILD and elucidated the differences and similarities of REILD, with the previously described radiation induced liver disease syndromes: radiation induced liver disease (RILD) and combined modality induced liver disease (CMILD) (Table 1).

**Table 1:** Definitions of radiation induced liver diseases

		<b>Definition*</b>	<b>Time of onset</b>
Radiation induced liver disease	"classic" RILD	RILD is caused by EBRT and characterized by anicteric ascites, hepatomegaly and an isolated elevation of ALP.	2-16 weeks (typically 4-8 weeks)
	"non-classical" RILD	"Classic" RILD, only combined with at least a fivefold elevation of the ULN of transaminases.	
Combined modality induced liver disease	CMILD	CMILD is caused by a combination of EBRT and chemotherapy and characterized by jaundice, hyperbilirubinemia, elevated AST and a less pronounced ALP elevation. It typically occurs 1-2 weeks after cessation of therapy (rang 1-4 weeks).	1-4 weeks (typically 1-2 weeks)

---

EBRT: external beam radiation therapy, ALP: alkaline phosphatase, ULN: upper limit of the normal value, AST: aspartate aminotransferase.

\* definitions according to Lawrence et al. (7)

All three syndromes are considered a form of sinusoidal obstructive syndrome (SOS) and include ascites, weight gain and liver function derailment, however contrary to RILD, both CMILD and REILD are characterized by an obligate elevation of bilirubin (7, 14). Despite their differences, REILD and RILD are used interchangeably in the current RE literature. Consequently, the incidence of REILD and its potential treatment options are not well known.

The primary aim of this study is to review the used definitions of unacceptable hepatotoxicity/ REILD after  $^{90}\text{Y}$  RE of hepatic malignancies. Secondly, the incidence of REILD, its natural course, its risk factors and its treatment options are investigated and a unifying diagnosis for this entity is proposed.

## **Methods**

### **Literature search (Figure 1)**

A systematic literature search was conducted within the Medline database. Only studies published since 2008 (i.e. the introduction of the term REILD by Sangro et al. (14)) were reviewed to assess which definitions of REILD are being used.

The following search terms were included: RILD/ radiation induced liver disease, REILD/ radioembolization induced liver disease or RILI/radiation induced liver injury, combined with the following terms: radioembolisation, radioembolization, SIRT, selective internal radiation therapy, Y90 or Yttrium-90.

Studies were included if a definition of REILD, a reference to a previously published definition of REILD or a definition of RILD in the setting of RE was given. Also included were studies reporting the incidence of REILD in their population.

Prospective and retrospective clinical studies and case series were selected for evaluation. Small studies (<10 patients) were excluded, as were studies evaluating part of a population which was previously published. There were no restrictions regarding the primary tumor (i.e. hepatocellular carcinoma, cholangiocarcinoma or metastases of various primaries), underlying liver disease (cirrhosis), prior interventions (chemotherapy, surgery, external beam radiation, prior RE) or microspheres used (glass or resin). Additional publications were retrieved by cross-referencing.

All included studies used the National Cancer Institute Common Terminology Criteria for Adverse Events (NCI-CTCAE), version 3.0, 4.02 or 4.03 (**Supplement 1**).

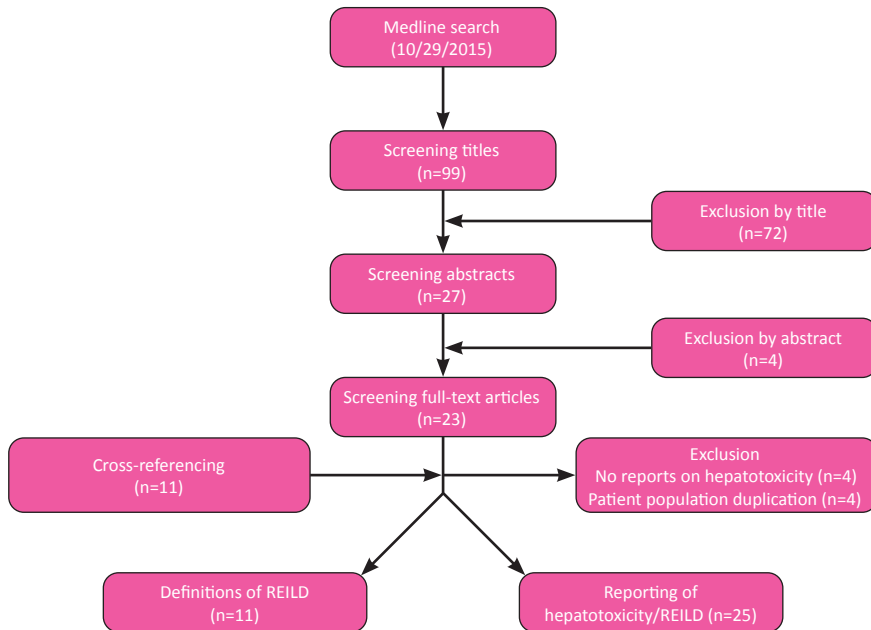


**Figure 1.** Literature search

## Results

Our search yielded 26 clinical studies in total (5, 6, 13-36). Review of these studies revealed that in most studies (15/26) no definition of REILD was mentioned. Remarkably, these 15 studies reported the incidence of REILD in their study population, without any clarification

of the definition applied. In eight of the remaining 11 articles either a definition of REILD was given or a reference was mentioned (**Table 2**) (14, 16, 17, 24, 25, 29, 30, 36). In the three other articles a definition of RILD was described in patients treated with RE (13, 15, 22). Results obtained from all 26 articles are presented on page 39.

In all articles, the bland descriptions of the clinical syndrome (**Figure 2**) included the presence of both ascites or increasing abdominal girth and jaundice or hyperbilirubinemia. Some definitions also required the absence of tumor progression or the presence of veno-occlusive disease / sinusoidal obstructive syndrome (SOS) at histological examination.

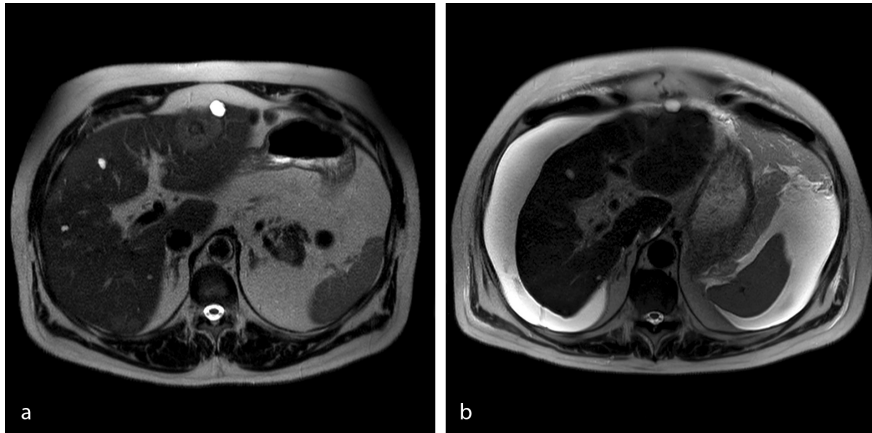


**Figure 2.** A patient with bilobar colorectal livermetastases. Segment 2 and 3 (2.3 GBq), segment 4 (2.4 GBq) and segment 6 and 7 (2.5 GBq) were treated during the first session. Twenty days later segment 5 and 8 were treated (4.5 GBq). a) A pre-treatment T2-weighted image, showing one of the metastases in the left liver lobe. b) The corresponding T2-weighted image acquired three months after RE treatment shows minimal reduction of the metastasis. However, a substantial amount of ascites, shrinkage of the liver and a nodular liver surface have developed. The patient's symptoms were consistent with a grade 4 REILD, requiring repeated paracentesis.

The time of onset of REILD differed considerably between studies. Studies on explants in the setting of transplantation reported signs of SOS in the non-tumorous parenchyma at 28-55 days after RE, but no signs of SOS within 14 days after RE (12, 13). Concordantly, there are no reports of REILD within two weeks after RE, and only a few clinical reports of REILD without histology diagnosed <1 month after <sup>90</sup>Y RE (15, 19, 28). In contrast, explant specimens obtained after four months showed primarily fibrotic changes, similar to reports of RILD (8, 13). In line with this, clinical reports of patients diagnosed with REILD after four months are rare (32, 37). Moreover, most authors exclude this late presentation by definition (**Table 2**). However, several authors do recognize the development of portal hypertension at long term follow-up after RE (25, 30, 37). Thus, based on the available data, REILD due to SOS seems to occur within a timespan of two weeks to four months.

### **Incidence**

The incidence of REILD was highly variable in smaller studies (0-31%), though in the larger series (>200 patients) incidences of 0-5.4% are consistently reported (**Table 3 and 4**). These differences can be explained either by the small patient populations (5, 14, 24), synchronous or prior extensive treatments (5, 14), or by a broad definition of REILD in terms of the clinical and biochemical threshold (17) or the defined time of onset (32).

### **Hepatotoxicity after RE**

The natural course of REILD was highly variable; it can either be transient and self-limiting or result in fulminant hepatic failure and death. However, hepatotoxicity after RE (any CTCAE grade; **Supplement 1**) was reported in up to 100% of cases, mostly grade 1-2 (5, 6, 14, 18-20, 22, 26-28, 30, 31, 33, 35, 38-41). Yet, consistent reports on liver biochemistry abnormalities plotted against the posttreatment interval were scarce. Bilirubin toxicity was seen more often in studies with HCC than in studies with metastatic disease (**Table 4**). To deduce the influence of underlying chronic liver disease we classified the included studies based on the proportion of HCC patients (and thus generally cirrhosis) in the reported study populations (**Tables 3 and 4**). In the HCC populations bilirubin toxicity grade 1-2 was observed in 43-55%, compared to 13-21% in the non-HCC populations. Grade 3-4 bilirubin toxicity was reported in 13-21% and 6-23% in HCC and non-HCC populations, respectively. However, mean pre-treatment total bilirubin levels were higher

**Table 2:** Available definitions of REILD

Author	Year	n	Definition of REILD
Sangro et al. (14)	2008	45	Potentially life-threatening liver damage characterized by jaundice and ascites developing 4 to 8 weeks after treatment, with pathologic changes consistent with VOD in the most severe cases.
Ruhl et al. (29)	2009	12	REILD is characterized by jaundice and ascites as a form of sinusoidal obstruction syndrome. Definition according to Sangro et al.
Nalesnik et al.* (13)	2009	13	A syndrome characterized by ascites with an onset approximately 2 to 4 weeks after irradiation. This may be accompanied by hyperbilirubinemia and tender hepatomegaly.
Kennedy et al.* (22)	2009	515	RILD has been described after external beam radiation and is widely acknowledged to be a clinical entity that can present with ascites 2 weeks to 4 months after hepatic radiation. Clinically, patients develop rapid weight gain, increased abdominal girth, liver enlargement, jaundice, and increased transaminase levels, particularly alkaline phosphatase.
Seidensticker et al. (30)	2012	34	REILD was diagnosed by clinical presentation of jaundice and ascites and a bilirubin increase of >50 $\mu$ mol/l (2,9 mg/dl). Definition according to the definition by Sangro et al.
Gil-Alzugaray et al. (17)	2013	260	REILD was defined as the appearance of a serum total bilirubin of 3 mg/dL or higher and ascites (clinically or by imaging) 1 to 2 months after RE in the absence of tumor progression or bile duct obstruction.
Lam et al. (25)	2013	247	REILD was suspected in the presence of signs and symptoms including jaundice, fatigue, ascites, and changes in laboratory values (elevated serum bilirubin, AST, ALT, alkaline phosphatase and ammonia; decreased albumin) in absence of hepatic tumor progression.
Fernandez et al. (16)	2014	14	Definition according to Sangro et al.
Zarva et al. (36)	2014	21	Definition according to Sangro et al.
Kwok et al. (24)	2014	30	REILD was defined as the appearance of a serum total bilirubin of 3 mg/dL (51 $\mu$ mol/L) or higher, plus new appearance of ascites within 3 months after RE, which could not be explained by tumor progression or bile duct obstruction. Definition according to Gil-Alzugaray et al.
Bester et al.* (15)	2014	427	REILD has a typical onset of 4 to 8 weeks after radioembolization and patients present with jaundice and ascites in the absence of tumor progression or bile duct dilatation.

\* Definition of RILD in a study solely involving RE treatments; consistent with the authors' definition of REILD.



**Table 3** Studies on <sup>90</sup>Y-RE for HCC

Author	Year	n	Child-Pugh score	Microspheres
Nalesnik et al. (13)	2009	13	100% cirrhosis; CP NR	Glass
Ruhl et al. (29)	2009	12	100%CPA	Resin
Hilgard et al. (19)	2010	108	CPA 76%, CPB 22%	Glass
Strigari et al. (32)	2010	73	CPA 79%, CPB 18%, CPC 3%	Resin
Golfieri et al. (18)	2013	325	255/325 cirrhosis, CPA 82%, CPB 18%	Resin
Gil-Alzugaray et al.* (17)	2013	88	100% cirrhosis; CP NR; HCC 98% CCC 2%	Resin
Fernandez et al. (16)	2014	14	100% cirrhosis; BCLC A 21%; B 21%;C 57%	Resin
Kwok et al. (24)	2014	30	CPA 83%; CPB 17%	Resin

CP = Child-Pugh score, BCLCA = Barcelona-Clinic Liver Cancer staging system, BSA = body surface area-based activity calculation, WLD = whole liver delivery (single session), SD = whole liver sequential delivery, LD = lobar delivery, LSD = lobar or segmental delivery, NR = not reported. - = dosimetric calculation for glass microspheres as described by the manufacturer.

Table 3 Continued

Dosimetric calculation	Delivery	REILD†	Remarks
NR	92% LD	NR	Histopathological study of explanted livers
BSA	92% SD 8% LD	0%	
NR	0% WLD	2.8% (0%)	
BSA	48% WLD 52% LD	31% (11%)	
Empiric, BSA or modified partition model	48% WLD	4.3% (0.9-3.4%)	3 deaths related to RE 11 probably related to RE
BSA or partition model	19% WLD	15%; (1.9%)**	Comparison of standard treatment protocol and modified protocol††
NR	0% WLD	0%	
Partition model, if possible. Otherwise BSA	NR	13% (NR)	

\*Gil-Alzugaray et al. Split population (n=260) into a cirrhosis group (n=88) and non-cirrhosis group (n=172). 1.9% of the entire population had grade 5 REILD toxicity (death); no record of presence of cirrhosis or not.

† (%) = REILD related death (% of the entire population).

†† Modified protocol: In general a 10-20% reduction in calculated activity (BSA method) for whole liver treatments, for selective treatments (≥2 liver segments spared) calculation of the activity according to the partition model. Also ursodeoxycholic acid and methyl-prednisolone for 2 months post-RE.

**Table 4** Studies on <sup>90</sup>Y-RE for primary and secondary malignancies

Author	Year	n	Tumor type	Microspheres
Sangro et al. (14)	2008	45	Various metastases, HCC (27%)	Resin
Jakobs et al. (20)	2008	30	Breast cancer metastases	Resin
Kennedy et al. (21)	2008	148	NET metastases	Resin
Kennedy et al. (22)	2009	515	Various, HCC (12%)	Resin
Van Hazel et al. (33)	2009	25	CRC metastases	Resin
Kosmider et al. (5)	2011	19	CRC metastases	Resin
Piana et al. (28)	2011	81	Various metastases, HCC (9%)	Resin
Klingenstein et al. (23)	2013	13	Uveal melanoma metastases	Resin
Paprottka et al. (27)	2012	42	NET metastases	Resin
Seidensticker et al. (30)	2012	34	Various metastasis	Resin
Gil-Alzugaray et al. * (17)	2013	172	HCC (16%), CCC, various metastases	Resin
Lam et al. (25)	2013	247	HCC (26%), CCC (11%), various metastases	Glass (n=66) Resin (n=181)
Peterson et al. (6)	2013	112	Various metastases and HCC (4%)	Resin
Smits et al. (31)	2013	59	Various metastases	Resin
Sofocleous et al. (35)	2013	14	CRC	Resin
Zarva et al. (36)	2014	21	CRC (24%), HCC (38%), CCC (5%)	Resin
Lewandowski et al. (26)	2014	214	CRC metastases	Glass
Bester et al. (15)	2014	427	Various metastases, HCC (6.8%), CCC (7.7%)	Resin
Saxena et al. (34)	2015	302	CRC	Resin

BSA = body surface area-based activity calculation, CCC = cholangiocarcinoma, CPB = Child-Pugh score B, CRC = colorectal, NET = neuro-endocrine tumor, HCC = hepatocellular carcinoma, LD = lobar delivery, LSD = lobar or segmental delivery, NR = not reported, SD = whole liver sequential delivery, WLD = whole liver delivery (single session).-: dosimetric calculation for glass microspheres as described by the manufacturer.

Table 4 Continued

Dosimetric calculation	Delivery	% REILD†	Remarks
BSA & partition model	73% WLD	20% (6.6%)	No cirrhosis
Empiric	100% WLD	3.3%(3.3%)	
BSA	37% WLD	0%	
74% BSA; 19% empiric	32% WLD	5.4% (5.4%)	
BSA	100% WLD	0%	Phase 1 dose escalation study with irinotecan. RE on day 2 or 3 of cycle 1
Empiric or BSA	100% WLD	26% (5%)	RE combined with systemic chemotherapy as first-line treatment
BSA; 25% dose reduction if previous chemo or TACE	5% WLD; 9% SD 86% LD	1% (1%)	
Empiric or BSA	85% WLD	7.8% (7.8%)	
BSA	57% WLD	0%	
BSA	50% WLD	8.8% (NR)	Comparison of WLD and SD
BSA for WLD, partition model if >2 segments were spared	63% WLD	8% (1.9%)*	Comparison of standard protocol and modified protocol††
Glass: - Resin: BSA	64% WLD; 9% SD 27% LSD	4.0% (0.8%)	20,6% cirrosis
BSA	77% WLD; 23% LD	1.8% (0%)	
BSA	64% WLD; 17% SD 19% LD	0%	CPB 10%
BSA	NR	0%	Phase 1 study with delivery of 70%, 85% or 100% of the calculated dose
BSA	No WLD	0%	Study regarding repeated RE
NR	83% SD; 17% LD	0%	
BSA	NR	2.3% (0%)	Comparison of toxicity in patients with and without prior hepatectomy
BSA	In principle WLD	0.3% (0.3%)	CPB 1%

\*Gil-Alzugaray et al. Split population (n=260): cirrhosis group (n=88) and non-cirrhotic group (n=172). 1.9% of the entire population had grade 5 REILD toxicity (death); no record of presence of cirrhosis or not. † (%) = REILD related death (% of the entire population). †† Modified protocol: In general a 10-20% reduction in calculated activity (BSA method) for whole liver treatments, for selective treatments ( $\geq 2$  liver segments spared) calculation of the activity according to the partition model. Also ursodeoxycholic acid and methyl-prednisolone for 2 months post-RE.

in the HCC populations; 13.7-20.5  $\mu\text{mol/l}$  compared to 10.3-15.4  $\mu\text{mol/l}$  in non-HCC populations. Gil-Alzugaray et al. (17) divided their population of 260 patients in a non-cirrhotic and cirrhotic group; baseline mean total bilirubin levels were 10.4  $\mu\text{mol/l}$  and 19.7  $\mu\text{mol/l}$ , respectively. REILD developed in 8% of non-cirrhotic patients and in 15% of cirrhotic patients (no p-value given). In other large studies the incidence of REILD was fairly similar in both groups, as was death due to REILD. Other liver biochemistry abnormalities were similar for the HCC and non-HCC populations (Table 5). In both groups most liver biochemistry abnormalities resolved spontaneously (6, 19, 28, 39). A return to the baseline bilirubin level typically occurred within 4-6 weeks (19, 28, 36, 39). Incidence of ascites after RE varied from 0-26% (5, 20, 30, 39, 42, 43). When reported, ascites was coincident with the liver biochemistry abnormalities.

**Table 5:** Range of incidences of all liver toxicities after RE according to grade and tumor type

	Bilirubin	Albumin	ALP	ALT	AST	INR	Ascites†
<b>HCC</b>							
grade 1-2	43-55	18-77	16-75	53-58	71	30-31	4-13
grade 3-4	6-19	0-18	0-4	0-5	19	2-3	
<b>Non-HCC</b>							
grade 1-2	13-21	57	21-62	43-87	21-87	-	0-26
grade 3-4	0-18	2-17	0-21	0-5	2-5	-	

Data are all ranges of data presented in the above mentioned studies, denoted in percentages (5, 6, 14, 18-20, 22, 26-28, 30, 31, 33, 35, 36, 38-41).

ALP= alkaline phosphatase, GGT= gamma glutamyl transpeptidase, ALT= alanine aminotransferase, AST= aspartate aminotransferase. † Ascites; not due to tumor progression and all CTCAE grades combined.

### Risk factors

Several risk factors for hepatotoxicity and REILD have been proposed (6, 14, 15, 17, 18, 22, 28, 30, 39, 44). Although younger age (<70 years) was initially identified as a risk factor (14), this was not confirmed by another study (18). Liver-directed treatments have been established as a risk factor, such as chemotherapy (either pre- or post-RE) (14, 17, 22, 26,

28), prior RE (25), prior external beam radiation therapy (44), other prior intra-arterial therapies (28) and the number of prior liver-directed treatments (22).

The reported risk factors tumor burden, prescribed and administered activity, and liver volume/weight all represent one common underlying risk factor: administered activity per target volume or absorbed dose. Indeed, Gil-Alzugaray et al. (17) found the activity per target volume to be a significant risk factor, with most cases occurring  $>0.8$  GBq/l. Single session whole liver treatment also increased the risk of hepatotoxicity (in contrast to sequential treatment of the right and left liver lobe with a six week interval) (17, 22, 30).

### **Treatment options**

Due to the low incidence of serious REILD only anecdotal reports of treatment options are available. The treatment of the underlying sinusoidal obstructive syndrome (SOS) in general is more elaborately described in two recent review articles (45, 46).

Supportive measures are most important. These include the avoidance of hepato- and nephrotoxic drugs and the reduction of the excessive extravascular volume (i.e. ascites, edema, pleural effusion) while securing the maintainance of the intravascular volume. This can be accomplished by diuretics, paracentesis and thoracocentesis. If sodium and fluid balance cannot be controlled adequately, transjugular intrahepatic portosystemic shunt (TIPS) placement and/or haemodialysis may be required. However, in an earlier report on TIPS in severe CMILD, at best temporarily improvements of liver function, creatinine levels or ascites were seen, with only 3/18 patients surviving  $\geq 6$  months (47).

Pharmacological options are not well established in SOS and REILD. Ursodeoxycholic acid is a hydrophilic bile acid, that reduces the amounts of endogenous hydrophobic bile acids, which can be hepatotoxic in cholestasis (45). Gil-Alzugaray et al. (17) report a significant reduction in the incidence of REILD after the introduction of a modified protocol, existing of ursodeoxycholic acid (600 mg/day) and methylprednisolone (4-8 mg/day) during two months after RE. However, the modified protocol also included concomitant 10-20% reduction of the administered  $^{90}\text{Y}$ -dose, providing an alternative explanation for the reduced incidence of REILD. In line with this suggestion, ursodeoxycholic acid and methylprednisolone were not independently associated with the REILD reduction. Of

note, mitigation of RILD by a combination of ursodeoxycholid acid, low molecular weight heparin and pentoxifylline has been reported after interstitial brachytherapy (48), whereas other studies report contradictory results on the use of low molecular weight heparin, corticosteroids and ursodeoxycholic acid in SOS (46). Of note, according to a recent Cochrane review (49), the use of ursodeoxycholic acid as a prophylaxis may decrease the incidence of SOS in stem cell transplant recipients.

Defibrotide is currently the most promising drug for SOS in general, although it is only available as an investigational drug in the United States (since 2007) and as a compassionate drug for severe SOS in Europe (since 2013). Defibrotide is a porcine-derived polydisperse polydeoxyribonucleotide, with anti-thrombotic, fibrinolytic, anti-adhesive and anti-inflammatory effects on microvascular endothelium, without enhancement of the systemic bleeding risk or compromise of anti-tumor effects (45). No mention of its specific use has been made in case of REILD.

Although, a protective effect of bevacizumab (monoclonal antibody directed against vascular endothelial growth factor) against the development of SOS (in case of oxaliplatin induced SOS) has been suggested (46, 50), Lam et al. (25) found no such beneficial effect of bevacizumab in REILD. Finally, a protective effect has been described for sorafenib in preclinical studies, but no data on patients are available (51).

## Discussion

Even though REILD is a multifactorial entity, the two key factors for its development seem to be the absorbed dose in non-tumorous parenchyma and a reduced functional liver reserve (due to cirrhosis or prior treatments).

First, accurate dose calculation is complex owing to the flow dynamics inherent to the (ab)normal liver architecture, the unknown tumor-to-non-tumor ratio and the unknown susceptibility to radiation of the non-tumorous parenchyma (52, 53). Moreover, some evidence indicates a difference in mean tolerable liver dose between different microspheres with a mean tolerable liver dose for 50% liver toxicity complication risk ( $TD_{50}$ ) of 100 Gy for glass  $^{90}\text{Y}$ -microspheres vs. a  $TD_{50}$  of 52 Gy for resin  $^{90}\text{Y}$ -microspheres (32, 53, 54). This

finding can be partly explained by the higher embolic load of the resin spheres, as a 20-60 times larger amount of resin spheres is injected (52).

Second, prediction of the functional liver reserve is difficult. The commonly used clinical scores (i.e. Child-Pugh score and MELD score) cannot reliably predict the actual functional liver reserve or risk of postoperative liver failure (55). Conversely, hepatobiliary scintigraphy can quantify liver function and account for regional differences (56). This technique could therefore be of value in case of repeated RE or downstaging with RE prior to surgery (57).

Late sequelae of RE and RE induced portal hypertension are increasingly reported (13, 37, 58, 59). In patients with cirrhosis another explanation for late liver function deterioration might be worsening of preexisting cirrhosis or even reactivation of latent hepatitis (17, 60). The exacerbation of chronic hepatitis in known hepatitis B or C carriers has been described in patients with CMILD, after chemoradiation, chemotherapy alone or TACE (60). In the current literature no such case after RE has been described.

Clinical and laboratory toxicity is commonly graded according to the CTCAE. REILD or RILD is not incorporated as a separate entity. On top of the inconsistent reports of REILD and varying definitions, few studies applied CTCAE criteria to define the grade of REILD; all but one omitting clarification of the graded adverse event (either the criteria for hepatic failure, bilirubin laboratory toxicity or otherwise) (6, 17, 32, 38).

Apart from TACE, other liver-directed treatments, such as stereotactic body radiation therapy (SBRT) and radiofrequency ablation (RFA), are also used to treat primary and secondary liver malignancies. Compared to SBRT and RFA, hepatotoxicity seems to be more prevalent in RE (61, 62). Tao et al. (61) reported an incidence of RILD after SBRT in 13 out of 499 patients (2.6%), with 11 cases occurring in patients with HCC (7% vs. 0.6% in metastatic disease). Hepatotoxicity after RFA is equally rare, but other major complications (eg. intra-abdominal hemorrhage, intestinal perforation, biliary damage and pneumothorax) are reported in 2% (62, 63). The essential difference between these locoregional treatments and RE is the size and number of lesions, as well as the fraction of the liver to be treated. Both SBRT and RFA require separate targeting of each lesion, resulting in a median of 1 treated lesion of limited size (63). In contrary, patients selected for RE generally have a high



tumor load (size and number), especially in metastatic disease, and are often ineligible for RFA or SBRT. Inevitably, a larger part of the non-tumorous parenchyma is involved in the treatment, resulting in more hepatotoxicity.

At present, phase III studies on RE are ongoing, underlining the importance of a well-defined definition and uniform grading system of REILD to establish reliable dose-effect relationships, to improve uniform reporting and to enhance the inter-study comparability. The recently published results of the first large phase III trial (SIRFLOX-study) emphasize the need for consistency, as their definition of hepatotoxicity was unclear and the long abandoned term “radiation hepatitis” was used (64).

Based on the current literature we propose the following definition of REILD: a symptomatic post-radioembolization deterioration in the ability of the liver to maintain its (normal or preprocedural) synthetic, excretory, and detoxifying functions. It is characterized by jaundice and the development/increase in ascites, hyperbilirubinemia and hypoalbuminemia developing  $\geq 2$  weeks – 4 months post-radioembolization, in the absence of tumor progression or biliary obstruction. Furthermore, hepatotoxicity after RE may be graded as follows:

- Grade 0: No liver toxicity (i.e. no CTCAE toxicity grade changes over baseline).
- Grade 1: Minor liver toxicity, limited to increased AST, ALT, ALP and/or GGT levels (all not exceeding newly developed grade 1 CTCAE toxicity).
- Grade 2: Moderate liver toxicity, with a self-limiting course. No medical intervention necessary.
- Grade 3: REILD, manageable with non-invasive treatments such as diuretics, ursodeoxycholic acid and steroids.
- Grade 4: REILD necessitating invasive medical treatment such as paracentesis, transfusions, haemodialysis or a transjugular intrahepatic portosystemic shunt (TIPS).
- Grade 5: Fatal REILD.

Similar to the consensus article of posthepatectomy liver failure (65) we propose to stratify or grade REILD according to the clinical presentation and required treatments, opposed to a grading system principally based on histopathology or elevated laboratory values. Our 5 point scale is also consistent with the adverse event reporting system according to the NCI-CTCAE.

The stratification of REILD according to its impact on patients' management seems clinically relevant and easily applicable, but its reproducibility still needs to be validated. Moreover, clinical stratification is very likely to be the best option, as histopathology after RE will often be lacking and laboratory values do not reflect the actual loss of liver function as a whole. Naturally, the use of this definition of REILD will lead to an increase in the reported incidence of REILD, as currently often only severe cases of REILD are reported (grade 4 or 5). However, consistent reporting of all grades of REILD will enhance our knowledge of its risk factors, prevention and treatment.

## **Conclusion**

RE-related hepatotoxicity is a very common complication, with a large variation in its severity, ranging from no symptomatology to fatal REILD. Currently, reporting of REILD is highly variable precluding valid comparison between studies, identification of risk factors and treatment developments. Standardized reporting of hepatotoxicity after RE will help to elucidate the absorbed dose - hepatotoxicity relationship, ultimately leading to improved patient selection and patient outcome.

## References

1. Dezso K, Bugyik E, Papp V, Laszlo V, Dome B, Tovari J, et al. Development of arterial blood supply in experimental liver metastases. *Am J Pathol.* 2009;175(2):835-43.
2. Salem R, Lewandowski RJ, Kulik L, Wang E, Riaz A, Ryu RK, et al. Radioembolization results in longer time-to-progression and reduced toxicity compared with chemoembolization in patients with hepatocellular carcinoma. *Gastroenterology.* 2011;140(2):497-507 e2.
3. Lau WY, Sangro B, Chen PJ, Cheng SQ, Chow P, Lee RC, et al. Treatment for hepatocellular carcinoma with portal vein tumor thrombosis: the emerging role for radioembolization using yttrium-90. *Oncology.* 2013;84(5):311-8.
4. Rosenbaum CE, Verkooijen HM, Lam MG, Smits ML, Koopman M, van Seeters T, et al. Radioembolization for treatment of salvage patients with colorectal cancer liver metastases: a systematic review. *J Nucl Med.* 2013;54(11):1890-5.
5. Kosmider S, Tan TH, Yip D, Dowling R, Lichtenstein M, Gibbs P. Radioembolization in combination with systemic chemotherapy as first-line therapy for liver metastases from colorectal cancer. *J Vasc Interv Radiol.* 22. United States: 2011 SIR. Published by Elsevier Inc; 2011. p. 780-6.
6. Peterson JL, Vallow LA, Johnson DW, Heckman MG, Diehl NN, Smith AA, et al. Complications after 90Y microsphere radioembolization for unresectable hepatic tumors: An evaluation of 112 patients. *Brachytherapy.* 2013;12(6):573-9.
7. Lawrence TS, Robertson JM, Anscher MS, Jirtle RL, Ensminger WD, Fajardo LF. Hepatic toxicity resulting from cancer treatment. *Int J Radiat Oncol Biol Phys.* 31. United States1995. p. 1237-48.
8. Sempoux C, Horsmans Y, Geubel A, Fraikin J, Van Beers BE, Gigot JF, et al. Severe radiation-induced liver disease following localized radiation therapy for biliopancreatic carcinoma: activation of hepatic stellate cells as an early event. *Hepatology.* 1997;26(1):128-34.
9. Pan CC, Kavanagh BD, Dawson LA, Li XA, Das SK, Miften M, et al. Radiation-associated liver injury. *Int J Radiat Oncol Biol Phys.* 2010;76(3 Suppl):S94-100.
10. Burton MA, Gray BN, Klemp PF, Kelleher DK, Hardy N. Selective internal radiation therapy: distribution of radiation in the liver. *Eur J Cancer Clin Oncol.* 1989;25(10):1487-91.
11. Gulec SA, Mesoloras G, Dezarn WA, McNeillie P, Kennedy AS. Safety and efficacy of Y-90 microsphere treatment in patients with primary and metastatic liver cancer: the tumor selectivity of the treatment as a function of tumor to liver flow ratio. *J Transl Med.* 5. England2007. p. 15.
12. Kennedy AS, Nutting C, Coldwell D, Gaiser J, Drachenberg C. Pathologic response and microdosimetry of (90)Y microspheres in man: review of four explanted whole livers. *Int J Radiat Oncol Biol Phys.* 2004;60(5):1552-63.
13. Nalesnik MA, Federle M, Buck D, Fontes P, Carr BI. Hepatobiliary effects of 90yttrium microsphere therapy for unresectable hepatocellular carcinoma. *Hum Pathol.* 40. United States2009. p. 125-34.
14. Sangro B, Gil-Alzugaray B, Rodriguez J, Sola I, Martinez-Cuesta A, Viudez A, et al. Liver disease induced by radioembolization of liver tumors: description and possible risk factors. *Cancer.* 2008;112(7):1538-46.
15. Bester L, Feitelson S, Milner B, Chua TC, Morris DL. Impact of prior hepatectomy on the safety and efficacy of radioembolization with yttrium-90 microspheres for patients with unresectable liver tumors. *Am J Clin Oncol.* 2014;37(5):454-60.

16. Fernandez-Ros N, Inarrairaegui M, Paramo JA, Berasain C, Avila MA, Chopitea A, et al. Radioembolization of hepatocellular carcinoma activates liver regeneration, induces inflammation and endothelial stress and activates coagulation. *Liver Int.* 2015;35(5):1590-6.
17. Gil-Alzugaray B, Chopitea A, Inarrairaegui M, Bilbao JJ, Rodriguez-Fraile M, Rodriguez J, et al. Prognostic factors and prevention of radioembolization-induced liver disease. *Hepatology.* 2013;57(3):1078-87.
18. Golfieri R, Bilbao JJ, Carpanese L, Cianni R, Gasparini D, Ezziddin S, et al. Comparison of the survival and tolerability of radioembolization in elderly vs. younger patients with unresectable hepatocellular carcinoma. *J Hepatol.* 2013;59(4):753-61.
19. Hilgard P, Hamami M, Fouly AE, Scherag A, Muller S, Ertle J, et al. Radioembolization with yttrium-90 glass microspheres in hepatocellular carcinoma: European experience on safety and long-term survival. *Hepatology.* 2010;52(5):1741-9.
20. Jakobs TF, Hoffmann RT, Fischer T, Stemmler HJ, Tatsch K, La Fougere C, et al. Radioembolization in patients with hepatic metastases from breast cancer. *J Vasc Interv Radiol.* 2008;19(5):683-90.
21. Kennedy AS, Dezarn WA, McNeillie P, Coldwell D, Nutting C, Carter D, et al. Radioembolization for unresectable neuroendocrine hepatic metastases using resin 90Y-microspheres: early results in 148 patients. *Am J Clin Oncol.* 31. United States 2008. p. 271-9.
22. Kennedy AS, McNeillie P, Dezarn WA, Nutting C, Sangro B, Wertman D, et al. Treatment parameters and outcome in 680 treatments of internal radiation with resin 90Y-microspheres for unresectable hepatic tumors. *Int J Radiat Oncol Biol Phys.* 2009;74(5):1494-500.
23. Klingenstein A, Haug AR, Zech CJ, Schaller UC. Radioembolization as locoregional therapy of hepatic metastases in uveal melanoma patients. *Cardiovasc Intervent Radiol.* 2013;36(1):158-65.
24. Kwok PC, Leung KC, Cheung MT, Lam TW, Szeto LT, Chou SQ, et al. Survival benefit of radioembolization for inoperable hepatocellular carcinoma using yttrium-90 microspheres. *J Gastroenterol Hepatol.* 2014;29(11):1897-904.
25. Lam MG, Louie JD, Iagaru AH, Goris ML, Sze DY. Safety of repeated yttrium-90 radioembolization. *Cardiovasc Intervent Radiol.* 2013;36(5):1320-8.
26. Lewandowski RJ, Memon K, Mulcahy MF, Hickey R, Marshall K, Williams M, et al. Twelve-year experience of radioembolization for colorectal hepatic metastases in 214 patients: survival by era and chemotherapy. *Eur J Nucl Med Mol Imaging.* 2014;41(10):1861-9.
27. Paprottka PM, Hoffmann RT, Haug A, Sommer WH, Raessler F, Trumm CG, et al. Radioembolization of symptomatic, unresectable neuroendocrine hepatic metastases using yttrium-90 microspheres. *Cardiovasc Intervent Radiol.* 2012;35(2):334-42.
28. Piana PM, Gonsalves CF, Sato T, Anne PR, McCann JW, Bar Ad V, et al. Toxicities after radioembolization with yttrium-90 SIR-spheres: incidence and contributing risk factors at a single center. *J Vasc Interv Radiol.* 2011;22(10):1373-9.
29. Ruhl R, Seidensticker M, Peters N, Mohnike K, Bornschein J, Schutte K, et al. Hepatocellular carcinoma and liver cirrhosis: assessment of the liver function after Yttrium-90 radioembolization with resin microspheres or after CT-guided high-dose-rate brachytherapy. *Dig Dis.* 2009;27(2):189-99.

30. Seidensticker R, Seidensticker M, Damm R, Mohnike K, Schutte K, Malfertheiner P, et al. Hepatic toxicity after radioembolization of the liver using (90)Y-microspheres: sequential lobar versus whole liver approach. *Cardiovasc Intervent Radiol.* 2012;35(5):1109-18.
31. Smits ML, van den Hoven AF, Rosenbaum CE, Zonnenberg BA, Lam MG, Nijsen JF, et al. Clinical and laboratory toxicity after intra-arterial radioembolization with (90)Y-microspheres for unresectable liver metastases. *PLoS One.* 8. United States2013. p. e69448.
32. Strigari L, Sciuto R, Rea S, Carpanese L, Pizzi G, Soriani A, et al. Efficacy and toxicity related to treatment of hepatocellular carcinoma with 90Y-SIR spheres: radiobiologic considerations. *J Nucl Med.* 51. United States2010. p. 1377-85.
33. van Hazel GA, Pavlakis N, Goldstein D, Olver IN, Tapner MJ, Price D, et al. Treatment of fluorouracil-refractory patients with liver metastases from colorectal cancer by using yttrium-90 resin microspheres plus concomitant systemic irinotecan chemotherapy. *J Clin Oncol.* 2009;27(25):4089-95.
34. Saxena A, Meteling B, Kapoor J, Golani S, Morris DL, Bester L. Is yttrium-90 radioembolization a viable treatment option for unresectable, chemorefractory colorectal cancer liver metastases? A large single-center experience of 302 patients. *Ann Surg Oncol.* 2015;22(3):794-802.
35. Sofocleous CT, Garcia AR, Pandit-Taskar N, Do KG, Brody LA, Petre EN, et al. Phase I trial of selective internal radiation therapy for chemorefractory colorectal cancer liver metastases progressing after hepatic arterial pump and systemic chemotherapy. *Clin Colorectal Cancer.* 2014;13(1):27-36.
36. Zarva A, Mohnike K, Damm R, Ruf J, Seidensticker R, Ulrich G, et al. Safety of repeated radioembolizations in patients with advanced primary and secondary liver tumors and progressive disease after first selective internal radiotherapy. *J Nucl Med.* 2014;55(3):360-6.
37. Kuo JC, Tazbirkova A, Allen R, Kosmider S, Gibbs P, Yip D. Serious hepatic complications of selective internal radiation therapy with yttrium-90 microsphere radioembolization for unresectable liver tumors. *Asia Pac J Clin Oncol.* 2014;10(3):266-72.
38. Bester L, Meteling B, Pocock N, Pavlakis N, Chua TC, Saxena A, et al. Radioembolization versus standard care of hepatic metastases: comparative retrospective cohort study of survival outcomes and adverse events in salvage patients. *J Vasc Interv Radiol.* 2012;23(1):96-105.
39. Goin JE, Salem R, Carr BI, Dancy JE, Soulen MC, Geschwind JF, et al. Treatment of unresectable hepatocellular carcinoma with intrahepatic yttrium 90 microspheres: factors associated with liver toxicities. *J Vasc Interv Radiol.* 16. United States2005. p. 205-13.
40. Salem R, Lewandowski RJ, Mulcahy MF, Riaz A, Ryu RK, Ibrahim S, et al. Radioembolization for hepatocellular carcinoma using Yttrium-90 microspheres: a comprehensive report of long-term outcomes. *Gastroenterology.* 2010;138(1):52-64.
41. Sangro B, Carpanese L, Cianni R, Golfieri R, Gasparini D, Ezziddin S, et al. Survival after yttrium-90 resin microsphere radioembolization of hepatocellular carcinoma across Barcelona clinic liver cancer stages: a European evaluation. *Hepatology.* 2011;54(3):868-78.
42. Ibrahim SM, Mulcahy MF, Lewandowski RJ, Sato KT, Ryu RK, Masterson EJ, et al. Treatment of unresectable cholangiocarcinoma using yttrium-90 microspheres: results from a pilot study. *Cancer.* 2008;113(8):2119-28.

43. Saxena A, Meteling B, Kapoor J, Golani S, Danta M, Morris DL, et al. Yttrium-90 radioembolization is a safe and effective treatment for unresectable hepatocellular carcinoma: a single centre experience of 45 consecutive patients. *Int J Surg*. 2014;12(12):1403-8.
44. Lam MG, Abdelmaksoud MH, Chang DT, Eclov NC, Chung MP, Koong AC, et al. Safety of 90Y radioembolization in patients who have undergone previous external beam radiation therapy. *Int J Radiat Oncol Biol Phys*. 2013;87(2):323-9.
45. Dignan FL, Wynn RF, Hadzic N, Karani J, Quaglia A, Pagliuca A, et al. BCSH/BSBMT guideline: diagnosis and management of veno-occlusive disease (sinusoidal obstruction syndrome) following haematopoietic stem cell transplantation. *Br J Haematol*. 2013;163(4):444-57.
46. Fan CQ, Crawford JM. Sinusoidal obstruction syndrome (hepatic veno-occlusive disease). *J Clin Exp Hepatol*. 2014;4(4):332-46.
47. Azoulay D, Castaing D, Lemoine A, Hargreaves GM, Bismuth H. Transjugular intrahepatic portosystemic shunt (TIPS) for severe veno-occlusive disease of the liver following bone marrow transplantation. *Bone Marrow Transplant*. 2000;25(9):987-92.
48. Seidensticker M, Seidensticker R, Damm R, Mohnike K, Pech M, Sangro B, et al. Prospective randomized trial of enoxaparin, pentoxifylline and ursodeoxycholic acid for prevention of radiation-induced liver toxicity. *PLoS One*. 2014;9(11):e112731.
49. Cheuk DK, Chiang AK, Ha SY, Chan GC. Interventions for prophylaxis of hepatic veno-occlusive disease in people undergoing haematopoietic stem cell transplantation. *Cochrane Database Syst Rev*. 2015;5:CD009311.
50. Imai K, Emi Y, Iyama KI, Beppu T, Ogata Y, Kakeji Y, et al. Splenic volume may be a useful indicator of the protective effect of bevacizumab against oxaliplatin-induced hepatic sinusoidal obstruction syndrome. *Eur J Surg Oncol*. 2014;40(5):559-66.
51. Nakamura K, Hatano E, Narita M, Miyagawa-Hayashino A, Koyama Y, Nagata H, et al. Sorafenib attenuates monocrotaline-induced sinusoidal obstruction syndrome in rats through suppression of JNK and MMP-9. *J Hepatol*. 2012;57(5):1037-43.
52. Walrand S, Hesse M, Jamar F, Lhommel R. A hepatic dose-toxicity model opening the way toward individualized radioembolization planning. *J Nucl Med*. 2014;55(8):1317-22.
53. Lam MG, Louie JD, Abdelmaksoud MH, Fisher GA, Cho-Phan CD, Sze DY. Limitations of body surface area-based activity calculation for radioembolization of hepatic metastases in colorectal cancer. *J Vasc Interv Radiol*. 2014;25(7):1085-93.
54. Chiesa C, Mira M, Maccauro M, Spreafico C, Romito R, Morosi C, et al. Radioembolization of hepatocarcinoma with (90)Y glass microspheres: development of an individualized treatment planning strategy based on dosimetry and radiobiology. *Eur J Nucl Med Mol Imaging*. 2015;42(11):1718-38.
55. Bennink RJ, Tulchinsky M, de Graaf W, Kadry Z, van Gulik TM. Liver function testing with nuclear medicine techniques is coming of age. *Semin Nucl Med*. 2012;42(2):124-37.
56. de Graaf W, van Lienden KP, van Gulik TM, Bennink RJ. (99m)Tc-mebrofenin hepatobiliary scintigraphy with SPECT for the assessment of hepatic function and liver functional volume before partial hepatectomy. *J Nucl Med*. 2010;51(2):229-36.

57. Bennink RJ, Cieslak KP, van Delden OM, van Lienden KP, Klumpen HJ, Jansen PL, et al. Monitoring of Total and Regional Liver Function after SIRT. *Front Oncol.* 2014;4:152.
58. Jakobs TF, Saleem S, Atassi B, Reda E, Lewandowski RJ, Yaghami V, et al. Fibrosis, portal hypertension, and hepatic volume changes induced by intra-arterial radiotherapy with 90Yttrium microspheres. *Dig Dis Sci.* 2008;53(9):2556-63.
59. Maleux G, Deroose C, Laenen A, Verslype C, Heye S, Haustermans K, et al. Yttrium-90 radioembolization for the treatment of chemorefractory colorectal liver metastases: Technical results, clinical outcome and factors potentially influencing survival. *Acta Oncol.* 2015:1-10.
60. Shim SJ, Seong J, Lee IJ, Han KH, Chon CY, Ahn SH. Radiation-induced hepatic toxicity after radiotherapy combined with chemotherapy for hepatocellular carcinoma. *Hepatol Res.* 2007;37(11):906-13.
61. Tao C, Yang LX. Improved radiotherapy for primary and secondary liver cancer: stereotactic body radiation therapy. *Anticancer Res.* 2012;32(2):649-55.
62. Vogl TJ, Farshid P, Naguib NN, Darvishi A, Bazrafshan B, Mbalisike E, et al. Thermal ablation of liver metastases from colorectal cancer: radiofrequency, microwave and laser ablation therapies. *Radiol Med.* 2014;119(7):451-61.
63. Wahl DR, Stenmark MH, Tao Y, Pollom EL, Caoili EM, Lawrence TS, et al. Outcomes After Stereotactic Body Radiotherapy or Radiofrequency Ablation for Hepatocellular Carcinoma. *J Clin Oncol.* 2016;34(5):452-9.
64. van Hazel GA, Heinemann V, Sharma NK, Findlay MP, Ricke J, Peeters M, et al. SIRFLOX: Randomized Phase III Trial Comparing First-Line mFOLFOX6 (Plus or Minus Bevacizumab) Versus mFOLFOX6 (Plus or Minus Bevacizumab) Plus Selective Internal Radiation Therapy in Patients With Metastatic Colorectal Cancer. *J Clin Oncol.* 2016.
65. Rahbari NN, Garden OJ, Padbury R, Brooke-Smith M, Crawford M, Adam R, et al. Posthepatectomy liver failure: a definition and grading by the International Study Group of Liver Surgery (ISGLS). *Surgery.* 2011;149(5):713-24.

## Supplementary material

**Supplement 1:** NCI-CTCAE grading system of REILD related toxicities

Lab	Grade	CTCAE version 3.0	CTCAE version 4.02	CTCAE version 4.03
<b>Bilirubin</b>	1	ULN-1.5 ULN	ULN-1.5 ULN	ULN-1.5 ULN
	2	>1.5-3.0 ULN	>1.5-3.0 ULN	>1.5-3.0 ULN
	3	>3.0-10.0 ULN	>3.0-10.0 ULN	>3.0-10.0 ULN
	4	>10.0 ULN	>10.0 ULN	>10.0 ULN
<b>ALP and GGT</b>	1	ULN – 2.5 ULN	ULN – 2.5 ULN	ULN – 2.5 ULN
	2	>2.5 – 5.0 ULN	>2.5 – 5.0 ULN	>2.5 – 5.0 ULN
	3	>5.0-20.0 ULN	>5.0-20.0 ULN	>5.0-20.0 ULN
	4	>20.0 ULN	>20.0 ULN	>20.0 ULN
<b>ALT and AST</b>	1	ULN – 2.5 ULN	ULN – 3.0 ULN	ULN – 3.0 ULN
	2	>2.5 – 5.0 ULN	>3.0 – 5.0 ULN	>3.0 – 5.0 ULN
	3	>5.0-20.0 ULN	>5.0-20.0 ULN or >5.0 ULN >2 weeks	>5.0-20.0 ULN
	4	>20.0 ULN	>20.0 ULN	>20.0 ULN
<b>Ascites</b>	1	Asymptomatic	Asymptomatic	Asymptomatic
	2	Medical intervention indicated	Medical intervention indicated	Medical intervention indicated
	3	Invasive procedure indicated	Invasive procedure indicated	Invasive procedure indicated
	4	Life-threatening	Life-threatening	Life-threatening
	5	Death	Death	Death

ALP= alkaline phosphatase, GGT= gamma glutamyl transpeptidase, ALT= alanine aminotransferase, AST= aspartate aminotransferase, ULN= upper limit of normal value







CHAPTER  
THREE

Toxicity comparison of yttrium-90  
resin and glass microspheres  
radioembolization

Manon N.G.J.A. Braat, Arthur J.A.T. Braat, Marnix G.E.H. Lam

*Quarterly Journal of Nuclear Medicine and Molecular Imaging 2022 Jun 28.*

## Abstract

### Background

To investigate the clinical, hematological and biochemical toxicity differences between glass and resin yttrium-90 (<sup>90</sup>Y)-microspheres radioembolization treatment of primary and metastatic liver disease.

### Methods

Between May 2014 and November 2016 all consecutive glass and resin <sup>90</sup>Y microspheres radioembolization treatments were retrospectively analyzed. Biochemical, hematological and clinical data were collected at treatment day, two weeks, one month and three-month follow-up. Post-treatment <sup>90</sup>Y PET/CTs were assessed for the absorbed doses in non-tumorous liver volume ( $D_{\text{NTLV}}$ ) and tumor volume ( $D_{\text{TV}}$ ). Biochemical, hematological and clinical toxicity were compared between glass and resin using chi-square tests and repeated ANOVA measures. Biochemical and clinical toxicity was correlated with  $D_{\text{NTLV,total}}$  by means of Pearson correlation and independent T-tests.

### Results

A total of 85 patients were included (n=44 glass, n=41 resin). Clinical toxicity the day after treatment (i.e. abdominal pain (p=0.000), nausea (p=0.000) and vomiting (p=0.003)) was more prevalent for resin. Biochemical and hematological toxicities were similar for both microspheres. The  $D_{\text{NTLV,total}}$  was significantly higher in patients with REILD grade  $\geq 3$  in the resin group (43.5 versus 33.3 Gy (p=0.050)). A similar non-significant trend was seen in the glass group: 95.0 versus 69.0 Gy (p=0.144).

### Conclusion

The clinical, hematological and biochemical toxicity of radioembolization treatment with glass and resin is comparable, however, post-embolization syndrome related complaints are more common for resin.

## Background

Currently, two types of yttrium-90 (<sup>90</sup>Y) microspheres for radioembolization are commercially available: glass microspheres (Therasphere<sup>®</sup>, Boston Scientific) and resin microspheres (SIR-Spheres<sup>®</sup>, SIRTEX). However, their acknowledged treatment indications vary. Glass microspheres have been granted a humanitarian device exemption by the United States Food & Drug administration (FDA) for the treatment of unresectable hepatocellular carcinoma (HCC), whereas resin microspheres have been granted a premarket approval by the FDA for the treatment of colorectal liver metastases (1).

Even though they use the same isotope (<sup>90</sup>Y), the physical characteristics of glass and resin microspheres differ considerably (1, 2). Glass and resin microspheres have comparable sizes (mean diameter of 25 micron versus 32 micron, respectively), but glass microspheres have a higher specific activity and gravity ( $\pm 2500$  Bq/microsphere versus  $\pm 50$  Bq/microsphere and 3.6 g/dL versus 1.6 g/dL, respectively). These differences resonate in the embolic effect of the treatment (due to the higher number of injected resin microspheres), but also flow dynamics and dose-effect relationships (1, 3, 4).

Innumerable studies have been conducted evaluating the efficacy and toxicity profile of the different microspheres separately, however, data on head-to-head comparison of the microspheres is scarce and mainly reserved for <sup>90</sup>Y-microspheres radioembolization in HCC (5-8).

In other populations than HCC patients (i.e. cholangiocarcinoma, liver metastases), little is known about the differences in clinical, hematological and biochemical toxicity between these microspheres. The aim of this study therefore was to investigate the clinical, hematological and biochemical toxicity differences between glass and resin <sup>90</sup>Y microspheres in both primary and metastatic liver disease.

## Methods

### Patients

Between May 2014 and November 2016, consecutively treated patients were included in this retrospective single center analysis. In 2015, the institution switched from resin microspheres to glass microspheres. Treatments before, after and during the transition period were included. Baseline characteristics were obtained, including age, sex, previous treatments, type of primary tumor, tumor burden and liver volumes. Treatment related characteristics included type of treatment, type of microsphere and injected activity.

Radioembolization treatment was performed according to international standards, after a standard preparatory simulation angiography with technetium-99m ( $^{99m}\text{Tc}$ )-macroaggregated albumin (MAA) (9, 10). The therapeutic activity of resin microspheres was calculated according to the body surface area (BSA) method, whereas the therapeutic activity of glass microspheres was calculated according to the MIRD (i.e. mono-compartment) model.

In May 2015, radioembolization-induced liver disease (REILD) prophylaxis was introduced, modelled on a previous publication by Gil-Alzugaray et al. (11). It consisted of ursodeoxycholic acid 600 mg daily for two months and prednisone 10 mg daily for one month, followed by 5 mg daily for the second month; all starting the day of treatment.

After treatment, patients remained in the hospital for one night (day one). Follow-up included a phone call with standardized questions by the treating physician at two weeks, and an outpatient clinic visit at one and three months. Adverse events were systematically registered in the patient files and scored according to the Common Terminology Criteria of Adverse Events (CTCAE 4.03). Other follow-up variables included prescribed treatment for REILD, presence of ascites at three months and date of progression. In case of evidenced progressive disease within three months follow-up, the clinical, hematological and biochemical changes after progression were excluded. In case of sequential whole liver treatments, only the first treatment was analyzed. All data acquired after the second treatment were regarded as missing.

The medical ethics committee of our institution waived the need for informed consent for this retrospective review.

### **Toxicity analysis**

Laboratory examinations were collected at multiple time points: baseline and at one, three and six months follow-up. These included total bilirubin, alkaline phosphatase (ALP), gamma-glutamyl transferase (GGT), aspartate aminotransferase (AST), alanine aminotransferase (ALT) hemoglobin, white blood cell count, thrombocytes and international normalized ratio (INR). The presence of hepatotoxicity was graded according to the proposed scoring system by Braat et al., in which REILD necessitating medical treatment is considered grade 3, REILD necessitating invasive treatment grade 4 and fatal REILD grade 5 (Chapter 2, page 48) (12).

### **$^{90}\text{Y}$ PET/CT imaging protocol and dosimetric analysis**

All  $^{90}\text{Y}$  PET/CTs were performed on the same PET/CT-scanner (Biograph mCT, Siemens Healthcare) within 24 hours after treatment administration. Imaging parameters included a total acquisition time of 30 minutes for two bed positions, TrueX and time-of-flight reconstruction, reconstruction using 4 iterations with 21 subsets and a 5 mm full-width at half maximum Gaussian post-reconstruction filter. A low dose CT was acquired for attenuation correction and anatomical reference.

The  $^{90}\text{Y}$  PET/CT scans were analyzed using Simplicit $^{90}\text{y}$  software (Mirada Medical Ltd, Oxford, UK). The  $^{90}\text{Y}$  PET/CT was registered to the last available diagnostic contrast-enhanced CT for liver and tumor delineation. Only rigid transformations were allowed in the image registration process. The non-tumorous liver was considered as one volume (NTLV), as well as the treated NTLV, non-treated NTLV and the tumor volume (TV). The absorbed doses in all these volumes were calculated (respectively  $D_{\text{NTLV,total}}$ ,  $D_{\text{NTLV,treated}}$ ,  $D_{\text{NTLV,non-treated}}$  and  $D_{\text{TV}}$ ). Biochemical, hematological and clinical toxicities were correlated with  $D_{\text{NTLV}}$ .

### **Statistics**

Descriptive statistics, chi-square tests and independent sample T-tests were used to explore baseline characteristics and baseline biochemical differences. Data with a normal and non-normal distribution are presented as mean  $\pm$  standard deviation and median (range), respectively.

Repeated measures ANOVA tests were used to compare the laboratory values over time (three months) between both microspheres, whereas chi-square tests were used for the presence of clinical toxicities (yes/no). Correlation between  $D_{\text{NTLV,total}}$  and biochemical toxicities was performed using a Pearson's correlation (Pearson's correlation coefficient = PCC). Clinical toxicities and  $D_{\text{NTLV,total}}$  were compared by means of independent T-tests.

All analyses were performed with IBM SPSS Statistics version 25.0.0.2. A p-value <0.05 was considered statistically significant.

## Results

Eighty-five consecutively treated patients were analyzed. Forty-four patients were treated with resin and 41 patients with glass, of whom 27/41 with <1 week shelf-life and 14/41 >1 week shelf-life.

Baseline characteristics of all patients are reported in **Table 1**. There were no differences in baseline characteristics besides the higher prevalence of colorectal cancer in the resin group ( $p=0.055$ ) and the more frequent use of REILD prophylaxis in the glass group ( $p=0.004$ ).

**Table 1.** Baseline patient characteristics

Characteristic	All (n=85)	Glass (n=41)	Resin (n=44)	p-value
<b>Age</b>	62 ± 26	63 ± 11	62 ± 21	0.648
<b>Sex</b>				
Male	51	26	25	0.535
Female	34	15	19	
<b>BMI</b>	25.5 ± 4.6	26.2 ± 5.1	25.0 ± 4.1	0.235
<b>WHO performance score</b>				
0	55	28	27	0.396*
1	21	11	10	
2	5	1	4	
3	0	0	0	
4	1	1	0	
<b>Tumor type</b>				
Colorectal cancer	36	13	23	0.055**
HCC	8	6	2	
NET	17	10	7	
Breast cancer	4	3	1	
Uveal melanoma	5	2	3	
Cholangiocarcinoma	9	3	6	
Other	6	4	2	
<b>Previous liver-directed treatment</b>				
Left hemihepatectomy	3	2	1	0.859**
Right hemihepatectomy	2	1	1	
Metastasectomy	13	7	6	
RFA	11	4	7	
TACE	2	2	0	
SBRT	2	1	1	
None	60	28	32	



**Table 1.** Continued

Characteristic	All (n=85)	Glass (n=41)	Resin (n=44)	p-value
<b>Previous systemic treatment</b>				
Cytotoxic chemotherapy	52	22	30	
Immunotherapy	3	0	3	
Hormonal therapy	3	2	1	
mTOR inhibitor	8	5	3	0.058**
PRRT	11	5	6	
Tyrosinase inhibitor	2	1	1	
None	16	12	4	
<b>REILD prophylaxis</b>				
None	60	21	39	
UDCA + prednisone	22	17	5	0.004
UDCA only	1	1	0	
Prednisone only	2	2	0	
<b>Liver tumor burden</b>				
0-25%	59	27	32	
25-50%	12	5	7	0.679
50-75%	7	2	5	
<b>Liver volume (ml)</b>	1993 ± 923	2019 ± 873	1969 ± 977	0.813

The baseline patient characteristics are summarized in this table. Values are given in mean ± standard deviation or number of patients (percentage of total).

\* Chi square test: ECOG score 0-1 vs 2-4

\*\* Chi square test: tumor type: colorectal cancer vs others; previous liver directed treatment: none vs hemihepatectomy vs others; previous systemic treatment: none vs cytotoxic chemotherapy vs others  
 Abbreviations: HCC = hepatocellular carcinoma, NET = neuroendocrine tumor, PRRT = peptide receptor radionuclide therapy, RFA=radiofrequency ablation, SBRT=stereotactic body radiotherapy, TACE = transarterial chemoembolization, UCDA = ursodeoxycholic acid

Treatment approach did not vary between glass and resin (**Table 2**). The percentage of treated liver was higher in the resin group (85% versus 71%; p=0.028). The mean  $D_{NTLV,treated}$  was 112 Gy for glass (108 Gy week 1 and 119 Gy week 2; p=0.590) and 42 Gy for resin (p<0.001).  $D_{TV}$  was also significantly higher in the glass group (205.0 Gy versus 64.9 Gy, p<0.001).

**Table 2.** Treatment characteristics

Characteristic	Glass (n=41)	Resin (n=44)	p-value
<b>Treatment</b>			
Whole liver	19	26	0.281*
Sequential	3	5	
Left lobar	1	3	
Right lobar	12	10	
(Super)selective	6	0	
<b>Injected dose (MBq)</b>	3643 ± 2533	1573 ± 434	<b>0.000</b>
<b>Shelf-life</b>			
Week 1	27		
Week 2	14	NA	
Lung shunt fraction with <sup>99m</sup> Tc-MAA	4.6 ± 4.4	5.4 ± 6.6	0.521
Liver volume (ml)	2019 ± 873	1969 ± 977	0.813
<b>Perfused liver volume</b>			
(in ml)	1433 ± 970	1620 ± 653	0.329
(in %)	71%	85%	<b>0.028</b>
<b>Total non-tumorous liver volume (ml)</b>	1701 ± 669	1590 ± 620	0.461
<b>Total non-tumorous liver volume absorbed dose (Gy)</b>	72.6	36.1	<b>0.000</b>
<b>Treated non-tumorous liver volume (ml)</b>	1092 ± 732	1240 ± 402	0.280
<b>Treated non-tumorous liver volume absorbed dose (Gy)</b>	111.9 ± 56.0	42.0 ± 16.0	<b>0.000</b>
<b>Treated tumor volume (ml)</b>	341 ± 456	379 ± 536	0.738
<b>Treated tumor volume absorbed dose (Gy)</b>	205.0 ± 155.6	64.9 ± 28.4	<b>0.000</b>

Values are given in mean ± standard deviation or number of patients.

\* Fisher exact test; whole vs partial treatment. NA = not applicable, <sup>99m</sup>Tc-MAA = technetium-99m-macro-aggregated albumin

Baseline biochemical and hematological values were not significantly different between the two treatment groups. At one month and three months, 78/85 and 57/85 patients could be assessed for adverse events, respectively. Bilirubin significantly increased over time, with a mean value of 10.8  $\mu\text{mol/L}$  (0.63 mg/dL) at baseline, 13.2  $\mu\text{mol/L}$  (0.77 mg/dL) at one month and 18.6  $\mu\text{mol/L}$  (1.09 mg/dL) at three months (**Table 3**). Albumin mildly decreased over time in the overall population; from 40.0 g/L to 38.0 g/L ( $p < 0.001$ ). Thrombocytes changed significantly over time, with a maximum decrease at one month (from 229/nL to 176/nL). No differences in biochemical and hematological toxicities between resin, glass with <1 week shelf-life and glass with >1 week shelf-life were observed. In the glass group, the changes over three months in bilirubin and albumin were correlated with  $D_{\text{NTLV,total}}$  (PCC=0.485;  $p=0.006$  and PCC=-0.482;  $p=0.006$ , respectively), contrary to the resin group. AST change over three months was correlated with the  $D_{\text{NTLV,total}}$  for the resin group (PCC=0.526;  $p=0.007$ ), but not for the glass group (**Table 4**). No other correlations were observed.

Abdominal pain and nausea were the most experienced clinical toxicities on day one, whereas fatigue was the most experienced adverse event at two weeks and one month. Abdominal pain, nausea and vomiting were all more prevalent after resin treatments ( $p < 0.001$ ,  $p < 0.001$  and  $p = 0.003$  respectively)(**Table 5**). Consequently, more analgesics were prescribed in this group ( $p < 0.001$ ). Sixteen patients treated with resin received additional opioids during treatment or after treatment on day one, contrary to one patient treated with glass. At two weeks, one month and three months, no differences in clinical toxicity or analgesic use were observed (except from nausea at one month;  $p = 0.041$ ). When clinical toxicities at day one were correlated with  $D_{\text{NTLV,total}}$  a significant higher  $D_{\text{NTLV,total}}$  was seen in the resin group for patients with abdominal pain (40.1 Gy versus 30.4 Gy;  $p = 0.041$ ).

The presence of ascites at three months and hepatotoxicity score were similar for the glass and resin group (**Table 5**). Fatal REILD occurred in one patient in each group and REILD necessitating paracentesis in three patients in each group. The  $D_{\text{NTLV,total}}$  was significantly higher in patients with REILD grade  $\geq 3$  in the resin group (43.5 versus 33.3 Gy ( $p = 0.050$ )). A similar non-significant trend was seen in the glass group: 95.0 versus 69.0 Gy ( $p = 0.144$ ) (**Table 6**).

**Table 3.** Laboratory toxicities

	Glass	Resin	Total	p-value*	CTCAE grades	Glass	Resin
	Mean (±SD)	Mean (±SD)	Mean (±SD)			CTCAE (n=41)(%)	CTCAE (n=44)(%)
<b>Bilirubin (μmol/L)</b>							
Baseline	10.6	10.8	10.7	<b>0.000</b>	<b>1</b> 2 3	3 0 0	2 1 0
1 month	13.2	12.8	13.1		<b>1</b> 2 3	3 0 1	0 2 0
3 months	18.7	18.5	18.6		<b>1</b> 2 3	3 2 1	2 5 0
<b>Albumin (g/L)</b>							
Baseline	40.5	40.2	40.4	<b>0.000</b>	<b>1</b> 2 3	2 0 0	6 0 0
1 month	39.1	38.1	39.0		<b>1</b> 2 3	2 1 0	6 0 0
3 months	38.6	36.8	38.0		<b>1</b> 2 3	1 0 0	5 2 0
<b>AST (U/L)</b>							
Baseline	64	42	56	0.246	<b>1</b> 2 3	19 2 2	26 0 0
1 month	48	50	49		<b>1</b> 2 3	20 3 1	27 2 0
3 months	68	61	65		<b>1</b> 2 3	24 1 3	19 3 1
<b>ALT (U/L)</b>							
Baseline	64	39	55	0.885	<b>1</b> 2 3	8 3 1	12 0 0
1 month	66	40	56		<b>1</b> 2 3	10 3 1	14 0 0
3 months	57	51	55		<b>1</b> 2 3	8 2 1	11 1 0

Table 3. Continued.

	Glass	Resin	Total	p-value*	CTCAE grades	Glass	Resin	
	Mean (±SD)	Mean (±SD)	Mean (±SD)			CTCAE (n=41)(%)	CTCAE (n=44)(%)	
<b>ALP (IU/L)</b>								
Baseline	232	224	228	<b>0.000</b>	<b>1</b>	17	21	
					<b>2</b>	3	4	
					<b>3</b>	5	3	
1 month	230	253	241		<b>1</b>	21	23	
					<b>2</b>	4	9	
					<b>3</b>	3	2	
3 months	336	352	343		<b>1</b>	14	13	
					<b>2</b>	9	7	
					<b>3</b>	3	4	
<b>GGT (U/L)</b>								
Baseline	278	222	256	<b>0.011</b>	<b>1</b>	16	16	
					<b>2</b>	7	11	
					<b>3</b>	10	13	
					<b>4</b>	3	0	
1 month	301	306	303		<b>1</b>	14	12	
					<b>2</b>	10	11	
					<b>3</b>	9	15	
					<b>4</b>	1	0	
3 months	370	465	407		<b>1</b>	5	3	
					<b>2</b>	13	8	
					<b>3</b>	11	12	
					<b>4</b>	4	1	
<b>Thrombocytes (/nL)</b>								
Baseline	221	247	231		<b>0.000</b>	<b>1</b>	5	9
						<b>2</b>	0	0
				<b>3</b>		1	0	
1 month	182	169	177	<b>1</b>		9	13	
				<b>2</b>		0	1	
				<b>3</b>		2	0	
3 months	191	201	195	<b>1</b>		7	7	
				<b>2</b>		0	3	
				<b>3</b>		2	0	

Glass: baseline: n=41, 1 month n=35, 3 months n=33. Resin: baseline: n=44, 1 month n=43, 3 months n=27.

\*p-values for laboratory toxicity differences over time; no significant differences were present in between the different microspheres. ALP = alkaline phosphatase, ALT = alanine aminotransferase, AST = aspartate aminotransferase, GGT = gamma-glutamyl transferase

**Table 4.** Correlation between the change in biochemical toxicities over three months and total non-tumorous liver absorbed dose

Toxicities	Pearson's correlation	p-value	Pearson's correlation	p-value
	Glass (n=33)		Resin (n=27)	
Bilirubin	0.485	0.006	-0.077	0.727
Albumin	-0.482	0.006	-0.006	0.981
AST	0.199	0.266	0.526	<b>0.007</b>
ALT	0.151	0.402	0.282	0.171
ALP	0.202	0.277	-0.174	0.405
GGT	0.109	0.552	0.055	0.793
Thrombocytes*	0.235	0.168	0.215	0.215

\* change over one month instead of three months. ALP = alkaline phosphatase, ALT = alanine aminotransferase, AST = aspartate aminotransferase, GGT = gamma-glutamyl transferase

**Table 5.** Clinical toxicity

	CTCAE grade	Glass (n=41)	Resin (n=44)	p-value*
<b>Abdominal pain</b>				
Day 1	<b>1</b>	6	22	<b>0.000</b>
	<b>2</b>	0	2	
	<b>3</b>	0	0	
2 weeks	<b>1</b>	9	18	0.132
	<b>2</b>	0	1	
	<b>3</b>	1	0	
1 month	<b>1</b>	12	11	0.509
	<b>2</b>	2	3	
3 months	<b>1</b>	7	7	0.437
	<b>2</b>	1	2	
<b>Nausea</b>				
Day 1	<b>1</b>	3	17	<b>0.000</b>
	<b>2</b>	0	2	
	<b>3</b>	0	0	
2 weeks	<b>1</b>	9	11	0.623
	<b>2</b>	2	0	
	<b>3</b>	0	0	
1 month	<b>1</b>	4	3	0.670
	<b>2</b>	3	3	
	<b>3</b>	0	1	
3 months	<b>1</b>	3	4	<b>0.041</b>
	<b>2</b>	0	3	
	<b>3</b>	0	1	
<b>Vomiting</b>				
Day 1	<b>1</b>	0	7	<b>0.003</b>
	<b>2</b>	0	1	
	<b>3</b>	0	1	
2 weeks	<b>1</b>	1	2	0.664
	<b>2</b>	0	0	
1 month	<b>1</b>	1	1	0.816
	<b>2</b>	1	2	
3 months	<b>1</b>	1	2	0.439
	<b>2</b>	0	0	

Table 5. Continued

	CTCAE grade	Glass (n=41)	Resin (n=44)	p-value*
<b>Fatigue</b>				
Day 1	1	2	6	0.198
	2	1	2	
2 weeks	1	22	25	0.554
	2	4	7	
1 month	1	17	17	0.846
	2	2	5	
3 months	1	8	5	0.148
	2	3	8	
	3	0	1	
<b>Ascites**</b>				
3 months	Absent	23	22	0.221
	Minimal	6	9	
	Moderate	6	2	
	Massive	1	4	
Hepatotoxicity score				
<b>Hepatotoxicity ***</b>				
3 months	0	4	8	
	1	19	17	
	2	8	6	
	3	1	3	
	4	3	3	
	5	1	1	

Glass: baseline: n=41, 2 weeks n=36, 1 month n=35, 3 months n=33. Resin: baseline: n=44, 2 weeks n=43, 1 month n=43, 3 months n=27. \* Chi square and Fisher exact tests were used to calculate the differences in clinical toxicities (no toxicity vs all CTCAE grades). \*\* Amount of ascites present on the 3-month follow up CT.

\*\*\* Grading according to Braat et al. (12)



**Table 6.** Comparison of the total non-tumorous liver absorbed dose and clinical toxicities

Toxicities	DNTLV <sub>total</sub> (in Gy)			
	Glass	p-value	Resin	p-value
<b>Abdominal pain at day one</b>				
CTCAE grade 0	71.6	0.693	30.4	<b>0.041</b>
CTCAE grade ≥1	78.0		40.1	
<b>Nausea at day one</b>				
CTCAE grade 0	74.1	0.418	36.7	0.800
CTCAE grade ≥1	56.2		35.5	
<b>Vomiting at day one</b>				
CTCAE grade 0	NA	NA	36.2	0.944
CTCAE grade ≥1			35.8	
<b>Fatigue at day one</b>				
CTCAE grade 0	71.1	0.321	34.8	0.237
CTCAE grade ≥1	97.6		42.2	
<b>Analgesics use at day one</b>				
Yes	72.7	0.960	33.8	0.196
No	70.8		40.3	
<b>Hepatotoxicity at three months*</b>				
Grade 0-2	69.0	0.144	33.3	<b>0.050</b>
Grade 3-5	95.0		43.5	

\* Grading according to Braat et al. (12). NA = not applicable

## Discussion

Though physical properties of glass and resin microspheres differ considerably, resulting in a different tolerable  $D_{\text{NTLV, total}}$  threshold, their overall biochemical, hematological and clinical toxicity were comparable. An exemption was the occurrence of the post-embolization syndrome (i.e. abdominal pain, nausea and vomiting), which was more frequent after

treatment with resin microspheres and led to more analgesics use. At two weeks these differences were resolved.

Glass and resin microspheres vary in size, specific activity and gravity, leading to substantial differences in non-radiation-related (e.g. embolic properties) and radiation-related properties (i.e. tolerable  $D_{\text{NTLV,total}}$ ) (1-4). Preclinical research in pigs showed that individual microspheres were more common than cluster formation after hepatic injection of 8-12 million resin microspheres (13). Another study in pigs showed a higher number of injected glass microspheres initially leads to the formation of more clusters without increase in cluster size (day 4-12 after calibration), but eventually also to an increase in the number of microspheres per cluster (day 12-16 after calibration) (14). Thus, treatments with higher numbers of microspheres result in more homogeneous dose distribution, while more heterogeneity leads to sparing of more sinusoids (i.e. NTLV), resulting in a higher tolerable  $D_{\text{NTLV,total}}$  (15, 16). Consequently, the tolerable  $D_{\text{NTLV,total}}$  is lower in resin treatments and in extended shelf-life glass treatments; whereas the embolic load is higher. This higher embolic load translates to our finding of significantly more post-embolization syndrome related complaints early after resin treatments and the correlation of abdominal pain on day one with the  $D_{\text{NTLV,total}}$ . Given the half-life of  $^{90}\text{Y}$ , this represents a toxicity related to higher embolic load, rather than the actual  $D_{\text{NTLV,total}}$ .

Previous studies reported fatigue and abdominal pain to be the most frequent encountered clinical toxicities, with similar profiles for glass and resin treatments (5, 7, 8, 17, 18). Unfortunately, in these studies, the timeline was often not specified and observations made in the first days after treatment were not reported. Only Ahmadzadehfar et al. reported on abdominal pain during resin treatments, with a significant decrease in pain if glucose 5% was used as delivery medium instead of sterile water (1.8% versus 44% of procedures;  $p < 0.001$ ) (19). In the present study, almost all resin treatments were performed using sterile water (the prescription-change for injection was approved by the FDA in October 2014). In 6/41 glass treatments and 24/44 resin treatments grade 1 or 2 abdominal pain was reported on day one; a finding at least partially attributable to the sterile water usage, supplementary to the higher embolic load of resin microspheres.

Biochemical and hematological toxicities were comparable with similar temporal changes for resin and glass treatments. This is in line with previous reports (7, 8, 17, 18). These similarities in toxicity profile, despite different absorbed doses, are largely explained by the microsphere distribution (due to the different specific activity, gravity and number of particles/ml) (15, 16).

Reports on the correlation of  $D_{\text{NTLV}}$  and toxicity are sparse and limited to severe hepatotoxicity (corresponding to grade 3-5 REILD in our classification (12)) in HCC patients, generally with underlying cirrhosis (3, 4, 20-22). Earlier studies on tolerable  $D_{\text{NTLV, total}}$  reported a TD50 of 52 Gy for resin and a TD50 of 97 Gy for glass in HCC populations (3, 4). However, even in these studies the number of whole liver treatments varied between microsphere types and the severity of the underlying cirrhosis was not consistently reported. Severe cirrhosis results in a lower tolerance of the NTLV and thus a lower tolerable absorbed dose (20). In contrast, partial liver treatment increases the tolerable dose of the NTLV. Allimant et al. reported a higher  $D_{\text{NTLV, treated}}$  in patients with REILD (78.9 Gy) compared to patients without REILD (53.8 Gy) in resin treatments for HCC with mean treated liver volumes of 30-32% (21). Also in the present study, a significantly higher  $D_{\text{NTLV, total}}$  in patients with REILD grade  $\geq 3$  was observed. In the studies with head-to-head comparison of both microspheres, REILD was not reported (5, 6, 18), or not present (7, 8).

A possible confounder of the comparison of the toxicity profile of the resin and glass treatments was the significantly more frequent use of REILD prophylaxis in the glass treatments. This prophylaxis was introduced after the publication by Gil-Alzugaray et al. (11). They reported a reduction in the incidence of REILD and CTCAE grade  $\geq 3$  toxicity after the introduction of their modified protocol (11). However, besides the REILD prophylaxis (UDCA + methylprednisolone), important and significant dose reductions were also applied. The exact contribution of the REILD prophylaxis to decreased toxicity therefore remains unclear. Our data on the effect of this prophylaxis are still being analyzed.

There are several other limitations to this study. Firstly, the retrospective nature and relatively small numbers, especially for glass treatments with extended shelf-life. Furthermore, the used activity calculation methods for both resin and glass microspheres

were also difficult to compare. Where the BSA-method for resin is empirical and prone to undertreat patients (23), mono-compartment modelling with MIRD for glass does not make a distinction between tumor and non-tumor compartments, potentially underdosing hypervascular tumors (i.e. HCC) and overdosing hypovascular tumors (i.e. mCRC) (24, 25). However, present data provides a real-world comparison in clinical practice.

Additional analysis of the  $D_{\text{NTLV,total}}$  on  $^{99\text{m}}\text{Tc}$ -MAA SPECT/CTs would have been interesting, as it enables the simulation of the  $D_{\text{NTLV,total}}$  for the different dosimetric methods. Previous studies have shown that the NTLV absorbed dose is accurately predictable on  $^{99\text{m}}\text{Tc}$ -MAA SPECT/CT for both microspheres/dosimetric methods (contrary to the tumor absorbed dose) (25-28); though still less accurate than a scout dose of the microsphere used in the actual treatment (29). Suffered hepatotoxicity is however related to the actual  $D_{\text{NTLV,total}}$  and only measurable on post-treatment  $^{90}\text{Y}$  PET/CT.

Evidence on dosimetry-based individualized treatment planning using both glass and resin treatments is still increasing, enabling smarter use and improved personalized treatment. Recently, Toskich et al. showed that specific activity was the most important predictor of complete pathological response after radiation segmentectomy in HCC patients treated with glass microspheres with a median dose of 314 Gy (31). This suggests an optimal specific activity or microspheres/ml range in segmental high-dose treatments. Better utilization of these different physical characteristics between and within microspheres (e.g. shelf-life) to fit individual patient needs requires further research.

## Conclusion

The clinical, hematological and biochemical toxicity profile of radioembolization treatment with glass and resin microspheres is comparable, however post-embolization syndrome related complaints the first days after treatment are more common with resin.

## References

1. Westcott MA, Coldwell DM, Liu DM, Zikria JF. The development, commercialization, and clinical context of yttrium-90 radiolabeled resin and glass microspheres. *Adv Radiat Oncol*. 2016;1(4):351-64.
2. Bult W, Vente MA, Zonnenberg BA, Van Het Schip AD, Nijsen JF. Microsphere radioembolization of liver malignancies: current developments. *Q J Nucl Med Mol Imaging*. 2009;53(3):325-35.
3. Strigari L, Sciuto R, Rea S, Carpanese L, Pizzi G, Soriani A, et al. Efficacy and toxicity related to treatment of hepatocellular carcinoma with 90Y-SIR spheres: radiobiologic considerations. *J Nucl Med*. 51. United States 2010. p. 1377-85.
4. Chiesa C, Mira M, Maccauro M, Spreafico C, Romito R, Morosi C, et al. Radioembolization of hepatocarcinoma with (90)Y glass microspheres: development of an individualized treatment planning strategy based on dosimetry and radiobiology. *Eur J Nucl Med Mol Imaging*. 2015;42(11):1718-38.
5. Biederman DM, Titano JJ, Tabori NE, Pierobon ES, Alshebeeb K, Schwartz M, et al. Outcomes of Radioembolization in the Treatment of Hepatocellular Carcinoma with Portal Vein Invasion: Resin versus Glass Microspheres. *J Vasc Interv Radiol*. 2016;27(6):812-21.e2.
6. Van Der Gucht A, Jreige M, Denys A, Blanc-Durand P, Boubaker A, Pomoni A, et al. Resin Versus Glass Microspheres for. *J Nucl Med*. 2017;58(8):1334-40.
7. Srinivas SM, Nasr EC, Kunam VK, Bullen JA, Purysko AS. Administered activity and outcomes of glass versus resin (90)Y microsphere radioembolization in patients with colorectal liver metastases. *J Gastrointest Oncol*. 2016;7(4):530-9.
8. Nezami N, Kokabi N, Camacho JC, Schuster DM, Xing M, Kim HS. Y radioembolization dosimetry using a simple semi-quantitative method in intrahepatic cholangiocarcinoma: Glass versus resin microspheres. *Nucl Med Biol*. 2018;59:22-8.
9. Salem R, Padia SA, Lam M, Bell J, Chiesa C, Fowers K, et al. Clinical and dosimetric considerations for Y90: recommendations from an international multidisciplinary working group. *Eur J Nucl Med Mol Imaging*. 2019;46(8):1695-704.
10. Levillain H, Bagni O, Deroose CM, Dieudonné A, Gnesin S, Gresser OS, et al. International recommendations for personalised selective internal radiation therapy of primary and metastatic liver diseases with yttrium-90 resin microspheres. *Eur J Nucl Med Mol Imaging*. 2021;48(5):1570-84.
11. Gil-Alzugaray B, Chopitea A, Inarrairaegui M, Bilbao JI, Rodriguez-Fraile M, Rodriguez J, et al. Prognostic factors and prevention of radioembolization-induced liver disease. *Hepatology*. 2013;57(3):1078-87.
12. Braat MN, van Erpecum KJ, Zonnenberg BA, van den Bosch MA, Lam MG. Radioembolization-induced liver disease: a systematic review. *Eur J Gastroenterol Hepatol*. 2017;29(2):144-52.
13. Bilbao JI, de Martino A, de Luis E, Diaz-Dorronsoro L, Alonso-Burgos A, Martinez de la Cuesta A, et al. Biocompatibility, inflammatory response, and recanalization characteristics of nonradioactive resin microspheres: histological findings. *Cardiovasc Intervent Radiol*. 2009;32(4):727-36.
14. Pasciak AS, Abiola G, Liddell RP, Crookston N, Besharati S, Donahue D, et al. The number of microspheres in Y90 radioembolization directly affects normal tissue radiation exposure. *Eur J Nucl Med Mol Imaging*. 2020;47(4):816-27.

15. Pasciak AS, Bourgeois AC, Bradley YC. A Microdosimetric Analysis of Absorbed Dose to Tumor as a Function of Number of Microspheres per Unit Volume in <sup>90</sup>Y Radioembolization. *J Nucl Med.* 2016;57(7):1020-6.
16. Walrand S, Hesse M, Jamar F, Lhomme R. A hepatic dose-toxicity model opening the way toward individualized radioembolization planning. *J Nucl Med.* 2014;55(8):1317-22.
17. Kallini JR, Gabr A, Thorlund K, Balijepalli C, Ayres D, Kanters S, et al. Comparison of the Adverse Event Profile of TheraSphere. *Cardiovasc Intervent Radiol.* 2017;40(7):1033-43.
18. Bhangoos MS, Karnani DR, Hein PN, Giap H, Knowles H, Issa C, et al. Radioembolization with Yttrium-90 microspheres for patients with unresectable hepatocellular carcinoma. *J Gastrointest Oncol.* 2015;6(5):469-78.
19. Ahmadzadehfar H, Meyer C, Pieper CC, Bundschuh R, Mucke M, Gärtner F, et al. Evaluation of the delivered activity of yttrium-90 resin microspheres using sterile water and 5 % glucose during administration. *EJNMMI Res.* 2015;5(1):54.
20. Chiesa C, Mira M, Maccauro M, Romito R, Spreafico C, Sposito C, et al. A dosimetric treatment planning strategy in radioembolization of hepatocarcinoma with <sup>90</sup>Y glass microspheres. *Q J Nucl Med Mol Imaging.* 2012;56(6):503-8.
21. Allimant C, Kafrouni M, Delicque J, Ilonca D, Cassinotto C, Assenat E, et al. Tumor Targeting and Three-Dimensional Voxel-Based Dosimetry to Predict Tumor Response, Toxicity, and Survival after Yttrium-90 Resin Microsphere Radioembolization in Hepatocellular Carcinoma. *J Vasc Interv Radiol.* 2018;29(12):1662-70 e4.
22. Garin E, Lenoir L, Edeline J, Laffont S, Mesbah H, Porée P, et al. Boosted selective internal radiation therapy with <sup>90</sup>Y-loaded glass microspheres (B-SIRT) for hepatocellular carcinoma patients: a new personalized promising concept. *Eur J Nucl Med Mol Imaging.* 2013;40(7):1057-68.
23. Lam MG, Louie JD, Abdelmaksoud MH, Fisher GA, Cho-Phan CD, Sze DY. Limitations of body surface area-based activity calculation for radioembolization of hepatic metastases in colorectal cancer. *J Vasc Interv Radiol.* 2014;25(7):1085-93.
24. Garin E, Tselikas L, Guiu B, Chalaye J, Edeline J, de Baere T, et al. Personalised versus standard dosimetry approach of selective internal radiation therapy in patients with locally advanced hepatocellular carcinoma (DOSISPHERE-01): a randomised, multicentre, open-label phase 2 trial. *Lancet Gastroenterol Hepatol.* 2021;6(1):17-29.
25. Bastiaannet R, Kappadath SC, Kunnen B, Braat AJAT, Lam MGEH, de Jong HWAM. The physics of radioembolization. *EJNMMI Phys.* 2018;5(1):22.
26. Jadoul A, Bernard C, Lovinfosse P, Gérard L, Lilet H, Cornet O, et al. Comparative dosimetry between. *Eur J Nucl Med Mol Imaging.* 2020;47(4):828-37.
27. Gnesin S, Canetti L, Adib S, Cherbuin N, Silva Monteiro M, Bize P, et al. Partition Model-Based <sup>99m</sup>Tc-MAA SPECT/CT Predictive Dosimetry Compared with <sup>90</sup>Y TOF PET/CT Posttreatment Dosimetry in Radioembolization of Hepatocellular Carcinoma: A Quantitative Agreement Comparison. *J Nucl Med.* 2016;57(11):1672-8.
28. Haste P, Tann M, Persohn S, LaRoche T, Aaron V, Mauxion T, et al. Correlation of Technetium-99m Macroaggregated Albumin and Yttrium-90 Glass Microsphere Biodistribution in Hepatocellular Carcinoma: A Retrospective Review of Pretreatment Single Photon Emission CT and Posttreatment Positron Emission Tomography/CT. *J Vasc Interv Radiol.* 2017;28(5):722-30.e1.

29. Chiesa C, Maccauro M. Ho microsphere scout dose for more accurate radioembolization treatment planning. *Eur J Nucl Med Mol Imaging.* 2020;47(4):744-7.
30. Smits MLJ, Dassen MG, Prince JF, Braat A, Beijst C, Buijnen RCG, et al. The superior predictive value of (166)Ho-scout compared with (99m)Tc-macroaggregated albumin prior to (166)Ho-microspheres radioembolization in patients with liver metastases. *Eur J Nucl Med Mol Imaging.* 2020;47(4):798-806.
31. Toskich B, Vidal LL, Olson MT, Lewis JT, LeGout JD, Sella DM, et al. Pathologic Response of Hepatocellular Carcinoma Treated with Yttrium-90 Glass Microsphere Radiation Segmentectomy Prior to Liver Transplantation: A Validation Study. *J Vasc Interv Radiol.* 2021;32(4):518-26.e1.









CHAPTER  
FOUR

**Prophylactic Medication During  
Radioembolization in Metastatic Liver  
Disease, is it Really Necessary?  
A Retrospective Cohort Study  
and Review of Literature**

Manon N.G.J.A. Braat, Sander C. Ebbers, Ahmed A. Alsultan, Atal O. Neek,  
Rutger C.G. Bruijnen, Maarten L.J. Smits, Joep de Bruijne,  
Marnix G.E.H. Lam, Arthur J.A.T. Braat

*Submitted for publication (Diagnostics)*

## **Abstract**

### **Purpose**

Trans-arterial radioembolization is a well-studied tumor reductive treatment for liver malignancies, however consensus and evidence regarding periprocedural prophylactic medication (PPM) is lacking. This study evaluated the efficacy of prednisolone plus ursodeoxycholic acid (P/UDCA) as PPM in a cohort of patients with liver metastases. Additionally, a structured (comprehensive) literature review on PPM is provided.

### **Methods**

A single center retrospective analysis from 2014 till 2020 was performed in patients treated with  $^{90}\text{Y}$ -glass microspheres for either neuroendocrine or colorectal liver metastases. Inclusion criteria were availability of at least three-months clinical, biochemical and imaging follow-up and post-treatment  $^{90}\text{Y}$ -PET/CT imaging for determination of whole non-tumorous liver absorbed dose ( $D_h$ ). Logistic regression models were used to investigate if variables (amongst which P/UDCA and  $D_h$ ) could be associated with either clinical toxicity, biochemical toxicity or hepatotoxicity.

### **Results**

Fifty-one patients received P/UDCA as post-treatment medication, whilst 19 did not. No correlation was found between toxicity and P/UDCA use.  $D_h$  was found to be a significant factor ( $p=0.05$ ) associated with biochemical toxicity. Literature review resulted in nine relevant articles including a total of 657 patients in which no consistent advice regarding PPM in general was provided.

### **Conclusion**

The necessity of prophylactic prednisolone and ursodeoxycholic acid use in radioembolization treatment cannot be supported in patients without underlying cirrhosis. No standardized international guideline or supporting evidence exists for PPM in radioembolization.

## Introduction

Trans-arterial radioembolization is a well-studied tumor reductive treatment for primary liver malignancies and liver metastases and has been proven to be safe and effective (1). The purpose of periprocedural prophylactic medication (PPM) in radioembolization is to ensure comfort and minimize side effects such as post-embolization syndrome, or potential complications like radioembolization-induced liver disease (REILD). However, only a limited number of studies investigate the actual efficacy of PPM in radioembolization, whilst several randomized controlled trials (SIRFLOX, FOXFIRE, FOXFIRE Global, SARAH, SIRVENIB, SORAMIC, EPOCH, DOSISPHERE-1) did not use or mention the use of standard PPM (1-7).

Differences in patient care amongst radioembolization centers exist, as there is no evidence based international standard to adhere to (8, 9). In recent CIRSE questionnaires, PPM use was highly variable, both pre-treatment and post-treatment. A minority of centers did not use PPM, whilst the remaining centers prescribed a variety of PPM in different combinations and doses (steroids, proton pump inhibitors, anti-emetics, analgesics, and antibiotics) (8, 9).

Based on a previous publication from Gil-Alzugaray et al. the use of prednisolone with ursodeoxycolic acid (P/UDCA) was introduced in several centers (10). Conclusive evidence for this approach is however lacking and recent guidelines do not mention the use of PPM (11). To this end, we performed a retrospective, single center cohort study to analyze the efficacy of P/UDCA and evaluate any relevant variables that should be taken into consideration in relation to post-treatment toxicity. Additionally, a structured literature search of all available evidence concerning general PPM in radioembolization is provided.

## Methods

### Cohort study

Data was collected on all consecutive patients treated with radioembolization from 2014 to October 2020. Retrospective analyses included patients with progressive liver dominant or liver-only colorectal liver metastases (CRLM) or neuroendocrine liver metastases (NELM), treated with <sup>90</sup>Y-glass microspheres (Therasphere®, Boston Scientific) as mono-

therapy (i.e. no concurrent systemic treatments). Including both CRLM and NELM would allow for analyzing differences between hypo- and hypervascular disease. Hepatocellular carcinoma patients were not analyzed, to avoid confounding by underlying liver disease. From 2016 to mid-2019, based on a previous publication from Gil-Alzugaray et al., P/UDCA was standard care in our center, consisting of ursodeoxycholic acid 600 mg daily for two months and prednisone 10 mg daily for one month, followed by 5 mg daily for the second month; all starting the day of treatment (10). Prior to 2016 and from mid-2019 onwards, no P/UDCA was prescribed.

Main inclusion and exclusion criteria were; baseline imaging and follow-up imaging at three months with either positron emission computed tomography / computed tomography (PET/CT) and multiphase contrast enhanced CT (CECT), full medical history (i.e. baseline and/or post-treatment clinical and laboratory adverse events) and availability of post-treatment  $^{90}\text{Y}$ -PET/CT for dosimetric analysis.

Simplicit $^{90}\text{y}$  software (Mirada Medical Ltd, Oxford, UK) was used for the dosimetric analysis. The  $^{90}\text{Y}$  PET/CT was registered to the last available diagnostic contrast-enhanced CT for liver and tumor delineation. The whole non-tumorous liver was considered as one volume, including both treated and non-treated parts, to calculate the whole non-tumorous liver absorbed dose ( $D_h$ ) (12).

Variables gathered were baseline patient characteristics (age, sex, World Health Organization performance status (WHO)), information on general PPM, treatment strategy (e.g. whole liver, lobar or selective approach), clinical adverse events measured in Common Terminology Criteria for Adverse Events (CTCAE) grades (version 5.0), biochemical toxicity, prescribed average absorbed dose to the treated volume,  $D_h$  in Gray (Gy), previous systemic therapies and previous liver-directed therapies.

REILD was defined as asymptomatic post-radioembolization deterioration in the ability of the liver to maintain its (normal or preprocedural) synthetic, excretory, and detoxifying functions according to Braat et al.; characterized by jaundice and the development of or increase in ascites, hyperbilirubinemia, and hypoalbuminemia developing at least 2 weeks – 4 months after treatment, in the absence of tumor progression or biliary obstruction” (13).

The medical ethics committee of our institution waived the need for informed consent for review of the data.

### **Procedures**

Patients' health status at baseline was established during pre-treatment consultations and pre-treatment simulations. Pre-treatment simulation consisted of hepatic angiography and administration of technetium-99m-macroaggregated albumin ( $^{99m}\text{Tc}$ -MAA), to exclude extrahepatic depositions of activity. Subsequently, therapeutic activity was calculated according to the so-called 'MIRD formula' (i.e. using an average absorbed dose to the treated volume), as prescribed by the manufacturer in the instructions for use. On the day of treatment, laboratory tests (i.e. bilirubin, alkaline phosphatase, aspartate aminotransferase, alanine aminotransferase, gamma-glutamyltransferase, lactate dehydrogenase and albumin) were performed as baseline measurement. Within 24 hours after treatment a  $^{90}\text{Y}$ -PET/CT was acquired to assess dose distribution. One and three months after radioembolization, patients were seen at out-patient clinic with laboratory testing and three months after radioembolization with evaluation imaging.

### **Statistical analysis**

Descriptive analyses were used to identify patient demographics and treatment characteristics. Three outcome measures were defined; Clinical and biochemical toxicities were scored according to CTCAE version 5.0 and hepatotoxicity score, according to Braat et al. (13). For the clinical and biochemical toxicity outcome measures a point total system was used to find a pattern, as most patients often only experience grade 1 events, but potentially on several fronts (e.g. fatigue, vomiting and fever all grade 1). Thus a point total system (i.e. summed CTCAE-scores) was assumed to give a better representation of patient data (as opposed to dichotomizing separate toxicities only). CTCAE scores were corrected for pre-treatment presence of CTCAE grades, i.e. the highest CTCAE grade post-treatment was included if it was higher than the CTCAE grade pre-treatment. However, if pre-treatment grade was equal to or greater than post-treatment grade, these toxicities were deemed unrelated to radioembolization and excluded in the analysis. In order to dichotomize the outcome measures, summed clinical and summed biochemical CTCAE-

scores, were defined as  $\leq 4$  vs  $> 4$ . For the hepatotoxicity score according to Braat et al. results were dichotomized to  $< 3$  vs  $\geq 3$  (i.e. without or with medical intervention) (13). The three outcome measures were tested independently; hepatotoxicity score was specifically designed for REILD only (encompassing clinical and biochemical toxicities and clinical follow-up), clinical toxicities are more generic (but affected by subjective physician reporting in a retrospective study) and biochemical toxicities, being observer-independent.

Individual variables were tested for collinearity by Spearman rank testing; WHO-performance status, tumor type, liver burden,  $D_{hr}$ , treatment approach (i.e. whole liver yes/no), previous chemotherapy, previous PRRT and liver-directed therapies. Finally, remaining non-correlated variables were dichotomized (in distinct categories or divided median-based) and assessed in binary uni- and multivariate logistic regression models to investigate a possible relationship with either of the three outcome measures. Findings were deemed statistically significant with a p-value of  $< 0.05$ .

### Literature search

A PubMed search was performed in November 2022 with the following key terms, along with all their respective variations, synonyms, combinations and MeSh terms: liver, radioembolization or selective internal radiation therapy (SIRT), octreotide, anti-emetics, antibiotics, analgesics, periprocedural, prophylactic, prophylaxis. The full search terminology can be found in **Supplemental table 2**.

Studies were included if patients were treated with radioembolization, including all commercially available particles (i.e.  $^{90}\text{Y}$ -glass,  $^{90}\text{Y}$ -resin or  $^{166}\text{Ho}$ ), and focused on pre-, peri- or postprocedural medication. Records of adverse events and follow-up of at least three months was required.

Careful note was taken of factors such as dosimetry, number of radioembolization procedures, concomitant chemotherapy, the number of adverse events and their respective CTCAE grades, and finally any relevant medical history noted in the articles. These factors were not mandatory, but used qualitatively (not standardized) to assess quality of the included studies.

## **Results**

### **Retrospective cohort study**

#### *Patient characteristics*

Seventy patients were included, 57% with CRLM and 43% with NELM. The study population was extensively pre-treated (Table 1) and mostly treated in salvage setting. The median prescribed average absorbed dose to the treatment volume was 120 Gy (range 30 – 300 Gy) for the entire population, including 54% whole-liver treatments (60% in mCRC and 45% in NELM). The median interval from calibration to therapy was 4 days (range 2-11 days). Median  $D_h$  was 58 Gy (range 5 – 139 Gy).

No patients were lost to follow-up within the first three months and there were no missing clinical data. Three patients had partial laboratory testing at one-month follow-up, whilst one other patient missed the three-months laboratory testing.

#### **Prophylactic medication**

Different combinations of PPM were given to patients (Table 2). Fifty-one patients received P/UDCA, whilst 19 patients did not. No specific PPM was prescribed in the CRLM patients. In the NELM population, none of the patients received periprocedural octreotide infusion or additional octreotide bolus. Five patients had a history of a biliary intervention (three biliodigestive anastomoses and two biliary stents), of which two patients received prophylactic antibiotics (one with biliodigestive anastomosis and one with biliary stent) (14). In three diabetic patients, prednisolone was consciously discarded to avoid hyperglycemias / diabetic dysregulation during follow-up (4%), but were included in the PU group.



**Table 1:** Baseline characteristics of 70 patients

<b>Characteristics</b>	
<b>Median Age (range)</b>	64 (42-86)
<b>Sex</b>	
Female	24 (34%)
Male	46 (66%)
<b>Tumor type</b>	
CRLM	40 (57%)
NELM	30 (43%)
NET grade 1	10 (33%)
NET grade 2	11 (37%)
NET grade 3	5 (17%)
NET grade unknown	4 (13%)
<b>WHO performance score</b>	
0	42 (60%)
1	25 (36%)
2	2 (3%)
3	1 (1%)
<b>Diabetes mellitus</b>	10 (14%)
<b>Previous therapies</b>	
<sup>177</sup> Lu-DOTATATE PRRT*	19 (27%)
4 cycles	7 (10%)
6 cycles	9 (13%)
8 cycles	2 (3%)
<b>Chemotherapy</b>	
1 line	14 (20%)
2 lines	15 (21%)
≥ 3 lines	13 (19%)

**Table 1:** Baseline characteristics of 70 patients

<b>Characteristics</b>	
<b>Embolotherapy</b>	6 (9%)
Ablation <sup>†</sup>	17 (24%)
Right sided hepatectomy	2 (3%)
Left sided hepatectomy	2 (3%)
Metastasectomy <sup>‡</sup>	14 (20%)
SBRT	2 (3%)
<b>Radioembolization approach</b>	
Whole liver	38 (54%)
Lobar	24 (34%)
Segmental	8 (11%)
<b>Interval calibration – therapy</b>	
≤ 7 days	37 (53%)
> 7 days	33 (47%)
<b>Liver volume (mL)</b>	
Median total liver (range)	1841 (821 – 4261)
Median healthy parenchyma (range)	1554 (787 – 3284)
Median tumor (range)	230 (0.4 – 1980)
Median tumor involvement in % (range)	15 (0.1 – 48)
<b>Dosimetry</b>	
Median prescribed average absorbed dose in Gy (range)	120 (30 – 300)
Median total <sup>90</sup> Y Activity in GBq (range)	2.7 (0.3 – 9.5)
Median D <sub>n</sub> in Gy (range)	58 (5 – 139)
D <sub>n</sub> > 75 Gy	18 (26%)

CRLM = colorectal liver metastasis, NELM = neuro-endocrine liver metastasis, NET = neuroendocrine tumor, PRRT = peptide receptor radionuclide therapy, SBRT = stereotactic body radiotherapy, WHO = World Health Organization, MIRD = Medical Internal Radiation Dosimetry, D<sub>n</sub> = absorbed dose in the total non-tumorous liver.

\*In NELM patients only. <sup>†</sup>In total 45 ablations (range 1-6) in 17 patients, either radiofrequency or microwave ablation. <sup>‡</sup>In total 26 metastasectomies (range 1-6) in 14 patients

**Table 2:** Prophylactic periprocedural medication combinations in retrospective cohort (n=70).

Prophylactic periprocedural medication	N	%
<b>Preprocedural medication</b>		
Dexamethasone + Ondansetron	61	87%
Dexamethasone only	1*	1%
Ondansetron only	3 <sup>†</sup>	4%
None	5	7%
<b>Postprocedural medication</b>		
Pantoprazole	62	89%
Prednisolone + ursodeoxycholic acid	51	73%
Ursodeoxycholic acid only	3	4%
None	8	11%
<b>All pre- and postprocedural medication</b>	51	73%
<b>No medication at all</b>	5	7%

\*Refrained from ondansetron, because of pre-existing ECG abnormalities

<sup>†</sup>Refrained from dexamethasone, because of diabetes mellitus

Following dosage was used; dexamethasone once 8 mg two hours before intervention; ondansetron once 8 mg two hours before intervention; prednisolone 10 mg daily for one month, subsequently 5 mg daily for one month; ursodeoxycholic acid 300 mg twice a day for two months; pantoprazole 40 mg once daily for six weeks.

**Table 3:** Adverse events according to CTCAE grading

CTCAE grade	1	2	3	4	5
<b>Clinical toxicity</b>					
Fatigue	55%	16%			
Abdominal pain	38%	7%	2%		
Other pain	4%	3%			
Nausea	37%	4%			
Vomiting	7%	3%			
Malaise	10%	2%			
Fever	10%	2%			
Loss of appetite	17%	4%			
<b>Biochemical toxicity*</b>					
Bilirubin	4%	2%	6%		
Alkaline phosphatase	44%	6%	3%		
Gamma-glutamyltransferase	39%	28%	11%	2%	2%
Aspartate aminotransferase	25%	6%			
Alanine aminotransferase	11%	4%			
Albumin	14%	3%	2%		
Lactate dehydrogenase	45%				
<b>Complications</b>					
Abscess				6%	
Clinical progressive disease			4%	6% <sup>†</sup>	
REILD <sup>‡</sup>				3%	
Radiation cholecystitis			2%		
<b>Hepatotoxicity</b>	24%	17%	1%	1%	

REILD = radioembolization induced liver disease.

\*Complete laboratory tests at 3 months follow-up missing for four patients (6%), <sup>†</sup>Requiring paracentesis, because of peritonitis carcinomatosa induced ascites. Progressive disease confirmed on imaging studies in all patients.

<sup>‡</sup>Overlap with hepatotoxicity score (13)

## Toxicity

New clinical toxicities resulting from the treatment were grade  $\geq 3$  in 6% (**Table 3**). New CTCAE grade  $\geq 3$  biochemical toxicities occurred 30 times in 21 patients (30%) (**Table 3**).

In total 14 patients developed a hepatotoxicity score  $\geq 2$ . Hepatotoxicity grade  $\geq 3$  (REILD) was diagnosed in 2 patients (3%) (13); one requiring paracentesis and medical intervention with a  $D_h$  of 139 Gy (lobar treatment) and one requiring only medical intervention with a  $D_h$  of 128 Gy (whole liver treatment). Eighteen patients (25%) exceeded the presumed  $D_h$  75 Gy threshold, of which eight patients (11%) developed hepatotoxicity score  $\geq 2$  (11). The remaining 8/14 patients with hepatotoxicity score of  $\geq 2$  had a median  $D_h$  of 54 Gy (range 19 – 73 Gy).

In the NELM group, no increased hormone-related complaints (e.g. carcinoid crisis) or infectious problems (e.g. liver abscess or cholangitis) were encountered. Four patients (6%), all without prior biliary interventions, developed a liver abscess at the site of a treated tumor, requiring intravenous antibiotic treatment and additional drainage or right-sided hepatectomy.

In 6 patients (9%), complaints probably related to the prophylaxis were reported (i.e. diarrhea following ursodeoxycolic acid or diabetic dysregulation during prednisolone use), resulting in early termination of P/UDCA.

## Efficacy of P/UDCA

Whole liver treatment and  $D_h$  showed significant collinearity ( $p < 0.001$ ), as well as previous treatments and tumor type (e.g. chemotherapy and CRC versus NELM and PRRT). To this end, whole liver treatment, previous chemotherapy and previous PRRT were excluded as variables in subsequent logistic regressions. Remaining non-correlated variables were; WHO performance score (0 or  $\geq 1$ ), tumor type (CRC or NELM), liver tumor burden (median-based:  $\leq 15\%$  vs.  $> 15\%$ ),  $D_h$  (median based;  $\leq 58$  Gy vs.  $> 58$  Gy) and P/UDCA (yes or no).

**Supplemental Table 3** shows the results of all analyses. In the analyses P/UDCA did not show any statistically significant relationship with any of the outcome measures (i.e. summed CTCAE clinical toxicity, summed CTCAE biochemical toxicity or hepatotoxicity score). None

of the investigated variables showed a significant relationship with the summed CTCAE clinical toxicity (**Supplemental Table 3**). Only  $D_h$  showed a significant relation with summed CTCAE biochemical toxicities, in both uni- and multivariate regression ( $p=0.05$ ). Liver tumor burden showed a significant relationship with the summed biochemical toxicities in only the multivariate analysis ( $p=0.04$ ).

### Literature search

The literature search yielded nine relevant studies pertaining a total of 850 radioembolizations in 657 patients treated with either  $^{90}\text{Y}$ -glass or  $^{90}\text{Y}$ -resin microspheres (**Figure 1**). Five studies used medication prophylactically and therapeutically; four studies used medication only therapeutically in response to adverse events. The most common PPM were proton pump inhibitors, analgesic medication and steroids (**Table 4**). Clinical adverse events grade 3 or higher occurred in 63 of 657 patients (9.6%). Only two studies took biochemical toxicity into consideration. A total of 52 patients (41.5%) in a combined patient size of 135 were recorded to experience grade  $\geq 3$  biochemical toxicity (15, 16).

There was no similarity concerning PPM between studies. Each treatment center differed in medication types, the duration of administration and indication for the PPM. Quality of included articles was variable. Three studies mentioned the indication for PPM; for prevention of a carcinoid crisis, hepatobiliary infections or REILD (10, 17, 18). Two studies mentioned the actual names of the administered medication and specifically attempted to investigate the efficacy of the administered PPM (10, 18). Two studies specifically mention that patients had no concurrent chemotherapy (16, 19). Three studies had no standardized way of adverse events reporting (i.e. CTCAE) (17, 20, 21). Only one of the included articles had a clear comparative cohort and none of the included articles reported adverse events related to PPM.

**Table 4:** Literature search results

Author (year)	Product	N (p)	Tumor types	Cirrhosis	Activity calculation method
King et al. (2008) (17)	Resin	34 (46)	NELM	NR	BSA
Stubbs et al. (2001) (21)	Resin	50 (50)	CRLM	NR	NR
Murthy et al. (2005) (15)	Resin	12 (17)	CRLM	NR	BSA & Empirical
Lim et al. (2005) (20)	Resin	29 (29)	CRLM	NR**	BSA
Pöpperl et al (2005) (19)	Resin	23 (23)	Mixed	NR	Empirical
Salem et al. (2011) (16)	Glass	123 (245)	HCC	86%	NR
Gil-Alzugaray et al. (2013) (10)	Resin	260	HCC	34%	BSA & partition modelling
Cholapranee et al. (2015)	Resin	SIRT 16 (24)* TACE 13 (24)	Mixed	NR	BSA
Devulapalli et al. (2018) (18)	Glass & resin	126 (92 glass, 88 resin) <sup>†</sup>	Mixed	NR	MIRD & BSA

AB = antibiotic prophylaxis, BSA = body surface area, CRLM = colorectal liver metastases, HCC = hepatocellular carcinoma, MIRD = Medical Internal Radiation Dosimetry, MVA = multivariate analysis, N = number of patients, NELM = neuroendocrine liver metastases, NR = Not reported, p = number of treatments, PPI = proton pump inhibitor, PPM = periprocedural prophylactic medication, SIRT = selective internal radiation therapy a.k.a. radioembolization.

**Table 4:** Continued.

GBq (range)	PPM	Comments and author's advice
Mean 1,99 (0.92-2.80)	Prophylactic: Octreotide + H2-antagonist for 1 month	No advice regarding PPM. No patients were coiled
Mean 2,27 (2,0-3,0)	Narcotics	No advice regarding PPM.
Mean 1.47 (0.63– 2.5)	Antiemetics, narcotic analgesics, supportive care, parenteral antibiotics	No mention of prophylactic medication or efficacy of periprocedural medication
NR	Antiemetics, Analgesics	Prophylactic H2-antagonist recommended. No risk factors for toxicity were found
Mean 2,5 (NR)	Analgesics, antiemetics, steroids, drugs for gastric protection and AB	No mention of the efficacy of PPM or advice concerning usage of PPM
NR	Prophylactic: five day PPI treatment after treatment	Mentions underscoring a lower need for in-patient resource utilization based on no hospitalization of patients included in the study
Mean NR (0.6 – 2.23)	Prophylactic: Ursodeoxycolic acid and methylprednisolone	Prescribed activity was reduced for all subgroups with 'modified protocol' (partition modelling and prophylaxis), and reduced the occurrence of REILD. In MVA, occurrence of REILD was reduced by the 'modified protocol'
NR	Extensive AB prophylaxis: oral levofloxacin 500 mg daily + metronidazole 500 mg twice daily.	No control group without AB prophylaxis. With AB no infectious complication in the SIRT group. 23% liver abscesses in the TACE group.
Glass: Median 2.36 (NR); Resin: Median 1.04 (NR)	Prophylactic: AB in 79%, various types. Most common: levofloxacin + metronidazole (43%)	Incidence of liver abscess is rare (7.9%). Bowel preparation and antibiotic prophylaxis were not associated with lower risk of infection.

\*Including 11 patients with a biliodigestive anastomosis (either pancreatic adenocarcinoma of cholangiocarcinoma as primary tumor) and 5 patients with a biliary stent placement. †Including 54 repeated treatments (in 47 patients), all with the same microsphere type as the initial treatment. \*\* Patients with liver decompensation or portal hypertension were excluded.



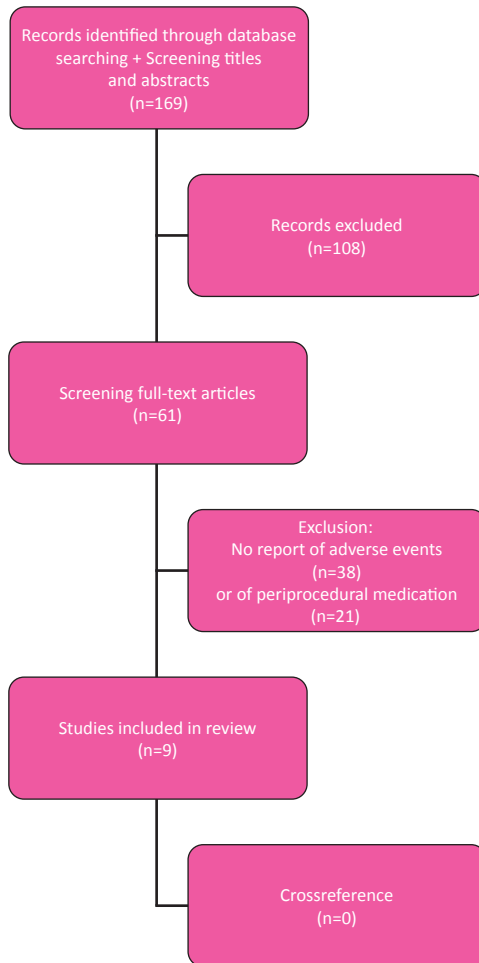


Figure 1. Flowchart

Three publications gave an advice concerning PPM. First, Lim et al., although not having used PPM in their study, advised adhering to the manufacturer's recommended prophylactic H2-antagonist administration (20). Paradoxically, the study mentioned that no risk factors for toxicity were found in their analysis. Second, Devulapalli et al. retrospectively researched the risk of hepatobiliary infections in patients with a hepatobiliary history being treated with radioembolization and prophylactic use of antibiotics and bowel preparation. A wide variation of prophylactic antibiotic treatment combinations was described and also contained a group not receiving any prophylaxis. The authors concluded that bowel preparation and antibiotic prophylaxis were not associated with lower risk of infection (18). Thirdly, Gil-Alzugaray et al. described a treatment protocol to reduce the number of REILD events (defined as bilirubin  $\geq 3$  mg/dL ( $\geq 51.3$   $\mu\text{mol/L}$ ) and presence of ascites clinically or on imaging). Their 'modified protocol' incorporated the use of prophylactic medication (ursodeoxycolic acid twice daily 300 mg and methylprednisolone 8 mg daily for one month followed by 4 mg daily for the subsequent month) and a 10-20% reduction in the calculated activity in whole liver treatments (up to 0.8 GBq/L in cirrhotic patients), while for selective treatments the partition model was used (with a target dose to the non-tumorous liver of 40 Gy in poor candidates, i.e. patients with cirrhosis or extensive pre-treatment with chemotherapy). The authors suggested that with this PMM protocol, the number of REILD cases can be reduced compared to their non-matched historical cohort (10). However, with the significant reduction in administered activity (in both cirrhotic and non-cirrhotic patients) the contribution of PPM to the decline in REILD is unclear.

Each treatment center in these publications had different protocols concerning patient hospitalization after treatment and adverse event recording. There was no mentioning of specific patient characteristics that influenced these protocols, apart from the study by Gil-Alzugaray et al. who were more cautious with patients having underlying cirrhosis or previous chemotherapy.

## Discussion

As a start to generate supporting data for PPM, this retrospective cohort study was conducted to investigate the effect of prednisolone and ursodeoxycholic acid (P/UDCA) after radioembolization to prevent REILD (i.e. hepatotoxicity score (13)), in line with the intention of and adopted from Gil-Alzugaray et al. (10). This study showed that in patients with CRLM or NELM treated with radioembolization, the use of P/UDCA as PPM or REILD-prophylaxis is not supported by conclusive evidence. The only probable variable that correlated with observed toxicity was whole non-tumorous liver absorbed dose ( $D_h$ ). Review of available literature revealed a wide variety of PPM use in literature, however none providing firm scientific evidence supporting specific PPM use. No guidelines mention the use of PPM. In line with the findings of previously published international questionnaires, no standardized PPM protocol exists for radioembolization (8, 9).

Gil-Alzugaray et al. treated patients with  $^{90}\text{Y}$  resin microspheres, investigating the effect of a so-called 'modified protocol'; a combination of dose reduction plus prophylaxis with P/UDCA as PPM. Their modified protocol was compared to a non-matched historical group (without prophylaxis or dose reduction). In the multivariate analysis, in non-cirrhotic patients, the modified protocol showed a statistically significant reduction in REILD cases, whilst methylprednisolone and ursodeoxycholic acid separately were no significant factors. No dosimetric data were available. Yet, the activity/target volume for whole liver treatments was significantly lower in the modified protocol group (1 vs. 0.77 GBq/L;  $p = 0.003$ ) (10). Interestingly, in their multivariate analysis, in cirrhotic patients the modified protocol did not reduce the number of REILD cases. Furthermore, nearly all REILD cases developed in patients with an activity/target volume of  $> 0.8$  GBq/L, which insinuates a significant effect of  $D_h$ .

The current cohort study and the study by Gil-Alzugaray et al. (whole liver treatments in non-cirrhotic patients in 57.8% and 63.4%, respectively) both failed to conclusively prove the usefulness of P/UDCA as PPM following radioembolization to prevent REILD. Both studies however, do insinuate that  $D_h$  is a more important variable.

Seidensticker et al. reported that the use of pentoxifylline, UDCA and low molecular weight heparin as prophylaxis after interstitial brachytherapy reduced the extent of radiation-induced liver damage (22). After radioembolization, using the same prophylaxis, no significant difference in hepatotoxicity was reported (23). Their definition of hepatotoxicity was non-standard and highly variable (based on bilirubin and/or ascites or imaging characteristics) and no control group without prophylaxis was selected in the radioembolization study. The value of this prophylactic extended regimen remains unclear.

Concerning other PPM (proton pump inhibitors (PPI), H2-antagonists and antibiotics), efficacy is even more questionable and proper evidence is lacking. Lim et al. advised H2-antagonists, because of gastroscopy proven gastrointestinal ulceration in 8% (4 patients, of which 3 biopsy proven) (20). The applicability of H2-antagonists or PPI in contemporary practice is debatable since most centers perform improved pre-treatment work-up with perprocedural conebeam-CT and <sup>99m</sup>Tc-MAA SPECT/CT to prevent extrahepatic deposition of activity. More recent studies looking at radiation absorbed doses to the stomach after left lobe treatments showed negligible absorbed doses (i.e. 13±9 Gy) and low rates of GI-ulceration (<3%) (24-27). Although questionable, in absence of a comparator group (i.e. without any form of PPM) no definitive judgement can be made on the efficacy of H2-antagonists or PPI.

Another interesting observation in our cohort was the development of liver abscesses following radioembolization in four patients, as this only occurred in patients without any prior biliary intervention. Contra-intuitive to daily practice, where liver abscess formation is feared in patients with a biliodigestive anastomosis, based on high occurrence rates after TACE (even under antibiotic prophylaxis) (14). This finding was indirectly supported by others, who did provide evidence for an increased risk of infectious complications in patients with prior biliary intervention, however without supporting evidence for the use of antibiotic prophylaxis or bowel preparation (28). Based on these studies and the sole occurrence of liver abscesses in non-biliary compromised patients in this cohort, antibiotic prophylaxis in patients with prior biliary intervention remains unsupported.

In this study the summed CTCAE grades of adverse events were used instead of individual CTCAE grades. As **Table 3** shows, most patients either experienced no or only grade 1 clinical adverse events/biochemical toxicities. There were some cases of grade  $\geq 2$  toxicity, but not enough to form a reliable sample size for accurate analysis per adverse event/biochemical toxicity. Hepatotoxicity as described by Braat et al. was also used to give a more holistic representation of the effect of radioembolization on the patient and REILD (13). It also provides a clear definition of REILD using clinical and biochemical parameters, as histopathological correlation is lacking and biochemical toxicity on its own does not reflect the actual loss of liver function. The number of serious clinical, biochemical and hepatotoxic adverse events in our population was limited, which hampered the analysis on PPM use on one hand, but further questioned the use of PPM to begin with on the other hand.

The relatively small number of studies found on this topic in literature convey that the efficacy of PPM in patients being treated with radioembolization is not a broadly researched subject and that there is no consistent trend in PPM protocols across treatment centers. The results of this retrospective cohort study and the literature search seem to be in line with the advice from Lim et al. and Devulapalli et al., that PPM has not proven to be effective in protecting against adverse events due to radioembolization.

The retrospective cohort study had several limitations, besides being a retrospective analysis, limiting the power to establish a reliable causal relationship, as there may have been unknown confounders left out of the regression model. Furthermore, the relatively small sample size ( $n=70$ ) limited the statistical power of our analyses. However, the structured practice did allow for a limited number of missing data and consistent timing of follow-up, which has been unchanged for years.

A limitation of the literature search is the limited number of articles discussing PPM and the lack of recent data (most studies were conducted before 2010). They should be considered as outdated, as the field of radioembolization has rapidly evolved over the past 10 years.

Future (prospective) studies on the toxicity of radioembolization should at least take note of PPM and important dosimetric values (i.e.  $D_h$ ). Preferably, more data is gathered to

investigate the efficacy of PPM in general, also considering the side-effects of PPM. As proper scientific evidence supporting the use of steroids, ursodeoxycholic acid, proton-pump inhibitors, octreotide infusion in neuroendocrine tumor patients and antibiotics in patients with a history of biliary interventions is lacking, use of any PPM cannot be advised or supported at the moment in patients with metastatic disease.

### **Conclusion**

No standardized international guideline or proper supporting evidence exists for any periprocedural medication in radioembolization. The use of prednisolone and ursodeoxycholic acid as prophylaxis was not supported. Whole non-tumorous liver absorbed dose was the only significant factor for hepatotoxicity.

## References

1. Gibbs P, GebSKI V, Van Buskirk M, Thurston K, Cade DN, Van Hazel GA, et al. Selective Internal Radiation Therapy (SIRT) with yttrium-90 resin microspheres plus standard systemic chemotherapy regimen of FOLFOX versus FOLFOX alone as first-line treatment of non-resectable liver metastases from colorectal cancer: the SIRFLOX study. *BMC Cancer*. 2014;14:897.
2. Vilgrain V, Abdel-Rehim M, Sibert A, Ronot M, Lebtahi R, Castera L, et al. Radioembolisation with yttrium-90 microspheres versus sorafenib for treatment of advanced hepatocellular carcinoma (SARAH): study protocol for a randomised controlled trial. *Trials*. 2014;15:474.
3. Gandhi M, Choo SP, Thng CH, Tan SB, Low AS, Cheow PC, et al. Single administration of Selective Internal Radiation Therapy versus continuous treatment with sorafenib in locally advanced hepatocellular carcinoma (SIRveNIB): study protocol for a phase iii randomized controlled trial. *BMC Cancer*. 2016;16(1):856.
4. Ricke J, Klumpen HJ, Amthauer H, Bargellini I, Bartenstein P, de Toni EN, et al. Impact of combined selective internal radiation therapy and sorafenib on survival in advanced hepatocellular carcinoma. *J Hepatol*. 2019;71(6):1164-74.
5. Ricke J, Schinner R, Seidensticker M, Gasbarrini A, van Delden OM, Amthauer H, et al. Liver function after combined selective internal radiation therapy or sorafenib monotherapy in advanced hepatocellular carcinoma. *J Hepatol*. 2021;75(6):1387-96.
6. Garin E, Tselikas L, Guiu B, Chalaye J, Edeline J, de Baere T, et al. Personalised versus standard dosimetry approach of selective internal radiation therapy in patients with locally advanced hepatocellular carcinoma (DOSISPHERE-01): a randomised, multicentre, open-label phase 2 trial. *Lancet Gastroenterol Hepatol*. 2021;6(1):17-29.
7. Mulcahy MF, Mahvash A, Pracht M, Montazeri AH, Bandula S, Martin RCG, 2nd, et al. Radioembolization With Chemotherapy for Colorectal Liver Metastases: A Randomized, Open-Label, International, Multicenter, Phase III Trial. *J Clin Oncol*. 2021;39(35):3897-907.
8. Reinders MTM, Mees E, Powerski MJ, Bruijnen RCG, van den Bosch M, Lam M, et al. Radioembolisation in Europe: A Survey Amongst CIRSE Members. *Cardiovasc Intervent Radiol*. 2018;41(10):1579-89.
9. Powerski MJ, Scheurig-Munkler C, Banzer J, Schnapauff D, Hamm B, Gebauer B. Clinical practice in radioembolization of hepatic malignancies: a survey among interventional centers in Europe. *Eur J Radiol*. 2012;81(7):e804-11.
10. Gil-Alzugaray B, Chopitea A, Inarrairaegui M, Bilbao JI, Rodriguez-Fraile M, Rodriguez J, et al. Prognostic factors and prevention of radioembolization-induced liver disease. *Hepatology*. 2013;57(3):1078-87.
11. Weber M, Lam M, Chiesa C, Konijnenberg M, Cremonesi M, Flamen P, et al. EANM procedure guideline for the treatment of liver cancer and liver metastases with intra-arterial radioactive compounds. *Eur J Nucl Med Mol Imaging*. 2022;49(5):1682-99.
12. Ebberts SC, van Roekel C, Braat M, Barentsz MW, Lam M, Braat A. Dose-response relationship after yttrium-90-radioembolization with glass microspheres in patients with neuroendocrine tumor liver metastases. *Eur J Nucl Med Mol Imaging*. 2022;49(5):1700-10.
13. Braat MN, van Erpecum KJ, Zonnenberg BA, van den Bosch MA, Lam MG. Radioembolization-induced liver disease: a systematic review. *Eur J Gastroenterol Hepatol*. 2017;29(2):144-52.

14. Cholapranee A, van Houten D, Deitrick G, Dagli M, Sudheendra D, Mondschein JI, et al. Risk of liver abscess formation in patients with prior biliary intervention following yttrium-90 radioembolization. *Cardiovasc Intervent Radiol.* 2015;38(2):397-400.
15. Murthy R, Xiong H, Nunez R, Cohen AC, Barron B, Szklaruk J, et al. Yttrium 90 resin microspheres for the treatment of unresectable colorectal hepatic metastases after failure of multiple chemotherapy regimens: preliminary results. *J Vasc Interv Radiol.* 2005;16(7):937-45.
16. Salem R, Lewandowski RJ, Kulik L, Wang E, Riaz A, Ryu RK, et al. Radioembolization results in longer time-to-progression and reduced toxicity compared with chemoembolization in patients with hepatocellular carcinoma. *Gastroenterology.* 2011;140(2):497-507 e2.
17. King J, Quinn R, Glenn DM, Janssen J, Tong D, Liaw W, et al. Radioembolization with selective internal radiation microspheres for neuroendocrine liver metastases. *Cancer.* 2008;113(5):921-9.
18. Devulapalli KK, Fidelman N, Soulen MC, Miller M, Johnson MS, Addo E, et al. (90)Y Radioembolization for Hepatic Malignancy in Patients with Previous Biliary Intervention: Multicenter Analysis of Hepatobiliary Infections. *Radiology.* 2018;288(3):774-81.
19. Popperl G, Helmberger T, Munzing W, Schmid R, Jacobs TF, Tatsch K. Selective internal radiation therapy with SIR-Spheres in patients with nonresectable liver tumors. *Cancer Biother Radiopharm.* 2005;20(2):200-8.
20. Lim L, Gibbs P, Yip D, Shapiro JD, Dowling R, Smith D, et al. A prospective evaluation of treatment with Selective Internal Radiation Therapy (SIR-spheres) in patients with unresectable liver metastases from colorectal cancer previously treated with 5-FU based chemotherapy. *BMC Cancer.* 2005;5:132.
21. Stubbs RS, Cannan RJ, Mitchell AW. Selective internal radiation therapy (SIRT) with 90Yttrium microspheres for extensive colorectal liver metastases. *Hepatogastroenterology.* 2001;48(38):333-7.
22. Seidensticker M, Seidensticker R, Damm R, Mohnike K, Pech M, Sangro B, et al. Prospective randomized trial of enoxaparin, pentoxifylline and ursodeoxycholic acid for prevention of radiation-induced liver toxicity. *PLoS One.* 2014;9(11):e112731.
23. Seidensticker M, Fabritius MP, Beller J, Seidensticker R, Todica A, Ilhan H, et al. Impact of Pharmaceutical Prophylaxis on Radiation-Induced Liver Disease Following Radioembolization. *Cancers (Basel).* 2021;13(9).
24. Gates VL, Hickey R, Marshall K, Williams M, Salzig K, Lewandowski RJ, et al. Gastric injury from (90)Y to left hepatic lobe tumors adjacent to the stomach: fact or fiction? *Eur J Nucl Med Mol Imaging.* 2015;42(13):2038-44.
25. Braat A, Kappadath SC, Ahmadzadehfar H, Stothers CL, Frilling A, Deroose CM, et al. Radioembolization with (90)Y Resin Microspheres of Neuroendocrine Liver Metastases: International Multicenter Study on Efficacy and Toxicity. *Cardiovasc Intervent Radiol.* 2019;42(3):413-25.
26. Braat A, Prince JF, van Rooij R, Bruijnen RCG, van den Bosch M, Lam M. Safety analysis of holmium-166 microsphere scout dose imaging during radioembolisation work-up: A cohort study. *Eur Radiol.* 2018;28(3):920-8.
27. van Roekel C, Bastiaannet R, Smits MLJ, Bruijnen RC, Braat A, de Jong H, et al. Dose-Effect Relationships of (166)Ho Radioembolization in Colorectal Cancer. *J Nucl Med.* 2021;62(2):272-9.
28. Geisel D, Powerski MJ, Schnapauff D, Colletinni F, Thiel R, Denecke T, et al. No infectious hepatic complications following radioembolization with 90Y microspheres in patients with biliodigestive anastomosis. *Anticancer Res.* 2014;34(8):4315-21.



## Supplementary material

**Supplemental Table 1**

---

<b>Grade 0</b>	No liver toxicity (i.e. no CTCAE toxicity grade changes over baseline).
<b>Grade 1</b>	Minor liver toxicity, limited to increased AST, ALT, ALP and/or GGT levels (all not exceeding newly developed grade 1 CTCAE toxicity).
<b>Grade 2</b>	Moderate liver toxicity, with a self-limiting course. No medical intervention necessary.
<b>Grade 3</b>	REILD, manageable with non-invasive treatments such as diuretics, ursodeoxycholic acid and steroids.
<b>Grade 4</b>	REILD necessitating invasive medical treatment such as paracentesis, transfusions, haemodialysis or a transjugular intrahepatic portosystemic shunt (TIPS).
<b>Grade 5</b>	Fatal REILD.

---

\*Grading according to Braat et al. (12)

ALP = alkaline phosphatase, ALT = alanine aminotransferase, AST = aspartate aminotransferase, GGT = gamma-glutamyl transferase, CTCAE = Common Terminology Criteria for Adverse Events, REILD = radioembolization-induced liver disease

**Supplemental Table 2:** Literature search strategy

**Main search string**

("radioembolic"[All Fields] OR "radioembolisation"[All Fields] OR "radioembolization"[All Fields] OR radioemboli\* [All Fields] OR "SIRT"[All fields] OR "selective internal radiation therapy"[All Fields] OR "TARE" [All Fields] OR "transarterial radioembolization"[All Fields])

**AND**

((("liver"[MeSH Terms] OR "liver"[All Fields] OR neoplasm metastasis[MeSH Terms] OR liver neoplasm[MeSH Terms]))

**AND**

((("octreotid"[All Fields] OR "octreotide"[MeSH Terms] OR "octreotide"[All Fields] OR "somatostatin"[All Fields] OR SSA[All Fields] OR "Anti-Bacterial Agents"[Mesh] OR "Antibiotic Prophylaxis"[Mesh] OR antibioti\* [All Fields] OR anti-emetic [All Fields] OR prophylaxis [All Fields] OR analgesics [All Fields] OR steroids[All Fields])

---

**Supplemental Table 3:** Logistic regression models

	Univariate				Multivariate			
	B	p	OR	95% CI	B	p	OR	95% CI
<b>Clinical toxicity</b>								
WHO	0.20	0.73	1.22	0.4–3.8	0.56	0.40	1.74	0.5–6.3
Tumor type	-1	0.08	0.35	0.1–1.1	-0.68	0.29	0.51	0.1–1.8
Liver burden	1.09	0.07	2.97	0.9–9.7	0.82	0.21	2.27	0.6–8.1
D <sub>h</sub>	-0.33	0.57	0.72	0.2–2.2	-0.42	0.50	0.66	0.2–2.2
LDT	-1.09	0.12	0.34	0.1–1.3	-1.15	0.14	0.32	0.1–1.4
P/UDCA	-0.15	0.82	0.86	0.2–3.1	-0.21	0.77	0.81	0.2–3.6
<b>Biochemical toxicity</b>								
WHO	-0.71	0.27	0.49	0.1–1.7	-0.84	0.25	0.43	0.1–1.8
Tumor type	0.11	0.86	1.11	0.3–3.6	-0.21	0.76	0.81	0.2–3.2
Liver burden	-1.16	0.07	0.31	0.1–1.1	<b>-1.45</b>	<b>0.04*</b>	<b>0.24</b>	<b>0.1–1.0</b>
D <sub>h</sub> <sup>†</sup>	<b>1.31</b>	<b>0.04*</b>	<b>3.71</b>	<b>1.0–13.1</b>	<b>1.37</b>	<b>0.05*</b>	<b>3.92</b>	<b>1.0–15.0</b>
LDT	-0.16	0.79	0.85	0.3–2.8	0.23	0.75	1.26	0.3–5.3
P/UDCA	0.13	0.85	1.14	0.3–4.7	0.04	0.96	1.04	0.2–5.0
<b>Hepatotoxicity</b>								
WHO	-1.08	0.12	0.34	0.1–1.3	-0.80	0.30	0.45	0.1–1.9
Tumor type	-0.72	0.23	0.49	0.1–1.6	-0.43	0.52	0.65	0.2–2.4
Liver burden	-0.43	0.48	1.54	0.5–5.0	0.22	0.74	1.25	0.4–4.6
D <sub>h</sub>	0.73	0.24	2.10	0.6–7.0	0.46	0.49	1.59	0.4–5.9
LDT	<b>-2.28</b>	<b>0.03*</b>	<b>0.10</b>	<b>0.0–0.8</b>	-1.97	0.07	0.34	0.1–1.2
P/UDCA	0.69	0.40	2.00	0.4–10.1	0.84	0.34	2.32	0.4–13.1

WHO = World Health Organization performance score, D<sub>h</sub> = whole healthy liver absorbed dose, LDT = liver directed treatment (i.e. whole liver: yes/nos. \*Indicates significance, p<0.05. †D<sub>h</sub> is the only significant factor in both uni- and multivariate logistic regression for biochemical toxicity, p<0.05. ) univariate and multivariate logistic regressions, only D<sub>h</sub> remains as significant factor: per 1 Gy D<sub>h</sub>, likelihood of developing >4 summed CTCAE biochemical toxicities increases by 3% (p=0.018).



The background of the slide is a dense, multi-colored pattern of small, round confetti pieces in various colors including white, yellow, green, blue, red, and pink.

## Part II

# Nuclear medicine perspectives on radioembolization



The background of the entire page is a dense field of multi-colored confetti, including shades of red, green, blue, yellow, and white.

# CHAPTER FIVE

## Hepatobiliary scintigraphy may improve radioembolization treatment planning in HCC patients

Manon N.G.J.A. Braat, Hugo W. de Jong, Beatrijs A. Seinstra,  
Mike. V. Scholten, Maurice A.A.J. van den Bosch, Marnix G.E.H. Lam

*European Journal of Nuclear Medicine and Molecular Imaging Research 2017 Dec; 7(1):2.*

## **Abstract**

### **Background**

Routine work-up for transarterial radioembolization, based on clinical and laboratory parameters, sometimes fails, resulting in severe hepatotoxicity in up to 5% of patients. Quantitative assessment of the pre-treatment liver function, and its segmental distribution, using hepatobiliary scintigraphy may improve patient selection and treatment planning. A case-series will be presented to illustrate the potential of this technique.

### **Methods**

HCC patients with cirrhosis (Child-Pugh A and B) underwent hepatobiliary scintigraphy pre- and three months post-radioembolization as part of a prospective study protocol, which was prematurely terminated because of limited accrual. Included patients were analyzed together with their clinical, laboratory and treatment data.

### **Results**

Pre-treatment corrected  $^{99m}\text{Tc}$ -mebrofenin liver uptake rates were marginal (1.8 – 3.0%/min/m<sup>2</sup>), despite acceptable clinical and laboratory parameters. Post-treatment liver functions seriously declined (corrected  $^{99m}\text{Tc}$ -mebrofenin liver uptake rates: 0.6-2.4%/min/m<sup>2</sup>), resulting in lethal radioembolization induced liver disease in two out of three patients.

### **Conclusion**

Hepatobiliary scintigraphy may be of added value during work-up for radioembolization, to estimate liver function reserve and its segmental distribution, especially in patients with underlying cirrhosis, for whom analysis of clinical and laboratory parameters may not be sufficient.

## Introduction

Transarterial radioembolization (RE) is an emerging treatment option for patients with hepatocellular carcinoma (HCC). Comparative studies have shown that RE outperforms transarterial chemoembolization (TACE) with regard to overall survival and time to progression, with a similar toxicity profile (1, 2). Similar results were reported in a recent randomized controlled trial in patients with HCC Barcelona Clinic Liver Cancer stage A/B (the Premiere trial; NCT00956930 (3)). Treatment planning however, is a balancing act between optimal efficacy and acceptable toxicity.

Lodging of radioactive microspheres in the functional liver parenchyma may result in radiation damage, consistent with sinusoidal obstruction syndrome at histopathology (4). The extent of the radiation damage depends on the percentage of functional liver within the treated volume, the tumor-to-non tumor ratio (TNR) and the regenerative capacity of the remaining functional liver parenchyma.

The functional liver remnant after RE is hard to predict, due to the heterogeneity of the radiation absorbed dose distribution, but may be crucial to prevent (severe) radioembolization-induced liver disease (REILD), especially in patients with a marginal liver function, as seen in cirrhosis or after chemotherapy.

Assessment of eligibility for RE is usually based on a combination of clinical, laboratory and imaging parameters, with special attention to performance score, bilirubin, albumin, portal vein thrombosis and ascites. Nonetheless, this evaluation can sometimes not predict serious toxicity after RE, with incidences of lethal REILD up to 5% in large series (5). There is definitively room for improvement.

Hepatobiliary scintigraphy with technetium-99m ( $^{99m}\text{Tc}$ )-mebrofenin is a dynamic quantitative liver function test; for example able to assess severity of fibrosis in hepatitis C positive patients (6). Furthermore, it can adequately predict the risk of postoperative liver failure, outperforming the Child-Pugh score and CT volumetry (7-9). De Graaf et al. reported that a liver remnant function cut-off value of  $2.69\%/ \text{min}/\text{m}^2$  (=body surface area corrected  $^{99m}\text{Tc}$ -mebrofenin hepatic uptake rate = cMUR) can accurately identify patients



at risk for postoperative liver failure, regardless of the presence of underlying liver disease (7). Moreover, an uptake below 2.2%/min/m<sup>2</sup> was reported to be associated with a 50% risk of lethal postoperative liver failure (8).

We hypothesized that quantitative assessment of remnant liver function using hepatobiliary scintigraphy can improve patient selection, complementary to routine assessment. In this case series three cases with pre- and Post-treatment hepatobiliary scintigraphies will be presented to illustrate the potential of this technique.

## Methods

### Patient selection

We reviewed the data of patients, who were initially included in a multicenter randomized controlled trial in 2012 comparing TACE and RE in patients with unresectable HCC (the TRACE study; NCT01381211 (10)). Unfortunately, this trial was prematurely terminated due to the lack of inclusions. Ultimately, in our hospital, three patients were included before study closure. The medical ethics committee of our institution waived the need for informed consent for review of the imaging data.

### Treatment

Before treatment, all patients underwent screening with dynamic contrast enhanced magnetic resonance imaging (MRI), bone scintigraphy and angiography. Subsequently, a surrogate particle, <sup>99m</sup>Tc-macroaggregated albumin (<sup>99m</sup>Tc-MAA) (TechnoScan LyoMaa, Mallinckrodt Medical, Petten, The Netherlands) was intra-arterially injected, directly followed by a <sup>99m</sup>Tc-MAA planar scintigraphy and single-photon emission computed tomography (SPECT)/CT. The <sup>99m</sup>Tc-MAA SPECT/CT was used to calculate the lung shunt fraction (LSF) and to detect other extrahepatic deposition.

RE was performed using yttrium-90 (<sup>90</sup>Y)-labeled glass microspheres (Theraspheres®, BTG International, London, England) according to international guidelines (11). On the same day a <sup>90</sup>Y-positron emission tomography (PET)/CT (mCT, Siemens Healthcare, Erlangen, Germany) was performed to assess the activity distribution. Our acquisition protocol was published earlier (12).

### **Hepatobiliary scintigraphy**

Additional to the standard work-up patients underwent a  $^{99m}\text{Tc}$ -mebrofenin hepatobiliary scintigraphy prior to and three months after RE. Our acquisition protocol is triphasic, similar to the protocol previously described by de Graaf et al. (13). A dual-head gamma camera (Symbia 16T, Siemens Healthcare, Erlangen, Germany) is positioned over the patient, including the heart and liver in the field of view. After intravenous administration of 200 MBq  $^{99m}\text{Tc}$ -mebrofenin (Bridatec, GE Healthcare) 36 dynamic anterior and posterior planar images are acquired over 10 minutes at 10 s per frame, using a low-energy high-resolution collimator (matrix 128 x 128; energy window 130-150 keV). Subsequently, a fast SPECT/CT is performed (matrix 128 x 128; 64 projections in total at 8 s/projection). A low dose CT is acquired for attenuation correction and anatomical reference. Thereafter, a second series of planar scintigraphic images is performed to evaluate biliary secretion (matrix 128 x 128; 30 frames at 60 s/frame).

### **Image analyses**

Analysis of the hepatobiliary scintigraphies was not performed until after treatment (in 2016).

The hepatobiliary scintigraphy data were processed using in-house-developed software (Volumetool (14)), similar to the method described by de Graaf et al. (13). A geometric mean dataset was calculated from the anterior and posterior planar projections of the first dynamic series ( $G_{\text{mean}} = \sqrt{(\text{anterior} \times \text{posterior})}$ ). Regions of interest (ROI's) were drawn on the planar  $G_{\text{mean}}$  dataset around the total image, cardiac blood pool and whole liver to calculate the  $^{99m}\text{Tc}$ -mebrofenin liver uptake rate (expressed in %/min), as previously described by Ekman et al. (15). This value was divided by the body surface area (BSA) to correct for inter-patient variability in metabolic needs (cMUR, expressed as %/min/ $\text{m}^2$ ). Liver and heart ROIs were placed so as to avoid spillover from one to the other. Subsequently, the whole liver was manually delineated on the SPECT/CT images, as well as the treated and non-treated volumes after correlation with Post-treatment  $^{90}\text{Y}$ -PET/CT; enabling assessment of both the volumes and contribution to the liver function. The latter was done by dividing the sum of counts in the ROI of the treated volume by the

total liver counts; representing the contribution of the treated volume to the total cMUR (as calculated on the  $G_{\text{mean}}$  dataset). The contribution of the non-treated volume was identically assessed. Activity in the hilar and extrahepatic bile ducts was excluded from the ROIs to avoid falsely increased regional activity due to biliary excretion.

The tumor absorbed dose and non-tumorous liver absorbed dose of the treated liver parenchyma were calculated using ROVER software (ABX-CRO Advanced Pharmaceutical Services, Dresden, Germany). For each patient, a volume of interest (VOI) was drawn on the  $^{90}\text{Y}$ -PET/CT in the tumors and in the non-tumorous treated liver tissue. To prevent erroneous overlap, the pre-treatment CT was used as a reference. The mean activity in Bq in the VOI was computed. Subsequently, a correction factor was applied to correct for the low number of positrons/Bq. The corrected activity at the time of  $^{90}\text{Y}$ -PET/CT acquisition was recalculated to the corrected activity at time of treatment by adjustment for the radioactive decay. Subsequently, the healthy liver absorbed doses were calculated as follows:

$$\text{Healthy liver absorbed dose (Gy)} = \frac{(50\text{Gy} * \text{Kg/GBq}) \times (\text{Corrected activity in GBq})}{(\text{VOI Volume in ml} \times 1.06 \text{ g/ml})/100}$$

### Case 1

A 74-years-old male with a history of liver cirrhosis due to alcohol abuse was diagnosed with a mass in the right liver lobe at ultrasonography. A subsequent liver CT revealed a multifocal, hypervascular mass in segment 5 and 8 of the liver with contrast washout, consistent with HCC. The largest tumor measured 3.7 cm (tumor involvement 1%). Cirrhosis, splenomegaly and gastro-esophageal varices were also present, but no ascites or portal vein thrombosis. The day of treatment he was graded as Child-Pugh grade A6 / ALBI score grade 1 (Table 1).

The LSF was 9%. He underwent a right lobar treatment (3,1 GBq, target dose 80 Gy). Post-treatment  $^{90}\text{Y}$ -PET/CT showed adequate targeting of the lesion in segment 5 (306 Gy) and 8 (376 Gy). The average absorbed dose of the non-tumorous liver parenchyma was 33 Gy.

**Table 1.** Liver biochemistry tests during follow-up

Case	Time to RE (days)	Bilirubin (mg/dL)	Albumin (g/L)	AST (U/L)	ALT (U/L)	ALP (U/L)	INR	Ascites	AFP (µg/L)
1	-1	0.9	31	72	60	252	1.24 <sup>a</sup>	no	750
	+12	1.2	30	75	51	326	-	minimal	-
	+35	1.1	27	107	59	290	3.49 <sup>a</sup>	-	-
	+65	1.1	24	60	47	286	5.79 <sup>a</sup>	diffuse	-
	+86	2.4	20	62	36	347	1.36 <sup>a</sup>	-	-
2	-1	1.9	27	76	60	115	1.38	minimal	140
	+14	4.3	25	96	58	138	-	moderate	-
	+18	6.7	22	72	84	67	1.8	diffuse	-
	+33	5.6	25	69	45	100	0.9	diffuse	-
	+61	8.2	23	69	170	126	1.7	massive	-
3	+95	11.1	23	250	212	153	-	massive	36
	0	1.6	25	61	46	122	1.18	minimal	270
	+14	2.5	28	80	50	143	1.16	moderate	210
	+30	2.3	22	58	32	126	1.20	moderate	-
	+71	2.2	23	63	37	144	1.20	moderate	-
+160	2.9	23	67	32	156	1.20	massive	5200	

AFP = alpha-fetoprotein, ALP = alkaline phosphatase, ALT = alanine aminotransferase, AST = aspartate aminotransferase, INR = international normalized ratio. <sup>a</sup> = under treatment with coumarine derivatives.

Twelve days after treatment he visited the outpatient clinic with complaints of increasing abdominal girth and weight. He was treated with a low sodium diet and diuretics. Six weeks thereafter he was readmitted because of decompensated cirrhosis with worsening encephalopathy. At three-month follow-up laboratory tests showed grade 2 bilirubin (2.4 mg/dL), grade 3 albumin (20 g/L), grade 1 ALP, AST and ALT toxicity and an elevated ammonia serum value (60 µmol/L). Concurrent liver CT showed ascites in all quadrants, shrinkage of the liver and partial necrosis of the HCC's (partial response of the smaller tumors and stable disease of the largest tumor).

Evaluation of the hepatobiliary scintigraphies showed a whole liver function decline from 3.0%/min/m<sup>2</sup> to 2.4%/min/m<sup>2</sup> (**Table 2**). The function of the treated right hemiliver declined from 2.3%/min/m<sup>2</sup> to 1.6%/min/m<sup>2</sup>, without evident hypertrophy of the left hemiliver (0.8%/min/m<sup>2</sup> vs 0.7%/min/m<sup>2</sup>).

He died four months after RE due to hepatic failure, probably caused by REILD.

**Table 2.** Hepatobiliary scintigraphy measurements at baseline and 3-month follow-up

Case		Baseline			3-month follow-up		
		Liver (total)	Liver (treated)	Liver (non-treated)	Liver (total)	Liver (treated)	Liver (non-treated)
1	Volume	2481	1845	636	1919	1357	562
	%	100	74	26	100	71	29
	cMUR	3.0	2.3	0.7	2.4	1.6	0.8
	%	100	77	23	100	67	33
2	Volume	1396	1178	285	1111	855	256
	%	100	84	16	100	77	23
	cMUR	1.8	1.6	0.2	0.6	0.4	0.2
	%	100	87	13	100	77	23
3	Volume	1288	881	407	1218	713	505
	%	100	68	32	100	59	41
	cMUR	2.2	1.5	0.7	1.8	0.8	1.0
	%	100	70	30	100	43	57

Volume (in ml); cMUR = BSA corrected <sup>99m</sup>Tc-mebrofenin uptake rate (in %/min/ m<sup>2</sup>).

## Case 2

A homeless 57-years-old male with a history of cirrhosis due to alcohol abuse was diagnosed with a multifocal HCC. MRI liver revealed four hypervascular lesions in segment 1 (1.0 cm), 5 (4.4 cm) and 8 (3.2 cm and 0.8 cm), consistent with HCC (tumor involvement 1%). Coexisting liver cirrhosis, portal hypertension and a moderate amount of ascites was

also present, but no portal vein thrombus. At diagnosis he had decompensated cirrhosis, which was recompensated five months later at treatment. He had a Child-Pugh grade B8 at treatment (ALBI grade 3) (Table 1). The LSF was 4%.

He underwent a right lobar treatment (2.5 GBq, target dose 100 Gy). The Post-treatment  $^{90}\text{Y}$ -PET/CT showed reasonable targeting, but also a relatively large amount of activity in the tumor-free segments 6 and 7 with an average absorbed dose of 91 Gy (Figure 1). The absorbed dose for the tumors in segment 1, 5 and 8 was 226 Gy, 63 Gy and 227 Gy, respectively. The absorbed dose of the smallest tumor (0.8 cm) could not reliably be measured.

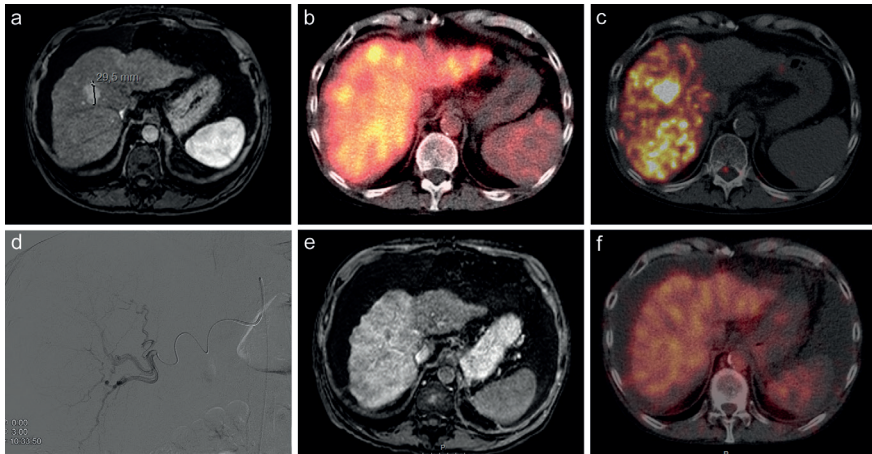


**Figure 1.** Pre- and Post-treatment images of case 2

On the arterial phase of the Pre-treatment MRI a hypervascular lesion in segment 8 is depicted on a background of liver cirrhosis, consistent with a HCC (a). Pre-treatment hepatobiliary scintigraphy shows a visually fairly homogenous  $^{99\text{m}}\text{Tc}$ -mebrofenin uptake with a defect in segment 8, corresponding to the HCC (b). Post-treatment  $^{90}\text{Y}$ -PET/CT shows good targeting of the HCC (227 Gy), but also a significant  $^{90}\text{Y}$  deposition in segment 7 (91 Gy) (c). At treatment angiography the endhole catheter tip was positioned at the bifurcation of the anterior and posterior right hepatic artery. The overdosage of the posterior sector is therefore most likely due to preferential flow (d). Post-treatment MRI and hepatobiliary scintigraphy show ascites and shrinkage of the cirrhotic liver with increased arterial enhancement of the treated lobe and decreased  $^{99\text{m}}\text{Tc}$ -mebrofenin uptake (e, f).

Fourteen days after treatment he was readmitted with increasing ascites and peripheral edema, consistent with decompensated cirrhosis. Two days later he developed a spontaneous bacterial peritonitis, successfully managed with albumin suppletion and antibiotics.

At three-month follow up his liver function had further declined to Child Pugh grade C11, with a grade 3 bilirubin toxicity (**Table 1**). Follow-up MRI at that time showed a partial response of all four lesions, consistent with the decrease in AFP levels. However, also massive ascites and shrinkage of the liver were noted.

At three-month follow-up his liver function had declined to  $0.6\%/min/m^2$  ( $1.8\%/min/m^2$  at baseline). The pre-treatment liver function was mainly located in the right hemiliver ( $1.6\%/min/m^2$ ). After RE this declined to  $0.4\%/min/m^2$ , without compensatory function increase of the left hemiliver (stable at  $0.2\%/min/m^2$ ).

He died four months after RE treatment due to definite REILD (**Figure 2**).

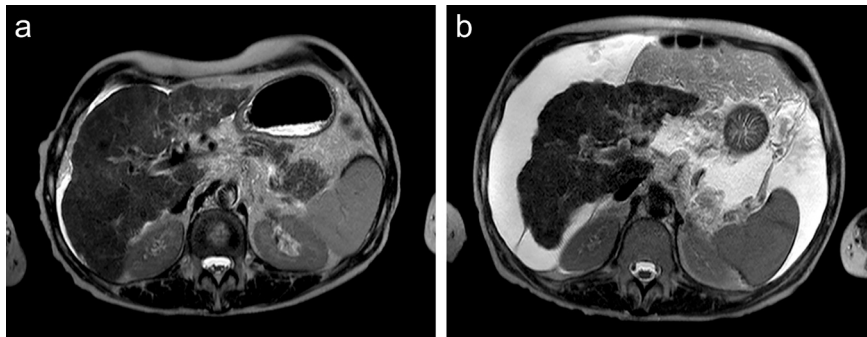


**Figure 2.** Pre- and Post-treatment T2 weighted images of case 2  
On the Pre-treatment image (A) a nodular surface of the liver is seen, consistent with cirrhosis. A small amount of ascites is present. Three months after treatment (B) the liver has atrophied impressively and the amount of ascites has substantially increased, consistent with REILD.

### Case 3

A 74-years-old male with a history of hepatitis B and cirrhosis (Child Pugh grade C11 / ALBI grade 3) was diagnosed with multifocal HCC, which was initially left untreated because of decompensated cirrhosis. After six months he was admitted because of severe hemorrhage of one lesion. He was treated with bland coiling of the arterial supply to this lesion. Another 12 months later his cirrhosis had recompensated (Child Pugh grade B8 / ALBI grade 2) and he opted for RE. At that time his MRI revealed a large HCC located in segment 7/8 (6.6 cm), in segment 4 (6.3 cm) and two smaller lesions in segment 6 (tumor involvement 19%). No portal vein thrombus was present. The LSF was 11%.

He underwent a right lobar treatment (2 GBq; target dose 120 Gy). The Post-treatment  $^{90}\text{Y}$ -PET/CT showed adequate targeting of lesions in segment 6 (243 Gy and 422 Gy) and segment 7/8 (309 Gy). The average absorbed dose of the non-tumorous parenchyma was 32 Gy. Subsequent treatment of segment 4 was cancelled, because of uncorrectable extrahepatic deposition and a LSF of 25% on  $^{99\text{m}}\text{Tc}$ -MAA SPECT/CT one month later.

Follow-up MRI at three and six months showed a partial response of the lesions in segment 6 and 7/8, but progressive growth of the lesion in segment 4. At three-month follow-up the function of the treated liver volume had declined to  $0.8\%/ \text{min}/\text{m}^2$  ( $1.5\%/ \text{min}/\text{m}^2$  at baseline), whereas the non-treated volume showed a minimal functional improvement from  $0.7\%/ \text{min}/\text{m}^2$  to  $1.0\%/ \text{min}/\text{m}^2$  (Figure 3), resulting in a decline of the total liver function from  $2.2\%/ \text{min}/\text{m}^2$  to  $1.8\%/ \text{min}/\text{m}^2$ .

He died one year after RE due to tumor progression (not due to REILD).



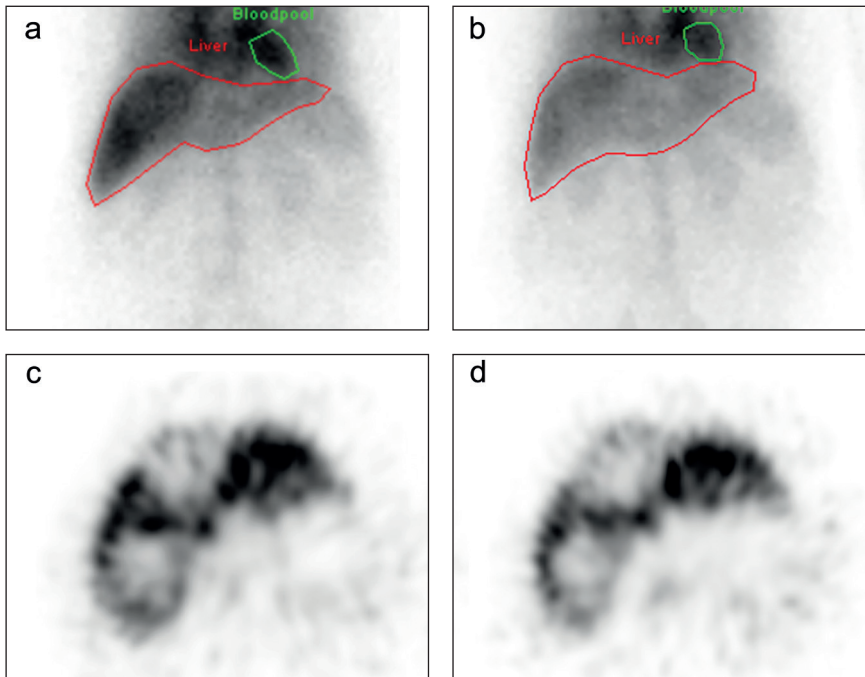


**Figure 3.** Pre- and Post-treatment hepatobiliary scintigraphy images of case 3. The Pre-treatment  $G_{\text{mean}}$  planar image (a) shows that  $^{99\text{m}}\text{Tc}$ -mebrofenin is mainly taken up in the right hemiliver. Centrally in the liver (segment 4) no uptake is seen, due to the presence of a large HCC (c). After treatment ( $G_{\text{mean}}$  planar (b), SPECT (d)) a decrease in total liver uptake is seen, primarily due to a decrease in uptake in the right hemiliver. The left hemiliver has hypertrophied slightly (b: red line, contouring the functional liver). On the SPECT images (c, d) the uptake in the left hemiliver is similar to the Pre-treatment images. The defect in the uptake in segment 4 remains, consistent with the untreated segment 4 lesion (d).

## Discussion

In this case series we presented three cases with a dismal outcome after lobar <sup>90</sup>Y glass microspheres RE treatment. The rapid clinical deterioration in the first two patients was due to REILD. In all three patients Pre-treatment clinical, laboratory and imaging parameters were within acceptable limits for safe treatment, but did not predict the severe toxicity encountered, even though all cases involved lobar treatments only.

Patients amendable for RE commonly have a compromised liver function due to cirrhosis or other underlying liver disease (e.g. prior chemotherapy). Most large published series applied limited exclusion criteria regarding the liver function, often confined to a total bilirubin of <2 mg/dL or <3 mg/dL (2, 16). Consequently, 18-44% of patients, who underwent RE for HCC, had a Child-Pugh B cirrhosis and in up to 2% even a Child-Pugh C cirrhosis (2, 16). In patients who undergo segmental or lobar treatment only, this is generally accepted. However, contrary to hepatectomy candidates, Pre-treatment quantitative segmental assessment of the liver function is often lacking (17). In other words: is the liver function of the non-treated lobe sufficient to compensate for radiation damage in the treated part of the liver?

Adequate assessment of the overall liver function is difficult due to the diversity of its functions (e.g. detoxification, synthesis, etc). Several clinical scoring systems (incorporating some of these functions) exist to estimate overall survival and eligibility for hepatectomy in patients with cirrhosis (18). Of these, the Child-Pugh score is best-known. However, considerable heterogeneity exists within the Child-Pugh categories, resulting in an unreliable prediction of liver failure after hepatectomy (19, 20). The recently introduced ALBI scoring system might be more successful in these predictions (19). The ALBI score has shown to be a successful predictor of survival after RE, though its correlation with hepatotoxicity is not known (21).

Contrary to the clinical scoring systems, hepatobiliary scintigraphy with SPECT/CT allows for quantification of a non-uniform distribution of the liver function, as often seen in cirrhosis (13). The visualization and quantification of possible regional differences in liver function can be crucial in large liver resections or segmental liver-directed treatments, as illustrated by our cases. In all cases a right lobar treatment was performed to spare the non-tumorous

liver parenchyma. Unfortunately, most of the functional liver tissue was located in the treated right hemiliver (70-87%), resulting in considerable liver function decline, both clinically and at hepatobiliary scintigraphy. Prior knowledge of these segmental differences probably would have led to a change in treatment strategy or renouncement (17, 22).

De Graaf et al. suggested a cMUR cut-off value of 2.69%/min/m<sup>2</sup>, after analysis of hepatobiliary scintigraphies of 55 patients before and after major hepatectomy (7). Nine of their patients developed postoperative liver failure (8/9 with compromised livers), which was lethal in 8/9 cases. The cut-off value of 2.69%/min/m<sup>2</sup> rightly identified all but one patient with postoperative liver failure. In contrary, CT volumetry-based cut-off values failed to identify two cases and in case of BSA corrected volumes even three cases. Furthermore, for hepatobiliary scintigraphy one cut-off value sufficed for both compromised and normal livers, whereas cut-off values for CT volumetry varied.

The cut-off value of 2.69%/min/m<sup>2</sup> implies a serious risk of liver failure in the presented cases, of whom two developed fatal REILD. Interestingly, the data in **Table 2** show no compensatory hypertrophy of the non-treated lobes in the first 2 cases, indicative of a severely compromised liver regeneration. However, in the third case the non-treated lobe had hypertrophied (25% volume increase) with a liver function increase of 43% from 0.7 to 1.0%/min/m<sup>2</sup>. The regeneration capacity in this case may explain the longer survival, as hypertrophy is known to continue up to 12 months after RE (23).

According to the device instruction manual for glass microspheres (24) a target dose of 120 Gy (range 80-150 Gy) is suggested for the treated liver volume, in principle ignoring the presence of underlying liver disease, TNR and liver volume (total volume and % treated volume). Yet, a definite relationship exists between the absorbed dose in the non-tumorous parenchyma ( $D_{ntp}$ ) and hepatotoxicity (25, 26). Chiesa et al. (25) identified a tolerance dose of 75 Gy for 15% RE-related hepatotoxicity ( $=TD_{15 \text{ whole liver}}$ ) in 43 HCC patients with a Child-Pugh A cirrhosis after lobar RE with glass microspheres (based on the <sup>99m</sup>Tc-MAA SPECT data). In contrary, 83% of their Child-Pugh B7 patients had RE-related liver failure at a mean liver dose <60 Gy (27). All Child-Pugh A patients (6/43) with hepatotoxicity had a mean liver dose >60 Gy and at least 58% of the liver volume treated. Our findings are consistent with these results.

Logically, also a positive relationship exists between tumor dose ( $D_{\text{tumor}}$ ) and tumor response (25, 26, 28). Garin et al. suggested a  $^{99m}\text{Tc}$ -MAA SPECT/CT based tumor response threshold dose (TTD) of 205 Gy for HCC treatment with glass microspheres, using measurements similar to ours (2 cc VOI in tumor and non-tumorous tissue) (29). This TTD is consistent with the findings of Chiesa et al. (217 Gy) (25). However, larger lesions require a higher  $D_{\text{tumor}}$ ; i.e. >1000 Gy for lesions >10 cc to achieve 50% tumor control probability (25). In our patients three out of four lesions > 10 cc were treated with >217 Gy (case 1: 306 Gy/ case 2: 226 Gy and 227 Gy/ case 3: 309 Gy). Yet, all lesions showed partial response, except the lesion in case 1. Nonetheless, target dose and volume planning in case of larger and/or necrotic lesions is more difficult. In these cases extra caution has to be taken with regard to treatment intensification or retreatments to prevent serious hepatotoxicity, especially in the presence of cirrhosis. Hepatobiliary scintigraphy may help in this patient selection.

This case series is obviously limited by patient number, caused by preliminary closure of the TRACE study in our hospital. However, it is the first case series on liver-directed RE that shows the potential benefit of imaging-based quantification of liver function and its segmental distribution, complementary to systemic assessment of overall liver function. Patients with a marginal Pre-treatment liver function, as suspected after routine evaluation, may be further screened by hepatobiliary scintigraphy for improved treatment planning. Definition and validation of thresholds for safe treatment should be based on clinical data. Large studies should answer questions with regard to the minimal acceptable remaining liver function and the numeric relation between the absorbed dose to the functional liver parenchyma and the decline in liver function Post-treatment.

## **Conclusion**

Based on this case series, hepatobiliary scintigraphy seems to be complementary to current patient selection based on clinical, laboratory and imaging parameters alone. Although thresholds for safe treatment should be determined and validated in large patient series, the potential of hepatobiliary scintigraphy to quantify segmental liver function, in contrast to overall liver function, seems imperative for RE treatment planning.

## References

- Lewandowski RJ, Kulik LM, Riaz A, Senthilnathan S, Mulcahy MF, Ryu RK, et al. A comparative analysis of transarterial downstaging for hepatocellular carcinoma: chemoembolization versus radioembolization. *Am J Transplant.* 2009;9(8):1920-8.
- Salem R, Lewandowski RJ, Kulik L, Wang E, Riaz A, Ryu RK, et al. Radioembolization results in longer time-to-progression and reduced toxicity compared with chemoembolization in patients with hepatocellular carcinoma. *Gastroenterology.* 2011;140(2):497-507 e2.
- Gordon AL, R; Hickey, R; Kallini, J; Gabr, A; Sato, K; Desai, K; Thornburg, B; Gates, V; Ganger, D. Prospective randomized phase 2 study of chemoembolization versus radioembolization in hepatocellular carcinoma: results from the PREMIERE trial. *Journal of Vascular and Interventional Radiology.* 2016;3(27).
- Kennedy AS, Nutting C, Coldwell D, Gaiser J, Drachenberg C. Pathologic response and microdosimetry of (90)Y microspheres in man: review of four explanted whole livers. *Int J Radiat Oncol Biol Phys.* 2004;60(5):1552-63.
- M.G.E.H. BMNvEKEZBAvdBMAAJL. Radioembolization Induced Liver Disease: a systematic review. *European Journal of Gastroenterology & Hepatology.* 2016:Accepted for publication.
- Kula M, Karacavus S, Baskol M, Deniz K, Abdulrezzak U, Tutus A. Hepatobiliary function assessed by 99mTc-mebrofenin cholescintigraphy in the evaluation of fibrosis in chronic hepatitis: histopathological correlation. *Nucl Med Commun.* 2010;31(4):280-5.
- de Graaf W, van Lienden KP, Dinant S, Roelofs JJ, Busch OR, Gouma DJ, et al. Assessment of future remnant liver function using hepatobiliary scintigraphy in patients undergoing major liver resection. *J Gastrointest Surg.* 2010;14(2):369-78.
- Dinant S, de Graaf W, Verwer BJ, Bennink RJ, van Lienden KP, Gouma DJ, et al. Risk assessment of posthepatectomy liver failure using hepatobiliary scintigraphy and CT volumetry. *J Nucl Med.* 2007;48(5):685-92.
- Erdogan D, Heijnen BH, Bennink RJ, Kok M, Dinant S, Straatsburg IH, et al. Preoperative assessment of liver function: a comparison of 99mTc-Mebrofenin scintigraphy with indocyanine green clearance test. *Liver Int.* 2004;24(2):117-23.
- Seinstra BA, Defreyne L, Lambert B, Lam MG, Verkooijen HM, van Erpecum KJ, et al. Transarterial radioembolization versus chemoembolization for the treatment of hepatocellular carcinoma (TRACE): study protocol for a randomized controlled trial. *Trials.* 2012;13:144.
- Giammarile F, Bodei L, Chiesa C, Flux G, Forrer F, Kraeber-Bodere F, et al. EANM procedure guideline for the treatment of liver cancer and liver metastases with intra-arterial radioactive compounds. *Eur J Nucl Med Mol Imaging.* 2011;38(7):1393-406.
- Elschot M, Vermolen BJ, Lam MG, de Keizer B, van den Bosch MA, de Jong HW. Quantitative comparison of PET and Bremsstrahlung SPECT for imaging the in vivo yttrium-90 microsphere distribution after liver radioembolization. *PLoS One.* 2013;8(2):e55742.
- de Graaf W, van Lienden KP, van Gulik TM, Bennink RJ. (99m)Tc-mebrofenin hepatobiliary scintigraphy with SPECT for the assessment of hepatic function and liver functional volume before partial hepatectomy. *J Nucl Med.* 2010;51(2):229-36.

14. Bol GH, Kotte AN, van der Heide UA, Legendijk JJ. Simultaneous multi-modality ROI delineation in clinical practice. *Comput Methods Programs Biomed.* 2009;96(2):133-40.
15. Ekman M, Fjalling M, Friman S, Carlson S, Volkmann R. Liver uptake function measured by IODIDA clearance rate in liver transplant patients and healthy volunteers. *Nucl Med Commun.* 1996;17(3):235-42.
16. Golfieri R, Bilbao JI, Carpanese L, Cianni R, Gasparini D, Ezziddin S, et al. Comparison of the survival and tolerability of radioembolization in elderly vs. younger patients with unresectable hepatocellular carcinoma. *J Hepatol.* 2013;59(4):753-61.
17. Shen S, Jacob R, Bender LW, Duan J, Spencer SA. A technique using 99mTc-mebrofenin SPECT for radiotherapy treatment planning for liver cancers or metastases. *Med Dosim.* 2014;39(1):7-11.
18. Ge PL, Du SD, Mao YL. Advances in preoperative assessment of liver function. *Hepatobiliary Pancreat Dis Int.* 2014;13(4):361-70.
19. Johnson PJ, Berhane S, Kagebayashi C, Satomura S, Teng M, Reeves HL, et al. Assessment of liver function in patients with hepatocellular carcinoma: a new evidence-based approach-the ALBI grade. *J Clin Oncol.* 2015;33(6):550-8.
20. Nagashima I, Takada T, Okinaga K, Nagawa H. A scoring system for the assessment of the risk of mortality after partial hepatectomy in patients with chronic liver dysfunction. *J Hepatobiliary Pancreat Surg.* 2005;12(1):44-8.
21. Hickey R, Mouli S, Kulik L, Desai K, Thornburg B, Ganger D, et al. Independent Analysis of Albumin-Bilirubin Grade in a 765-Patient Cohort Treated with Transarterial Locoregional Therapy for Hepatocellular Carcinoma. *J Vasc Interv Radiol.* 2016.
22. Bennink RJ, Cieslak KP, van Delden OM, van Lienden KP, Klumpen HJ, Jansen PL, et al. Monitoring of Total and Regional Liver Function after SIRT. *Front Oncol.* 2014;4:152.
23. Theysohn JM, Ertle J, Muller S, Schlaak JF, Nensa F, Sipilae S, et al. Hepatic volume changes after lobar selective internal radiation therapy (SIRT) of hepatocellular carcinoma. *Clin Radiol.* 2014;69(2):172-8.
24. Nordion. Theraspheres Manual [www.therasphere.com](http://www.therasphere.com).
25. Chiesa C, Mira M, Maccauro M, Spreafico C, Romito R, Morosi C, et al. Radioembolization of hepatocarcinoma with (90)Y glass microspheres: development of an individualized treatment planning strategy based on dosimetry and radiobiology. *Eur J Nucl Med Mol Imaging.* 2015;42(11):1718-38.
26. Strigari L, Sciuto R, Rea S, Carpanese L, Pizzi G, Soriani A, et al. Efficacy and toxicity related to treatment of hepatocellular carcinoma with 90Y-SIR spheres: radiobiologic considerations. *J Nucl Med.* 2010;51(9):1377-85.
27. Chiesa C, Mira M, Maccauro M, Romito R, Spreafico C, Sposito C, et al. A dosimetric treatment planning strategy in radioembolization of hepatocarcinoma with 90Y glass microspheres. *QJ Nucl Med Mol Imaging.* 2012;56(6):503-8.
28. Garin E, Lenoir L, Edeline J, Laffont S, Mesbah H, Poree P, et al. Boosted selective internal radiation therapy with 90Y-loaded glass microspheres (B-SIRT) for hepatocellular carcinoma patients: a new personalized promising concept. *Eur J Nucl Med Mol Imaging.* 2013;40(7):1057-68.
29. Garin E, Lenoir L, Rolland Y, Edeline J, Mesbah H, Laffont S, et al. Dosimetry based on 99mTc-macroaggregated albumin SPECT/CT accurately predicts tumor response and survival in hepatocellular carcinoma patients treated with 90Y-loaded glass microspheres: preliminary results. *J Nucl Med.* 2012;53(2):255-63.



The background of the entire page is a dense field of multi-colored confetti, including shades of red, green, blue, yellow, and white.

# CHAPTER SIX

## A pilot study on hepatobiliary scintigraphy to monitor regional liver function in yttrium-90 radioembolization

Sandra van der Velden, Manon N.G.J.A. Braat, Tim A. Labeur, Mike V. Scholten,  
Otto M. van Delden, Roelof J. Bennink, Hugo W.A.M. de Jong, Marnix G.E.H. Lam

*Journal of Nuclear Medicine* 2019 Oct; 60(10):1430-1436.



## Abstract

### Background

Radioembolization is increasingly used as a bridge to resection (i.e. radiation lobectomy). It combines ipsilateral tumor control with the induction of contralateral hypertrophy to facilitate lobar resection. The aim of this pilot study was to investigate the complementary value of hepatobiliary scintigraphy (HBS) before and after radioembolization in the assessment of the future remnant liver.

### Methods

Consecutive patients with liver tumors who underwent HBS before and after yttrium-90 (<sup>90</sup>Y) radioembolization were included. Regional (treated/non-treated) and whole liver function and volume were determined on HBS and CT. Changes in regional liver function and volume were correlated with the functional liver absorbed doses, determined on <sup>90</sup>Y-PET/CT. In addition, the correlation between liver volume and function change was evaluated.

### Results

Thirteen patients (10 HCC, 3 mCRC) were included. Liver function of the treated part declined after radioembolization (HBS-pre: 4.0 %/min/m<sup>2</sup>; HBS-post: 1.9 %/min/m<sup>2</sup>; p=0.001 ), while the function of the non-treated part increased (HBS-pre: 1.4 %/min/m<sup>2</sup>; HBS-post: 2.8 %/min/m<sup>2</sup>; p=0.009 ). Likewise, the treated volume decreased (pre-treatment: 1118.7 ml (360.4 – 1790.8); post-treatment: 870.7 ml (441.0 – 1327.6) p=0.003 ), while the non-treated volume increased (pre-treatment: 412.7 ml (107.2 – 910.8); post-treatment: 577.6 ml (193.5 – 1278.4) p=0.005). Bland-Altman analysis revealed a large bias (29%) between volume decrease and function decrease in the treated part and wide limits of agreement (-7.7 – 65.6 % point). The bias between volume and function change was smaller (-6.0%) in the non-treated part of the liver, but limits of agreement were still wide (-117.9 – 106.7 % point).

### Conclusion

Radioembolization induces regional changes in liver function that are accurately detected by HBS. Limits of agreement between function and volume changes were wide, showing large individual differences. This implicates that HBS may have a complementary role in the management of patients treated with radioembolization.

## Introduction

In radioembolization, radioactive microspheres (e.g. yttrium-90 ( $^{90}\text{Y}$ ) or holmium-166 ( $^{166}\text{Ho}$ )) are injected in (branches of) the hepatic artery (1). The microspheres primarily lodge in the tumor, resulting in a high radiation absorbed tumor dose, while part of the microspheres will lodge in the 'healthy' functional liver, irradiating functional liver tissue. When only part of the liver is treated, the radiation damage induces a decrease in functional liver volume in the treated part and an increase in functional liver volume in the non-treated part (2). This may have implications for subsequent treatments, including surgical resection of the involved part of the liver.

There has been a growing interest in radioembolization as a bridge to transplant (3), and more recently as a bridge to resection (4) (i.e. radiation lobectomy), especially in hepatocellular carcinoma (HCC) patients. Although considered curative, many patients are excluded from surgery because of inadequate future liver remnant (FLR) volume. Radioembolization has been found to effectively induce FLR volumetric hypertrophy, while simultaneously providing tumor control. As such, it may have benefits over portal vein embolization (PVE), the current standard of care in these patients (4).

Currently, management of patients for radiation lobectomy is based on clinical, laboratory and imaging parameters (e.g. volumetry). Liver function is tested using blood markers (e.g. bilirubin, albumin, etc.) and clinically derived scores (e.g. Child-Pugh, MELD, etc.). Although this gives an indication of global liver function, liver function may actually be heterogeneously distributed, especially in patients with known underlying liver disease such as cirrhosis or large/unilateral liver tumors. Hypertrophy of the FLR may therefore be insufficient for subsequent resection. A better understanding of the dose-effect relationship between radioembolization and FLR hypertrophy, in combination with a more accurate assessment of FLR in terms of functional liver reserve, may lead to better selection, planning, and monitoring of patients who have an indication for radiation lobectomy.

Quantitative total and regional liver function can be measured using hepatobiliary scintigraphy (HBS) with technetium-99m ( $^{99\text{m}}\text{Tc}$ )-mebrofenin (Bridatec, GE Healthcare B.V.,

Eindhoven, the Netherlands). HBS with  $^{99m}\text{Tc}$ -mebrofenin prior to hepatectomy adequately predicts the risk of post-surgical liver failure (5-7). A cut-off value of 2.69 %/min/m<sup>2</sup> (body surface area corrected  $^{99m}\text{Tc}$ -mebrofenin uptake rate) in the FLR was reported to accurately identify patients at risk of liver failure, regardless of underlying liver disease, improving the pre-surgical work-up based on liver volumetry alone (6-8).

Two case studies (9,10) reported on the feasibility of HBS to monitor regional liver function changes after radioembolization. The aim of this pilot study was to investigate the potential complementary value of regional function assessment in the management of radiation lobectomy by analyzing the correlation between regional liver function and volume changes.

## Methods

### Patient selection

All patients treated with radioembolization (n=356) between April 2012 and February 2018 were reviewed. All patients who underwent HBS pre- and post-treatment (n=17) were evaluated. Two patients were excluded from the study, because the post-treatment HBS was acquired more than four months after treatment (i.e. 17 and 7.5 months). One patient was excluded because of additional liver-directed treatment (i.e. radio frequency ablation) between radioembolization and post-treatment HBS, and one patient was excluded because of treatment with holmium-166 ( $^{166}\text{Ho}$ ) microspheres and not yttrium-90 ( $^{90}\text{Y}$ ) microspheres. Hence, data of 13 patients were retrospectively analyzed. Three of these patients were earlier included in a case series by Braat et al. (9). The medical ethics committee waived the need for informed consent.

### Radioembolization

The regular work-up included three-phase computed tomography (CT) and/or magnetic resonance imaging (MRI) and clinical/laboratory assessment of liver function. Prior to radioembolization treatment, all patients underwent a safety procedure. During this procedure, a scout dose of approximately 150 MBq  $^{99m}\text{Tc}$  macro-aggregated albumin ( $^{99m}\text{Tc}$ -MAA) (TechneScan LyoMaa, Mallinckrodt Medical, Petten, the Netherlands) was

intra-arterially injected. Immediately after,  $^{99m}\text{Tc}$ -MAA planar scintigraphy was obtained, followed by  $^{99m}\text{Tc}$ -MAA single-photon computed tomography (SPECT)/CT. The lung shunt fraction was determined on planar scintigraphy, SPECT/CT was used to detect extrahepatic depositions.

All patients were treated with  $^{90}\text{Y}$  glass microspheres (Theraspheres<sup>®</sup>, BTG International, London, Great Britain). The administered activity was calculated using the MIRD model (11). The procedure was performed according to international guidelines (12).

### **Hepatobiliary scintigraphy**

After intravenous administration of approximately 200 MBq of  $^{99m}\text{Tc}$ -mebrofenin, a dual head gamma camera (Symbia T16, Siemens Healthcare, Erlangen, Germany) was positioned over the patient, including the heart and liver in the field of view. The gamma camera was mounted with a low-energy high-resolution collimator. The acquisition protocol consisted of three phases (13). First, 36 dynamic anterior and posterior images were acquired with a frame duration of 10 seconds (matrix: 128 x 128, energy window: 140 keV  $\pm$  7.5%, zoom: 1.00). Second, a fast SPECT/CT was acquired (matrix: 128 x 128, energy window: 140 keV  $\pm$  7.5%, 64 projections, 8 s/projection, zoom: 1.45). A low-dose CT was acquired for attenuation correction and a diagnostic contrast-enhanced CT (CECT) was acquired for anatomical reference. In the last phase, 30 dynamic planar frames were acquired with a frame duration of 60 seconds (matrix: 128 x 128, energy window: 140 keV  $\pm$  7.5%, zoom: 1.00) to evaluate biliary excretion. We will refer to HBS acquired prior to treatment as HBS-pre and HBS acquired after treatment as HBS-post.

### **$^{90}\text{Y}$ -PET/CT**

On the same day or the day after radioembolization,  $^{90}\text{Y}$  positron emission tomography (PET)/CT (Siemens Biograph mCT Time-Of-Flight (TOF)) was acquired to assess the activity distribution. Acquisition time was 15 minutes per bed position (30 minutes total) and consecutive bed positions overlapped approximately 43%. A low-dose CT (120 kVp, 40 mAs) was acquired for attenuation correction. PET images were reconstructed using the ordinary Poisson ordered subset expectation maximization reconstruction method, including resolution recovery, TOF information, and attenuation, random and scatter

correction. Images were reconstructed using 4 iterations and 21 subsets and were smoothed with a 5 mm full-width-at-half-maximum Gaussian filter. The reconstructed voxel size was 3.9 x 3.9 x 4.0 mm<sup>3</sup>.

## Image analysis

### *Hepatobiliary scintigraphy*

HBS was analyzed similar to the method described by de Graaf et al. (13). A geometric mean dataset was calculated from the anterior and posterior dynamic projections of the first acquisition phase. Regions of interest around the total image, liver and cardiac blood pool were manually delineated. Subsequently, the <sup>99m</sup>Tc-mebrofenin uptake rate (MUR) expressed in %/min was calculated according to the method of Ekman et al. (14). The liver uptake rate was divided by the body surface area (cMUR, expressed in %/min/m<sup>2</sup>) to correct for variability in metabolic need.

Regional liver uptake values were determined on SPECT using Simplicit<sup>90Y</sup>™ software (Mirada Medical Limited, Oxford, Great Britain). The accompanying CECT was used for anatomical reference. When no CECT was obtained during HBS, the low-dose CT scan used for attenuation correction was rigidly registered to a previously acquired CECT scan. When no CECT was available (n = 2), the low-dose CT was rigidly registered to an MRI for anatomical reference.

The whole liver and tumors were semi-automatically delineated on CECT. The hilar and extrahepatic bile ducts were excluded from the whole liver volume of interest (VOI). After rigid registration with post-treatment <sup>90</sup>Y-PET/CT, the liver VOI was manually divided into a treated (excluding tumors) and non-treated part, based on the <sup>90</sup>Y distribution. The function of the treated and non-treated part was subsequently calculated as follows (7):

$$cMUR_i = \frac{C_i}{C_{liver}} \cdot cMUR_{liver^j}$$

where  $cMUR_i$  is the liver uptake rate in VOI  $i$  (i.e. treated or non-treated part),  $C_i$  the number of counts in VOI  $i$ ,  $C_{liver}$  the number of counts in the whole liver and  $cMUR_{liver}$  the liver uptake rate calculated from the dynamic planar images. Besides liver uptake rate, volumes [ml] of the different VOIs were also obtained from Simplicity<sup>90Y</sup>.

### **<sup>90</sup>Y-PET/CT**

Functional liver parenchyma absorbed dose was calculated using Simplicity<sup>90Y</sup>™ software. The <sup>90</sup>Y-PET/CT images were rigidly registered to the CECT used to analyze HBS-pre to allow the use of identical VOIs.

### **Statistical analysis**

Statistical analysis was performed using the Python module Scipy version 0.16.0 (Python Software Foundation, <https://www.python.org/>). Categorical variables were described as frequencies (percentage) and continuous data was expressed as median (range). Due to the limited sample size, data did not follow a normal distribution. Therefore, differences between groups were tested with the non-parametric Wilcoxon signed-rank test. Correlation between variables was tested using the Spearman correlation coefficient  $\rho$ . Correspondence between measurements was analyzed using Bland-Altman plots. A p-value of 0.05 or less was considered significant.

### **Results**

Between April 2012 and February 2018, 13 patients (11 male, 2 female) underwent an HBS within four months before and after radioembolization treatment, thereby fulfilling the inclusion criteria. Patient characteristics can be found in **Table 1**. Ten patients had hepatocellular carcinoma (HCC) and three patients had metastases from a colorectal carcinoma (mCRC). The treatment intent was palliative in five patients and eight patients underwent radioembolization for downstaging and/or induction of hypertrophy to enable hepatectomy. Five patients were successfully resected. The other patients had either progression of disease ( $n = 2$ ) or insufficient remnant liver function for subsequent surgery ( $n=1$ ).

**Table 1.** Patient characteristics.

<b>Characteristic (n=13)</b>	
<b>Age (y)</b>	68 (50-78)
<b>Sex</b>	
Male	11 (85%)
Female	2 (15%)
<b>Primary malignancy</b>	
HCC	10 (77%)
mCRC	3 (23%)
<b>Treatment</b>	
Lobar	11 (85%)
Right	11 (85%)
Left	0 (0%)
Superselective	2 (15%)
<b>Administered <sup>90</sup>Y activity (GBq)</b>	2.58 (1.17 – 7.11)
<b>Time from <sup>90</sup>Y calibration to treatment (days)<sup>†</sup></b>	9 (2 – 11)
<b>Estimated number of administered microspheres<sup>†</sup></b>	4.81 <sup>‡</sup> (1.71 <sup>‡</sup> – 13.8 <sup>‡</sup> )
<b>Average absorbed <sup>90</sup>Y dose (Gy)</b>	
Treated part	102.9 (71.8 – 125.3)
Functional parenchyma	83.4 (71.6 – 117.0)
Tumor	174.3 (66.7 – 335.8)
<b>Time from HBS-pre to treatment (days)</b>	26 (10 – 64)
<b>Time from treatment to HBS-post (days)</b>	92 (58 – 111)
<b>Cirrhosis</b>	6 (46%)
<b>Portal hypertension</b>	4 (31%)
<b>Blood marker at baseline (HBS-pre)</b>	9 (5 – 31)

Table 1. Continued.

<b>Characteristic (n=13)</b>	
<b>Bilirubin (<math>\mu\text{mol/L}</math>)</b>	
Albumin (g/L)	39.6 (30.2 – 46.1)
AST (U/L)	52 (22 – 313)
ALT (U/L)	45 (12 – 113)
GGT (U/L)	108 (66 – 386)
ALP (U/L)	142 (62 – 199)
INR*	1.03 (0.82 – 1.40)
ALBI score	-2.83 (-3.21 – -1.58)
Grade 1	10 (77%)
Grade 2	3 (23%)
Grade 3	0 (0%)
<b>Blood marker at follow-up (HBS-post)</b>	
Bilirubin ( $\mu\text{mol/L}$ )*	10 (5 – 164)
Albumin (g/L)	38.7 (20.2 – 45.0)
AST (U/L)	51 (24 – 403)
ALT (U/L)	36 (8 – 232)
GGT (U/L)	204 (66 – 804)
ALP (U/L)	176 (73 – 347)
INR*	1.06 (0.84 – 1.74)
ALBI score*	-2.60 (-3.13 – -0.55)
Grade 1	6 (50%)
Grade 2	3 (25%)
Grade 3	3 (25%)

Continuous values are expressed as median (range). Categorical values are expressed as frequencies (percentage). HCC = hepatocellular carcinoma, mCRC = metastatic colorectal carcinoma, AST = aspartate aminotransferase, ALT = alanine aminotransferase, GGT = gamma-glutamyltransferase, ALP = alkaline phosphatase, INR = international normalized ratio, ALBI = albumin-bilirubin. † n = 8; \* n = 12



In general, treatment-induced toxicity within three months after treatment was mild. Median follow-up was 7 (1 – 30) months. Three patients died within six months after treatment, of whom two died due to radioembolization induced liver disease (REILD) (9) and one patient died due to rapid tumor progression after radioembolization treatment.

HBS whole liver function (pre- and post-treatment) was correlated with bilirubin (pre-treatment: Spearman  $\rho=-0.73$ ,  $p=0.004$ ; post-treatment: Spearman  $\rho=-0.64$ ,  $p=0.025$ ), albumin (pre-treatment: Spearman  $\rho=0.63$ ,  $p=0.021$ ; post-treatment: Spearman  $\rho=0.80$ ,  $p=0.001$ ), aspartate aminotransferase (AST) (pre-treatment: Spearman  $\rho=-0.68$ ,  $p=0.010$ ; post-treatment: Spearman  $\rho=-0.84$ ,  $p<0.001$ ), and international normalized ratio (INR) (pre-treatment: Spearman  $\rho=-0.58$ ,  $p=0.046$ ; post-treatment: Spearman  $\rho=-0.51$ ,  $p=0.090$ ). When bilirubin and albumin were combined into the ALBI score (15), the correlation was even stronger (pre-treatment: Spearman  $\rho=-0.75$ ,  $p=0.003$ ; post-treatment: Spearman  $\rho=-0.85$ ,  $p<0.001$ ). Whole liver volume did not correlate with bilirubin, albumin, AST, INR or any other blood value at baseline or follow-up.

HBS whole liver and regional (treated/non-treated) liver function and volume at baseline and follow-up of each individual patient can be found in the supplementary material (**Supplemental Table 1**). Overall, liver function of the treated part declined after radioembolization (**Figure 1**)(HBS-pre: 4.0 %/min/m<sup>2</sup> (1.4 – 7.2); HBS-post: 1.9 %/min/m<sup>2</sup> (0.4 – 3.8);  $p=0.001$ ), while the function of the non-treated part increased (HBS-pre: 1.4 %/min/m<sup>2</sup> (0.2 – 6.4); HBS-post: 2.8 %/min/m<sup>2</sup> (0.1 – 6.5);  $p=0.009$ ) (**Figure 2a and 3a**). The increase in function of the non-treated part did not fully compensate the decline in function of the treated part. This was reflected by the decrease in whole liver function seen in most patients (HBS-pre: 6.3 %/min/m<sup>2</sup> (1.8 – 11.0); HBS-post: 5.1 %/min/m<sup>2</sup> (0.6 – 10.6);  $p=0.009$ ). In only one patient, whole liver function increased after treatment, mainly due to a large increase in liver function in the non-treated part (+98.4%), while the function of the treated part only showed a minor decline (-5.6%). In two patients, liver function declined in the non-treated part of the liver. One had a limited liver function at baseline (whole liver: 1.8 %/min/m<sup>2</sup>; non-treated liver: 0.2 %/min/m<sup>2</sup>) and died four months after treatment as a result of definite REILD (9). The other patient had massive tumor progression in both the treated and non-treated part of the liver and died five months after treatment.

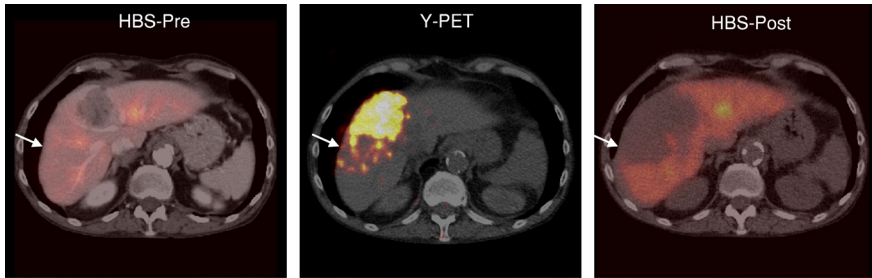


**Figure 1.** Example of regional liver function decline after  $^{90}\text{Y}$  radioembolization. Part of the functional liver parenchyma received a high absorbed dose of  $^{90}\text{Y}$  (103 Gy on the functional liver, 231 Gy on the tumor). This was reflected on HBS-post, where that particular part of the functional liver lost most of its function (HBS-pre: 2.4 %/min/m<sup>2</sup>; HBS-post: 0.6 %/min/m<sup>2</sup>).

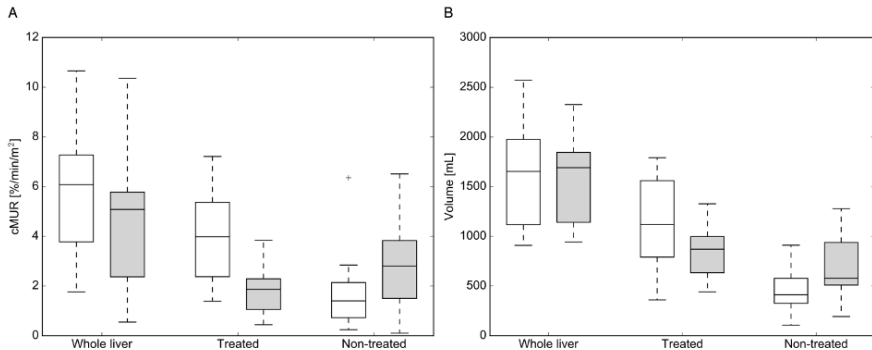


**Figure 2.** (a) Boxplot of liver function obtained from HBS-pre (white) and HBS-post (grey). Whole liver function declined (HBS-pre: 6.3 %/min/m<sup>2</sup> (1.8 – 11.0); HBS-post: 5.1 %/min/m<sup>2</sup> (0.6 – 10.6);  $p=0.009$ ). Liver function in the treated part declined (HBS-pre: 4.0 %/min/m<sup>2</sup> (1.4 – 7.2); HBS-post: 1.9 %/min/m<sup>2</sup> (0.4 – 3.8);  $p=0.001$ ). Liver function in the non-treated part increased (HBS-pre: 1.4 %/min/m<sup>2</sup> (0.2 – 6.4); HBS-post: 2.8 %/min/m<sup>2</sup> (0.1 – 6.5);  $p=0.009$ ). (b) Boxplot of liver volume pre- (white) and post-treatment (grey). Whole liver volume was stable (pre-treatment: 1683.3 ml (983.5 – 3112.5); post-treatment: 1792.4 ml (1012.4 – 3161.2);  $p=0.600$ ). Healthy liver volume in the treated part decreased (pre-treatment: 1118.7 ml (360.4 – 1790.8); post-treatment: 870.7 ml (441.0 – 1327.6);  $p=0.003$ ), while the non-treated volume increased (pre-treatment: 412.7 ml (107.2 – 910.8); post-treatment: 577.6 ml (193.5 – 1278.4);  $p=0.005$ ).

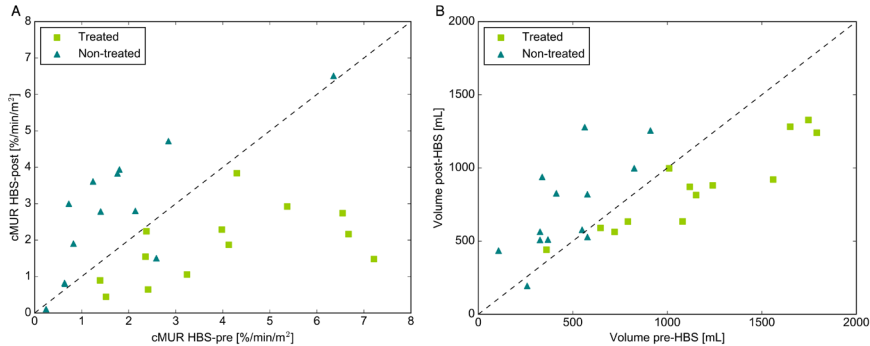


**Figure 3.** (a) Liver function obtained from the HBS-pre and HBS-post and (b) liver volume pre- and post-treatment for each individual patient. Points above the dashed line indicate function/volume increase, points below the dashed line indicate function/volume decline.

In most patients ( $n=12$ ), treated volume decreased (pre-treatment: 1118.7 ml (360.4 – 1790.8); post-treatment: 870.7 ml (441.0 – 1327.6);  $p=0.003$ ), while the non-treated volume increased (pre-treatment: 412.7 ml (107.2 – 910.8); post-treatment: 577.6 ml (193.5 – 1278.4);  $p=0.005$ ) (Figures 2b, 3b and 4). Whole liver volume, however, did not change significantly after radioembolization (pre-treatment: 1683.3 ml (983.5 – 3112.5); post-treatment: 1792.4 ml (1012.4 – 3161.2);  $p=0.600$ ). For two patients, both with cirrhotic livers, volume of the non-treated part decreased after radioembolization. One of these patients also had a decrease in liver function and died of REILD four months after treatment, as described above. The other patient had a slight increase of function in the non-treated part (+29.2%), but died four months after treatment due to hepatic failure (probably REILD, whole liver function post-treatment: 2.4 %/min/m<sup>2</sup>) (9).

No correlation was found between the absorbed dose in the treated functional liver tissue and the absolute function change ( $cMUR_{post} - cMUR_{pre}$ ) in the treated functional liver tissue (Spearman  $p=-0.31$ ,  $p=0.310$ ), nor was a correlation found between absorbed dose and volume change (Spearman  $p=-0.09$ ,  $p=0.768$ ). However, the three patients who received

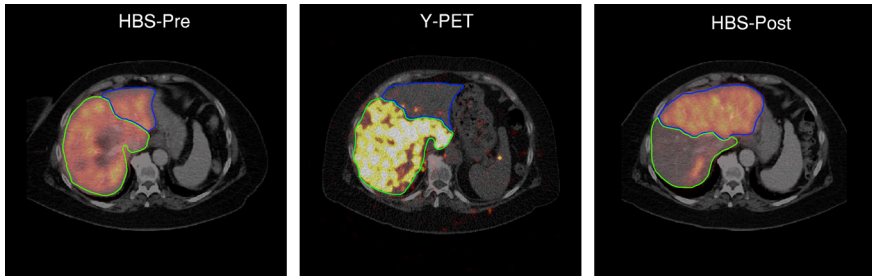


**Figure 4.** Example of volume decrease in the treated part of the liver (-41%) with compensatory increase in volume of the non-treated part (+178%). The functional liver parenchyma obtained a high absorbed dose of  $^{90}\text{Y}$  (105 Gy on functional liver, 145 Gy on the tumor). This particular part of the liver lost most of its function (HBS-pre: 7.2 %/min/m<sup>2</sup>; HBS-post: 1.5 %/min/m<sup>2</sup>). The non-treated part increased in function (HBS-pre: 1.2 %/min/m<sup>2</sup>; HBS-post: 3.6 %/min/m<sup>2</sup>).

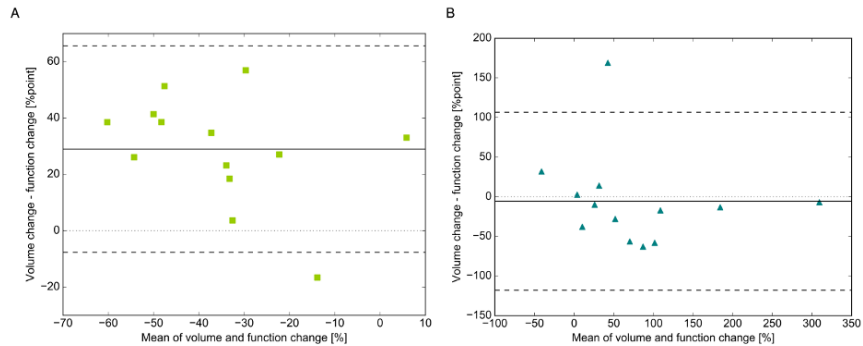


**Figure 5.** Bland-Altman plot of the relative change in volume versus the relative change in function in (a) the treated part (bias: 29.0%, limits of agreement: -7.68 – 65.60 % point) and (b) the non-treated part (bias: -6.0%, limits of agreement: -117.9 – 106.7 % point). Solid line indicates mean, dashed lines indicate limits of agreement (mean  $\pm$  1.96\*std).

the highest absorbed dose (average absorbed dose > 104.5 Gy) showed a larger function decline (cMUR change < -3.8 %/min/m<sup>2</sup>) than the patients receiving a lower absorbed dose (cMUR change > -2.4 %/min/m<sup>2</sup>) (p=0.007). Interestingly, these three patients also showed the largest function increase (cMUR change > 2.1 %/min/m<sup>2</sup>) in the non-treated part (p=0.011). No such relationships were observed for absorbed dose versus volume change.

Whole liver volume and whole liver function showed no correlation at baseline (Spearman p=-0.07, p=0.817). Bland-Altman analysis revealed a large bias of 29.0% and wide limits of agreement (-7.68 – 65.60 % point) for relative changes in the treated part (**Figure 5a**). In the non-treated part, this bias was -6.0% (**Figure 5b**), but the limits of agreement were still wide (-117.9 – 106.7 % point). In both the treated and non-treated part of the liver, the individual differences were large.

Large individual differences between function and volume changes in the non-treated lobe were found: 10/13 patients had an increase of both function and volume with a median relative difference between percent function and volume increase of 61% (range 2 - 134%), 1/13 patients had a decrease of both with a relative difference of 127%, and 2/13 patients had an increase of one parameter and a decrease of the other. The relative effect in the non-treated lobe was larger for function than for volume in 10/13 patients.

In two patients, the difference between function change and volume change of the non-treated part were not concordant. One patient (patient 5; **Supplemental Table 1**) showed a large volume increase in the non-treated part (+127.0%), while function decreased (-41.9%). The other patient (patient 2; **Supplemental Table 1**) showed a decrease in volume (-8.6%), but liver function in the non-treated part increased nonetheless (+29.2%).

## Discussion

Lobar radioembolization induces a decrease in function and volume in the treated part and an increase in function and volume in the non-treated part of the liver. The limits of agreement between relative function and volume change were wide, reflecting large individual differences. This may implicate a complimentary role for regional function

assessment with HBS in the selection and treatment planning of patients undergoing radioembolization, especially in patients undergoing lobar radioembolization with the aim to induce contralateral hypertrophy as a bridge to surgery with curative intent (i.e. radiation lobectomy) (2).

The concept of radiation lobectomy has been shown to be a feasible and effective treatment modality as a bridge to surgery in HCC patients, as an alternative to portal vein embolization (PVE) (4). With a median interval between <sup>90</sup>Y (glass microspheres) radioembolization and resection of 2.9 months (interquartile range [IQR]: 2-5 months), the median FLR hypertrophy was 23.3% (IQR: 10-48%) after radiation lobectomy. Complete, 50-99%, and <50% pathologic tumor necrosis was identified in 14 (45%), 10 (32%), and 7 (23%) tumors, confirming interval disease control (4). Palard et al. (16) showed a relationship between functional liver absorbed dose and FLR hypertrophy in 73 HCC patients who received lobar radioembolization using <sup>90</sup>Y glass microspheres. Patients who received a functional liver absorbed dose >88 Gy had a 92% chance of an FLR hypertrophy of at least 10% versus 66% for patients who received <88 Gy ( $p < 0.05$ ). Interestingly, the tumor absorbed dose, tumor size, baseline FLR volume, and Child-Pugh score also influenced FLR hypertrophy, illustrating the multifactorial physiological process of FLR hypertrophy (16).

The physiology of FLR hypertrophy is poorly understood. From the lengthy experience with PVE, however, it is known that embolization, diverting flow towards the FLR, plays a role. The embolizing properties for each radioembolization product vary considerably, and in the case of <sup>90</sup>Y glass microspheres also depends on the interval between calibration and administration (i.e. week 1-2 microspheres). This should be taken into account. The previously mentioned study by Palard et al. (16) was performed with less embolic week 1 microspheres, but it may be expected that dose-effect relationships will be different for the more embolic week 2 <sup>90</sup>Y glass microspheres. In our study a mix of week 1 and week 2 treatments was used for logistic reasons.

In our study, patients receiving the highest average functional liver absorbed dose also showed the largest function decrease in the treated part and the largest function increase in the non-treated part. In contrast, no such pattern was seen in the relationship between

absorbed dose and volume change, with large individual differences between function and volume changes. With increasing attention to personalized dosimetry-based treatment planning, further investigations regarding the relation between function change and absorbed dose is required and could have relevant clinical implications.

HBS with SPECT/CT allows for an accurate quantification of regional liver function. This may improve the future work-up of patients who are candidates for radioembolization, reducing the risk of hepatotoxicity. In a small case-series of three patients, we previously showed that discrepancies between lab values and liver function assessment using HBS may lead to dismal outcomes, that potentially could have been prevented if regional HBS results would have been taken into account (9). The suggested cMUR cut-off value of 2.69 %/min/m<sup>2</sup> for liver surgery (7) may be lower for lobar radioembolization, since radiation damage is a more gradual process compared to resection, and liver function may increase up to 12 months after radioembolization, both in treated and the non-treated part of the liver (17). Establishing the relationship between functional liver absorbed dose and functional changes is expected to lead to optimization of treatment planning by taking a pre-specified FLR function into account.

Although the largest series to date, the main limitation of this pilot study is the small cohort size. Due to the retrospective nature, no correlation with outcome measures (i.e. survival or hepatotoxicity) was possible, and a clear dose-effect relationship could not be established. Furthermore, liver function evaluation was only performed at three months, while the non-treated volume increases up to nine months after treatment (2). It would be interesting to assess liver function and volume after a longer period of time following radioembolization (i.e. follow-up of 9-12 months).

The next step towards the clinical implementation of HBS as a complementary imaging modality in radioembolization work-up would be a large prospective validation study, in which baseline and follow-up HBS would be compared to outcome measures. In addition, the relation between radiation absorbed dose and function change and the relation between FLR function and toxicity should be investigated to fully understand the potential of using HBS as an additional patient selection criterion, and possibly a parameter for individualized dosimetry-based treatment planning.

## **Conclusion**

Radioembolization induces regional changes in liver function that are accurately detected by HBS. Limits of agreement between function and volume changes after lobar radioembolization were wide, showing large individual differences. This implicates that HBS may have a complementary role in the management of patients for radiation lobectomy.



## References

1. Braat AJAT, Smits MLJ, Braat MNGJA, et al. <sup>90</sup>Y Hepatic Radioembolization: An Update on Current Practice and Recent Developments. *J Nucl Med.* 2015;56:1079-1087.
2. Vouche M, Lewandowski RJ, Atassi R, et al. Radiation lobectomy: Time-dependent analysis of future liver remnant volume in unresectable liver cancer as a bridge to resection. *J Hepatol.* 2013;59:1029-1036.
3. Gabr A, Abouchaleh N, Ali R, et al. Comparative study of post-transplant outcomes in hepatocellular carcinoma patients treated with chemoembolization or radioembolization. *Eur J Radiol.* 2017;93:100-106.
4. Gabr A, Abouchaleh N, Ali R, et al. Outcomes of Surgical Resection after Radioembolization for Hepatocellular Carcinoma. *J Vasc Interv Radiol.* 2018;29:1502-1510.e1.
5. Bennink RJ, Dinant S, Erdogan D, et al. Preoperative Assessment of Postoperative Remnant Liver Function Using Hepatobiliary Scintigraphy. *J Nucl Med.* 2004;45:965-971.
6. Dinant S, de Graaf W, Verwer BJ, et al. Risk Assessment of Posthepatectomy Liver Failure Using Hepatobiliary Scintigraphy and CT Volumetry. *J Nucl Med.* 2007;48:685-692.
7. de Graaf W, van Lienden KP, Dinant S, et al. Assessment of future remnant liver function using hepatobiliary scintigraphy in patients undergoing major liver resection. *J Gastrointest Surg.* 2010;14:369-378.
8. Chapelle T, Op De Beeck B, Huyghe I, et al. Future remnant liver function estimated by combining liver volumetry on magnetic resonance imaging with total liver function on <sup>99m</sup>Tc-mebrofenin hepatobiliary scintigraphy: Can this tool predict post-hepatectomy liver failure? *Hpb.* 2016;18:494-503.
9. Braat MNGJA, de Jong HW, Seinstra BA, Scholten M V., van den Bosch MAAJ, Lam MGEH. Hepatobiliary scintigraphy may improve radioembolization treatment planning in HCC patients. *EJNMMI Res.* 2017;7.
10. Bennink RJ, Cieslak KP, van Delden OM, et al. Monitoring of Total and Regional Liver Function after SIRT. *Front Oncol.* 2014;4:1-5.
11. Gulec SA, Mesoloras G, Stabin M. Dosimetric Techniques in <sup>90</sup>Y-Microsphere Therapy of Liver Cancer : The MIRD Equations for Dose Calculations. 2016:1209-1212.
12. Giammarile F, Bodei L, Chiesa C, et al. EANM procedure guideline for the treatment of liver cancer and liver metastases with intra-arterial radioactive compounds. *Eur J Nucl Med Mol Imaging.* 2011;38:1393-1406.
13. de Graaf W, van Lienden KP, van Gulik TM, Bennink RJ. <sup>99m</sup>Tc-Mebrofenin Hepatobiliary Scintigraphy with SPECT for the Assessment of Hepatic Function and Liver Functional Volume Before Partial Hepatectomy. *J Nucl Med.* 2010;51:229-236.
14. Ekman M, Fjälling M, Friman S, Carlson S, Volkmann R. Liver uptake function measured by iodida clearance rate in liver transplant patients and healthy volunteers. *Nucl Med Commun.* 1996;17:235-242.
15. Johnson PJ, Berhane S, Kagebayashi C, et al. Assessment of liver function in patients with hepatocellular carcinoma: A new evidence-based approach - The albi grade. *J Clin Oncol.* 2015;33:550-558.
16. Palard X, Edeline J, Rolland Y, et al. Dosimetric parameters predicting contralateral liver hypertrophy after unilobar radioembolization of hepatocellular carcinoma. *Eur J Nucl Med Mol Imaging.* 2018;45:392-401.
17. Theysohn JM, Ertle J, Müller S, et al. Hepatic volume changes after lobar selective internal radiation therapy (SIRT) of hepatocellular carcinoma. *Clin Radiol.* 2014;69:172-178.

## Supplementary material

**Supplemental Table 1:** Function and volume before and after radioembolization for the thirteen included patients. The relative change is indicated between bracket

Case		Function			Volume		
		Whole liver [%/min/m <sup>2</sup> ]	Treated [%/min/m <sup>2</sup> ]	Non-treated [%/min/m <sup>2</sup> ]	Whole liver [ml]	Treated [ml]	Non-treated [ml]
1	Pre-RE:	2.2	1.4	0.6	1140.1	646.7	368.4
	Post-RE:	1.8 (-19.1%)	0.9 (-35.8%)	0.8 (+24.5%)	1173.4 (+2.9%)	590.3 (-8.7%)	510.3 (+35.5%)
2	Pre-RE:	3.0	2.4	0.6	2385.3	1790.8	577.5
	Post-RE:	2.4 (-20.7%)	1.5 (-34.4%)	0.8 (+29.2%)	1792.4 (-24.9%)	1240.3 (-30.7%)	528.0 (-8.6%)
3	Pre-RE:	1.8	1.5	0.2	1439.6	1152.6	258.5
	Post-RE:	0.6 (-69.2%)	0.4 (-70.7%)	0.1 (-57.1%)	1012.4 (-29.7%)	814.5 (-29.3%)	193.5 (-25.1%)
4	Pre-RE:	8.6	6.7	1.8	1683.3	1240.4	412.7
	Post-RE:	6.0 (-29.8%)	2.2 (-67.5%)	3.8 (+117.4%)	1728.4 (+2.7%)	880.7 (-29.0%)	826.3 (+100.2%)
5	Pre-RE:	5.2	2.4	2.6	1335.7	721.0	563.1
	Post-RE:	2.3 (-56.4%)	0.6 (-73.3%)	1.5 (-41.9%)	2041.2 (+52.8%)	562.9 (-21.9%)	1278.4 (+127.0%)
6	Pre-RE:	4.5	2.4	1.4	3112.5	1118.7	577.2
	Post-RE:	5.7 (+26.2%)	2.2 (-5.6%)	2.8 (+98.4%)	3161.2 (+1.6%)	870.7 (-22.2%)	819.8 (+42.0%)
7	Pre-RE:	6.3	4.0	2.1	2646.7	1746.5	825.0
	Post-RE:	5.1 (-17.9%)	2.3 (-42.5%)	2.8 (+30.8%)	2371.9 (-10.4%)	1327.6 (-24.0%)	997.8 (+20.9%)
8	Pre-RE:	11.0	4.3	6.4	983.5	360.4	549.2
	Post-RE:	10.6 (-3.1%)	3.8 (-10.7%)	6.5 (+2.4%)	1052.8 (+7.0%)	441.0 (+22.4%)	577.6 (+5.2%)
9	Pre-RE:	6.5	3.2	2.8	2212.3	1080.6	910.8
	Post-RE:	5.6 (-8.1%)	1.1 (-67.4%)	4.7 (+65.8%)	2042.2 (-7.7%)	634.7 (-41.3%)	1255.4 (+37.8%)
10	Pre-RE:	8.7	7.2	1.2	1963.6	1560.2	337.9
	Post-RE:	5.1 (-40.8%)	1.5 (-79.5%)	3.6 (+190.9%)	1880.0 (-4.3%)	920.8 (-41.0%)	938.1 (+177.6%)
11	Pre-RE:	6.3	5.4	0.8	2015.7	1650.3	326.7
	Post-RE:	4.9 (-23.3%)	2.9 (-45.6%)	1.9 (+130.7%)	1861.1 (-7.7%)	1281.5 (-22.3%)	563.8 (+72.6%)
12	Pre-RE:	7.3	6.5	0.7	1120.3	1009.5	107.2
	Post-RE:	5.7 (-21.3%)	2.7 (-58.1%)	3.0 (+312.8%)	1437.3 (+28.3%)	997.6 (-1.2%)	435.1 (+305.9%)
13	Pre-RE:	6.2	4.1	1.8	1252.5	791.1	326.5
	Post-RE:	6.0 (-4.5%)	1.9 (-54.7%)	3.9 (+118.4%)	1234.4 (-1.4%)	633.7 (-19.9%)	507.7 (+55.5%)





# CHAPTER SEVEN

**Radioembolization-induced changes in  
hepatic  $^{18}\text{F}$ FDG metabolism in  
non-tumorous liver parenchyma**

Manon N. Braat, Caren van Roekel, Marnix, G. Lam, Arthur J. Braat

*Diagnostics* 2022 Oct 17;12(10):2518.

## Abstract

### Background

$^{18}\text{F}$ FDG-PET/CT is increasingly used for response assessment after oncologic treatment. Known response criteria for  $^{18}\text{F}$ FDG-PET/CT use healthy liver parenchyma as reference-standard. However,  $^{18}\text{F}$ FDG liver metabolism may change as a result of the therapy given. The aim of this study was to assess change in  $^{18}\text{F}$ FDG liver metabolism after hepatic  $^{90}\text{Y}$  resin radioembolization.

### Methods

$^{18}\text{F}$ FDG-PET/CTs prior to radioembolization, one and three months after radioembolization (consistent with the PERCIST comparability criteria) and  $^{90}\text{Y}$ -PET/CTs were analyzed using 3 cm VOIs; FDG-activity concentration and absorbed dose were measured. A linear mixed-effects logistic regression and logistic mixed-effects model were used to assess the correlation between the FDG-activity concentration, absorbed dose and biochemical changes.

### Results

The median  $\text{SUL}_{\text{VOI,liver}}$  at baseline was 1.8 (range 1.2-2.8). The mean change in  $\text{SUL}_{\text{VOI,liver}}$  per month increase in time was 0.05 (95%CI 0.02-0.09),  $p < 0.001$ . The median absorbed dose per VOI was 31.3 Gy (range 0.1-82.3 Gy). The mean percent change in  $\Delta\text{SUL}_{\text{VOI,liver}}$  for every Gy increase in absorbed dose was -0.04 (95%CI -0.22 - 0.14),  $p = 0.67$ . The  $\text{SUL}_{\text{blood}}$  and  $\text{SUL}_{\text{spleen}}$  showed no increase.

### Conclusions

$^{18}\text{F}$ FDG metabolism in the liver parenchyma is significantly, but mildly increased after radioembolization, and therefore can interfere with its use as a threshold for therapy-response.

## Introduction

More and more  $^{18}\text{F}$ FDG-PET/CT studies are performed for response evaluation, as anatomical imaging modalities lack adequate response assessment, useful and consistent response criteria and/or have minor prognostic value (1). In light of these limitations of anatomical imaging, two distinct response assessment criteria were defined for  $^{18}\text{F}$ FDG-PET: EORTC criteria since 1999 (2) and PERCIST criteria since 2009 (1). Their differences are outlined in **Supplemental table 1**. Mean and maximum standard uptake value ( $\text{SUV}_{\text{mean}}$  and  $\text{SUV}_{\text{max}}$ ) corrected for body weight in a 2D region of interest (ROI) in the most metabolic part of as many tumors as possible are used in EORTC (2), while SUV corrected for the lean body mass (= SUL) in a stringent volume of interest (VOI) of  $1\text{ cm}^3$  centered at the most metabolic active part of up to 5 tumors (=SUL<sub>peak</sub>) is used in PERCIST (1). Additionally, PERCIST uses a SUL<sub>mean</sub> assessment of the right lobe of the liver (or bloodpool) for  $^{18}\text{F}$ FDG-PET comparability at different time points and as a threshold to define response.

In light of the PERCIST criteria and its use of a VOI in the right liver lobe to assess  $^{18}\text{F}$ FDG-PET comparability, multiple test-retest studies in healthy volunteers or former cancer patients showed that quantification of the physiologic activity concentration of  $^{18}\text{F}$ FDG was similar over longer periods of time, including the liver parenchyma (3). However, studies performed in oncologic patients, mainly lymphoma patients, showed that some types of chemotherapy had an effect on healthy liver parenchyma, leading to an increase in mean liver activity on  $^{18}\text{F}$ FDG-PET (4, 5). This poses a problem with the current response assessment criteria used in lymphoma patients, the Deauville criteria (6-10), in which response is based on a (visual) assessment, comparing tumor uptake to liver uptake. Theoretically, response after treatment could be wrongfully overestimated.

For the treatment of hepatic malignancies, radioembolization has gained terrain the last decades. During that time, multiple studies have used  $^{18}\text{F}$ FDG-PET/CT for response assessment and applied the PERCIST criteria (11, 12). However, concomitant non-target embolization and radiation of the non-tumorous liver parenchyma (=NTLP) may lead to a localized and systemic inflammatory reaction (13, 14). And eventually, changes consistent with sinusoidal obstruction syndrome (SOS) and fibrosis can develop (15).

We hypothesized that  $^{18}\text{F}$ FDG activity concentration in NTLP changes after radioembolization, leading to misinterpretation and possible overestimation of response using this activity concentration as a threshold in the PERCIST criteria. In this study, it was investigated whether  $^{18}\text{F}$ FDG activity concentration in NTLP changes after radioembolization, and whether alternative reference values can be used.

## Methods

### Study population

This retrospective monocenter study comprises all patients treated with  $^{90}\text{Y}$  resin microspheres (SIRTeX Medical, Sydney) in our center from 2009 till July 2015, with an  $^{18}\text{F}$ FDG-PET/CT prior ( $=^{18}\text{F}$ FDG-PET/CT<sub>prior</sub>) and one and/or three months after treatment ( $=^{18}\text{F}$ FDG-PET/CT<sub>follow-up</sub>). Patients were only included if the  $^{18}\text{F}$ FDG-PET/CTs met the PERCIST criteria (**Supplemental table 1**) and if a  $^{90}\text{Y}$ -PET/CT was performed within 24 hours after radioembolization for regional dose calculation on NTLP.

The institutional medical ethics committee waived the need for informed consent for this retrospective review.

### Radioembolization treatment

After a pre-treatment hepatic arteriography to evaluate the vascular anatomy, a simulation was performed with the injection of  $^{99\text{m}}\text{Tc}$ -macroaggregated albumin (MAA) into the hepatic artery / arteries. Standard planar and SPECT images of  $^{99\text{m}}\text{Tc}$ -MAA were obtained for particle distribution assessment and to exclude relevant liver–lung shunting and extrahepatic depositions. In a separate session,  $^{90}\text{Y}$  resin microspheres were injected in the hepatic artery/arteries after ensuring adequate catheter placement (similar to the  $^{99\text{m}}\text{Tc}$ -MAA injection position). The therapeutic activity of  $^{90}\text{Y}$  resin microspheres was calculated according to the body surface area method.

### $^{18}\text{F}$ FDG-PET/CT imaging protocols

All  $^{18}\text{F}$ FDG-PET/CTs at all time points were performed on the same PET/CT-scanner (Biograph mCT, Siemens Healthcare, Erlangen, Germany). All patients fasted for at least 6 hours prior to intravenous  $^{18}\text{F}$ FDG administration (2.0 MBq/kg) and the patient's blood glucose level

was determined prior to tracer injection ( $<11.1$  mmol/l). Imaging parameters included a three-dimensional acquisition technique with a 216 mm field of view, 3 minutes per bed position, and ordered subset expectation maximization iterative reconstruction, including a Gaussian filter, 4 iterations, and 21 subsets. Measurements were performed on image reconstructions according to the EARL criteria (16).

### **$^{90}\text{Y}$ -PET/CT imaging protocol**

All  $^{90}\text{Y}$ -PET/CTs were performed on the same PET/CT-scanner (Biograph mCT, Siemens Healthcare, Erlangen, Germany) within 24 hours after treatment. Imaging parameters included a total acquisition time of 30 minutes for 2 bed positions, TrueX and time-of-flight reconstruction, reconstruction using 4 iterations with 21 subsets and a 5 mm full-width at half maximum Gaussian post-reconstruction filter. A low dose CT was acquired for attenuation correction and anatomical reference.

### **Non-tumorous liver parenchyma analysis**

All  $^{18}\text{F}$ FDG-PET/CT and  $^{90}\text{Y}$ -PET/CT scans were analyzed using ROVER software (ABX, Radeberg, Germany). A 3 cm VOI in the right lobe of a normal liver is a robust method for the identification of the  $\text{SUL}_{\text{mean}}$  (17) and is applied in the PERCIST criteria as a threshold parameter. To assess the NTLF activity concentration the liver was separated into three regions, consistent with the three supplying arteries: the left hemiliver (i.e. the left hepatic artery (LHA)), the right hemi-liver (i.e. the right hepatic artery (RHA)) and segment 4 (i.e. the middle hepatic artery (MHA) or segment 4 artery). Segment 4 was considered a separate region, as the MHA can be separately injected.

Spheric VOIs (3 cm in diameter) were placed in the NTLF of all three liver regions and in the spleen. If one of the regions was too diffusely involved by malignancy to accommodate a 3 cm VOI, no VOI was placed. In case of a (extended) right-sided hemihepatectomy a second VOI was placed in the remaining liver. Cylindrical VOIs with a 2 cm diameter were placed in the ascending, descending and abdominal aorta, without inclusion of the aortic wall (to avoid elevated  $^{18}\text{F}$ FDG-uptake due to atherosclerosis).



The  $^{18}\text{F}$ FDG-PET/CT<sub>follow-up</sub> of each patient was registered to the  $^{18}\text{F}$ FDG-PET/CT<sub>prior</sub>. ROIs were automatically co-registered onto the  $^{18}\text{F}$ FDG-PET/CT<sub>follow-up</sub>, but manually corrected if the automatic placement of the VOI did not correspond to the location of the VOI on the  $^{18}\text{F}$ FDG-PET/CT<sub>prior</sub>.  $\text{SUL}_{\text{mean}}$  and  $\text{SUL}_{\text{max}}$  were calculated for all VOIs.

The same parameters were registered for the spleen, as well as the splenic volume. Splenic volume is known to increase after radioembolization, however it is unknown whether FDG activity concentration changes are correlated to splenic volume changes (18).

In addition, all  $^{90}\text{Y}$ -PET/CTs were registered to the  $^{18}\text{F}$ FDG-PET/CT<sub>prior</sub> and the liver VOIs co-registered onto the  $^{90}\text{Y}$ -PET/CT, thus enabling a read-out of the absorbed dose (MBq/ml) in the same three regional VOIs. In a previous report we validated the use of ROVER software for absorbed dose estimation on  $^{90}\text{Y}$ -PET/CT (19).

All measurements on the  $^{18}\text{F}$ FDG-PET/CT<sub>prior</sub> were performed by one physician (MB; >10 years of experience).

### Biochemical changes

Laboratory examinations at the time of each PET/CT were noted, including: liver function tests (total bilirubin, alkaline phosphatase, gamma-glutamyl transferase (GGT), aspartate aminotransferase (AST), alanine aminotransferase (ALT)) and coagulation parameters (thrombocytes, international normalized ratio (INR), partial thromboplastin time (PTT), activated partial thromboplastin time (APTT) and thrombin time (TT)). The common terminology criteria for adverse events (CTCAE) version 5.0 was used for grading biochemical toxicities. The presence of  $\geq 2$  CTCAE grade  $\geq 1$  laboratory adverse events was regarded as clinically relevant biochemical toxicity.

Biochemical changes were correlated with changes in  $^{18}\text{F}$ FDG uptake in NTLF.

### Statistical analysis

Descriptive statistics were used to explore baseline and treatment characteristics. The change in  $\text{SUL}_{\text{liver}}$  (the average of all VOIs per patient),  $\text{SUL}_{\text{VOI,liver}}$ ,  $\text{SUL}_{\text{spleen}}$  and  $\text{SUL}_{\text{blood}}$  over time was assessed using linear mixed-effect regression models, to account for clustered

data. Nested models were compared using Akaike's Information Criterion. A model with a random slope only fitted the data best for all parameters. Time was used as a continuous independent variable. In the analyses of  $\text{SUL}_{\text{liver}}$  and  $\text{SUL}_{\text{VOI,liver}}$ , injected activity (MBq) (patient-level) and the absorbed dose per VOI (VOI-level) were included as co-variables, to adjust for possible confounding.

The association between parenchymal-absorbed dose and change in  $\text{SUL}_{\text{VOI,liver}}$  (represented as  $\Delta\text{SUL}_{\text{VOI,liver}}$ ) was also analyzed using a linear mixed-effect regression model with a random slope, with absorbed dose as the continuous independent variable.

A logistic mixed-effects model was used to assess the association between presence of clinically relevant biochemical toxicity (using the cut-off definition as described above) per time point and change in  $\text{SUL}_{\text{VOI,liver}}$ . The analysis was adjusted for response to therapy (coded as yes/no progressive disease) as a possible confounder. All statistical analyses were done with R statistical software, version 3.6.2 for Windows. We reported effect estimates with associated 95% confidence intervals and corresponding two-sided p-values.

## Results

A total of 292 patients were screened, of whom 43 patients underwent both an  $^{18}\text{F}$ FDG-PET/CT<sub>prior</sub> and  $\geq 1$   $^{18}\text{F}$ FDG-PET/CT<sub>follow-up</sub> and an  $^{90}\text{Y}$ -PET/CT. Sixteen patients were excluded, because they did not meet the PERCIST criteria for inter-study comparison of  $^{18}\text{F}$ FDG-PET/CT. One additional patient was excluded because of too diffuse liver metastases to accommodate a 3 cm VOI in the NTL. Twenty-six patients were included, with 35  $^{18}\text{F}$ FDG-PET/CTs<sub>follow up</sub> (total of 61  $^{18}\text{F}$ FDG-PET/CTs), resulting in a total of 62 VOIs<sub>liver</sub> that were analyzed in this study (**Figure 1**). Nine patients had two  $^{18}\text{F}$ FDG-PET/CTs<sub>follow up</sub>, the remaining 17 patients had one  $^{18}\text{F}$ FDG-PET/CT<sub>follow up</sub> at one month (n=9) or three months (n=8). Baseline characteristics are presented in **Table 1**.

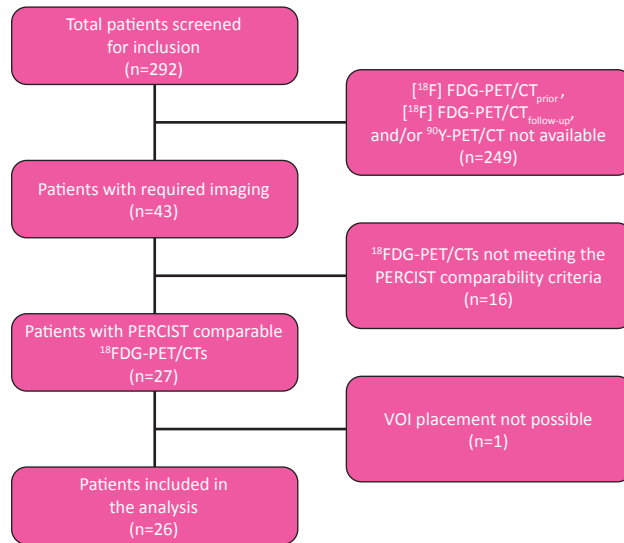


**Figure 1.** Flowchart of the study

The median post-injection time was 64,5 minutes, 62,3 minutes and 65 minutes at <sup>18</sup>FDG-PET/CT<sub>prior</sub> and the one and three month <sup>18</sup>FDG-PET/CT<sub>follow-up</sub>, respectively (Table 2). The median absorbed dose per VOI was 31.3 Gy (range 0.1-82.3 Gy). Overall, the median  $SUL_{VOI,liver}$  at baseline was 1.8 (range 1.2-2.8). A significant increase in  $SUL_{VOI,liver}$  over time was found: the mean change in  $SUL_{VOI,liver}$  per month increase in time was 0.05 (95%CI 0.02-0.09),  $p=0.00088$  (Figure 2)(Table 3). The mean percent change in  $\Delta SUL_{VOI,liver}$  for every Gy increase in dose was -0.04 (95%CI -0.22 - 0.14),  $p=0.67$ . At a patient level, the median  $SUL_{VOI}$  (average of all VOIs of the liver parenchyma) was 1.8 (range 1.5-2.3). The mean change in  $SUL_{VOI}$  per month increase in time was 0.05 (95%CI 0.01-0.08);  $p=0.016$  (Table 3).

**Table 1.** Baseline characteristics of included patients

<b>Characteristics</b>	
<b>Total number of evaluable patients</b>	26
<b>Sex</b>	
Male	16
Female	10
<b>Median age in years (range)</b>	66 (34-79)
<b>Median time from baseline F-18 FDG-PET/CT to Y-90-RE in days (range)</b>	24 (1-44)
<b>Median weight in kg (range)</b>	82 (57-110)
<b>Number of patients known with diabetes mellitus</b>	1
<b>Number of patients with use of anti-diabetic medication</b>	1
<b>Primary tumor</b>	
Colorectal carcinoma	25
Pancreatic adenocarcinoma	1
<b>Prior locoregional treatment</b>	
Extended right hemihepatectomy	3
Left hemihepatectomy + one metastasectomy in the right hemiliver	1
Multiple metastasectomies	3
Radiofrequency ablation	1
<b>Median injected activity in MBq (range)</b>	1484 (345-2164)
<b>Treatment</b>	
Whole liver delivery	22
Sequential delivery	1
Lobar treatment	3
<b>Prior systemic treatment</b>	26
<b>No. of systemic treatment lines</b>	
1	9
2	12
3	4
4	1

RE=radioembolization

Overall, the incidence of biochemical toxicity was low. CTCAE grade 3 toxicity was only found for bilirubin, GGT and APTT (**Table 4A**). PTT, INR and TT were slightly prolonged in three, three and one patient(s), respectively. The results of the logistic regression models showed a non-significant association between clinically relevant biochemical toxicity and change in  $SUL_{VOI}$  (at a patient level) (95%CI 0.0006-333.29),  $p=0.90$  (**Table 4B**) (**Figure 3**).

**Table 2.**  $^{18}F$ FDG-PET/CT specifications and measurements of this study population

Time after RE	Baseline	One month	Three months
Number of examinations	26	18	17
	Median (range)		
Serum glucose level in mmol/l	6.4 (5.1-9.8)	6.3 (4.2-10.3)	6.6 (4.4-10.4)
Post-injection time in minutes	64.5 (56-85)	62.5 (58-78)	65 (51-86)
Injected activity in MBq/kg	2.03 (1.81-2.37)	2.03 (1.66-2.50)	1.94 (1.69-2.62)
$SUL_{mean}$ segment 2-3	1.8 (1.5-2.2)	1.9 (1.5-2.6)	1.95 (1.6-2.4)
$SUL_{mean}$ segment 4	1.7 (1.5-2.1)	1.7 (1.6-2.1)	1.8 (1.6-2.2)
$SUL_{mean}$ right hemiliver	1.9 (1.2-2.8)	1.7 (1.3-2.6)	1.9 (1.7-2.5)
$SUL_{mean}$ spleen	1.4 (1.1-2.0)	1.5 (0.9-1.9)	1.5 (1.3-1.9)
$SUL_{mean}$ bloodpool	1.3 (1.03-1.63)	1.27 (1.00-1.87)	1.23 (1.00-1.70)

**Table 3.** Relation of  $SUL_{VOI}$  over time based on linear mixed effects regression analyses

Independent variable	Mean change in $SUL_{VOI}$ per month increase in time (95%CI); p-value	
$SUL_{VOI}$ (patient-level)	Unadjusted 0.05 (0.01-0.08); 0.016	Adjusted (for administered activity Y90) 0.03 (-0.04-0.1); 0.38
$SUL_{VOI,liver}$ (VOI-level)	Unadjusted 0.05 (0.02-0.09), 0.00088	Adjusted (for absorbed dose per VOI) 0.05 (0.02-0.08); 0.00084

Numbers represent the different times of biochemical toxicity determination per patient. Some patients had measurements at two follow-up times so numbers do not equal total number of patients.

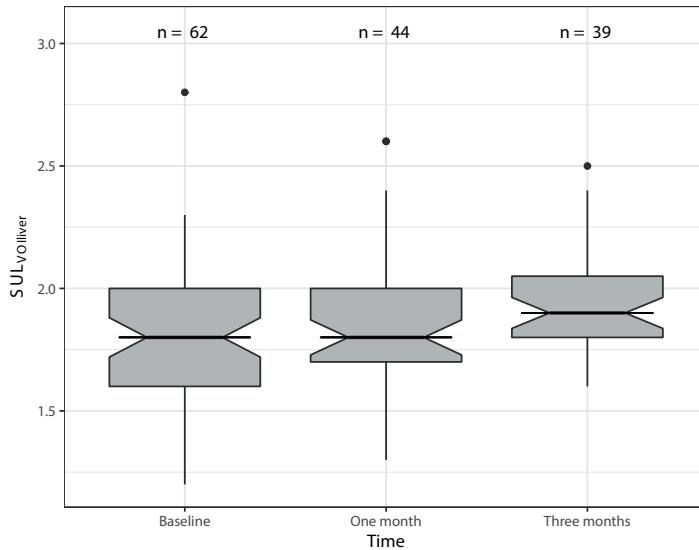


**Table 4A.** Incidence of biochemical toxicity between baseline and three months after radioembolization, according to CTCAE version 5.

CTCAE grade	1	2	3
Alanine aminotransferase	11		
Alkaline phosphatase	6	3	
Aspartate aminotransferase	14	1	
Bilirubin	5	1	1
Gamma-glutamyl transferase	3	5	3
Thrombocytes	9	2	
APTT	13	1	1

**Table 4B.** Relation between  $SUL_{VOL,liver}$  and clinically relevant biochemical toxicity, based on mixed-effects logistic regression analyses with  $SUL_{VOL,liver}$  as the independent variable.

Clinically relevant biochemical toxicity yes versus no		
Dependent variable	Odds ratio for clinically relevant biochemical toxicity for every month increase in $SUL_{VOL,liver}$ (95% CI); p-value	
	Unadjusted model	Adjusted model (for progressive disease)
Clinically relevant biochemical toxicity (based on laboratory parameters) (no n=14, yes n=21)	0.42 (0.0006-296.82); 0.69	0.48 (0.0006-333.29); 0.90

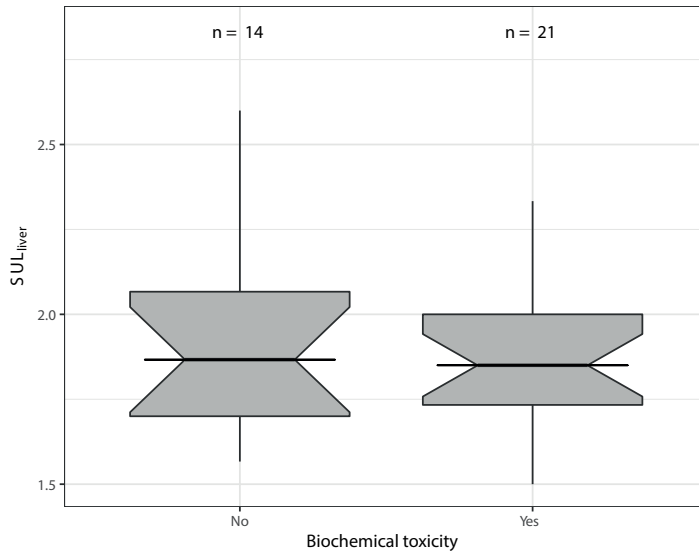


**Figure 3.** Difference in  $SUL_{liver}$  (patient-level) versus biochemical toxicity. Numbers represent the different times of biochemical toxicity determination per patient. Some patients had measurements at two follow-up times so numbers do not equal total number of patients.

For  $\text{SUL}_{\text{blood}}$ , no significant increase or decrease over time was found; mean change in  $\text{SUL}_{\text{blood}}$  per month increase in time was  $-0.012$  (95%CI  $-0.05$ - $0.03$ ),  $p=0.57$  (**Figure 4A**).  $\text{SUL}_{\text{spleen}}$  was also stable over time; mean change per month increase in time of  $0.005$  (95%CI  $-0.04$ - $0.05$ ),  $p=0.83$  (**Figure 4B**), while splenic volume did significantly increase over time;  $49$  mL increase in volume per month (95%CI  $32$ - $65$ ,  $p=0.0011$ ) (**Figure 4C**).

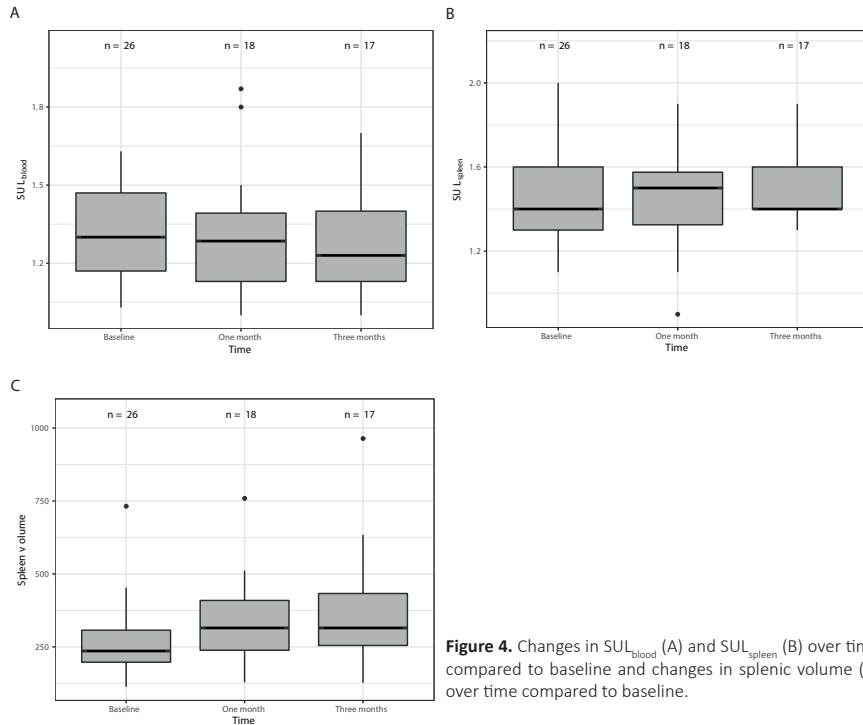


**Figure 4.** Changes in  $\text{SUL}_{\text{blood}}$  (A) and  $\text{SUL}_{\text{spleen}}$  (B) over time compared to baseline and changes in splenic volume (C) over time compared to baseline.



## Discussion

Our data showed that after  $^{90}\text{Y}$  radioembolization the  $^{18}\text{F}$ FDG activity concentration ( $\text{SUL}_{\text{VOI, liver}}$ ) in the collateral targeted NTLP is significantly increased compared to baseline. Though the  $\text{SUL}_{\text{VOI, liver}}$  increase was minimal with a mean change in  $\text{SUL}_{\text{VOI, liver}}$  per month increase in time of 0.05 of a median  $\text{SUL}_{\text{VOI, liver}}$  at baseline of 1.8, this may influence quantitative assessments of liver activity concentration as used in PERCIST. The influence on routine visual response assessment remains unclear, but will be minimal. Mild changes in  $^{18}\text{F}$ FDG activity concentration however could be noticed in our study visually (**Figure 5**).

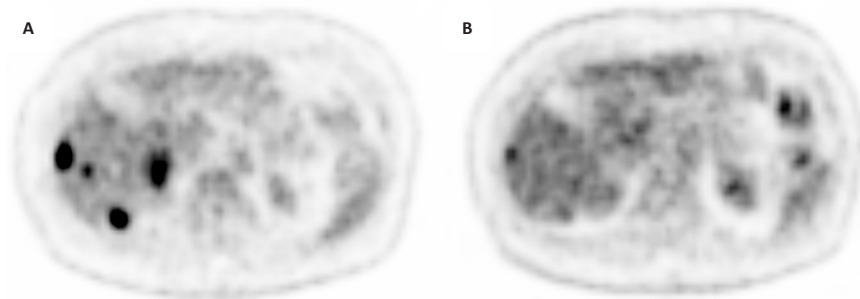


**Figure 5.** Case example of visual increase of  $^{18}\text{F}$ FDG activity concentration in non-tumorous liver tissue. A 75-year-old woman with colorectal liver metastases underwent a  $^{18}\text{F}$ FDG-PET/CT<sub>prior</sub> (A) and a  $^{18}\text{F}$ FDG-PET/CT<sub>follow-up</sub> (B) 15 days prior and 29 days after radioembolization, respectively. The images are similarly scaled (0-7  $\text{SUV}_{\text{lean body mass}}$ ). One month after radioembolization a reduced  $^{18}\text{F}$ FDG activity concentration is seen in the metastases, but the background non-tumorous liver activity concentration has visually increased ( $\text{SUL}_{\text{VOI, liver}}$  increase from 1,8 to 2,4 in the  $\text{VOI}_{\text{right liver}}$ ).

Multiple reports on increased  $^{18}\text{F}$ FDG uptake in the liver after chemoradiation therapy for esophageal cancer were published, with focal as well as diffuse patterns (20-22, 23). However, only one publication touched upon the  $^{18}\text{F}$ FDG uptake pattern in normal liver parenchyma one month after radioembolization, with no changes compared to baseline (24). Unfortunately, additional data were lacking and no correlation was made with the absorbed dose.

Remarkably, we did not find association between the median absorbed dose and the change in  $\text{SUL}_{\text{VOI,liver}}$ . In contrast, Nakahara et al. reported a direct visual correspondence to the radiation dose distribution and the pattern of increased  $^{18}\text{F}$ FDG uptake in the liver in a patient after chemoradiation therapy for esophageal cancer (23). The lack of association in our data may be due to the limited patient number and the limited spread in absorbed doses between the VOIs.

The explanation for the increased  $^{18}\text{F}$ FDG liver activity concentration after radioembolization is largely unknown. Local inflammation seems plausible, though this is not confirmed in the existing (though scarce) histopathology literature (15, 25-27). In vitro assessment of ovarian cancer cell lines after radiotherapy showed swelling and increased  $^3\text{H}$ FDG uptake in the surviving cells (28); a similar phenomenon may be present in hepatocytes after radioembolization. However, the most plausible explanation may be increased  $^{18}\text{F}$ FDG uptake due to sinusoidal obstruction syndrome (SOS). Several authors reported signs of SOS developing within the first three months after radioembolization (15, 26, 27). And as shown by Kim et al. in 35 patients with SOS after platin-based chemotherapy, SOS can lead to a significantly increased  $^{18}\text{F}$ FDG liver activity concentration (29). The possible explanation they offer is passive  $^{18}\text{F}$ FDG tracer stasis, due to endothelial cell injury and peliotic changes. The increase in  $\text{SUL}_{\text{liver}}$  in their study (12%) was considerably higher than in our data, yet similar to our findings, the activity concentration in the bloodpool remained unchanged, unlike the splenic  $^{18}\text{F}$ FDG activity concentration (which increased significantly in the moderate to severe cases of SOS in their study). As blood pool  $^{18}\text{F}$ FDG activity concentration seems unchanged at different time points after injection, in different patient populations and even after chemotherapy, it may be the best reference value for patients treated with radioembolization (4, 6-9, 29, 30).

Although PERCIST aims to unify response assessment with  $^{18}\text{F}$ FDG-PET, in our study 30.8% of the patients with a  $^{18}\text{F}$ FDG-PET/CT at baseline and follow-up were excluded based on the PERCIST timing and scan criteria (apart from the liver SUL criterion). This is consistent with most publications that show mean exclusion percentages of 22.6% - 38.3% for PERCIST response assessment, due to the strict criteria for scan comparability (**Supplemental table 1**) (9, 10, 31). Major restrictions include the difference in post-injection scanning time (<15 min)

and a minimum of 50 minutes post injection scanning. Unfortunately, these are significant factors in SUV measurements and a major logistical problem for most nuclear medicine departments. As shown in several test-retest studies, the interval between injection and acquisition is a significant parameter for underestimating liver activity (30-33). This may be explained by the abundance of the enzyme glucose-6-phosphatase in the liver, causing continuous glycolysis and decrease in FDG retention (34). Thus, it is essential to minimize the differences in FDG uptake-time between scans, to ensure a consistent threshold for PET-based response assessment (as used in PERCIST, Deauville criteria, etc.). The post-injection times between  $^{18}\text{F}$ FDG-PET/CTs in our study were not significantly different (**Table 2**). However, in 5/26 of the right liver VOIs the  $\text{SUL}_{\text{VOI, liver}}$  was  $\geq 0,3$  SUL unit change; violating the scan restrictions according to the PERCIST criteria. In these cases radioembolization-induced increased  $^{18}\text{F}$ FDG liver activity concentration would have resulted in exclusion. Yet, these minimal changes in  $\text{SUL}_{\text{VOI}}$  will probably not be clinically relevant in routine visual response assessment. But with the increased use of the modified PERCIST criteria the reference threshold of the  $\text{VOI}_{\text{liver}}$  is lowered, and use of a more robust reference value in clinical studies is advisable (35).

Comparison of  $^{18}\text{F}$ FDG liver activity concentration with earlier reported results is difficult, due to differences in quantification and/or correction of  $^{18}\text{F}$ FDG uptake; i.e. the use of ROIs or VOIs, the use of  $\text{SUV}_{\text{max}}$  or  $\text{SUV}_{\text{mean}}$  or total lesion/liver glycolysis (TLG), correction for body surface area (BSA) vs body weight vs lean body mass (LBM). Only LBM corrected SUV (SUL) is not significantly affected by body weight, contrary to BSA-corrected or body weight-corrected SUV. All calculations are not affected by age, blood glucose, diabetes and sex (3, 4, 30). Therefore, in our study SUL was chosen for all measurements, consistent with the PERCIST criteria.

There are a few limitations in this study; foremost the small patient number with consistently acquired PET/CTs according to the PERCIST guidelines. A patient cohort with only lobar treatments, enabling an in-patient comparison with non-treated NTLF, would be better by avoiding inter-patient biological differences. Additionally, comparison of patients treated with different commercially available microspheres (with their differing specific activity) could help to further evaluate the role of  $^{18}\text{F}$ FDG-PET/CT as an follow-up tool after

radioembolization. And given the expanding use of both external beam radiotherapy and radioembolization and increasing use of  $^{18}\text{F}$ FDG-PET/CT for response assessment further research is required.

### **Conclusion**

$^{18}\text{F}$ FDG liver activity concentration in the background liver ( $\text{SUL}_{\text{vol}}$ ) is mildly, but significantly increased after radioembolization, and therefore can interfere with the use of the background liver firstly as a threshold for therapy-response and secondly as a comparability criterion in the PERCIST criteria. An alternative and more consistent threshold is  $^{18}\text{F}$ FDG activity concentration in the blood pool ( $\text{SUL}_{\text{blood}}$ ).

## References

1. Wahl RL, Jacene H, Kasamon Y, Lodge MA. From RECIST to PERCIST: Evolving Considerations for PET response criteria in solid tumors. *J Nucl Med.* 2009;50 Suppl 1:122s-50s.
2. Young H, Baum R, Cremerius U, Herholz K, Hoekstra O, Lammertsma AA, et al. Measurement of clinical and subclinical tumour response using [18F]-fluorodeoxyglucose and positron emission tomography: review and 1999 EORTC recommendations. European Organization for Research and Treatment of Cancer (EORTC) PET Study Group. *Eur J Cancer.* 1999;35(13):1773-82.
3. Skougaard K, Nielsen D, Jensen BV, Hendel HW. Comparison of EORTC criteria and PERCIST for PET/CT response evaluation of patients with metastatic colorectal cancer treated with irinotecan and cetuximab. *J Nucl Med.* 2013;54(7):1026-31.
4. Paquet N, Albert A, Foidart J, Hustinx R. Within-patient variability of (18)F-FDG: standardized uptake values in normal tissues. *J Nucl Med.* 2004;45(5):784-8.
5. Kanstrup IL, Klausen TL, Bojsen-Moller J, Magnusson P, Zerahn B. Variability and reproducibility of hepatic FDG uptake measured as SUV as well as tissue-to-blood background ratio using positron emission tomography in healthy humans. *Clin Physiol Funct Imaging.* 2009;29(2):108-13.
6. Boktor RR, Walker G, Stacey R, Gledhill S, Pitman AG. Reference range for intrapatient variability in blood-pool and liver SUV for 18F-FDG PET. *J Nucl Med.* 2013;54(5):677-82.
7. Chiaravalloti A, Danieli R, Abbatiello P, Di Pietro B, Travascio L, Cantonetti M, et al. Factors affecting intrapatient liver and mediastinal blood pool (1)(8)F-FDG standardized uptake value changes during ABVD chemotherapy in Hodgkin's lymphoma. *Eur J Nucl Med Mol Imaging.* 2014;41(6):1123-32.
8. Ceriani L, Suriano S, Ruberto T, Zucca E, Giovannella L. 18F-FDG uptake changes in liver and mediastinum during chemotherapy in patients with diffuse large B-cell lymphoma. *Clin Nucl Med.* 2012;37(10):949-52.
9. Rubello D, Gordien P, Morliere C, Guyot M, Bordenave L, Colletti PM, et al. Variability of Hepatic 18F-FDG Uptake at Interim PET in Patients With Hodgkin Lymphoma. *Clin Nucl Med.* 2015;40(8):e405-10.
10. Fencl P, Belohlavek O, Harustiak T, Zemanova M. The analysis of factors affecting the threshold on repeated 18F-FDG-PET/CT investigations measured by the PERCIST protocol in patients with esophageal carcinoma. *Nucl Med Commun.* 2012;33(11):1188-94.
11. Barrington SF, Qian W, Somer EJ, Franceschetto A, Bagni B, Brun E, et al. Concordance between four European centres of PET reporting criteria designed for use in multicentre trials in Hodgkin lymphoma. *Eur J Nucl Med Mol Imaging.* 2010;37(10):1824-33.
12. Bagni O, Filippi L, Schillaci O. The role of (18)F-FDG positron emission tomography in the follow-up of liver tumors treated with (90)Yttrium radioembolization. *Am J Nucl Med Mol Imaging.* 2015;5(3):220-32.
13. Fernandez-Ros N, Inarrairaegui M, Paramo JA, Berasain C, Avila MA, Chopitea A, et al. Radioembolization of hepatocellular carcinoma activates liver regeneration, induces inflammation and endothelial stress and activates coagulation. *Liver Int.* 2015;35(5):1590-6.
14. Chew V, Lee YH, Pan L, Nasir NJM, Lim CJ, Chua C, et al. Immune activation underlies a sustained clinical response to Yttrium-90 radioembolisation in hepatocellular carcinoma. *Gut.* 2019;68(2):335-46.

15. Nalesnik MA, Federle M, Buck D, Fontes P, Carr BI. Hepatobiliary effects of 90yttrium microsphere therapy for unresectable hepatocellular carcinoma. *Hum Pathol.* 40. United States 2009. p. 125-34.
16. Kaalep A, Sera T, Oyen W, Krause BJ, Chiti A, Liu Y, et al. EANM/EARL FDG-PET/CT accreditation - summary results from the first 200 accredited imaging systems. *Eur J Nucl Med Mol Imaging.* 2018;45(3):412-22.
17. Viner M, Mercier G, Hao F, Malladi A, Subramaniam RM. Liver SULmean at FDG PET/CT: interreader agreement and impact of placement of volume of interest. *Radiology.* 2013;267(2):596-601.
18. Lam MG, Banerjee A, Louie JD, Sze DY. Splenomegaly-associated thrombocytopenia after hepatic yttrium-90 radioembolization. *Cardiovasc Intervent Radiol.* 2014;37(4):1009-17.
19. van den Hoven AF, Rosenbaum CE, Elias SG, de Jong HW, Koopman M, Verkooijen HM, et al. Insights into the Dose-Response Relationship of Radioembolization with Resin 90Y-Microspheres: A Prospective Cohort Study in Patients with Colorectal Cancer Liver Metastases. *J Nucl Med.* 2016;57(7):1014-9.
20. Grant MJ, Didier RA, Stevens JS, Beyder DD, Hunter JG, Thomas CR, et al. Radiation-induced liver disease as a mimic of liver metastases at serial PET/CT during neoadjuvant chemoradiation of distal esophageal cancer. *Abdom Imaging.* 2014;39(5):963-8.
21. Iyer RB, Balachandran A, Bruzzi JF, Johnson V, Macapinlac HA, Munden RF. PET/CT and hepatic radiation injury in esophageal cancer patients. *Cancer Imaging.* 2007;7:189-94.
22. Wong JJ, Anthony MP, Lan Khong P. Hepatic radiation injury in distal esophageal carcinoma: a case report. *Clin Nucl Med.* 2012;37(7):709-11.
23. Nakahara T, Takagi Y, Takemasa K, Mitsui Y, Tsuyuki A, Shigematsu N, et al. Dose-related fluorodeoxyglucose uptake in acute radiation-induced hepatitis. *Eur J Gastroenterol Hepatol.* 2008;20(10):1040-4.
24. Bienert M, McCook B, Carr BI, Geller DA, Sheetz M, Tutor C, et al. 90Y microsphere treatment of unresectable liver metastases: changes in 18F-FDG uptake and tumour size on PET/CT. *Eur J Nucl Med Mol Imaging.* 2005;32(7):778-87.
25. Bilbao JI, de Martino A, de Luis E, Diaz-Dorransoro L, Alonso-Burgos A, Martinez de la Cuesta A, et al. Biocompatibility, inflammatory response, and recanalization characteristics of nonradioactive resin microspheres: histological findings. *Cardiovasc Intervent Radiol.* 2009;32(4):727-36.
26. Sangro B, Gil-Alzugaray B, Rodriguez J, Sola I, Martinez-Cuesta A, Viudez A, et al. Liver disease induced by radioembolization of liver tumors: description and possible risk factors. *Cancer.* 2008;112(7):1538-46.
27. Pasciak AS, Abiola G, Liddell RP, Crookston N, Besharati S, Donahue D, et al. The number of microspheres in Y90 radioembolization directly affects normal tissue radiation exposure. *Eur J Nucl Med Mol Imaging.* 2020;47(4):816-27.
28. Higashi K, Clavo AC, Wahl RL. In vitro assessment of 2-fluoro-2-deoxy-D-glucose, L-methionine and thymidine as agents to monitor the early response of a human adenocarcinoma cell line to radiotherapy. *J Nucl Med.* 1993;34(5):773-9.
29. Kim H, Baek SE, Moon J, Roh YH, Lee N, Cho A. Increased hepatic FDG uptake on PET/CT in hepatic sinusoidal obstructive syndrome. *Oncotarget.* 2016;7(42):69024-31.

30. Kuruva M, Mittal BR, Abrar ML, Kashyap R, Bhattacharya A. Multivariate analysis of various factors affecting background liver and mediastinal standardized uptake values. *Indian J Nucl Med.* 2012;27(1):20-3.
31. Yuan H, Tong DK, Vardhanabhuti V, Khong PL. Factors that affect PERCIST-defined test-retest comparability: an exploration of feasibility in routine clinical practice. *Clin Nucl Med.* 2015;40(12):941-4.
32. Hofheinz F, Apostolova I, Oehme L, Kotzerke J, van den Hoff J. Test-Retest Variability in Lesion SUV and Lesion SUR in (18)F-FDG PET: An Analysis of Data from Two Prospective Multicenter Trials. *J Nucl Med.* 2017;58(11):1770-5.
33. Hofheinz F, Maus J, Zschaeck S, Rogasch J, Schramm G, Oehme L, et al. Interobserver variability of image-derived arterial blood SUV in whole-body FDG PET. *EJNMMI Res.* 2019;9(1):23.
34. Torizuka T, Tamaki N, Inokuma T, Magata Y, Sasayama S, Yonekura Y, et al. In vivo assessment of glucose metabolism in hepatocellular carcinoma with FDG-PET. *J Nucl Med.* 1995;36(10):1811-7.
35. Deipolyi AR, England RW, Ridouani F, Riedl CC, Kunin HS, Boas FE, et al. PET/CT Imaging Characteristics After Radioembolization of Hepatic Metastasis from Breast Cancer. *Cardiovasc Intervent Radiol.* 2020;43(3):488-94.

## Supplementary material

**Supplemental Table 1.** PERCIST criteria

PERCIST	
<b>Main criteria</b>	
Patient preparations	4-6 hours fasting
Serum glucose level	< 200 mg/dl (<11,1 mmol/l)
Injected activity	Center dependent, but within 20% difference between scans
Measurement unit	1. SUVLBM = SUL 2. SULpeak = 1 cm <sup>3</sup> VOI
Glucose correction	No
Timing restrictions	PET at least 10 days after last chemotherapy 8-12 weeks after external beam radiotherapy
Scan restrictions	>50 minutes p.i. < 15 min difference in p.i. times between studies. (but always > 50 min p.i.) Normal liver SUL must be within 20% (and < 0,3 SUL units) between baseline and follow-up scans Always same scanner, same model, same reconstructions
Partial volume correction	No
Correlation with other tissues*	3 cm diameter VOI in right liver lobe, expressed in SULmean + SD. If liver is affected or VOI cannot be placed: 1 cm diameter axial (ROI) with 2 cm diameter in z-axis (= ellipse VOI)
<b>Measurements</b>	
Tumor	SULpeak VOI centered around hottest point in tumor foci (around maximum SUL pixel; which also should be noted)
Number of lesions	Most intense hypermetabolic tumors Up to 5 lesions (up to 2 per organ) 2 cm in diameter (though smaller lesions with sufficient uptake might be included). Baseline tumor uptake: > 1,5 x SULmean,liver + 2 SDs SULmean,liver Or > 2 x SULmean,bloodpool + 2 SDs SULmean,mediastinum
Follow up measurements	Most intense lesions, not necessarily the same lesions
<b>Additional parameters</b>	
Definition response:	
Calculation	Sum of PERCIST lesions
Complete metabolic response	Visual disappearance of all metabolic active tumors
Partial metabolic response	>30% reduction and at least 0,8 unit decline in SULpeak
Stable disease	Between partial response and progressive disease
Progressive metabolic disease	>30% increase and at least 0,8 unit increase in SULpeak or new metabolic active tumors or >75% increase in TLG

SUV = standardized uptake value, LBM = lean body mass, SUL = SUV corrected for lean body mass, p.i. = post-injection, SD = Standard deviation, TLG = total lesion glycolysis. \* modified PERCIST 1.0: threshold for minimal metabolically measurable tumor activity is 1.5 x mean liver SUL instead of 1.5 x mean liver SUL + 2 SDs (as in the conventional PERCIST)





The background of the slide is a dense, multi-colored pattern of small, round confetti pieces in various colors including white, yellow, green, blue, red, and pink. The text is overlaid on this pattern.

## Part III

### Radiological perspectives on radioembolization



The background of the entire slide is a dense, multi-colored confetti pattern. The confetti consists of small, round, multi-colored beads in various colors including red, yellow, green, blue, purple, and white, scattered across the entire surface.

CHAPTER  
EIGHT

**The caudate lobe –  
the blind spot in radioembolization  
or an overlooked opportunity?**

**Manon N.G.J.A. Braat, Andor F. van den Hoven, Pieter J. van Doormaal,  
Rutger C. Bruijnen, Marnix G.E.H. Lam, Maurice A.A.J. van den Bosch**

*Cardiovascular and Interventional radiology 2016 Jun;39(6):847-54.*

## Abstract

### Purpose

The caudate lobe (CL) is impartial to the functional left and right hemi-liver and has outspoken inter-individual differences in arterial vascularization. Unfortunately, this complexity is not specifically taken into account during radioembolization treatment (RE), potentially resulting in under- or overtreatment of the CL. The objective of this study was to evaluate the CL coverage in RE and determine the detection rate of the CL arteries on CT angiography during work-up.

### Methods

In all consecutive patients who underwent RE treatment between May 2012 – January 2015  $^{99m}\text{Tc}$ -MAA SPECT/CT and post-treatment scans ( $^{90}\text{Y}$ -bremsstrahlung SPECT/CT,  $^{90}\text{Y}$ -PET/CT, or  $^{166}\text{Ho}$ -SPECT/CT) were reviewed for activity in the CL. Pre-treatment CT angiographies were reviewed for the visibility of the CL arteries.

### Results

Eighty-two patients were treated. In 32/82 (39%) the CL was involved. In 6/32 (19%) patients no activity was seen on the post-treatment scan in the CL, whereas in 40/50 (80%) patients without CL tumor-involvement the CL was treated.  $^{99m}\text{Tc}$ -MAA SPECT/CT and final post-treatment scans were discordant in 16/78 (21%).  $^{99m}\text{Tc}$ -MAA SPECT/CT had a positive and negative predictive value of 94% and 46% respectively for activity in the CL after RE. In untreated CLs significant hypertrophy was observed with a median volume increase of 33% ( $p=0,02$ ). CL arteries were seldom visible on the pre-treatment CT; the identification rate was 12-17%.

### Conclusion

Currently in RE treatments, targeting or sparing of the CL is highly erratic and independent of tumor-involvement. Intentional treatment or bypassing of the CL seems worthwhile to either improve tumor coverage or enhance functional liver remnant.

## **Introduction**

The caudate lobe (segment 1 and 9 according to Couinaud's classification) is not regarded as a distinct part of the functional left or right hemiliver, due to its highly variable vascular anatomy. Cadaveric dissection and radiologic studies have found a range of 1-5 arterial branches supplying the caudate lobe (CL), with 2-3 branches being the most common (1, 2). These branches can originate from the right hepatic artery (RHA), left hepatic artery (LHA), middle hepatic artery (MHA)/segment 4 artery (S4A) and/or the right posterior hepatic artery (RPHA). At dissection Lee et al. identified a CL branch originating from the RHA or RPHA in 38/45 livers (84%) and a branch originating from the LHA in 20/45 livers (44%) (1). Hence, dual supply of the CL is a common normal variant.

The CL is usually not targeted separately during RE treatments, nor is its volume and vascularization considered during prescribed activity calculations. The latter is of lesser importance during whole liver treatments with the catheter positioned in the common (CHA) or proper hepatic artery (PHA). However, in most treatments the RHA and LHA are separately injected, which necessitates a division of the planned target volume.

The aim of this study was to evaluate the effect of RE treatment on the CL and its relation to CL tumor-involvement. Secondly, we determined the visibility of CL arteries on CT angiography and the associated inter-observer reproducibility.

## **Methods**

### **Study population and design**

Between May 2012 – January 2015 86 consecutive radioembolization candidates with both primary and secondary liver tumors underwent RE treatment. All patients had unresectable tumors and were refractory to standard treatment. We retrospectively reviewed the imaging data related to the RE treatment. The medical ethics committee of our institution has waived the need for informed consent for the review of imaging data from RE patients.

## Treatment

All patients underwent screening with  $^{18}\text{F}$ FDG-PET and multiphase liver CT. All CT scans were acquired on an integrated PET/CT scanner (Biograph mCT, Siemens Healthcare, Erlangen, Germany) with 40 detector rows, using a matrix size of 512 x 512, rotation time of 0.4-0.5 sec, pitch of 0.9-1.2, and fixed 120 kV tube potential.

For the CT 150-185 ml (depending on body weight) Iopromide 300 mg/ml (Ultravist, Bayern Schering Pharma AG, Berlin Germany) was injected at a rate of 5 ml/s followed by a 50 ml saline chaser. Two CT protocols were applied in this population, differing only in arterial phase (early or late arterial phase). The arterial phase was either obtained with a post-threshold delay (abdominal aorta enhancement > 100HU) of 20 sec at a tube current of 150 mAs or with a post-threshold delay of 10 sec at a tube current of 150 mAs or 200 mAs (200 mAs in patients >85 kg). The portal venous phase was obtained with equal parameters.

Subsequently, a pre-treatment angiography (DSA) was performed. Approximately 150 MBq technetium-99m-macroaggregated albumin ( $^{99\text{m}}\text{Tc}$ -MAA) (TechneScan LyoMaa, Mallinckrodt Medical, Petten, The Netherlands) was intra-arterially injected, followed by a  $^{99\text{m}}\text{Tc}$ -MAA planar scintigraphy and single-photon emission computed tomography (SPECT)/CT (Symbia 16T, Siemens Healthcare, Erlangen, Germany).

RE was performed using yttrium-90 ( $^{90}\text{Y}$ )-labeled resin microspheres (Sir-Spheres, SIRTex, Lane Cove, Australia) according to international guidelines or Holmium-166 poly(L-lactic acid) microspheres ( $^{166}\text{Ho}$ ) as previously described (3). The positions of the endhole catheter tip, defining injection position(s) during RE treatment were similar to the  $^{99\text{m}}\text{Tc}$ -MAA injection position(s). Depending on the microspheres used, a  $^{90}\text{Y}$ -bremsstrahlung SPECT/CT,  $^{90}\text{Y}$ -positron emission tomography (PET)/CT, or  $^{166}\text{Ho}$ -SPECT/CT was performed to assess the distribution of the activity. Our acquisition protocols were published earlier (3, 4). Only patients that underwent post-treatment imaging were included.

## Image analyses

All images were stored in a picture archiving and communication system. For analysis of the arterial supply and CL volume the images were exported, anonymized, and loaded into OsiriX (version 5.8, 32-bit, MacOS X).

Two radiologists (MB and PJVD) scored the presence, number and origin of the CL arteries on CT angiography. They were blinded for all patient data, including angiographies and post-treatment scans. If present, the origin was marked by each of the observers. To assess the volumetric changes of the CL one observer (MB) manually segmented the CL on the pre-treatment liver CT and on the last available abdominal CT. CL tumor(s) were excluded from the volume. In case of repeated RE treatment, the last CT before the second treatment was used. Only first treatments were analyzed.

The deposition of activity in the CL was assessed after treatment by  $^{90}\text{Y}$  bremsstrahlung SPECT/CT,  $^{90}\text{Y}$ -PET/CT, or  $^{166}\text{Ho}$ -SPECT/CT. CL deposition was considered present if the majority (>2/3) of the CL showed activity. The  $^{99\text{m}}\text{Tc}$ -MAA SPECT/CT was assessed in a similar fashion. The presence of CL tumor(s), activity on the post-treatment scan and  $^{99\text{m}}\text{Tc}$ -MAA SPECT/CT, as well as the CL volumes were scored by one observer (MB), at different time points. In case of doubt, a second reader (ML) was consulted and a consensus was reached.

## Statistics

Descriptive statistics and independent-samples T-tests were used to explore baseline characteristics and CL artery origin locations. Data with a normal and non-normal distribution are presented as mean  $\pm$  standard deviation and median (range) respectively.

A Wilcoxon rank sum test was used to test for differences in CL volume between patients. A Wilcoxon signed rank test was used to assess intra-individual changes in the CL volume.

Chi-square tests and Fisher's exact tests were used to compare the visibility of CL arteries and the  $^{99\text{m}}\text{Tc}$ -MAA SPECT/CT and post-treatment scans in relation to the presence of tumor.

All analyses were performed with IBM SPSS Statistics version 22. A p-value < 0.05 was considered statistically significant.



## Results

A total of 86 patients underwent RE treatment and post-treatment imaging. Four patients were excluded because of prior CL resection. The baseline characteristics of the remaining 82 patients are presented in **Table 1**.

In 32 patients (39%) a tumor was located in the CL. Patients with CL tumor-involvement had a higher liver tumor burden than those without CL tumor-involvement, with a median of 19% and 7.5% respectively ( $p=0.015$ ). All patients with >50% tumor burden ( $n=4$ ) had CL tumor-involvement.

### CL activity (Table 2)

In 6/32 (19%) patients with CL tumor-involvement no activity was seen on the post-treatment scan in the CL (**Figure 1**). Conversely, 40/50 (80%) patients without CL tumor showed activity in the CL. There was no association between post-treatment CL activity and CL tumor involvement or microsphere type.

CL volumetric measurements were possible in 57/82 (70%). The median interval between measurements was 153 days (21-827 days). After RE, the median CL volume increased from 36 ml to 48 ml in patients with an untreated CL (median volume increase 33% (range -1-243%);  $p=0.02$ ). In patients with a treated CL, a non-significant decrease from 38 ml to 32 ml was observed.

Additionally,  $^{99m}\text{Tc}$ -MAA SPECT/CTs and post-treatment scans were compared. In 13/24 (54%) cases with a negative  $^{99m}\text{Tc}$ -MAA SPECT/CT the post-treatment scan did show activity in the CL. Conversely, in 3/14 negative post-treatment scans the  $^{99m}\text{Tc}$ -MAA SPECT/CT did show activity in the CL. These results correspond to a positive predictive value of 94%, negative predictive value of 46%, false negative rate of 54% and false positive rate of 6%.

Review of the DSAs of the negative post-treatment scans revealed that in all cases the LHA, RHA (and sometimes MHA) were separately injected. Review of the DSAs of the discrepant  $^{99m}\text{Tc}$ -MAA SPECT/CTs and post-treatment scans revealed no consistent explanation (**Supplement 1**) (**Figure 2 and 3**).

**Table 1.** Baseline characteristics

Characteristic	All patients (n=82)	CL tumor (n=32)	No CL tumor (n=50)	p-value*
<b>Age (years)</b>	64 ± 11	64 ± 10	64 ± 11	NS
<b>Sex</b>				
Male	47 (57%)	19 (59%)	28 (56%)	NS
Female	35 (43%)	13 (41%)	22 (44%)	
<b>BMI</b>	27 ± 4	27 ± 5	27 ± 4	NS
<b>Primary tumor</b>				
CRC	57 (70%)	22 (69%)	35 (70%)	NS
Cholangiocarcinoma	8 (10%)	5 (16%)	3 (6%)	
Uveal melanoma	6 (7%)	1 (3%)	5 (10%)	
Breast carcinoma	4 (5%)	3 (9%)	1 (2%)	
Others <sup>a</sup>	7 (9%)	1	6	
<b>Liver tumor burden</b>				
<25%	73 (89%)	25 (78%)	48 (96%)	<b>0.02</b>
25-50%	5 (6%)	3 (9%)	2 (4%)	
>50%	4 (5%)	4 (13%)	0	
<b>Previous liver treatment</b>				
Right hemihepatectomy <sup>b</sup>	5 (6%)	3 (9%)	2 (4%)	NS
Segmentectomy/ metastasectomy	7 (9%)	3 (9%)	4 (8%)	
RFA	1 (1%)	1 (3%)	0	
<b>Treatment</b>				
Whole liver in one session	71 (90%)	27 (84%)	47 (94%)	NS
Sequential lobar	5 (6%)	3 (9%)	2 (4%)	
Lobar (right-sided)	3 (4%)	2 (6%)	1 (2%)	
<b>Microsphere</b>				
<sup>90</sup> Y	52 (63%)	18 (56%)	34 (68%)	NS
<sup>166</sup> Ho	30 (37%)	14 (44%)	16(32%)	
<b>Post-treatment scan</b>				
<sup>90</sup> Y-SPECT	2 (2%)	0	2 (4%)	NS
<sup>90</sup> Y-PET	50 (61%)	18 (56%)	32 (64%)	
<sup>166</sup> Ho-SPECT	27 (27%)	13 (41%)	14 (44%)	
<sup>166</sup> Ho-PET	2 (2%)	1 (3%)	1 (2%)	
MRI <sup>c</sup>	1 (1%)	0	1 (2%)	

<sup>a</sup> Pancreatic carcinoma (n=2), Gastric carcinoma (n=1), Thymoma (n=1), oesophageal carcinoma (n=1), NET (n=1), RCC (n=1)

<sup>b</sup> Right hemihepatectomy (n=1), extended right hemihepatectomy (n=4)

<sup>c</sup>No <sup>166</sup>Ho- SPECT imaging was performed in one case, though deposition of <sup>166</sup>Ho microspheres in the CL was clearly seen on follow-up MRI.

\* p<0,05 is considered significant. NS = not significant.

**Table 2.** Comparison of treatments with and without CL activity

	Activity in CL	No activity in CL	p-value*
<b>CL tumor</b>			
Yes	26 (81%)	6 (19%)	0.889
No	40 (80%)	10 (20%)	
<b>Microsphere</b>			
<sup>90</sup> Y	43 (83%)	9 (17%)	0.569
<sup>166</sup> Ho	23 (77%)	7 (23%)	
<b>CL volume pre-treatment</b>			
(in ml) <sup>a</sup>	38 (2-154)	36 (19-80)	
<b>CL volume post-treatment (in ml)<sup>a</sup></b>			
	32 (0-115)	48 (9-244)	
<b>Activity in CL on <sup>99m</sup>Tc-MAA SPECT/CT scan<sup>b</sup></b>			
Yes	51 (80%)	3 (21%)	<0.001†
No	13 (20%)	11 (79%)	

<sup>a</sup> In 24/79 cases follow-up did not include a portal venous CT-scan for volume measurements. Caudate lobe tumor(s) were subtracted from the volume of the caudate lobe; the volume of 0 ml corresponds to a caudate lobe that is completely engulfed by tumor. Values expressed in median (range).

<sup>b</sup> In 4 cases no <sup>99m</sup>Tc-MAA SPECT/CT was performed; only a <sup>166</sup>Ho-scout SPECT-CT.

\* Fisher's exact test

†  $p < 0.05$  is considered significant. Significant differences are marked.

### CL arteries

44 patients were scanned in the early arterial phase and 38 patients in the late arterial phase. In 10/82 (12%) patients both observers identified one CL artery, whereas in four cases only one rater identified a CL artery. In 68/82 (83%) both observers could not identify a CL artery. The specific proportion of agreement including the exact origin of a CL artery was 95% (78/82). A CL artery originated from the LHA (n=4), RHA (n=3), CHA (n=2) and PHA (n=1). In 11/32 (34%) cases with CL tumor-involvement a CL artery was identified, compared to 3/50 (6%) cases without CL tumor-involvement ( $p=0.002$ ). Visibility of the CL arteries was not related to the presence of activity in the CL after RE or to the pre-treatment CL volume.

Nearly all visible CL arteries (12/14, 85%) were detected on the early arterial phase.

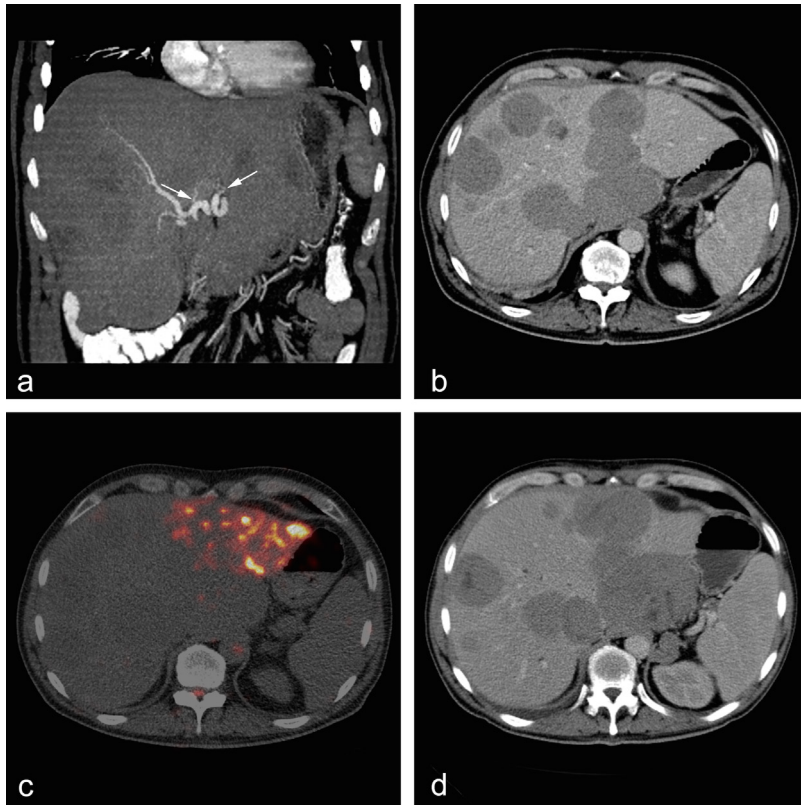


**Figure 1.** Failure to treat a CL metastasis in a patient with bilobar metastases of an uveal melanoma. a) On the coronal maximum intensity projection (MIP) image of the early arterial phase (post-threshold delay of 10 sec) two CL arteries can be identified. One branch arising from the RHA and one arising from the LHA; only the branch arising from LHA was identified by both raters. b) A large metastasis is present in the CL, mainly occupying the Spigelian lobe. The patient was treated with  $^{90}\text{Y}$  with sequential deliveries; the left lobe was treated six weeks after the right lobe had been treated. c) The  $^{90}\text{Y}$ -PET-CT of the left treatment shows no activity in the CL, similar to the treatment of the right lobe (not shown). d) The CECT obtained 6 months after RE treatment of the left lobe shows progression of the lesion in the CL, whereas the lesions in the right lobe are still smaller than on the baseline scan (compare to image b).



**Figure 2.** Unintentional CL targeting during  $^{99m}\text{Tc}$ -MAA administration in a patient with bilobar colorectal liver metastases, but no CL metastasis. DSA of the endhole catheter position during  $^{99m}\text{Tc}$ -MAA injection. A large caliber CL artery (arrow) was mistakenly interpreted as the artery of segment 4, resulting in massive accumulation of  $^{99m}\text{Tc}$ -MAA in the CL at  $^{99m}\text{Tc}$ -MAA SPECT-CT (**Figure 3a**).

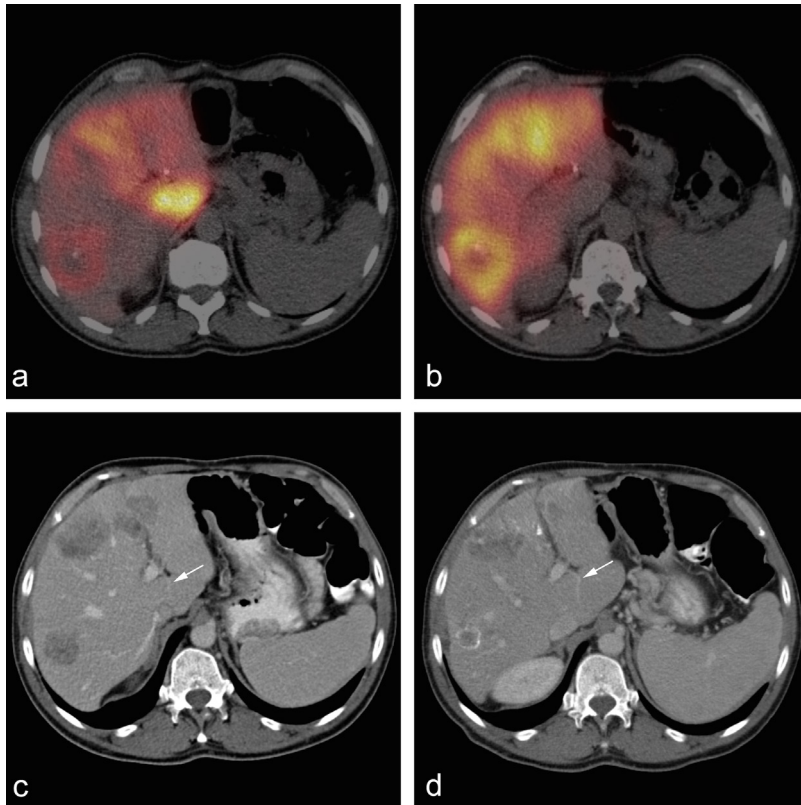


**Figure 3.** Unintentional CL targeting (clinical example of **Figure 2** continued). a)  $^{99m}\text{Tc}$ -MAA SPECT-CT: massive accumulation of  $^{99m}\text{Tc}$ -MAA in the CL. At RE treatment this easily identifiable artery was intentionally bypassed. b)  $^{166}\text{Ho}$ -SPECT/CT after RE treatment: no activity in the CL. Contrast enhanced CT pre-treatment (c) and follow-up at six months after RE (d) at the level of a portal branch arising from the left portal vein (arrow): hypertrophy of the CL with a volume increase of 279% (24 ml to 67 ml).

## Discussion

Our results show that the CL was often treated, regardless of CL tumor-involvement or identification of its arteries. Identification of the CL arteries on CT was suboptimal, but when visible there was often CL tumor-involvement.

In this context, it is important to address the highly variable and complicated anatomy of the CL. The CL is subdivided into 3 parts: the paracaval portion, Spigelian lobe and caudate process (1). Vascular supply of these parts varies considerably with 1-6 portal branches and 1-5 arterial branches (1, 2). The paracaval portion and caudate process are nearly always supplied by the RHA, whereas the Spigelian lobe can be supplied by the LHA, RHA or MHA/S4A or a combination (1, 2).

Separate assessment of the parenchymal territories of the CL arteries mandates a high spatial resolution; i.e. higher than most acquired post-treatment scans. Therefore the CL was considered adequately treated if more than two-thirds showed activity. Hence, in some cases not all CL arteries will have been injected with particles (**Figure 4**). Currently only one report on the presence of activity in the CL has been published. Gates et al. found  $^{99m}\text{Tc}$ -MAA activity in the CL in 19/51 (37%) patients after proximal RHA injection (5). In comparison, 79% of our patients showed CL activity, pleading for a substantial contribution of the LHA or more proximal branches.

Another important consideration is treatment planning. In our practice, the CL is incorporated in the right hemi-liver volume (presumed RHA territory) for activity calculations. Considering the variable inter-individual arterial anatomy and CL volume, this might lead to errors in planned target volume, and under- or overdosage of the CL or the adjacent arterial territory.

Also, the potential contribution of parasitized extrahepatic arteries has to be considered, especially in hepatocellular carcinoma (HCC). Several small studies have been published on intra-arterial treatments of CL HCC (2, 6, 7). All report multiple cases with 2-4 CL arteries and at least one case with a feeding artery arising from the right inferior phrenic artery. This necessitates not only a proximal injection during angiography or C-arm CT to evaluate all CL arteries but also a search for possible extrahepatic sources.

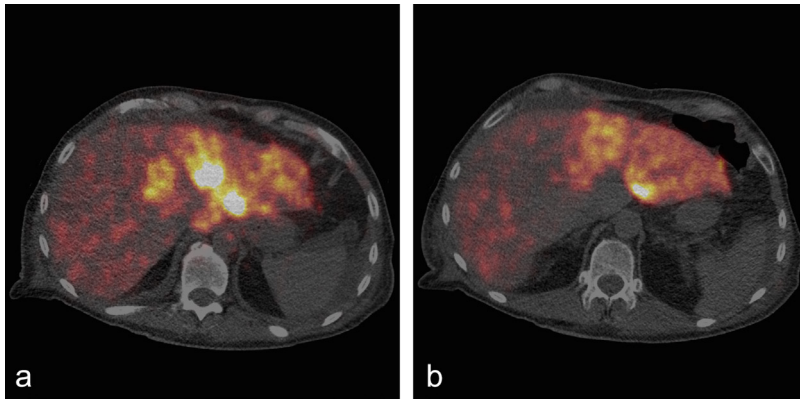


**Figure 4.** Unnecessary partial treatment of the CL in a patient with bilobar liver metastases of a neuroendocrine tumor without CL tumor-involvement. The patient was treated in a single whole liver session.  $^{90}\text{Y}$ -PET-CT after RE treatment: two levels are shown (a-b). Due to intrahepatic shunting (not shown) the left liver lobe received a larger part of the dose. a) In the cranial part of the Spigelian lobe accumulation of  $^{90}\text{Y}$  is clearly seen. b) The caudal part of the Spigelian lobe and caudate process show no activity (even less than the right lobe).

A large number of our patients (39%) had CL tumor-involvement. This is considerably higher than in previously published hepatectomy and TACE series with an incidence of 4.5-7.5% (2, 6, 8). Consistent with our findings, these studies observed a higher liver tumor burden in patients with CL involvement. This difference in incidence is probably attributable to the higher tumor burden in patients referred for RE and the increased prevalence of metastases.

We observed a surprising discordance between the deposition of the  $^{99\text{m}}\text{Tc}$ -MAA and  $^{90}\text{Y}$  or  $^{166}\text{Ho}$  in the CL.  $^{99\text{m}}\text{Tc}$ -MAA particles vary substantially from  $^{90}\text{Y}$  and  $^{166}\text{Ho}$  particles. The larger size, specific gravity, injected particle load, injected volume and embolic potential of the latter two are known to cause stasis and potential retrograde reflux (9). Reflux or redistribution into the proximal branching CL arteries is most likely the cause of this discordance, especially since direct comparison of the injection positions revealed no consistent differences.



Hypertrophy of untreated lobes is a known by-effect of RE treatment. Some advocate replacing portal vein embolization with radiation lobectomy to induce hypertrophy whilst treating the underlying liver tumors (10). In these cases sparing of a tumor-free CL could be beneficial, either as bridge to surgery or as important functional liver remnant in case of repeated RE treatments (Figure 5).

Caudate lobe resections have high complication rates and mortality rates, together with smaller tumor-free margins, more positive resection margins and higher recurrence rates (8). Ibrahim et al. report on RE treatment of eight CL HCC, resulting in downstaging in four patients and subsequent liver transplantation in three (7). Thus, RE might be an attractive option for downstaging and diminishing positive resection margins in CL resections.

This study is most importantly limited by its retrospective design. Identification of CL arteries is notoriously difficult on two-dimensional DSA projections due to their unknown origin and number, small caliber and overlap with other hepatic arteries (2, 6). During the pre-treatment angiography the CL arteries were not selectively examined and the DSA images available for review were not acquired in a standardized fashion and only at one projection angle, prohibiting reliable review of the CL artery origins. C-arm CT could benefit their detection (6), yet was not consistently acquired.

## **Conclusion**

Though the CL is often neglected during RE planning or treatment, its consideration seems worthwhile. If CL tumor-involvement is present, identification of its feeding arteries is necessary to obtain a comprehensive treatment result. Moreover, intentional sparing of a tumor-free CL should be endeavored to enhance the future functional liver remnant for additional liver directed therapies.

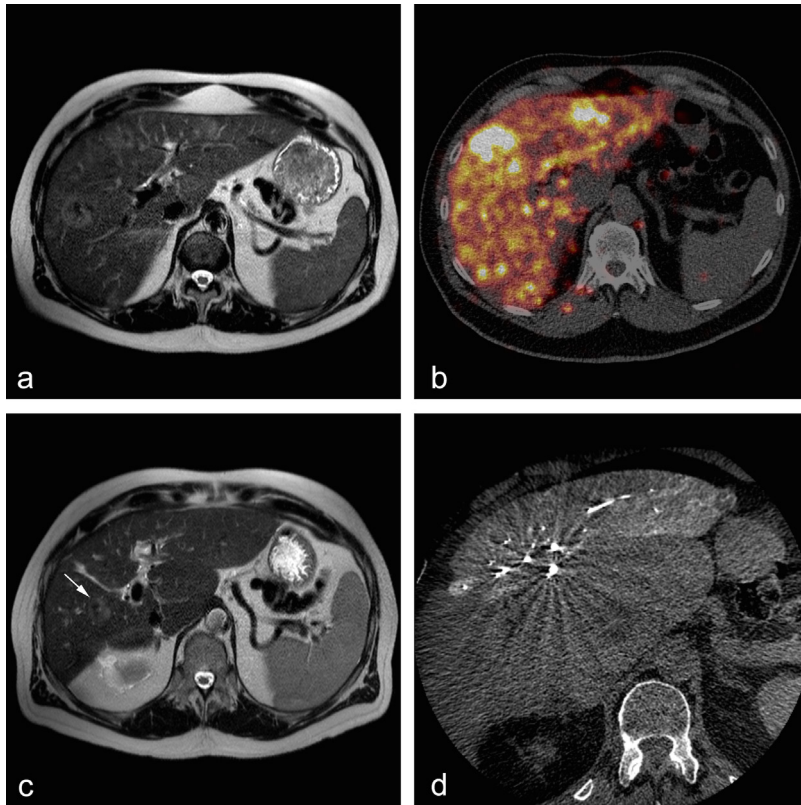


**Figure 5.** Compensatory hypertrophy after intentional sparing of the CL in a patient with colorectal liver metastases, not involving the CL. a) Pre-treatment T2-weighted image of the liver with multiple bilobar metastases. The CL has a volume of 68 ml. b)  $^{90}\text{Y}$ -PET-CT after the first RE treatment, showing no accumulation of  $^{90}\text{Y}$  in the CL (non-intentional). c) T2-weighted image obtained nine months after RE treatment. The CL has hypertrophied to a volume of 308 ml. A persisting metastasis is seen in liver segment 6 (arrow). Because of the good initial response to RE treatment and absent extrahepatic disease, this patient has now undergone two retreatments. As the CL continued to be free of metastases it was intentionally bypassed during these retreatments. d) C-arm CT image obtained during the first retreatment. The catheter is positioned relatively distal in the left hepatic artery (LHA); no parenchymal enhancement of the hypertrophied CL is seen.

## References

1. Lee UY, Murakami G, Han SH. Arterial supply and biliary drainage of the dorsal liver: a dissection study using controlled specimens. *Anatomical science international*. 2004;79(3):158-66.
2. Yoon CJ, Chung JW, Cho BH, Jae HJ, Kang SG, Kim HC, et al. Hepatocellular carcinoma in the caudate lobe of the liver: angiographic analysis of tumor-feeding arteries according to subsegmental location. *Journal of vascular and interventional radiology : JVIR*. 2008;19(11):1543-50; quiz 50.
3. Elschot M, Vermolen BJ, Lam MG, de Keizer B, van den Bosch MA, de Jong HW. Quantitative comparison of PET and Bremsstrahlung SPECT for imaging the in vivo yttrium-90 microsphere distribution after liver radioembolization. *PLoS one*. 2013;8(2):e55742.
4. Elschot M, Nijsen JF, Lam MG, Smits ML, Prince JF, Viergever MA, et al. ((9)(9)m)Tc-MAA overestimates the absorbed dose to the lungs in radioembolization: a quantitative evaluation in patients treated with (1)(6)(6)Ho-microspheres. *European journal of nuclear medicine and molecular imaging*. 2014;41(10):1965-75.
5. Gates VL, Singh N, Lewandowski R, Spies SM, Salem R. INTRA-ARTERIAL HEPATIC SPECT/CT IMAGING USING TECHNETIUM-99M MACRO-AGGREGATED ALBUMIN IN PREPARATION FOR RADIOEMBOLIZATION. *Journal of nuclear medicine : official publication, Society of Nuclear Medicine*. 2015.
6. Choi WS, Kim HC, Hur S, Choi JW, Lee JH, Yu SJ, et al. Role of C-arm CT in identifying caudate arteries supplying hepatocellular carcinoma. *Journal of vascular and interventional radiology : JVIR*. 2014;25(9):1380-8.
7. Ibrahim SM, Kulik L, Baker T, Ryu RK, Mulcahy MF, Abecassis M, et al. Treating and downstaging hepatocellular carcinoma in the caudate lobe with yttrium-90 radioembolization. *Cardiovasc Intervent Radiol*. 2012;35(5):1094-101.
8. Thomas RL, Lordan JT, Devalia K, Quiney N, Fawcett W, Worthington TR, et al. Liver resection for colorectal cancer metastases involving the caudate lobe. *The British journal of surgery*. 2011;98(10):1476-82.
9. Bult W, Vente MA, Zonnenberg BA, Van Het Schip AD, Nijsen JF. Microsphere radioembolization of liver malignancies: current developments. *The quarterly journal of nuclear medicine and molecular imaging : official publication of the Italian Association of Nuclear Medicine (AIMN) [and] the International Association of Radiopharmacology (IAR), [and] Section of the So*. 2009;53(3):325-35.
10. Garlipp B, de Baere T, Damm R, Irmischer R, van Buskirk M, Stubs P, et al. Left-liver hypertrophy after therapeutic right-liver radioembolization is substantial but less than after portal vein embolization. *Hepatology (Baltimore, Md)*. 2014;59(5):1864-73.

## Supplementary material

### Supplement 1.

Review of the DSA of the negative and discordant  $^{99m}\text{Tc}$ -MAA SPECT/CT and post-treatment scans

Review of the DSA of the negative post-treatment scans revealed that in all of these cases the LHA, RHA (and sometimes the MHA) were separately injected. Secondly, the angiographies of the discrepant  $^{99m}\text{Tc}$ -MAA SPECT/CT and post-treatment scans were reviewed. In 3 cases CL activity was seen on the  $^{99m}\text{Tc}$ -MAA SPECT/CT but not on the post-treatment scan. In one case a large caliber CL artery was mistakenly interpreted as the artery of segment 4 at the pre-treatment angiography and consequently intentionally bypassed at the eventual RE treatment (**Figure 2 and 3** in the original manuscript). In another case the injection position at the  $^{99m}\text{Tc}$ -MAA was slightly more proximal in the RHA than at the RE treatment, though no extra arterial branches were identified in between these 2 injection positions on the angiography. In the last case the injection positions were similar for the proximal LHA and RHA, only the MHA was injected slightly more distal at the RE treatment (<1 cm). In this last case no explanation for the discrepancy could be identified.

In the 13 cases with a negative  $^{99m}\text{Tc}$ -MAA SPECT/CT and a positive post-treatment scan catheter positions were similar for the  $^{99m}\text{Tc}$ -MAA injection and final treatment in all but two cases. In the first case the  $^{99m}\text{Tc}$ -MAA was injected in the CHA, whereas the catheter was positioned in 3 distal branches of the LHA and proximal in the RHA at final RE treatment. In the last case the injection position in the RHA at the RE treatment was approximately 1 cm more proximal than at  $^{99m}\text{Tc}$ -MAA injection. Hence, no conclusive explanation for the discrepant results between the  $^{99m}\text{Tc}$ -MAA SPECT/CT's and positive post-treatment scans could be identified.



# CHAPTER NINE

## Liver CT for vascular evaluation during radioembolization work-up: comparison of an early and late arterial phase protocol

Andor F. van den Hoven, Manon N.G.J.A. Braat, Jip F. Prince, Pieter J. van Doormaal,  
Maarten S. van Leeuwen, Marnix G.E.H. Lam, Maurice A.A.J. van den Bosch

*European Radiology* 2017 Jan; 27(1):61-69.

## **Abstract**

### **Objectives**

Compare right gastric (RGA) and segment 4 artery (S4A) origin detection rates during radioembolization work-up between early and late arterial phase liver CT protocols, and determine inter-rater reproducibility.

### **Methods**

One hundred consecutive patients were included who underwent liver CT between May 2012 – January 2015 with an early or late arterial phase protocol (n=50 each, 10 vs. 20 sec post-threshold delay). RGA and S4A origin detection rates, assessed by two raters, and CNR of the hepatic artery relative to the portal vein were compared between both protocols. Inter-rater reproducibility measures were determined.

### **Results**

The first-second rater scored the RGA origin as visible in 58-65% (specific proportion of agreement [SPA] 82%,  $\kappa=0.62$ ); S4A origin in 96-89% (SPA 94%,  $\kappa=0.54$ ). Thirty-six percent of RGA origins not detectable by DSA were identified on CT. Origin detection rates were not significantly different for early/late arterial phases. Mean CNR was higher in the early arterial phase protocol (1.7 vs. 1.2,  $p<0.001$ ).

### **Conclusion**

A 10-second delay arterial phase protocol does significantly not improve the detection rate of small intra- and extrahepatic branches, despite increased CNR. RGA origin detection requires further optimization, whereas S4A/MHA origin detection is adequate, with good inter-rater reproducibility.

## Introduction

Radioembolization has evolved as a safe and effective treatment option in patients with liver tumors that are not resectable and are refractory to standard systemic therapy (1). Since this treatment encompasses the injection of radioactive microspheres via a microcatheter positioned in the hepatic arteries, it is essential to perform a thorough assessment of the hepatic arterial anatomy before treatment (2).

Intra-procedural imaging with digital subtraction angiography (DSA) – and nowadays increasingly C-arm cone beam CT (C-arm CT) – has been considered the gold standard for vascular evaluation (3). However, since modern multidetector computed tomography (CT) scanners enable high-resolution, multi-phasic, multi-planar imaging of the liver, the arterial vasculature can already be evaluated on CT before the pre-treatment angiography. This has two distinctive advantages. First, CT images can depict the spatial relation between arterial branches and liver parenchyma or gastro-intestinal organs in three dimensions, at high resolution, with a wide field of view. Most importantly, timely assessment of the anatomy enables the establishment of a treatment strategy ahead of time, and results in increased confidence of the operator during the treatment procedure (4).

In our center, a standardized triphasic liver CT protocol encompassing a late arterial, portal venous and equilibrium phase had been used to evaluate the liver parenchyma and vasculature in all patients with liver malignancies, including radioembolization candidates (5-7). The imaging delay of the arterial phase (post-threshold delay of 20 sec) was chosen to allow for detection of hypervascular tumors, but it is questionable whether a late arterial phase is best suited for evaluation of the arterial vasculature.

We noticed in clinical practice that contrast enhancement of the portal vein often obscures the origin of small arterial branches that need to be identified, especially the right gastric artery (RGA) and segment 4 artery (S4A). An early arterial phase with a delay of 10 seconds may reveal the RGA and S4A origin better due to a higher contrast to noise ratio (CNR) of the hepatic artery relative to the portal vein. Furthermore, it remains uncertain how well the RGA and S4A origins can be visualized on liver CT in the population of heavily pre-treated radioembolization patients, and how reproducible these observations are when comparing different raters.



Hence, the purpose of this study was to compare RGA and S4A origin detection rates during radioembolization work-up between early and late arterial phase liver CT protocols, and to determine inter-rater reproducibility.

## **Methods**

### **Study design**

We performed a prospective development study in accordance with the IDEAL recommendations (8). A triphasic liver CT (from now on referred to as standard protocol) was already part of our routine work-up for radioembolization. Tumor detection and localization was not the primary purpose of these scans, since recent other imaging was available in all patients and the liver CT was combined with an  $^{18}\text{F}$ -fluorodeoxyglucose positron emission tomography ( $^{18}\text{FDG}$ -PET) scan.

To improve the visualization of small arterial branch origins, we adjusted our liver CT protocol (from now on referred to as new protocol). The performance of the novel scan protocol was tested by using a historical cohort of patients previously scanned with the standard protocol as comparison.

The medical ethics committee of our institution approved this study and waived the need for informed consent for reviewing imaging data on radioembolization patients in our center.

### **Study population**

A total of 100 patients (50 patients each for both protocols) would be required to demonstrate a 30% difference in RGA detection rate (80% for the new protocol vs. 50% for the standard protocol) with a power of 0.90, at an alpha-level of 0.05 (sample size calculation with 'Power and Sample Size Calculation' version 3.1.2 for MacOSX).

All patients with unresectable and chemorefractory liver tumors who underwent a pre-treatment liver CT in combination with a  $^{18}\text{FDG}$ -PET scan on the same CT scanner, before undergoing a preparatory angiography as part of the radioembolization work-up, were eligible for study participation. Starting in December 2013, 50 consecutive patients were

selected for the new liver CT protocol. A group of 50 consecutive patients who had been scanned earlier using the standard protocol was selected for comparison. Patients with a technical scan failure or those without a preparatory angiography were excluded. Baseline patient characteristics for both groups were compared to ensure a valid comparison.

### **Technique, equipment and scan settings**

On the day before the examination, all patients received 1000 ml of water-soluble contrast solution (Telebrix Gastro 300 mg/ml) per os to enhance the detection of peritoneal disease and lymphadenopathy. In the new protocol, Mannitol solution (100 ml, 15%) was given orally before the scan to stimulate gastric emptying and create a negative contrast with adjacent contrast enhanced vessels. Subsequently, 150-185 ml (depending on body weight) Iopromide 300 mg/ml contrast agent (Ultravist, Bayern Schering Pharma AG, Berlin Germany) was injected with a double syringe injector in the antecubital vein at a rate of 5 ml/s, followed by a 50 ml NaCl chaser.

All CT scans were acquired under breath-hold on an integrated PET/CT scanner (Biograph mCT, Siemens Healthcare, Erlangen, Germany) with 40 detector rows, using a matrix size of 512 x 512, rotation time of 0.4-0.5 sec, pitch of 0.9-1.2, and fixed 120 kV tube potential.

The *standard protocol* consisted of a late arterial, portal venous and an equilibrium phase, which were obtained with a post-threshold (abdominal aorta enhancement > 100 HU) delay of 20, 55 and 300 sec, respectively. A tube current of 150 mAs was used in the arterial and equilibrium phase, and 225 mAs for the portal venous phase. Slice thickness/increment were 0.9/0.7 cm for the arterial phase, and 1.5/1.0 cm for the portal venous and equilibrium phase.

The *new protocol* consisted of an arterial phase with a shortened post-threshold delay of 10 sec, and an unchanged timing of the portal venous phase. No equilibrium phase was acquired.

In this protocol, tube current was dependent on the weight of the patient: 150 mAs in patients < 85 kg, and 200 mAs in patients ≥ 85 kg. In all phases, slice thickness/increment was 0.9/0.7 mm.

The technique used during the preparatory angiography has been published before and confirms to current standards of clinical practice (9,10). DSA images were acquired on an Allura Xper FD20 system (Philips, Best, The Netherlands).

### **Image analyses**

All images were anonymized and loaded into OsiriX (version 5.8, 32-bit, MacOS X) for image analyses.

Two independent raters, an abdominal radiologist (MB) and an interventional radiologist (PJvD), were asked to score: visibility of the RGA origin (yes/no), location of the RGA origin (arrow appointing the region of interest), visibility of the S4A/MHA origin (yes/no), location of the S4A/MHA origin/origins (arrow), ability to distinguish two separate branches to S4a and S4b (yes/no). The raters were instructed to score the origin as not visible when in doubt.

The origins were evaluated on the thin slices (1 mm thickness/ 0,7 mm increment). Use of a maximum intensity projection (MIP) with a reconstructed slice thickness of 4 mm and/or the use of multiplanar reconstruction was optional. Scans of patients who had previously undergone surgery in which the RGA was sacrificed or segment 4 was resected were considered non-evaluable.

The S4A was termed a middle hepatic artery (MHA) when originating in-between a (r) LHA and (r)RHA, as a branch from the CHA or PHA. No true PHA exists in patients with an aberrant hepatic artery, therefore, the RGA or S4A origin was called after the non-aberrant arterial branch if originating distal to the origin of the gastroduodenal artery (GDA) (4).

A third rater (AvdH) independently scored the origin of the RGA on digital subtraction angiography (DSA) to establish a reference standard for correct identification of the RGA origin on CT. This was not done for the S4A score, since DSA cannot provide topographical landmarks to distinguish between liver segments. Unfortunately, C-arm CT images were not available in all patients. The third rater also assessed the individual hepatic arterial anatomy as described earlier (4), and measured the signal to noise ratio (SNR) of the hepatic arteries and portal veins, as well as the contrast to noise ratio (CNR) of the hepatic

arteries relative to the portal vein. Circular ROIs with a diameter of 3-6 mm were drawn in the hepatic artery and the portal vein at approximately the same level in the liver hilum on axial slice MIP (8mm reconstructed slice thickness) images of the arterial phase, and the mean and standard deviation (SD) of the signal (in HU) were noted. The following equations were used:

### Statistical analysis

Descriptive analyses were performed to give an overview of baseline patient characteristics,

$$\text{SNR} = \frac{\text{Mean (HU)}}{\text{SD (HU)}} \quad (\text{Equation 1})$$

$$\text{CNR} = \frac{\text{Mean}_{\text{arteries}} - \text{Mean}_{\text{portal vein}}}{\sqrt{\frac{1}{2} (\text{SD}_{\text{arteries}}^2 + \text{SD}_{\text{portal vein}}^2)}} \quad (\text{Equation 2})$$

and RGA/S4A origin locations. Data with a normal and non-normal distribution are presented as mean  $\pm$  standard deviation and median (range).

A two-sided unpaired student's T-test was used to test for differences in mean arterial and portal SNR, and mean CNR, between the standard and the new protocol.

A chi-square test was used to compare the standard protocol and the new protocol with regard to the rate of correct RGA origin localization (using DSA as a reference standard), and S4A origin detection.

Specific proportion of agreement and kappa statistics were used to indicate inter-rater agreement and reliability for the RGA and S4A origin detection.

All analyses were performed with R Studio version 0.98.1102 for MacOSX. A p-value  $< 0.05$  was considered statistically significant.

## Results

### Patients and scans

Between December 2013 and January 2015, 58 patients were scanned according to the new protocol for liver CT, and were found eligible for inclusion in this study. Eight of these patients were excluded, because the scan was performed on another CT scanner ( $n = 6$ ), or because no angiography was performed ( $n = 2$ ). Between May 2012 and December 2013, 63 patients had undergone a standard triphasic liver CT. Twelve of these patients were not selected for the control group, because the scan was acquired on another CT scanner ( $n = 9$ ), no angiography was performed ( $n = 2$ ), or due to technical failure of the CT scan ( $n = 1$ ). Both groups were comparable with regard to baseline patient characteristics and hepatic arterial anatomy (**Table 1 and 2**).

### Origin of the RGA

Five scans (standard protocol  $n = 4$ , new protocol  $n = 1$ ) were not evaluable for the assessment of the RGA origin, due to previous gastric ( $n = 4$ ) or pancreatic ( $n = 1$ ) surgery involving the RGA, leaving 46 scans evaluable for the standard protocol and 49 scans for the new protocol (see **Figure 1** for a clinical example of both protocols).

The RGA origin was identified in 70/95 patients (74%) on DSA, and in 55/95 (58%) and 62/95 (65%) on CT for raters one and two respectively (**Table 3**). This corresponds to the following test characteristics for CT, taking DSA as reference standard (range for raters 1-2): positive predictive value 84-85%, negative predictive value 40-48%, false positive rate 36-36%, false negative rate 24-34%.

The specific proportion of agreement in CT scores between both raters was 78/95 (82%), and the reliability was substantial with a Cohen's kappa of 0.62 (confidence limits 0.46 – 0.78). Both raters appointed the same RGA origin in all cases with a visible RGA.

The RGA origin location was correctly identified on CT by rater one in 54% and 69% of patients scanned with the standard and new protocol respectively ( $p=0.19$ ); for rater two, this was 65% and 67% respectively ( $p=0.99$ ).

**Table 1.** Baseline patient characteristics

Characteristic	Entire cohort (n = 100)	Standard protocol (n = 50)	New protocol (n = 50)
<b>Age</b>	64 ± 10 years	63 ± 11 years	65 ± 11 years
<b>Sex</b>			
Male	54 (54%)	24 (48%)	30 (60%)
Female	46 (46%)	26 (52%)	20 (40%)
<b>BMI</b>	27 ± 4	27 ± 5	27 ± 4
<b>Liver tumor burden</b>			
< 25%	83 (83%)	42 (84%)	41 (82%)
25-50%	12 (12%)	6 (12%)	6 (12%)
> 50%	5 (5%)	2 (4%)	3 (6%)
<b>Liver tumor type</b>			
CRC	66 (66%)	31 (62%)	35 (70%)
Cholangioca	11 (11%)	6 (12%)	5 (10%)
Uvea melanoma	8 (8%)	4 (8%)	4 (8%)
Mammaca	5 (5%)	3 (6%)	2 (4%)
Other	10 (10%)	6 (12%)	4 (8%)
<b>Previous surgery involving</b>			
S4A	6 (6%)	2 (4%)	4 (8%)
RGA	5 (5%)	4 (8%)	1 (2%)

The baseline patient characteristics are summarized in this table, for the entire cohort and for both protocols separately. Values are given in mean ± standard deviation or number of patients (percentage of total).

In 28 patients, there was discordance between the appointed RGA origin on CT (for both raters) and DSA. These cases were revisited to determine the potential source of discordance. In 13 cases, the origin was appointed on DSA, but not on CT, which may be explained by a very small caliber of the RGA (n = 5), an intimate anatomical course of the RGA parallel to one of the major intrahepatic arterial branches (n = 4), no apparent reason (n = 2), flow dynamics prohibiting contrast-filling of the RGA (n = 1), and metal artifacts

**Table 2.** Individual hepatic arterial anatomy

<b>Anatomical variant</b>	<b>Entire cohort (n = 100)</b>	<b>Standard protocol (n = 50)</b>	<b>New protocol (n = 50)</b>
<b>Standard anatomy</b>	54 (54%)	29 (58%)	25 (50%)
<b>Early branching pattern</b>	19 (19%)	9 (18%)	10 (20%)
Early branching LHA	2 (2%)	1 (2%)	1 (2%)
Early branching RHA	1 (1%)	0	1 (2%)
Trifurcation of CHA	13 (13%)	7 (14%)	6 (12%)
Quadrifurcation of CHA	3 (3%)	1 (2%)	2 (4%)
<b>Aberrant hepatic arteries</b>	27 (27%)	12 (24%)	15 (30%)
rLHA [LGA, S2-3]	8 (8%)	2 (4%)	6 (12%)
rLHA [LGA, S2-4]	2 (2%)	1 (2%)	1 (2%)
aLHA [LGA, S2]	2 (2%)	1 (2%)	1 (2%)
rRHA [SMA, S5-8]	9 (9%)	5 (10%)	5 (10%)
rRHA [SMA, S4-8]	0	0	0
aRHA [SMA, S5+8]	1 (1%)	0	1 (2%)
rLHA + rRHA [SMA, S5-8]	1 (1%)	0	1 (2%)
rCHA [SMA]	4 (4%)	3 (6%)	1 (2%)

The hepatic arterial configuration is summarized in this table, for the entire cohort and for both protocols separately. Values are given in number of patients (percentage of total). Aberrant hepatic arteries are indicated as type of variant [origin, segmental vascularization pattern].

around the RGA origin on CT caused by surgical clips (n = 1). Conversely, in 10 cases the RGA origin was seen on CT but not on DSA, which may be explained by no apparent reason (n = 4), a poor quality of the DSA images (n = 3), a hidden course of the RGA due to overprojection in anterior view (n = 1), and too few available DSA images (n = 1). In the remaining 8 cases, a different origin was appointed on CT than on DSA, which may be explained by a very small difference in localization (for example difference between CHA and PHA, n = 3) and the presence of two RGA branches with different origins (n = 2).

According to the CT scores of raters 1-2, the RGA originated from the LHA in 47-51% of patients, PHA in 21-23%, CHA in 10-13%, GDA in 5-9%, RHA in 6-8%, S4A/MHA in 3-4%, and SMA in 2%.

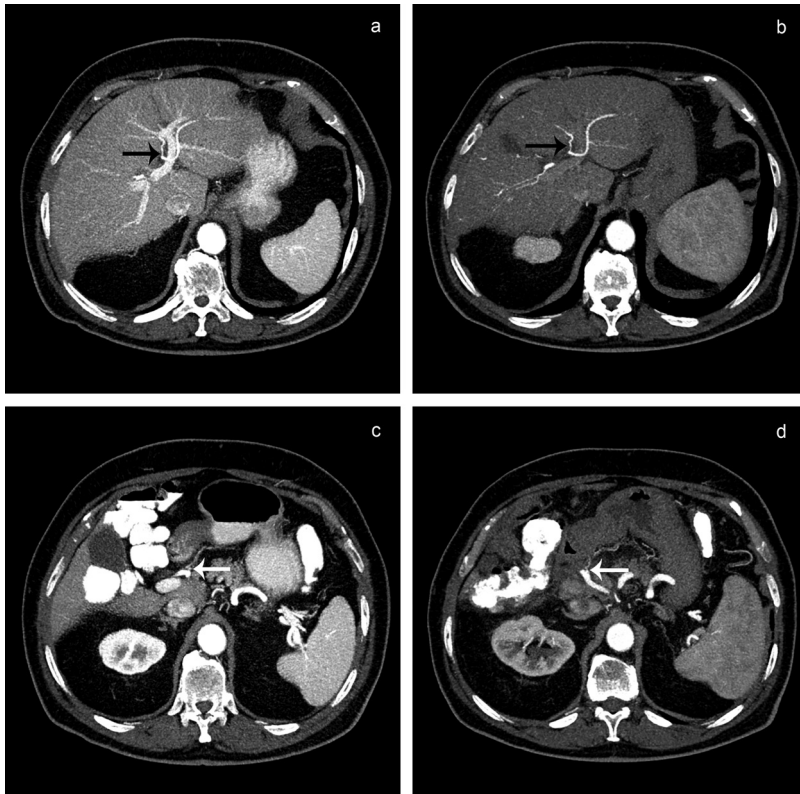


**Figure 1.** Comparison of maximum intensity projections of liver CT images with the standard (a, c) and the new arterial phase protocol (b, d) in the same patient, acquired on the same scanner. Note that the new protocol is easier to evaluate due to an increased CNR for the hepatic artery relative to the portal vein, but the origins of the S4A (a, b, black arrow) and the RGA (c, d, white arrow) are nonetheless visible in both protocols.



**Table 3.** Origin detection of the RGA

	DSA (n = 95)	CT rater 1 (n = 95)	CT rater 2 (n = 95)
<b>Origin of RGA visible?</b>			
Yes	70 (74%)	55 (58%)	62 (65%)
No	25 (26%)	40 (42%)	33 (35%)
<b>RGA origins</b>			
CHA	6 (9%)	8 (15%)	7 (11%)
GDA	3 (4%)	5 (9%)	3 (5%)
PHA	18 (26%)	11 (21%)	15 (24%)
LHA	35 (49%)	26 (47%)	29 (47%)
S4A/MHA	3 (5%)	2 (4%)	2 (3%)
RHA	5 (7%)	3 (6%)	5 (8%)
SMA	0	0	1 (2%)
	<b>Standard protocol</b> (n = 46)	<b>New protocol</b> (n = 49)	
<b>RGA origin correctly identified on CT (DSA as reference test)</b>			
Rater 1	25 (54%)	34 (69%)	
Rater 2	30 (65%)	33 (67%)	

The RGA origin and its detection rate is summarized for DSA and CT (both raters) in this table. Values are given in number of patients (percentage of total). No true PHA exists in patients with an aberrant hepatic artery, therefore, the RGA was called after the non-aberrant arterial branch if originating distal to the origin of the gastroduodenal artery (GDA).

### Origin of the S4A/MHA

Six scans (standard protocol n = 2, new protocol n = 4) were not evaluable for the assessment of the S4A/MHA origin, due to previous liver surgery involving segment 4, leaving 48 scans evaluable for the standard protocol and 46 scans for the new protocol.

The first and second rater scored the origin of the S4A/MHA as visible in 90/94 (96%) and 84/94 (89%) respectively (Table 4). The detection rate of the S4A/MHA origin did not differ significantly between the standard and the new protocol: 96% vs. 96% scored by rater one, and 87% vs. 91% (p=0.79) scored by rater two.

**Table 4.** Origin detection of the S4A/MHA on CT

	Entire cohort (n = 94)	Standard protocol (n = 48)	New protocol (n = 46)
<b>Origin of S4A/MHA visible?</b>			
<i>Rater 1</i>	90 (96%)	46 (96%)	44 (96%)
Yes	90 (96%)	46 (96%)	44 (96%)
No	4 (4%)	2 (4%)	2 (4%)
<i>Rater 2</i>			
Yes	84 (89%)	42 (87%)	42 (91%)
No	10 (11%)	6 (13%)	4 (9%)
<b>S4A/MHA origins</b>			
<i>Rater 1</i>	4 (4%)	1 (2%)	3 (7%)
CHA	4 (4%)	1 (2%)	3 (7%)
PHA	3 (3%)	3 (7%)	0
LHA	51 (57%)	28 (61%)	23 (52%)
rLHA	2 (2%)	1 (2%)	1 (2%)
RHA	25 (28%)	13 (28%)	12 (27%)
rRHA	0	0	0
LHA + RHA	4 (4%)	0	4 (9%)
rLHA + RHA	1 (1%)	0	1 (2%)
<i>Rater 2</i>			
CHA	4 (5%)	1 (2%)	3 (7%)
PHA	4 (5%)	4 (10%)	0 (0%)
LHA	47 (56%)	26 (62%)	21 (50%)
rLHA	1 (1%)	1 (2%)	0
RHA	23 (27%)	10 (24%)	13 (31%)
rRHA	0	0	0
LHA + RHA	4 (5%)	0	4 (10%)
rLHA + RHA	1 (1%)	0	1 (2%)

The S4A/MHA origin and its detection rate is summarized for both raters in this table, for the entire cohort and for both protocols separately. Values are given in number of patients (percentage of total).

The specific proportion of agreement in visibility of the S4A/MHA origin between both raters was 88/94 (94%). The reliability was moderate; Cohen's kappa was 0.54 (confidence limits 0.23 – 0.86). There was a disagreement between both raters in the appointed S4A/MHA origin location on CT in 4 patients.

According to raters 1-2, segment 4 was vascularized exclusively by a S4A originating from the LHA in 56-57% of patients, from the RHA in 27-28%, from a rLHA in 1-2% and never from a rRHA. A MHA originated from the CHA in 4-5% of patients, and from the PHA in 3-5%. A dual-type S4A originated from the LHA + RHA in 4-5% of patients, and from a rLHA + RHA in 1%.

Rater one and two indicated that they could clearly distinguish two separate arterial branches to the superior (S4a) and inferior (S4b) part of S4 in 18/94 (19%) and 10/94 (11%) of patients. These two branches originated from a different main hepatic arterial branch (LHA + RHA or rLHA + RHA) in five of these patients, and originated from the same main hepatic arterial branch in the rest of the cases.

### **SNR and CNR**

The mean arterial SNR was not different for both protocols: 7.5 and 7.4 for the new protocol and the standard protocol respectively (95% CI for the difference in means: -1.2 – 1.5;  $p=0.83$ ). The mean portal SNR was significantly lower in the new protocol compared with the standard protocol: 7.4 vs. 9.7 (95% CI for the difference in means: -3.2 – -1.3;  $p<0.000$ ). This resulted in a significantly higher mean CNR of the hepatic arteries relative to the portal vein in the standard protocol: 1.7 vs. 1.2 (95% CI for the difference in means: 0.4 – 0.7;  $p<0.000$ ).

### **Discussion**

The purpose of this study was to compare RGA and S4A/MHA origin detection rates during radioembolization work-up between early and late arterial phase liver CT protocols, and to determine inter-rater reproducibility. The new protocol with the early arterial phase did not significantly improve the detection rate of small intra- and extrahepatic branches, despite a higher CNR of the hepatic arteries relative to the portal vein. Furthermore, the

RGA origin detection was lower than that of the S4A (58-65% vs 89-96%) in our study. However, when identified, the inter-rater agreement of the origin localization was high for both the RGA (82%) and S4A (94%). The inter-rater reliability was moderate and substantial, respectively.

The RGA origin detection rate on CT (around 60%) can be considered suboptimal. By comparison with DSA, we found a low negative predictive value (40-48%) and relatively high false negative rate (24-34%), indicating that the inability to find the RGA origin on CT does not signify the same for DSA. Reviewing discordant cases revealed that the RGA origin may not be visualized on CT because of a small caliber, an intimate anatomical course parallel to another branch, flow dynamics prohibiting contrast filling, or metal artifacts. The high positive predictive value (84-85%), and good inter-rater agreement, on the other hand, suggest that the necessity to coil-embolize the RGA or advance the microcatheter beyond its origin to avoid harmful extrahepatic deposition of radioactive microspheres, can already be evaluated in patients with a visible origin of the RGA on pre-treatment liver CT. In some cases, CT actually revealed the origin of the RGA better, which may be explained by poor DSA image quality, overprojection of branches in the anterior view, or too few available DSA images.

The S4A/MHA origin detection rate is much higher, which has several important benefits. Depending on the hepatic arterial configuration of an individual patient, it can be decided to use the S4A/MHA as a separate site of administration, include it in a more proximal injection position, or coil-embolize it to induce intrahepatic redistribution of blood flow (6, 11). Furthermore, it allows pre-treatment activity calculations to be performed with knowledge of the segment 4 vascularization. This is crucial to avoid under- or overdosing of segment 4 when performing radioembolization on a single-session basis, and it may contribute to a more reliable distribution of  $^{99m}\text{Tc}$ -macroaggregated albumin ( $^{99m}\text{Tc}$ -MAA) during a routine pre-treatment procedure (12, 13). Interestingly, we found that the typical distinction of segment 4 into an upper (4a) and lower segment (4b) as based on the portal vascularization, could only be made in 11-19% of patients.

The radiologists in our center prefer the early arterial phase for vascular evaluation due to the increased ease of use associated with the higher CNR on maximum intensity projections. It should, however, be noted that the 10-second delay can be too short to allow for optimal enhancement of hypervascular tumors. In these patients, the use of an early and late arterial phase (10 and 20 second post-threshold delay respectively) may be considered if no other imaging is available to substitute tumor evaluation.

C-arm CT has vastly improved the possibilities for intra-procedural imaging. It allows for 3D-imaging of contrast-enhanced vessels in relation to surrounding soft tissue, and we have previously demonstrated that C-arm CT is capable of showing the intra- and extrahepatic arterial perfusion territory of target branches during radioembolization work-up (14). It may, therefore, be regarded as the new gold standard for vascular evaluation. Unfortunately, we could not use C-arm CT as reference standard, because it was not available in all study patients. We used DSA instead for the RGA origin detection, but lack of topographical landmarks to distinguish between liver segments makes DSA unsuitable to assess the S4A origin. It should be noted that the excellent capacities of C-arm CT do not render optimization of pre-procedural imaging useless. An accurate assessment of the hepatic arterial anatomy before the preparatory angiography enables discussing and defining a treatment strategy ahead of time, and increases time-efficiency as well as operator confidence during the preparatory angiography (6).

Our study had several limitations. First, our sample size was based on an assumption of a reasonable number of patients to compare both protocol groups, because specific detection rates for this study population were lacking. Yet, baseline characteristics were comparable. Furthermore, we allowed raters to use both MIP and non-MIP images to detect the RGA and S4A origins. For CNR assessment, we used MIP images only. We believe that this has attributed to the difference in results for the CNR measurements and origin detection assessments. In clinical practice radiologists are, however, also not restricted to a specific method to evaluate images. In addition, we tried to blind the raters for the type of protocol used in a scan, but because the difference in CNR was so explicit and the gastric preparation was slightly different in both protocols, they could still differentiate between both protocol types. Finally, we only evaluated the origin of the RGA and S4A,

because these branches are present in all patients and have important implications. However, in some patients other small arterial branches are also important such as the artery to segment 1, extrahepatic branches to the pancreas or duodenum, and parasitized extrahepatic arteries. Further research needs to clarify whether these branches and their origin can be visualized on pre-treatment CT.

CT hardware and acquisition protocols are continually evolving. In this study, we focused on the arterial phase delay timing, but changes in other technical parameters may lead to further improvements of the liver CT acquisition protocol. The use of a higher contrast agent concentration and injection rate, a patient-tailored scan delay based on a test bolus of contrast agent, and scanning at lower energy levels are among the most promising developments (7, 15, 16).

## **Conclusion**

A 10-second delay arterial phase protocol does not significantly improve the detection rate of small intra- and extrahepatic branches, despite increased CNR of the hepatic arteries relative to the portal vein. Ease of use with this protocol needs to be weighed against the lesser sensitivity for hypervascular tumor detection. The RGA origin detection rate is currently suboptimal, whereas the S4A/MHA origin detection rate is much higher, with good inter-rater reproducibility. Nevertheless, CT remains important for preprocedural planning, because it may reveal arterial anatomy not discernible on DSA.

## References

- Kennedy A (2014) Radioembolization of hepatic tumors. *J Gastrointest Oncol* 5:178–89. doi: 10.3978/j.issn.2078-6891.2014.037
- Lewandowski RJ, Sato KT, Atassi B, et al. (2007) Radioembolization with 90Y microspheres: angiographic and technical considerations. *Cardiovasc Intervent Radiol* 30:571–92. doi: 10.1007/s00270-007-9064-z
- Ugurel MS, Battal B, Bozlar U, et al. (2010) Anatomical variations of hepatic arterial system, coeliac trunk and renal arteries: An analysis with multidetector CT angiography. *Br J Radiol* 83:661–667. doi: 10.1259/bjr/21236482
- Van den Hoven AF, van Leeuwen MS, Lam MGEH, van den Bosch MAAJ (2014) Hepatic Arterial Configuration in Relation to the Segmental Anatomy of the Liver; Observations on MDCT and DSA Relevant to Radioembolization Treatment. *Cardiovasc Intervent Radiol* 1–12.
- Wicherts D a, de Haas RJ, van Kessel CS, et al. (2011) Incremental value of arterial and equilibrium phase compared to hepatic venous phase CT in the preoperative staging of colorectal liver metastases: an evaluation with different reference standards. *Eur J Radiol* 77:305–11. doi: 10.1016/j.ejrad.2009.07.026
- Van den Hoven AF, van Leeuwen MS, Lam MGEH, van den Bosch M a J (2014) Hepatic Arterial Configuration in Relation to the Segmental Anatomy of the Liver; Observations on MDCT and DSA Relevant to Radioembolization Treatment. *Cardiovasc Intervent Radiol*. doi: 10.1007/s00270-014-0869-2
- Rengo M, Bellini D, De Cecco CN, et al. (2011) The optimal contrast media policy in CT of the liver. Part II: Clinical protocols. *Acta radiol* 52:473–480. doi: 10.1258/ar.2011.100500
- McCulloch P, Cook J a, Altman DG, et al. (2013) IDEAL framework for surgical innovation 1: the idea and development stages. *BMJ* 346:f3012. doi: 10.1136/bmj.f3012
- Van den Hoven AF, Smits MLJ, de Keizer B, et al. (2014) Identifying Aberrant Hepatic Arteries Prior to Intra-arterial Radioembolization. *Cardiovasc Intervent Radiol*. doi: 10.1007/s00270-014-0845-x
- Mahnken AH, Spreafico C, Maleux G, et al. (2013) Standards of practice in transarterial radioembolization. *Cardiovasc Intervent Radiol* 36:613–22. doi: 10.1007/s00270-013-0600-8
- Abdelmaksoud MHK, Louie JD, Kothary N, et al. (2011) Consolidation of hepatic arterial inflow by embolization of variant hepatic arteries in preparation for yttrium-90 radioembolization. *J Vasc Interv Radiol* 22:1364–1371. e1. doi: 10.1016/j.jvir.2011.06.014
- Van den Hoven AF, Prince JF, van den Bosch MAAJ, Lam MGEH (2014) Hepatic radioembolization as a true single-session treatment. *J Vasc Interv Radiol* 25:1143–4. doi: 10.1016/j.jvir.2014.01.037
- Wongergem M, Smits MLJ, Elschot M, et al. (2013) 99mTc-macroaggregated albumin poorly predicts the intrahepatic distribution of 90Y resin microspheres in hepatic radioembolization. *J Nucl Med* 54:1294–301. doi: 10.2967/jnumed.112.117614
- Van den Hoven AF, Prince JF, de Keizer B, et al. (2015) Use of C-Arm Cone Beam CT During Hepatic Radioembolization: Protocol Optimization for Extrahepatic Shunting and Parenchymal Enhancement. *Cardiovasc Intervent Radiol*. doi: 10.1007/s00270-015-1146-8
- Rengo M, Bellini D, De Cecco CN, et al. (2011) The optimal contrast media policy in CT of the liver. Part I: Technical notes. *Acta radiol* 52:467–472. doi: 10.1258/ar.2011.100499
- Schneider JG, Wang ZJ, Wang W, et al. (2014) Patient-tailored scan delay for multiphase liver CT: Improved scan quality and lesion conspicuity with a novel timing bolus method. *Am J Roentgenol* 202:318–323. doi: 10.2214/AJR.12.9676







The background of the entire page is a dense, multi-colored confetti of small, round beads in various colors including red, yellow, blue, green, purple, and white. The text is centered and overlaid on this background.

# CHAPTER TEN

**The value of a dual arterial phase CT  
protocol in the preparation  
of radioembolization in  
neuroendocrine liver metastases**

**Manon N.G.J.A. Braat, Rutger C.G. Bruijnen, Maarten L.J. Smits,  
Arthur J.A.T. Braat, Marnix G.E.H. Lam**

*Submitted for publication (Cardiovascular and Interventional Radiology)*

## **Abstract**

### **Objectives**

To evaluate the addition of an early arterial phase (EAP) to the pre-radioembolization multiphase CT in patients with neuro-endocrine tumor liver metastases (NELM), for vascular anatomy assessment and prediction of response.

### **Material and methods**

From October 2014 to September 2018, all patients who underwent the extended multiphase CT protocol pre-radioembolization and had  $\geq 1$  NELM  $>10$  mm were included. The origin of small arteries was assessed on early and late arterial phases by two raters, including inter-observer agreement. Regions-of-interest (ROIs) were drawn in up to three NELM per patient to determine the enhancement in Hounsfield units (HU) in each contrast phase. Response was assessed according to RECIST 1.1.

### **Results**

Forty-four patients were included. No significant difference was observed in the origin detection between both arterial phases. The agreement on the origin was similar for both arterial phases with substantial inter-observer agreement for the cystic artery in the EAP ( $K = 0.631$ ), but only fair to moderate agreement for all other arteries.

Ninety-three lesions (33 patients) were evaluable for tumor enhancement and response. Responding lesions (i.e. 43/93 lesions) had significantly higher HU values in all contrast phases compared to non-responding lesions.

### **Conclusion**

No added value was found for the EAP in the assessment of small arterial branches or response prediction. Hypervascularity is associated with an improved durable response at six months.

## Introduction

Liver metastases and primary liver tumors are primarily supplied by the hepatic artery, contrary to foremost portal supply of the normal liver parenchyma (1). This difference is the rationale for embolization-based liver-directed treatments, including chemo-embolization and radioembolization.

In radioembolization, tumor response is dependent on the tumor-absorbed dose (2-4). Ideally, tumor response and hepatotoxicity can be predicted prior to treatment and used as a selection criterion and as input for treatment planning. Currently, the best predictor for the anticipated tumor-absorbed dose is the dose distribution on the technetium-99m macroaggregated albumin (Pulmocis®, CIS-bio International) or holmium-166 (<sup>166</sup>Ho) microspheres scout dose (QuiremScout®, Quirem Medical) single photon emission computed tomography (SPECT)-CT. The projected dose distribution of these scout particles is used to calculate the prescribed activity considering all compartments of interest (i.e. tumor, lung and normal liver) by use of the partition model or by voxel-based dosimetry. (5) Unfortunately, prediction of the distribution of intra-arterially administered particles in a non-invasive fashion is impossible. However, adequate pre-treatment imaging serves as an important tool to improve patient selection and potentially avoid redundant scout dose procedures.

At present, baseline multiphase CT is mainly acquired to assess intra- and extrahepatic tumor load, as well as the arterial anatomy of the hepatic artery and its branches. However, hypervascular tumors are likely to interfere with the detection of small vessels due to their similar attenuation in the arterial phase, especially in case of a high tumor load, as is often the case in neuroendocrine tumor liver metastases (NELM). In our institution, an early arterial phase (EAP) was introduced in the work-up for radioembolization, because of its superior artery-to-liver contrast. The downside of an EAP however, is decreased visibility of hypervascular liver lesions, resulting in underdetection. This makes the EAP unsuitable for tumor response evaluation using Response Evaluation Criteria In Solid Tumors (RECIST) and mRECIST (6-8).

A scan protocol was specifically designed for hypervascular liver tumors, including four

phases; early arterial phase (EAP), late arterial phase (LAP), portal venous phase and equilibrium phase. Hence, the purpose of this study was to evaluate this multiphase CT protocol prior to radioembolization, specifically evaluating artery detection, inter-observer agreement and lesion enhancement.

## Methods

### Study design

This was a single center, retrospective study. Between October 2014 (at the introduction of the dual arterial phase protocol) and September 2018 all patients with NELM who underwent a multiphase CT with the new protocol were extracted from the picture archiving and communication system (PACS). Patients were only included if they had at least one NELM of >10 mm and DSA imaging of the angiography procedures was available. Patients underwent radioembolization treatment with either <sup>90</sup>Y glass microspheres (TheraSphere®, Boston Scientific) or <sup>166</sup>Ho microspheres (QuiremSpheres®, Quirem Medical).

The medical ethics committee of our institution waived the need for informed consent for review of the imaging data.

### Image acquisition

All CT scans were acquired on the same CT-scanner (Brilliance ICT, Philips): 128 detector rows/256 slices, using a matrix size of 512 x 512, rotation time of 0.4 sec, pitch of 0.9, and fixed 120 kV tube potential. Depending on the body weight, 150-185 ml Iopromide 300 mg/ml contrast agent (Ultravist, Bayern Schering Pharma AG) was injected in the antecubital vein at a rate of 5 ml/sec, followed by a 50 ml saline chaser.

The imaging protocol consisted of an EAP, LAP, portal venous phase and equilibrium phase, obtained with a post-threshold (abdominal aorta enhancement > 100 HU) delay of 10, 20, 55 and 300 seconds, respectively (Figure 1). In patients < 85 kg, a tube current of 200 mAs was applied in the portal venous phase, and 150 mAs in the other phases (>85 kg: tube currents of 250 mAs and 200 mAs, respectively). Slice thickness/increment were 0.9/0.7 cm for all phases.

DSA images (Xellera, Philips) were acquired during the scout procedure and/or therapeutic procedure.

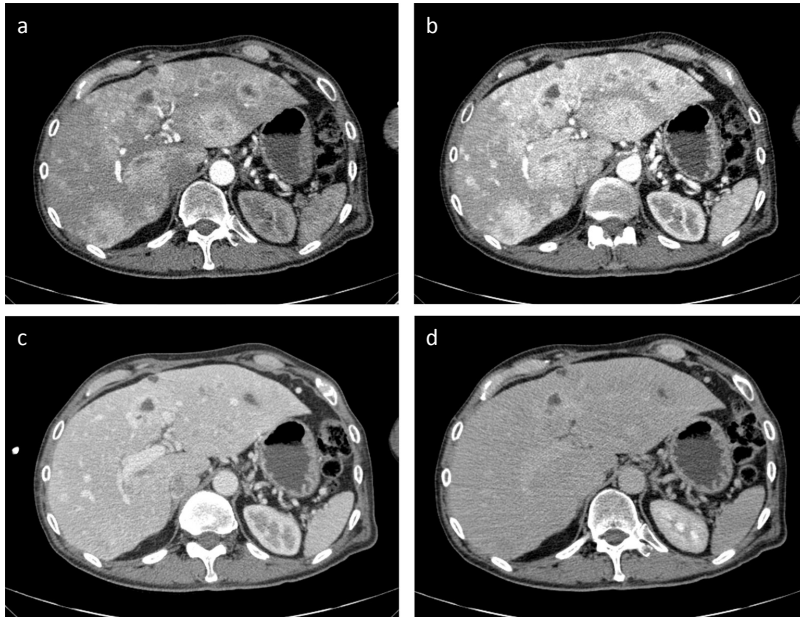


**Figure 1.** Dual arterial phase liver CT protocol. Example of the dual arterial phase CT protocol, consisting of an early arterial phase (a), a late arterial phase (b), a portal venous phase (c) and an equilibrium phase (d). Note the superior contrast-to-background ratio on the early arterial phase compared to the late arterial phase. This is due to more avid lesion enhancement and perilesional shunting in the late arterial phase.

### Image analyses

All images were stored in PACS and anonymized. The origin of the following arteries was assessed by two raters (MB (> 10 years' experience in abdominal radiology) and RB (interventional radiologist; > 10 years' experience with radioembolization)): right gastric artery (RGA), cystic artery (CA), segment 4 artery (S4A), caudate lobe arteries (CLA) and falciform artery. Rater two (RB) also scored the artery origins on DSA, to allow comparison between CT phases and DSA. Arteries sacrificed during previous surgery were considered

non-evaluable. Artery origins were assessed on the axial thin slice images, but for detection also maximum intensity projection and coronal image reconstructions were allowed.

Hepatic tumor load was calculated on the LAP by manual delineation and divided in two groups (<25% or >25%). For lesion enhancement assessment and response assessment, up to three lesions were selected on the LAP as target lesions (according to RECIST 1.1). Enhancement of these lesions was assessed objectively by drawing an as large as possible ROI over each lesion (excluding necrotic areas and large vessels). The ROI was drawn on the LAP and copied onto the other phases. As imaging was acquired during inspiration breath hold and patients did not leave the scanning table, additional image registration steps were unnecessary.

Standard clinical follow-up consisted of clinical evaluation at two weeks, one month, three and six months, and CT at three and six months.

Objective response of the target lesions was defined according to RECIST 1.1 on multiphase liver CTs, acquired six months after radioembolization. In case of sequential treatments, only the treated volume(s) with at least six months follow-up was evaluated. Lesion objective response was dichotomized between responding lesions (complete response (CR) = 100% tumor reduction and partial response (PR) = > 30% tumor reduction) or non-responding lesions (both stable disease (SD) and progressive disease (PD), having  $\leq$  30% tumor reduction).

### **Statistics**

Descriptive statistics were used to explore baseline characteristics. Data with a normal distribution are presented as mean  $\pm$  standard deviation.

The proportion of visible origins was compared between the raters for each arterial CT phase by chi-square tests or Fisher's exact tests. Inter-observer agreement on the artery origins was tested by Cohen's kappa (K), as well as agreement between the arterial phases and DSA (9).

Fisher's exact tests were used to compare the origin detection between patients with a tumor load <25% and >25%. Bootstrapped independent-samples T-tests were used to test the differences in HU-value between responding and non-responding lesions in all contrast-phases. All analyses were performed with IBM SPSS Statistics version 26. A p-value < 0.05 was considered statistically significant.

## Results

### Patients and scans

Forty-four patients with NELM underwent the dual arterial phase protocol in preparation of radioembolization treatment (of whom 28 as part of a prospective clinical study, the HEPAR PLuS study) (10). The baseline data are presented in **Table 1**. All EAP and LAP (n=44) were assessed for the artery origins. No patients had to be excluded because of imaging insufficiencies. Patients were either treated with <sup>166</sup>Ho microspheres (n=27) or <sup>90</sup>Y glass microspheres (n=17).

In the response analysis, an additional 11/44 patients were excluded (deceased before first response evaluation (n=1), no follow-up imaging obtained at six months (n=10)). The remaining 33 patients had a total of 93 lesions in the treated volume evaluable according to RECIST 1.1 (**Table 1**).

### Inter-observer agreement on arterial phase CT

The origin of the RGA was identified in more patients in the EAP (30 vs. 20 patients for rater one (p=0.048) and 37 vs. 32 patients for rater two (p=0.265)) (**Table 2**). It mostly originated from the left hepatic artery. The inter-observer agreement of both raters on the RGA origin was moderate for the EAP (K=0.527) and fair for the LAP (K=0.381) (**Table 3**).

The origin of the S4A was identified in nearly all patients on both arterial CT phases (43/44) (**Table 2**), mostly originating from the LHA. Interobserver agreement was moderate (EAP: K=0.480 and LAP: K=0.554).

A prior cholecystectomy was performed in 10 patients. The origin of the CA was identified in most patients on the EAP and LAP by both rater one (30/34 vs. 29/34) and rater two (34/34 vs. 33/34), i.e. non-significant. Substantial agreement was found for EAP (K=0.631) and moderate agreement for LAP (K=0.496).



**Table 1.** Baseline patient characteristics

Characteristic	All patients (n = 44)	RECIST evaluable patients (n=33)
<b>Age</b>	62,5 ± 8	62 ± 9
<b>Sex</b>		
Male	31	25
Female	13	8
<b>Weight</b>		
≤ 85 kg	30	22
>85 kg	14	11
<b>Tumor origin</b>		
Pancreas	12	9
Small intestine	12	9
Lung	5	3
Colon or rectum	6	5
Stomach	2	1
Unknown	7	6
<b>Tumor grade</b>		
1	16	12
2	23	17
3	2	1
Unknown	3	3
<b>Previous systemic treatment</b>		
PRRT	36	30
Chemotherapy	2	1
Embolization with alcohol foam particles	1	0
<b>Microsphere</b>		
<sup>90</sup> Y (glass)	17	9
<sup>166</sup> Ho	27	24
<b>Liver tumor burden</b>		
0-25%	28	22
25-50%	12	9
50-75%	2	2
Unknown	2	0

**Table 1.** Continued.

Characteristic	All patients (n = 44)	RECIST evaluable patients (n=33)
<b>Treatment</b>		
Whole liver	20	11
Sequential whole liver	3	3
Left lobe	3	16
Right lobe	18	3
<b>Injected dose (MBq)</b>		
<sup>166</sup> Ho	6942 ± 2638	6972 ± 2713
<sup>90</sup> Y	3756 ± 2202	3481 ± 1481
<b>Previous surgery involving</b>		
CA	10	NA
RGA	1	

The baseline patient characteristics are summarized in this table. Values are given in mean ± standard deviation or number of patients. CA = cystic artery; NA = not applicable; PRRT = peptide receptor radionuclide therapy; RECIST = response evaluation criteria in solid tumors; RGA = right gastric artery

Rater one identified a CLA origin in 13/44 cases in the EAP vs. 8/44 in the LAP. Rater two identified more CLA origins in the LAP (LAP: 18/44 vs. EAP: 14/44). Both differences were not significant. Agreement was fair for EAP (K=0.292) and LAP (K=0.265).

The falciform artery was identified with doubt in one case by rater one and in four cases by rater two.

### Agreement of arterial phase CT and DSA

The origin of the RGA was detected in 26/43 patients on DSA. The specific portion of agreement between both modalities on the origin of the RGA was 14/43 for the EAP (K=0.269) and 12/43 for the LAP (K=0.177). The S4A was identified in 44/44 patients on DSA. The specific portion of agreement between the EAP and DSA was 34/44 vs. 37/44 for the LAP and DSA. Agreement was moderate for both EAP (K=0.407) and LAP (K=0.551). The CA origin was detected in 29/34 cases on the DSA with a similar specific portion of agreement on the origin (22/34) and a similar agreement in both arterial phases (EAP: K=0.512 and LAP: K=0.538).

**Table 2.** Origin detection of the arteries on CT and DSA

CT phase	EAP	LAP	EAP	LAP	EAP	LAP	EAP	LAP
<b>Origins</b>	<b>RGA1</b>	<b>S4A</b>	<b>CA2</b>	<b>CLA</b>				
<i>Rater 1</i>								
CHA	2	2	0	0	1	1	0	0
GDA	1	0	0	0	0	1	1	0
PHA	5	3	7	5	0	0	1	1
LHA	20	14	28	28	3	3	2	1
S4A/MHA	0	0	-	-	0	1	2	1
RHA	2	1	8	10	26	23	7	5
<b>Total</b>	<b>30</b>	<b>20</b>	<b>43</b>	<b>43</b>	<b>30</b>	<b>29</b>	<b>13</b>	<b>8</b>
<i>Rater 2</i>								
CHA	1	2	0	0	0	0	0	0
GDA	2	1	0	0	0	0	1	0
PHA	7	8	4	1	2	0	3	2
LHA	25	19	30	33	3	4	4	8
S4A/MHA	0	0	-	-	0	0	0	0
RHA	2	2	9	9	29	29	6	10
<b>Total</b>	<b>37</b>	<b>32</b>	<b>43</b>	<b>43</b>	<b>34</b>	<b>33</b>	<b>14</b>	<b>20</b>
	<b>DSA</b>	<b>DSA</b>	<b>DSA</b>	<b>DSA</b>				
<b>Origins</b>	<b>RGA1</b>	<b>S4A</b>	<b>CA2</b>	<b>CLA</b>				
<i>Rater 2</i>								
CHA	0	0	0	0				
GDA	0	0	0	0				
PHA	12	0	0	1				
LHA	11	38	0	1				
S4A/MHA	0	-	0	0				
RHA	3	6	29	5				
<b>Total</b>	<b>26</b>	<b>44</b>	<b>29</b>	<b>7</b>				

1 = one patient after partial gastrectomy excluded; 2 = ten patients after cholecystectomy excluded. CA = cystic artery; CI = confidence interval; CHA = common hepatic artery; CLA = caudate lobe artery; DSA = digital subtraction angiography; GDA = gastroduodenal artery; LHA = left hepatic artery; NS = no significant kappa value; PHA = proper hepatic artery; RGA = right gastric artery; RHA = right hepatic artery; S4A = segment 4 artery/middle hepatic artery. A second segment 4 artery was identified in 7 cases on the EAP and in 4 cases on the LAP by rater 1. Rater 2 identified a second S4A in 14 and 12 cases, respectively. In the EAP both raters agreed on a second S4 artery in 3 cases, in the LAP only in 1 case. The origins of the RGA, S4A and CLA are summarized for both raters in this table for both protocols separately. Values are given in number of patients.

**Table 3.** Inter-observer agreement

CT phase	EAP	LAP	EAP	LAP	EAP	LAP	EAP	LAP
<b>Origins</b>	<b>RGA<sup>1</sup></b>		<b>S4A</b>		<b>CA<sup>2</sup></b>		<b>CLA</b>	
Specific portion of agreement on origin <sup>3</sup> Inter-observer	23/43	14/43	31/44	34/44	25/34	21/34	5/44	3/44
Cohen's Kappa <sup>3</sup> Inter-observer	0.527	0.381	0.480	0.554	0.631	0.496	0.292	0.265
Specific portion of agreement on origin <sup>4</sup> (CT vs. DSA)	14/43	12/43	34/44	37/44	22/34	22/34	1/44	1/44
Cohen's Kappa <sup>5</sup> (CT vs. DSA)	0.269	0.177	0.407	0.551	0.512	0.538	NS	NS

1 = one patient after partial gastrectomy excluded. 2 = ten patients after cholecystectomy excluded. 3 = agreement between rater 1 and rater 2 on the origin of the arteries. 5 = agreement between CT and DSA, rated by rater 2, on the origin of the arteries. CA = cystic artery; CLA = caudate lobe artery; NS = no significant kappa value; RGA = right gastric artery; S4A/MHA = segment 4 artery/middle hepatic artery

In only 7/44 patients a CLA origin was identified on DSA, with agreement on the origin in only one case in both EAP and LAP. The falciform artery was not identified in any patient on DSA.

### Influence of tumor load on origin detection

The tumor load was <25% in 28 patients and >25% in 14 patients (missing data in two). The detection of the origin of the RGA, S4A and CLA in both arterial phases and rated by both raters was not influenced by increasing tumor load.

### Lesion enhancement

At six-months follow-up, 43/93 lesions were considered responding lesions (CR 2/93 and PR 41/93) and 50/93 lesions were non-responding (SD 47/93 and PD 3/93). In all phases, a significant difference in absolute HU value was present between the responding and non-responding lesions (**Table 4**), with the most pronounced difference in the LAP and portal venous phase, of ca. 20 HU.

**Table 4.** Tumor enhancement (n=93)

HU value	Responding lesions		Non-responding lesions		p-value
	Mean ± SD	95% CI	Mean ± SD	95% CI	
Early arterial phase	83 ± 28	75-92	68 ± 28	60-77	<b>0.014</b>
Late arterial phase	117 ± 34	107-127	97 ± 45	84-112	<b>0.025</b>
Portal venous phase	114 ± 23	107-121	95 ± 34	85-105	<b>0.003</b>
Equilibrium phase	89 ± 11	84-91	78 ± 20	72-84	<b>0.007</b>

Independent-samples T-test (+bootstrapping).

CI = confidence interval; SD = standard deviation

## Discussion

The purpose of this study was to evaluate the value of a multi-phase CT protocol consisting of two arterial phases (EAP and LAP), a portal venous phase and equilibrium phase in patients prior to radioembolization. The approach was twofold. Firstly, to assess the visibility of the origins of common important branches on both arterial phases and determine the inter-observer agreement, as work-up for the angiography procedures. Origin detection of all arteries was less accurate than expected, and similar for both arterial phases with slight to moderate inter-observer agreement. Additionally, the lesion enhancement on multiple CT phases and its value in the prediction of tumor response was assessed, to assess the feasibility of the protocol to improve patient selection. A significant difference in absolute HU value was observed between responding lesions and non-responding lesions with the most pronounced difference in the LAP (20 HU difference,  $p=0.025$ ).

Acquisition of both arterial phases is a challenge for both patient and radiographer. During EAP and LAP the table has to move to the original position, and patients have to expire, inspire and hold their breath repeatedly. This limits the acquisition to fast multislice CT-scanners (at least 64 slice). However, if table movement is the time-limiting factor, the LAP can be acquired in the opposite direction (feet to head).

In clinical routine, the EAP is often preferred for vascular anatomy assessment due to its superior contrast with the background (**Figure 1**). This is in line with earlier studies on

arterial assessment in radioembolization work-up (11, 12). Van den Hoven et al. compared the detection of the RGA and S4A between EAP and LAP in two groups of 50 patients each, mostly suffering from colorectal liver metastases (11). No differences were found in detection of the origin of the RGA and S4A. Yet, the specific portion of agreement for the S4A (94%) and RGA (82%) origin was substantially higher compared with the present study (77-84% and 28-33%, respectively).

Although an improved detection rate of the origin of important arterial branches by including EAP could not be established, EAP imaging may still be of help, e.g. to check for tumor feeding vessels, to evaluate selective arterial vasculature and branching patterns, to exclude parasitized feeders, to evaluate the feasibility for catheterization of small branches, and to use as a navigation map during angiography (13). These (more case specific) benefits were not specifically studied.

The detection of a CLA origin was considerably higher on both arterial phases compared to DSA (**Table 2**). A possible explanation is the high variability of its origin(s) together with the lack of anatomic reference to the caudate lobe on DSA.

Contrary to most radioembolization studies, tumor response was assessed at six months instead of three months (**Figure 2**). However, prior studies on radioembolization in NELM presented durable responses at six months (10, 14, 15). Braat et al. reported improved disease control rates at six months, when compared to three months post-radioembolization. Consequently, a longer interval for tumor response assessment was chosen (16).

This study has several limitations, besides a small population and being of retrospective nature. The differences in detection of some important arterial branches were used to assess the added value of the EAP to our protocol. As mentioned above, the potential savings in time, cone-beam CT use or additional procedures were not investigated.

The used protocol did not include an unenhanced phase, omitting the measurement of absolute enhancement. HU measurement was preferred over the more commonly used subjective assessment of lesion hypervascularity (3, 14, 17). Visual assessment of

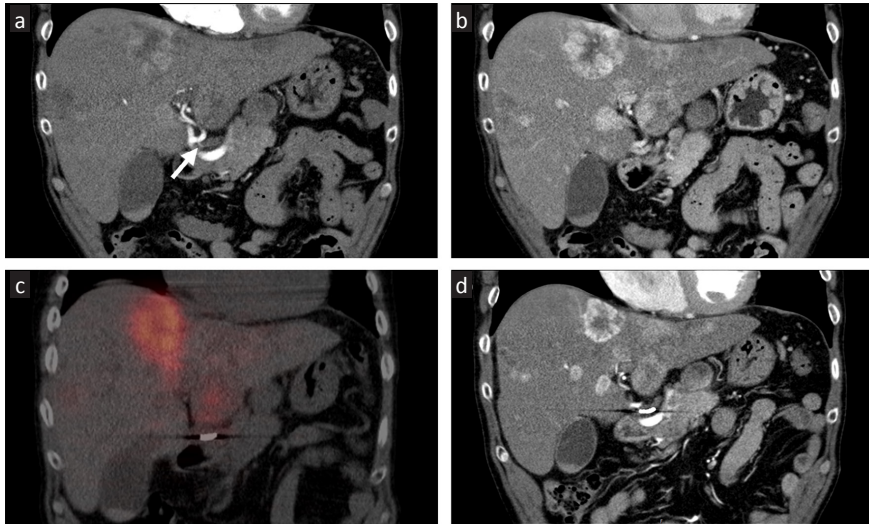


**Figure 2.** A 66-year-old male with NELM who was screened for radioembolization using the dual arterial phase protocol. In the EAP both raters identified the RGA as originating from the LHA (arrow in A), whilst they both failed to identify the RGA in the LAP (B). The “background enhancement” was increased compared to the EAP, due to both lesion and venous enhancement, complicating the identification of the RGA. The avidly enhancing lesion in segment 4A/8 showed sufficient  $^{166}\text{Ho}$  accumulation after treatment (C) and a 33% reduction in size according to RECIST six months after treatment (D). Note the coils in the RGA.

hypervascularity is common practice, however, coinciding steatosis may limit assessment. Steatosis increases the lesion-to-background ratio and may falsely identify lesions as hypervascular.

In the present study, not only enhancement in the LAP was indicative of response, but also in all three other phases (Table 3). Arterial lesion enhancement prior to radioembolization was subjectively assessed in a few studies (3, 14, 18, 19), two of which including NELM patients. Similar to our results, they showed that hypervascularity on CT was an indicator

of tumor response (3) or progression-free survival (14). Morsbach et al. reported that arterial perfusion differentiated best between responders and non-responders four months after radioembolization (19). However, the arterial HU value was also predictive of response with a mean HU of  $80 \pm 24$  for responders (in line with our EAP findings; **Table 3**).

The hypervascularity of NELM may favor higher tumor-to-liver ratios, resulting in higher tumor absorbed doses. In this study no correlation was made with absorbed dose. Prior studies on dosimetry in NELM have shown a dose-response relationship (3, 20).

Furthermore, tumor inhomogeneity was not studied. The ROI was placed in a relatively homogeneous enhancing part of the lesion, whereas response was assessed for the entire lesion. Mosconi et al. showed that not only the mean LAP HU value, but also the homogeneity in the LAP of in toto segmented cholangiocarcinomas was higher in objective responders after radioembolization (21).

Fine-tuning of patient selection and treatment using non-invasive pre-treatment imaging remains desirable. Promising developments for further improvements include the use of artificial intelligence tools, for example for segmentation purposes and to assess enhancement and tumor inhomogeneity (21). Another promising development is the use of dual energy CT; it enables quantification of lesion enhancement without a prior unenhanced CT and has the potential to increase artery and lesion detection using virtual monoenergetic images (22).

## **Conclusion**

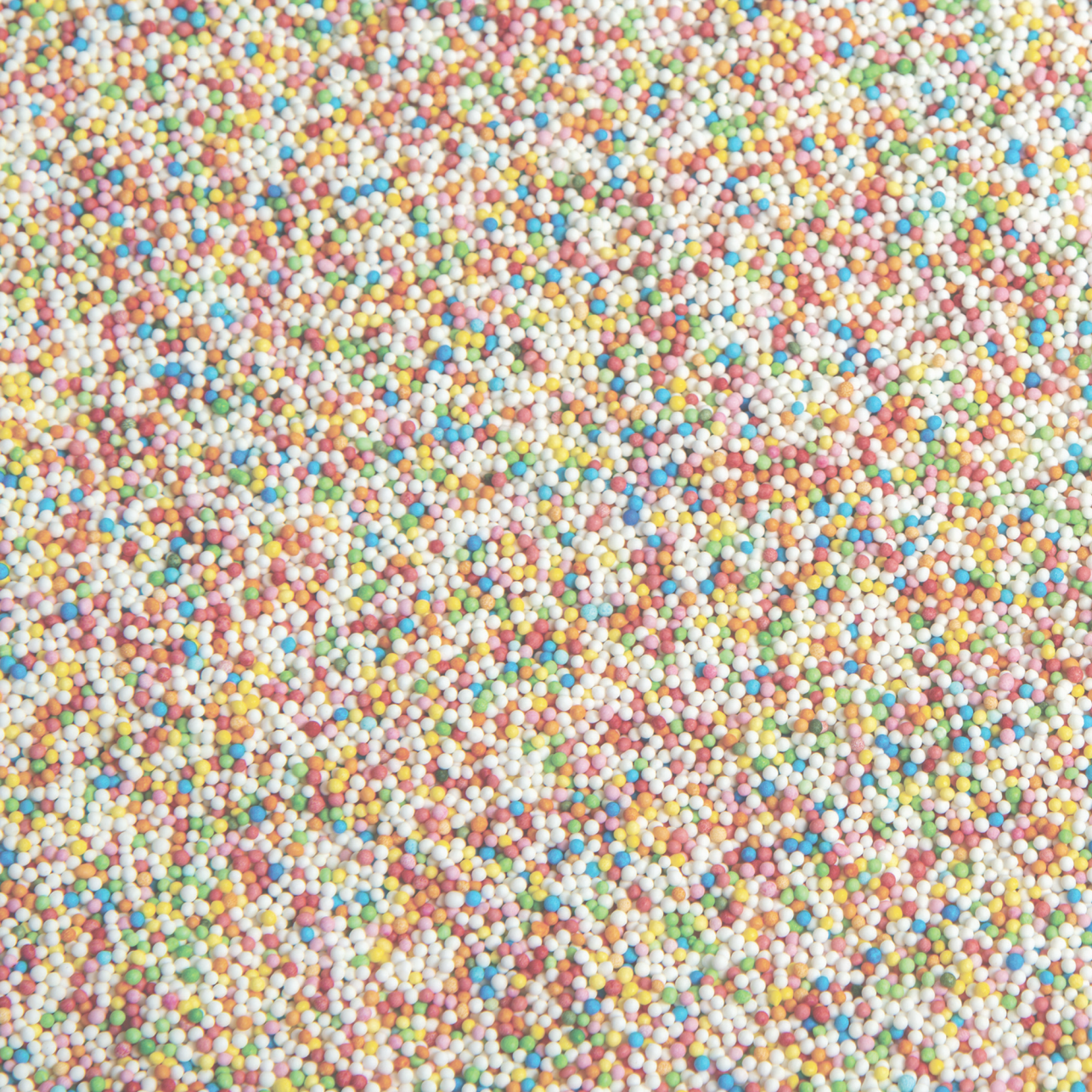
The addition of the early arterial phase to our CT protocol did not result in significantly improved detection of small arterial branches or improved inter-observer agreement. In NELM, hypervascularity, quantified by HU values in all contrast phases, is associated with an improved durable response at six months.



## References

1. Breedis C, Young G. The blood supply of neoplasms in the liver. *Am J Pathol.* 1954;30(5):969-77.
2. van den Hoven AF, Rosenbaum CE, Elias SG, de Jong HW, Koopman M, Verkooijen HM, et al. Insights into the Dose-Response Relationship of Radioembolization with Resin 90Y-Microspheres: A Prospective Cohort Study in Patients with Colorectal Cancer Liver Metastases. *J Nucl Med.* 2016;57(7):1014-9.
3. Chansanti O, Jahangiri Y, Matsui Y, Adachi A, Geeratikun Y, Kaufman JA, et al. Tumor Dose Response in Yttrium-90 Resin Microsphere Embolization for Neuroendocrine Liver Metastases: A Tumor-Specific Analysis with Dose Estimation Using SPECT-CT. *J Vasc Interv Radiol.* 2017;28(11):1528-35.
4. van Roekel C, Bastiaannet R, Smits MLJ, Bruijnen RC, Braat AJAT, de Jong HWAM, et al. Dose-effect relationships of holmium-166 radioembolization in colorectal cancer. *J Nucl Med.* 2020.
5. Ho S, Lau WY, Leung TW, Chan M, Ngar YK, Johnson PJ, et al. Partition model for estimating radiation doses from yttrium-90 microspheres in treating hepatic tumours. *Eur J Nucl Med.* 1996;23(8):947-52.
6. Portugaller HR, Stacher R, Komaz G, Aschauer M, Hausegger KA, Szolar DH. [The value of different spiral CT phases in the detection of liver metastases]. *Rofo.* 2002;174(4):452-8.
7. Paulson EK, McDermott VG, Keogan MT, DeLong DM, Frederick MG, Nelson RC. Carcinoid metastases to the liver: role of triple-phase helical CT. *Radiology.* 1998;206(1):143-50.
8. Ronot M, Cuccioli F, Dioguardi Burgio M, Vullierme MP, Hentic O, Ruszniewski P, et al. Neuroendocrine liver metastases: Vascular patterns on triple-phase MDCT are indicative of primary tumour location. *Eur J Radiol.* 2017;89:156-62.
9. Landis JR, Koch GG. The measurement of observer agreement for categorical data. *Biometrics.* 1977;33(1):159-74.
10. Braat AJAT, Bruijnen RCG, van Rooij R, Braat MNGJ, Wessels FJ, van Leeuwen RS, et al. Additional holmium-166 radioembolisation after lutetium-177-dotatate in patients with neuroendocrine tumour liver metastases (HEPAR PLuS): a single-centre, single-arm, open-label, phase 2 study. *Lancet Oncol.* 2020;21(4):561-70.
11. van den Hoven AF, Braat MN, Prince JF, van Doormaal PJ, van Leeuwen MS, Lam MG, et al. Liver CT for vascular mapping during radioembolisation workup: comparison of an early and late arterial phase protocol. *Eur Radiol.* 2017;27(1):61-9.
12. Braat MN, van den Hoven AF, van Doormaal PJ, Bruijnen RC, Lam MG, van den Bosch MA. The Caudate Lobe: The Blind Spot in Radioembolization or an Overlooked Opportunity? *Cardiovasc Intervent Radiol.* 2016;39(6):847-54.
13. Weber M, Lam M, Chiesa C, Konijnenberg M, Cremonesi M, Flamen P, et al. EANM procedure guideline for the treatment of liver cancer and liver metastases with intra-arterial radioactive compounds. *Eur J Nucl Med Mol Imaging.* 2022;49(5):1682-99.
14. Sommer WH, Ceelen F, García-Albéniz X, Paprottka PM, Auernhammer CJ, Armbruster M, et al. Defining predictors for long progression-free survival after radioembolisation of hepatic metastases of neuroendocrine origin. *Eur Radiol.* 2013;23(11):3094-103.
15. Braat A, Ahmadzadehfar H, Kappadath SC, Stothers CL, Frilling A, Deroose CM, et al. Radioembolization with (90)Y Resin Microspheres of Neuroendocrine Liver Metastases After Initial Peptide Receptor Radionuclide Therapy. *Cardiovasc Intervent Radiol.* 2020;43(2):246-53.

16. Braat AJAT, Kappadath SC, Ahmadzadehfar H, Stothers CL, Frilling A, Deroose CM, et al. Radioembolization with. *Cardiovasc Intervent Radiol.* 2019;42(3):413-25.
17. Sato KT, Omary RA, Takehana C, Ibrahim S, Lewandowski RJ, Ryu RK, et al. The role of tumor vascularity in predicting survival after yttrium-90 radioembolization for liver metastases. *J Vasc Interv Radiol.* 2009;20(12):1564-9.
18. Boas FE, Brody LA, Erinjeri JP, Yarmohammadi H, Shady W, Kishore S, et al. Quantitative Measurements of Enhancement on Preprocedure Triphasic CT Can Predict Response of Colorectal Liver Metastases to Radioembolization. *AJR Am J Roentgenol.* 2016;207(3):671-5.
19. Morsbach F, Sah BR, Spring L, Puijpe G, Gordic S, Seifert B, et al. Perfusion CT best predicts outcome after radioembolization of liver metastases: a comparison of radionuclide and CT imaging techniques. *Eur Radiol.* 2014;24(7):1455-65.
20. Ebbers SC, van Roekel C, Braat MNGJ, Barentsz MW, Lam MGEH, Braat AJAT. Dose-response relationship after yttrium-90-radioembolization with glass microspheres in patients with neuroendocrine tumor liver metastases. *Eur J Nucl Med Mol Imaging.* 2022;49(5):1700-10.
21. Mosconi C, Cucchetti A, Bruno A, Cappelli A, Bargellini I, De Benedittis C, et al. Radiomics of cholangiocarcinoma on pretreatment CT can identify patients who would best respond to radioembolisation. *Eur Radiol.* 2020;30(8):4534-44.
22. Muenzel D, Lo GC, Yu HS, Parakh A, Patino M, Kambadakone A, et al. Material density iodine images in dual-energy CT: Detection and characterization of hypervascular liver lesions compared to magnetic resonance imaging. *Eur J Radiol.* 2017;95:300-6.





CHAPTER  
ELEVEN

General discussion

During the last decade, radioembolization evolved rapidly as a treatment for liver malignancies, leading to many new diagnostic insights, treatment insights and concurrent scientific challenges. Developments occurred across the board; e.g. better imaging tools (including the increased use of cone-beam CT), new catheters and the abandonment of standard prophylactic embolization of side branches, the increasing use of personalized dosimetry and the development of dosimetry calculation software (1-3).

The aim of this thesis was to gain insight in hepatotoxicity after radioembolization and research some potential strategies to improve patient selection and avoid clinically relevant hepatotoxicity, i.e. symptomatic radioembolization-induced liver disease (REILD). In the first part of this discussion the differences between radioembolization products and their relation to dose-effect relationships will be discussed. Thereafter, the currently used definitions of REILD will be reviewed including an interpretation of (un)acceptable (hepato)toxicity. In the second part of this discussion the potential use of hepatobiliary scintigraphy for patient selection will be reviewed. Lastly, the currently used response evaluation criteria will be evaluated and future directions will be discussed.

### **Differences between radioembolization products and their relation to dose-effect relationships**

Currently, three types of microspheres are commercially available (**Table 1**): yttrium-90 ( $^{90}\text{Y}$ ) glass microspheres (TheraSphere<sup>®</sup>, Boston Scientific),  $^{90}\text{Y}$  resin microspheres (SIR-Spheres<sup>®</sup>, SIRTEX) and  $^{166}\text{Ho}$  poly (L-lactic acid) microspheres (QuiremSpheres<sup>®</sup>, Terumo). In addition to their difference in matrix and isotope used, other differences exist (**Table 1**).  $^{90}\text{Y}$  glass microspheres have a higher density and higher specific activity than both  $^{90}\text{Y}$  resin and  $^{166}\text{Ho}$  microspheres. This will influence both the flow dynamics during treatment and the dose-effect relationships (4, 5). Unfortunately,  $^{90}\text{Y}$  resin and glass microspheres are still regularly lumped together in study analyses (6, 7), neglecting their inherent different specific activity and resultant difference in injected dose and tolerable non-tumorous liver absorbed dose.

**Table 1.** Differences in the commercially available microspheres (8-13)

	SIR-spheres®	TheraSphere®	QuiremSpheres®
Matrix	Resin	Glass	Poly-L-lactic acid
Diameter (mean, range)	32 µm (30-60 µm)	25 µm (20-30 µm)	30 µm (15-60 µm)
Density	1.6 g/ml	3.3 g/ml	1.4 g/ml
Isotope	<sup>90</sup> Y	<sup>90</sup> Y	<sup>166</sup> Ho
β-energy	2.28 MeV	2.28 MeV	1.81 MeV
γ-energy	-	-	81 keV (6.7%)
Half-life	64.1 h	64.1 h	26.8 h
Specific activity	50 Bq	1250-2500 Bq (depending on shelf-life)	340 Bq
Number of microspheres for 3 GBq	40-50 million	1-8 million	20-30 million
Target volume dose*	50 Gy	80-150 Gy	60 Gy
Tolerable non-tumorous liver absorbed dose	30 Gy** / 40 Gy	50 Gy** / 90 Gy	40 Gy** / 60 Gy

\* according to manufacturers instructions for use

\*\* in case of a compromised liver function (for Theraspheres: an upper threshold dose of 50 Gy in patients with a bilirubin of >1.1 mg/dl)

Microspheres of lower specific activity are typically injected in higher numbers to establish their target dose. A higher number of injected microspheres results in the formation of more microsphere clusters in the target volume (tumor and non-tumorous liver), thus a more homogeneous dose distribution (14, 15). Consequently, more liver sinusoids will be targeted and the tolerable non-tumorous liver absorbed dose will decrease (5, 16). This effect will be even more pronounced if arterial stasis occurs (4). <sup>90</sup>Y glass microspheres have virtually no embolic potential, resulting in full delivery of the prescribed dose (17). In <sup>90</sup>Y resin treatments early stasis has been reported in approximately 20% of treatments (4). As a result, the prescribed dose will not always be fully delivered and/or microspheres will deviate to the hepatic vascular bed, increasing the non-tumorous liver absorbed dose (5, 15). A side note in case of <sup>90</sup>Y glass microspheres is that in clinical treatments the shelf-life / post-calibration time can vary (normally between 2-14 days). A longer shelf-life results in <sup>90</sup>Y decay before treatment, i.e. a lower specific activity at treatment and hence a higher

number of injected microspheres. Yet, only at 16 days post-calibration the specific activity will approach the specific activity of  $^{90}\text{Y}$  resin microspheres (15).

The influence of the higher specific gravity of  $^{90}\text{Y}$  glass microspheres remains unclear. Theoretically, this could result in a higher absorbed dose to the dorsal liver segments (given the supine patient position during treatment).

Besides microsphere distribution (i.e. dose distribution), the regenerative potential of the liver is also relevant. In case of cirrhosis, the liver function and its regenerative potential is decreased (18, 19). As a result the maximum tolerable non-tumorous liver dose decreases (20). In the study by Chiesa et al., using  $^{90}\text{Y}$  glass microspheres, a normal tissue complication probability (NTCP) of 15% was observed at a non-tumorous liver absorbed dose of 90 Gy and 49 Gy in Child-Pugh A patients with a bilirubin  $<1.1$  mg/dL and  $\geq 1.1$  mg/dL, respectively. Due to the differences in product characteristics, different tolerable non-tumorous liver absorbed doses for  $^{90}\text{Y}$  glass,  $^{90}\text{Y}$  resin and  $^{166}\text{Ho}$  are recommended in patients with a compromised liver function (e.g. cirrhosis or heavy chemotherapeutic pre-treatment) (Table 1) (12, 13).

### **Defining hepatotoxicity in the short-term and in the long-term; is there a difference?**

Lodging of microspheres into the liver sinusoids results in radiation-induced changes in the normal liver parenchyma (15, 21, 22). As a consequence varying degrees of hepatotoxicity can develop – depending on the extent of non-tumorous liver parenchyma involvement and the presence of underlying disease – ranging from clinically occult biochemical changes to symptomatic REILD (15, 21, 23, 24).

Symptomatic REILD is a seriously debilitating, potentially lethal condition, but fortunately rarely reported (0-5% in large patient series) (1, 24). A large heterogeneity exists in the definition of REILD and its reporting, prohibiting a meaningful comparison between studies and various treatment strategies.

In **Chapter 2** a comprehensive definition of REILD is described, building forward on the initial definition of Sangro et al. (21). In that study REILD was diagnosed if a serum

total bilirubin of  $\geq 51.3 \mu\text{mol/L}$  and ascites (clinically or by imaging) developed within 3 months following radioembolization in the absence of tumor progression or bile duct obstruction. We proposed an adjusted definition with a five-point grading scale, similar to the posthepatectomy liver failure and Common Terminology Criteria for Adverse Events (CTCAE) grading scales (25). Unfortunately, both definitions are not widely used in literature today, nor in large prospective clinical trials, leading to inconsistency in the reporting and grading of REILD (26-29).

Histopathological features of REILD are largely compatible with sinusoidal obstruction syndrome (SOS) (21, 22, 30). Interestingly, in the CTCAE version 5.0 (November 2017) SOS is first added to the list of adverse events. This classification partially resembles our grading system (Table 2), with similar definitions of grade 1, 4 and 5, while grade 2 is similar to our grade 3.

**Table 2.** Comparison of both scoring systems

	CTCAE version 5.0 Sinusoidal obstruction syndrome	Hepatotoxicity score (Chapter 2)
<b>Grade</b>		
1	–	Minor liver toxicity, limited to increased AST, ALT, ALP and/or GGT levels (all not exceeding newly developed grade 1 CTCAE toxicity).
2	Blood bilirubin 2-5 mg/dL; minor interventions required (i.e., blood product, diuretic, oxygen).	Moderate liver toxicity, with a self-limiting course. No medical intervention necessary.
3	Blood bilirubin 5 mg/dL; coagulation modifier indicated (e.g., defibrotide); reversal of flow on ultrasound.	REILD, manageable with non-invasive treatments such as diuretics, ursodeoxycholic acid and steroids.
4	Life-threatening consequences (e.g., ventilatory support, dialysis, plasmapheresis, peritoneal drainage).	REILD necessitating invasive medical treatment such as paracentesis, transfusions, haemodialysis or a transjugular intrahepatic portosystemic shunt (TIPS).
5	Death.	Fatal REILD.

ALP = alkaline phosphatase, ALT = alanine aminotransferase, AST = aspartate aminotransferase, GGT = gamma-glutamyl transferase, CTCAE = Common Terminology Criteria for Adverse Events, REILD = radioembolization-induced liver disease. Bilirubin conversion factor (mg/dL to  $\mu\text{mol/L}$ ) = 17.1



In the CTCAE v5.0 criteria treatment with defibrotide (an antithrombotic and profibrinolytic drug) is advised in case of grade 3 SOS. Treatment with defibrotide has not been reported in literature in case of REILD. Therefore, grade 3 is currently not applicable for REILD. Still, uniformity in the reporting of REILD is necessary for adequate comparison of data. The use of the CTCAE v5.0 criteria could be a potentially useful tool to allow standardized reporting and data comparison.

An important shortcoming in the definitions of REILD is the phrase “in the absence of tumor progression”. Does REILD really only occur in the absence of tumor progression? In contrast, some studies even stated that all liver dysfunction or liver related adverse events in case of progression were considered as REILD (2, 31). This dichotomy is not consistent with real-life: tumor progression and REILD can coexist, especially in case of poorly targeted tumors, i.e. a low tumor-to-non-tumor ratio. Van Doorn et al. reported the long-term response of hepatocellular carcinoma (HCC) patients following radioembolization treatment (after the exclusion of patients with REILD in the first four months post-treatment) separating the causes of death into four categories (tumor related, liver related, combined tumor and liver related, and unknown) (32). As much as 40% of the studied population had a combined cause of death, supporting the necessity of a change in the definitions regarding “the absence of tumor progression”.

Based on the available literature in 2017, we added a timeline to REILD development:  $\geq 2$  weeks – 4 months post-radioembolization, classifying it as a short-term adverse event. This timeline is based on the limited available histopathology data with almost all specimens acquired  $< 8$  weeks after radioembolization (14, 21, 22). This timeline is similar to the Baltimore and Seattle criteria for SOS in bone marrow transplant patients after a combination of chemotherapy and total body irradiation: 20-21 days after hematopoietic cell transplantation (33).

Long-term or chronic hepatotoxicity (i.e.  $> 4$  months after radioembolization) is a frequently reported, but difficult to discriminate entity, given the possible confounding by often underlying (progressive) liver disease in patients with HCC and cirrhosis or by accumulation of toxicity in heavily pre-treated patients (11, 32, 34, 35). Furthermore, the data are limited due to the limited survival of most patients treated with radioembolization.

Patients with HCC often have an underlying chronic liver disease with advanced fibrosis or cirrhosis. Mortality due to cirrhotic related complications in this fragile patient group – regardless of the development of HCC – is frequent, being the 12<sup>th</sup> leading cause of death in the United States (36). It is important to distinguish patients with compensated liver cirrhosis from patients with decompensated liver cirrhosis, since the clinical outcome and prognosis is vastly different (37, 38). The development of at least one sign of decompensated liver cirrhosis results in a significant increase in liver related mortality. For example, the development of one none-bleeding sign of decompensated liver disease (commonly ascites) is associated with a five-year mortality of 55-80% compared to 25% before the development of signs of decompensated liver disease (37). One-year survival of cirrhotic patients without an HCC in a European population was 88%, 75% and 56% for Child-Pugh A, B and C, respectively (39). Conversely, in the study by Johnson et al. the one-year survival in a similar patient group was 100%, 82% and 63% for ALBI grade 1, 2 and 3, respectively (40).

In a cohort of HCC patients with a Child-Pugh A cirrhosis, Chiesa et al. observed an almost constant incidence of liver decompensating events more than six months after lobar <sup>90</sup>Y glass radioembolization, after an initial peak at two months (11). Liver decompensation was defined as the occurrence of any of the six following features: total bilirubin > 3 mg/dL, international normalized ratio > 2.2, clinically detectable ascites, encephalopathy, oesophageal varices bleeding and death. Also, in the patient group with an injected liver volume of < 40% (mostly segmental treatments) and a baseline bilirubin of < 1.1 mg/dL (=18.8 µmol/L) no liver decompensation events were reported, regardless of the absorbed dose to the injected parenchyma.

Van Doorn et al. analyzed the development of liver decompensation (defined as the development of a Child-Pugh  $\geq$  B7) more than four months after radioembolization (the end of the REILD definition timeline) in HCC patients undergoing radioembolization treatment with a median baseline Child-Pugh score of A5 (73% cirrhotic patients) (32). The hypothesis of the study being that the damage to the non-tumorous liver would result in a functional decline of the liver and could partly explain the lack of a survival benefit seen in patients undergoing radioembolization when compared to sorafenib. Lobar or more

extensive treatments were performed in 71/85 patients. After exclusion of 16/85 patients, who developed REILD within four months after radioembolization, another 38/69 patients developed a Child-Pugh  $\geq$  B7 more than four months after treatment (30 patients needing medical intervention). The corresponding ALBI score of the total study population (n=69) declined from -2.8, SD 0.37 at baseline to -2.1, SD 0.73 at the end of follow-up ( $p < 0.001$ ; median follow-up 30 months). The baseline ALBI score was the only significant predictor of liver decompensation at last follow-up. Treatment-related death occurred in 28/69 patients at last follow-up (10 liver related, 18 combined liver and tumor related). No dosimetry data were available. Still, the median overall survival of this population was longer than the median overall survival of a matched cohort of HCC patients treated with sorafenib (16 months vs. eight months). This finding was in line with the dosimetric analysis of the SARA study, in which patients with an ALBI grade 1,  $< 25\%$  tumor load and a tumor dose  $> 100$  Gy had a longer overall survival than patients treated with sorafenib (41).

Clearly, the development of long-term hepatotoxicity, i.e. late-onset liver decompensation after radioembolization is a multi-factorial entity, depending on the pre-treatment liver function, treated volume fraction and non-tumorous liver absorbed dose. The stabilization in liver decompensation incidence six months after radioembolization (consistent with the natural history of cirrhosis), the predictive value of the pre-treatment ALBI scores, and the increasing liver decompensation and mortality with increasing ALBI grades in cirrhotic patients without a coexisting HCC, advocate for an important role of the preexisting cirrhosis in radioembolization-induced long-term hepatotoxicity (11, 31, 32, 40, 41).

Signs of portal hypertension on imaging are regularly reported after radioembolization in cirrhotic and non-cirrhotic patients. These signs include splenomegaly, an increasing diameter of the main portal vein or splenic vein and the development of portosystemic collaterals (34, 42-44). However, complications of newly developed portal hypertension in previously non-cirrhotic patients were only anecdotally reported following radioembolization. Gutierrez et al. reported a case-series of three patients with complications of portal hypertension after  $^{90}\text{Y}$  resin treatment of colorectal liver metastases (CRLM), all pre-treated with oxaliplatin-based chemotherapy regimens (FOLFOX). Oxaliplatin is known to cause sinusoidal injury and SOS, being reported in 59% of resected

liver specimens after hepatectomy (45). Furthermore, in the study by Emmons et al., including 498 patients with CRLM treated with <sup>90</sup>Y resin, 72 of the 347 patients available for toxicity analysis (21%) experienced grade  $\geq 3$  hepatotoxicity within the first six months, with more bilirubin and albumin grade 3-4 toxicity in patients receiving radioembolization as a third line therapy (compared to first and second line,  $p=0.008$ ) (46). This pleads for a combined etiology of these long-term complications.

Patients with neuroendocrine tumor liver metastases (NELM) are more often treatment-naïve and increased overall survival rates after radioembolization are reported with a median overall survival of 28-33 months (median overall survival of 58 months in liver-only disease) (34, 35). Avoidance of clinically overt long-term toxicity is therefore crucial in this patient population. Tomozawa et al. observed signs of portal hypertension on imaging in 29% of patients at one-year follow-up without reporting any complications (34). Signs of portal hypertension were more frequently seen after bilobar treatments and included ascites (17%), splenomegaly (21%) and varices (7%). Long-term grade 3 hyperbilirubinemia or the onset of ascites were rare after radioembolization of NELM (34, 35).

In view of the scarce clinically relevant long-term toxicity of radioembolization in patients with liver metastases, the benefit of the treatment (reduction of hormonal complaints and/or increased overall survival) outweighs the risks in selected patient populations (10, 47).

### **How much toxicity is acceptable?**

Almost all patients develop some form of (transient) radioembolization-related toxicity consisting of a post-embolization syndrome characterized by fever, abdominal pain and leukocytosis or laboratory changes (24). In **Chapter 3** the clinical and biochemical toxicities after resin and glass <sup>90</sup>Y radioembolization were described. In that study, 73% of all patients (31/41 glass + 31/44 resin) had a hepatotoxicity score of  $\leq 2$  based on the REILD score proposed in **Chapter 2**, meaning no medical intervention was needed. Nevertheless, with an eye on the quality of life, we need to clearly define what constitutes unacceptable toxicity for patients undergoing radioembolization. Furthermore, patients with underlying (chronic) liver disease and advanced fibrosis or cirrhosis have a significant greater risk of radioembolization-induced hepatotoxicity (20, 48). Pre-treatment assessment of

underlying liver disease and damage is therefore warranted to distinguish high risk patients from patients with healthy background liver parenchyma as is often the case in non-pretreated metastatic patients (e.g. up to one third of NELM patients) (34).

### **HCC patients**

Most patients with an HCC have underlying cirrhosis (ca. 81% in the Netherlands) with various etiology (49). Contrary to the non-invasive, image-based diagnosis of HCC in cirrhotic patients (50), the pre-treatment diagnosis of HCC in a non-cirrhotic liver is based on histopathologic examination. In tandem hepatological evaluation is warranted to assess the liver function, portal hypertension and potential underlying (chronic) liver disease. This includes the analysis of the liver's synthetic, excretory and detoxifying functions, using clinical scores, such as the Child-Pugh score, MELD score and ALBI score (**Table 2, Chapter 1**).

After the introduction of the ALBI score, several authors chose to analyze the toxic effect of radioembolization by use of either the ALBI score as a continuous variable or the ALBI grade (31, 32, 40, 44, 51). The ALBI grades categorize cirrhotic patients into three distinct prognostic groups. This grading system was validated in multiple cohorts (with or without coexisting HCC, and with or without sorafenib treatment for HCC) and has a higher degree of discriminative power compared to the Child-Pugh score (40).

Lescure et al. analyzed the ALBI scores in 222 patients (85% cirrhosis, 91% Child-Pugh A) with advanced HCCs (68% BCLC C) after one radioembolization treatment (96% lobar treatments). The one-year survival was approximately 75%, 50%, and 35% for ALBI grade 1, 2 or 3, respectively (based on their Kaplan Meier curves). The median overall survival was 24.0 months, 12.9 months and 8.3 months for ALBI grade 1, 2 and 3, respectively. In a patient population with similar baseline patient and HCC characteristics (apart from ca. 60% extrahepatic spread) treated with atezolizumab plus bevacizumab or sorafenib the one-year survival was 67.2% and 54.6%, respectively (no data on the ALBI scores) (52). Certainly, median overall survival of patients without extrahepatic disease was longer than in patients with extrahepatic disease: 22.8 vs. 17.8 months for atezolizumab plus bevacizumab (16.9 vs. 9.7 months for sorafenib) (53).

The ALBI score and baseline Child-Pugh score also correlated with hepatotoxicity and REILD (31, 32, 54). In the study by Lescure et al. the ALBI score increased with a median of  $0.35 \pm 0.45$ , whereas in the study by Ricke et al. (SORAMIC trial, 80% cirrhosis and 68% BCLC C at baseline) the mean increase in ALBI score was 0.79 in the patient group undergoing radioembolization plus sorafenib treatment with a stronger increase in patients with a Child-Pugh A6 score compared to Child-Pugh A5 (31, 51). To put this number into perspective: a bilirubin of 8  $\mu\text{mol/L}$  and albumin of 43 g/L result in an ALBI score of -3.06, hence an increase of 0.79 will result in one grade deterioration. By contrast, only one patient (0.6%) in the radioembolization plus sorafenib group of the SORAMIC trial developed grade 3/4 liver dysfunction (not further specified) and none of the patients developed radiation hepatitis (i.e. REILD). Overall grade  $\geq 3$  toxicities did not occur more frequently in the radioembolization plus sorafenib group compared to the sorafenib-only group (51, 55). It is difficult to put these data into perspective with regard to relevant hepatotoxicity, given the lack of data on dosimetry in this study.

In studies randomizing between radioembolization and sorafenib the incidence of treatment-related grade  $\geq 3$  toxicity was lower for radioembolization (30.6% vs. 52.1%,  $p=0.0002$ ), while radioembolization was noninferior to sorafenib treatment with regard to overall survival (26, 27, 55). In comparison, the more recently approved atezolizumab plus bevacizumab combination therapy resulted in as much as 56.6% grade  $\geq 3$  toxicity (4.6% grade 5) (52). It remains unclear if and to what extent these toxicities lead to additional treatments and interfere with quality of life. Based on the current literature, the one-year and median overall survival rates after radioembolization are at least comparable to currently available systemic HCC treatments for BCLC C patients, even with the treatment-related (hepato)toxicity taken into account.

More importantly, in patients with a high tumor absorbed dose and/or a non-cirrhotic liver overall survival after radioembolization is superior compared to sorafenib treated HCC patients with similar baseline characteristics (2, 6, 11, 41, 56, 57). Taken the safety and efficacy into consideration it seems reasonable to accept substantial grade  $\geq 3$  (hepato) toxicity in patients with advanced HCC; at least over 50% grade  $\geq 3$  toxicity with grade 5 toxicity in up to 5% (i.e. comparable to treatment with atezolizumab plus bevacizumab).

Especially, if this means that more well-selected patients (e.g. patients with low ALBI scores / Child-Pugh A5 scores, low perfused volumes and high tumor-to-non-tumor ratios on  $^{99m}\text{Tc}$ -MAA scintigraphy) can be treated with a tumoricidal absorbed dose, leading to an increased overall survival.

### **Metastatic liver disease**

Colorectal liver metastases (CRLM) are the most commonly treated and studied metastases with regard to radioembolization, and together with HCC the only reimbursed indication in the Netherlands. Unfortunately, the largest randomized trials (FOXFIRE, SIRFLOX, FOXFIRE global and EPOCH) compare radioembolization with and without either first line or second line chemotherapy (28, 29). As expected, the incidence of hepatotoxicity is higher in the combined treatment groups. In the combined analysis of the SIRFLOX and FOXFIRE trials grade  $\geq 3$  toxicity was present in 380 of 571 patients (67%) in the FOLFOX only group vs. 375 of 507 patients (74%) in the FOLFOX plus radioembolization group ( $p=0.0089$ ) (28). However, serious adverse events (SAEs) related to radioembolization were reported in only 16.4% of patients in the FOLFOX plus radioembolization group, whereas SAEs related to FOLFOX were reported in 32.5% in this group. Also, in the study by Emmons et al., including 498 patients with CRLM treated with  $^{90}\text{Y}$  resin, 21% experienced grade  $\geq 3$  hepatotoxicity (23% other grade  $\geq 3$  toxicities), which confirmed this finding (46). Taken together, toxicity seems limited compared to regular chemotherapy regimens.

Obviously, the extent to which toxicity is acceptable is related to the intended treatment aim; i.e. curative (e.g. downstaging to surgery) or palliative. As chemotherapy lines progress, more patients become chemotherapy unresponsive and intolerant (58). In a palliative setting, radioembolization can serve as a less toxic, though effective treatment regarding progression-free survival, overall survival and symptom relief (10, 29, 59). Grade 3-5 toxicity after radioembolization should be equally acceptable as after regular chemotherapy lines. Intended downstaging is different and almost always involves treatment of only one lobe or less, i.e. lobar or segmental treatment. Limiting the perfused volume lessens the extent of the hepatotoxicity, which is directly related to the non-tumorous liver absorbed dose (10, 11, 60). Conversely, Coskun et al. showed that the kinetic growth rate of the non-embolized lobe is higher, when a higher non-tumorous liver

absorbed doses is reached in the embolized lobe, using  $^{90}\text{Y}$  resin microspheres (61). This could be due to the higher absolute embolic load, especially in  $^{90}\text{Y}$  resin microspheres (as suspected based on the early observed clinical toxicity in **Chapter 3**). Given the interval (8-10 weeks) this is however probably also genuinely dose-related (similar to the patients with the highest non-tumorous liver absorbed dose in **Chapter 6**). In case of an insufficient function of the future liver remnant prior to resection, radioembolization has the benefit of combining downstaging with future liver remnant hypertrophy induction. The decline in function of the embolized lobe is not complete, leaving room for considerable dose-related toxicity in the embolized lobe (grade < 5) (62, 63). Therefore, treatment-related life-shortening toxicity will be limited for this indication. And, even in less desirable tumor targeting (i.e. higher non-tumorous liver absorbed dose) there is potential benefit in the form of accelerated hypertrophy, prompting the question: should we increase the accepted non-tumorous liver absorbed dose in downstaging treatments?

### **Possible value of hepatobiliary scintigraphy in radioembolization**

Cirrhosis is a complex entity with distortion of the hepatic architecture as a hallmark, leading to an increase in intrahepatic vascular resistance by histological changes (i.e. narrowing of the sinusoids) and an imbalance between vasoconstrictors and vasodilators (64, 65). By means of the hepatic arterial buffer response (among other mechanisms), the hepatic arterial contribution to the sinusoid perfusion increases from 20% to 40% in well-compensated cirrhosis (66, 67). Furthermore, vasodilators, such as nitric oxide cause dilation of the terminal hepatic arterioles (diameter 15-35  $\mu\text{m}$ ) lowering the hepatic arterial resistance, whilst the sinusoidal availability of nitric oxide is reduced (64, 67). Theoretically, the increase hepatic arterial flow and enlarged terminal hepatic arteriole diameter leads to an increased inflow of microspheres and more distally located microspheres in the cirrhotic non-tumorous parenchyma during radioembolization treatments. This theory could partly explain 1) the negative effect of the severity of cirrhosis on treatment outcomes with regard to (clinically relevant) hepatotoxicity and 2) the consequential lower non-tumorous liver absorbed dose tolerability (11, 31, 32). A similar effect was seen in the results of the indocyanine green (ICG) clearance tests in the study by Fernandez et al. (43). The ICG retention at 15 minutes (ICG R15) increased from 10.9% to 20.7% at two months



(normal value 0-10%), mainly owing to patients with an abnormal ICG R15 at baseline.

Though the mechanism of hepatic uptake for ICG and  $^{99m}\text{Tc}$ -mebrofenin is identical, no difference in the pre-radioembolization body surface area (BSA) corrected hepatic mebrofenin uptake rate (cMUR) was seen between patients with and without late onset liver dysfunction following radioembolization in the HCC Child-Pugh A patient population of Labeur et al.; even though the cMUR correlates well with bilirubin, albumin and the ALBI score (ALBI score,  $p=0.001$ ) (62). The post-radioembolization cMUR however showed a trend towards decreased total liver cMUR in patients with liver dysfunction.

Interestingly, in our studies (**Chapter 5** and **6**), as well as in the other studies on hepatobiliary scintigraphy in radioembolization patients an initial functional decline was reported in the non-treated lobe (62, 63). In the study of Labeur et al., the cMUR declined after radioembolization from 2.4 to 2.0%/ml/min/m<sup>2</sup> in the non-treated lobes after a median of 6 weeks ( $p=0.808$ ), whereas in the study of Allimant et al. the median functional decline in Child-Pugh A cirrhotic patients was -26% compared to baseline at 2 weeks and -8% and -6% at one and two months, respectively (62, 63). Subsequently, a functional increase to 120% was seen at three months in the non-treated lobe (63). These consistent findings suggest a real functional decline in the non-treated lobe in the first three months after radioembolization.

Several mechanisms could play a role in the functional decline of the non-treated lobe. One possible explanation is a rise in portal resistance and hepatic venous pressure gradient directly after radioembolization treatment, consistent with the fast development of splenomegaly post-treatment (42, 68, 69). ICG R15 is known to correlate well with the hepatic venous pressure gradient, which is the golden standard for assessing portal hypertension (70). Moreover, histopathologic changes leading to increased resistance, such as periportal fibrosis, are seen in pig's livers four weeks after radioembolization (14, 15). Although these histopathologic changes only occur in the treated lobe, they do alter the total portal pressure and flow velocity. The portal venous bed is a passive vascular bed in contrast to the arterial vascular bed (65). Consistent with Hagen-Poiseuille's law (**Table 3**) a change in the total diameter of a vascular bed will result in exponentially larger changes

in the vascular pressure gradient (65). These pressure changes are reflected by the increase in spleen size and decreased platelet counts early after treatment (**Chapter 3**) (69).

Furthermore, all aforementioned studies on hepatobiliary scintigraphy after radio-embolization used  $^{90}\text{Y}$  glass microspheres (**Chapter 6**) (62, 63), consequently the arterial embolization is neglectable (17). Therefore, the decreased uptake of mebrotfenin is not likely influenced by alterations in the hepatic arterial flow. Even if the arterial flow is altered, the arterial buffer response is more likely to increase the arterial flow to the non-embolized lobe (to compensate for the reduced portal flow) and synchronously and partially compensate for the decreased mebrotfenin uptake.

**Table 3.** Hagen – Poiseuille’s law of fluid dynamics

**Hagen-Poiseuille’s equation**

$$\Delta P = 128 \mu L Q / \pi r^4$$

P = pressure,  $\mu$  = fluid viscosity, L = length of the cylindrical pipe, r = radius of the pipe, Q = volumetric flow rate

Another potential explanation is the alteration in the uptake and intracellular transit of the  $^{99\text{m}}\text{Tc}$ -mebrotfenin (71). Many different liver diseases lead to apoptosis of hepatocytes, together with a release of cytokines. Some cytokines (e.g. tumor necrosis factor  $\alpha$  and interleukin-6) downregulate the transporters necessary for the uptake of bilirubin and  $^{99\text{m}}\text{Tc}$ -mebrotfenin (i.e. organoid anion transporting polypeptide 1B1 and 1B3, and multidrug resistance protein 2) (71, 72). Fernandez et al. reported an significant elevation in interleukin-6 after radioembolization, up to 207% compared to baseline after 24 hours (43). Interleukin-6 levels remained elevated until two months after treatment (no data afterwards available), with a more pronounced elevation in segmental treatments (compared to lobar). No significant change in the levels of tumor necrosis factor  $\alpha$  was observed (43). Interleukin-6 mediated downregulation of the transporters could explain the initial pronounced decrease in uptake of  $^{99\text{m}}\text{Tc}$ -mebrotfenin. Furthermore, an elevation in bilirubin concentrations is also seen after radioembolization (**Chapter 3**), which returns to normal or stabilizes at grade 1 toxicity after a median of 29 days in the majority of patients (60%) (23, 43, 73). Competitive inhibition due to the increased bilirubin levels

could further decrease  $^{99m}\text{Tc}$ -mebrofenin uptake (72).

The gradual increase in cMUR in the non-treated lobe, after an initial decline at two weeks, is less difficult to explain. Signs of recanalization with embedding of the microspheres in the vessel walls were reported by Bilbao et al. eight weeks after radioembolization. As a result, the portal resistance will decline. Rassam et al. reported on the microcirculatory alterations after portal vein embolization (PVE) with an increase in perfused vessel density and sinusoidal diameter in the non-embolized lobe 23 days after PVE, without changes in the microvascular flow (74). Whether similar changes occur after radioembolization is unclear. The volumetric increase of the non-embolized lobe is however much slower after radioembolization compared to PVE (75). Conceivably, the increase in perfused vessel density is therefore also slower. The potential increase in the total area of portal vascular bed and known increase in diameter of the portal vein in the non-embolized lobe (as reported 4.5 months after treatment (42)), will likely further reduce the portal pressure. Together, this could partially explain the improved uptake of  $^{99m}\text{Tc}$ -mebrofenin (14). Furthermore, reversal of the downregulation of the hepatic transporters can be assumed at some point, also enabling recovery of the  $^{99m}\text{Tc}$ -mebrofenin uptake.

Another important finding that could be deduced from the temporal changes in liver function recovery as measured on hepatobiliary scintigraphy is the timing of sequential treatments (63). Sequential whole liver treatments (i.e. right and left lobe treatment split) may result in less hepatotoxicity than single session whole liver treatments (48, 60). Obviously, this is also dosimetry-related. The rationale behind sequential treatment is to allow the liver time to recover before the second radioembolization hit is administered. Nowadays, the advocated interval is most commonly 4-8 weeks in both cirrhotic and non-cirrhotic patients (34, 57), whereas the slower liver function recovery in the study of Allimant et al. advocates a longer interval of at least three months. This may increase the chance of interval progression, yet reduce the chance of severe cumulative hepatotoxicity (13).

Hepatobiliary scintigraphy has proven its value in liver surgery and after PVE, outperforming CT-volumetry-based assessment (19, 76, 77). In surgery the outcome is a sudden reduction

in liver tissue volume and function. In PVE, the liver is cut off of its main blood and oxygen supply (70-80%), resulting in a fast functional and volumetric increase on the non-treated contralateral side (77, 78). In both PVE and surgery, the increase in function exceeds the volumetric increase in both compromised and non-compromised livers (76-78). Also, for both compromised and non-compromised livers the same cut-off value for a future liver remnant function can be used: 2.69%/min/m<sup>2</sup> (18). In radioembolization, the embolic effect is minimal, especially when using <sup>90</sup>Y glass microspheres. Moreover, the hepatic artery is only responsible for approximately 20% of the blood and oxygen supply in non-cirrhotic livers. This seems to translate to a much slower increase in function and volume in the non-embolized lobe (62, 63, 75, 79). Contrary to PVE and liver in situ splitting surgical techniques the anti-tumoral effect of radioembolization in combination with an increase in function and volume of the non-embolized lobe allows for this longer interval. So, the question is when and in which cases could hepatobiliary scintigraphy be useful with regard to radioembolization treatments?

For one, it could be useful in patients with severely compromised livers, e.g. Child-Pugh  $\geq 7$  or with a baseline bilirubin  $> 18.8 \mu\text{mol/L}$  (1.1 mg/dL) (similar to case 2 in **Chapter 5**) to reevaluate the treatment plan with regard to the perfused volume, and injected and predicted non-tumorous liver absorbed dose. Hepatotoxicity / functional liver decline is related to the non-tumorous whole liver absorbed dose (8, 10, 62). However, liver function is often not homogeneously distributed in patients with underlying liver disease (80). Also, the distribution of the injected microspheres in the treated lobe is very heterogeneous, leading to a heterogeneous dose distribution. This will result in heterogeneous and difficult to predict loss of liver function (5, 14-16). Given this multifactorial nature of the treatment (e.g. treatment volume, non-tumorous whole liver absorbed dose) and large inter-patient variability, a cMUR cut-off value prior to radioembolization treatment is difficult to define. Therefore, the added value of a pre-treatment hepatobiliary scintigraphy to the normal clinical and laboratory work-up is still under debate. Referring to the case in **Chapter 5**: hepatobiliary scintigraphy may be useful in selected cases, specifically in patients with a poor baseline liver function and a potential heterogeneous distribution, to adapt the treatment volume/plan to the liver function distribution.

Another possible indication for pre-radioembolization hepatobiliary scintigraphy could be planned re-treatments after previous whole liver injection or right lobar treatments to assess the regional differences in function and match these with the planned injected volume(s). Lastly, its most common use probably will be post-radioembolization pre-surgery measurement of the future liver remnant function.

### **Response assessment; how and when?**

The previous paragraphs focused on hepatotoxicity as a result of radioembolization treatment. Radioembolization is, however, foremost an anti-tumoral treatment for patients with liver-dominant or liver-only disease aimed at improving survival and quality of life. Liver metastases are often the limiting factor for survival, especially in patients with colorectal liver metastases (CRLM) and neuroendocrine liver metastases (NELM). In reality, tumor response is only useful as a proxy for progression-free and overall survival, which is even more disputable in regional, e.g. liver-directed therapies, including radioembolization. Contrary to systemic therapies, extrahepatic disease is not treated, but is logically included in the response criteria. Derivative endpoints are frequently adopted, such as liver-only progression-free survival.

Multiple response criteria are used (**Table 4**), both morphologic (in case of computed tomography (CT), magnetic resonance imaging (MRI)) and metabolic (in case of  $^{18}\text{F}$ -fluorodeoxyglucose positron emission tomography/CT ( $^{18}\text{F}$ FDG-PET/CT)). The most commonly used morphologic criteria are the Response Evaluation Criteria in Solid Tumor (RECIST 1.1). Though RECIST 1.1 is most commonly used for the evaluation of radioembolization, it has shown to be a poor predictor of response and overall survival for CRLM, NELM, as well as HCC and cholangiocarcinoma (6, 7, 81-86). Morphologic criteria that also take tumor density on contrast-enhanced CT into account outperform RECIST 1.1 with regard to the prediction of overall survival and progression-free survival, while maintaining substantial to excellent inter-observer agreement (7, 82, 84). This is true for both hypervascular and hypovascular lesions. Hypervascular lesions, such as HCC and NELM, are often assessed applying the modified RECIST (mRECIST) criteria to the late arterial phase CT or MRI images (**Table 4**). Although mRECIST outperforms RECIST with regard to overall survival prediction in HCC patients after radioembolization, even in these patients the Choi

criteria (measured on the portal venous phase!) or other criteria (e.g. volumetric iodine uptake, as measured on the late arterial phase) are superior (6, 7, 87, 88).

The Choi criteria were first introduced to evaluate response to Imatinib in gastro-intestinal stroma cell tumors; a relatively hypervascular tumor prior to treatment (89). Still, the Choi criteria have shown to accurately identify responders after radioembolization in hypovascular tumor types, including cholangiocarcinoma and CRLM (82, 84).

A noteworthy downside of density measurements is that they are not transposable to MRI studies. However, MRI has its own additional imaging features of response, such as a decrease in ADC value (90). Response evaluation on MRI is often reserved for HCC, cholangiocarcinoma, or CRLM prior to resection. In  $^{90}\text{Y}$  radioembolization treatments MRI evaluation is straightforward, using mRECIST or RECIST as appropriate. In case of  $^{166}\text{Ho}$  the susceptibility artefacts may hamper response evaluation. Besides being a beta-emitting radio-isotope,  $^{166}\text{Ho}$  also emits gamma photons (81 keV, 6.7%) and is highly paramagnetic (91). The latter enables visualization of  $^{166}\text{Ho}$  microspheres on MRI, either for dosimetric purposes or during clinical follow-up / response assessment (92). In patients after radiation lobectomy or other patients with foci of dense  $^{166}\text{Ho}$  microspheres depositions (such as adequately targeted tumors), the paramagnetic properties of  $^{166}\text{Ho}$  result in considerable susceptibility artefacts that interfere with tumor measurements (**Figure 1**).

$^{18}\text{F}$ FDG-PET/CT is mostly used in the response evaluation of patients with liver metastases (mainly CRLM) with a superior predictive value after radioembolization compared to morphologic criteria, especially in early assessments (at 4-6 weeks) (82, 83, 93, 94). The most commonly used metabolic response criteria are the EORTC and PERCIST criteria (**Table 4**) (10, 81-83). Other ways of response assessment include changes in standardized uptake value (SUV)-based parameters, such as change in  $\text{SUV}_{\text{max}}$ ,  $\text{SUV}_{\text{peak}}$  or metabolic tumor volume and total lesion glycolysis (TLG) (8, 93).

The timing of response evaluation depends on the tumor type, the treatment intent, chosen response criteria and chosen modality.  $^{18}\text{F}$ FDG-PET/CT has proven its use in early response prediction in CRLM radioembolization treatments by the use of TLG reduction, the EORTC or PERCIST 1.0 criteria. In the study by Jongen et al. TLG reduction of CRLM

**Table 4.** Common response criteria for oncologic assessment

	RECIST 1.1	mRECIST	Choi criteria
Measurement method	Measurement of the longest cross-sectional diameter	Measurement of the longest cross-sectional diameter of the arterial enhancing portion of the lesion	Measurement of the longest cross-sectional diameter and measurement of the CT attenuation coefficient in HU (by drawing a ROI around the margin of the entire lesion)
Calculation method	Sum of up to 5 target lesions	Sum of target lesions	Sum of target lesions and calculation of a patient-based HU <sub>mean</sub>
CR	Disappearance of all target lesions	Disappearance of any intratumoral arterial enhancement in all target lesions	Disappearance of all target lesions
PR	At least a 30% decrease in the sum of the greatest unidimensional diameters of target lesions	At least 30% decrease in the sum of unidimensional diameters of viable target lesions	Decrease in lesion size $\geq$ 10% or decrease in lesion density $\geq$ 15%
SD	Any cases that do not qualify for either CR, PR or PD	Any cases that do not qualify for either CR, PR or PD	Any cases that do not qualify for either CR, PR or PD
PD	An increase of at least 20% in the sum of the diameters of target lesions	An increase of at least 20% in the sum of the diameters of viable target lesions	Increase in tumor size $\geq$ 10% and does not meet PR criteria by tumor density
Modality	(Contrast enhanced) CT or MRI	Contrast enhanced CT or MRI	Contrast enhanced CT
Contrast phase	Possible on all	Late arterial phase	Portal venous phase

CR = complete response, HU = Hounsfield unit, LD = longest diameter, PR = partial response, SD = stable disease, PD = progressive disease

Table 4. Continued

	WHO criteria	EORTC	PERCIST 1.0
Measurement method	Bidimensional measurement (product of longest diameter and greatest perpendicular diameter)	Measurement of the SUV <sub>BSA, max</sub> and SUV <sub>BSA, mean</sub> in the most avid part of the lesion	Measurement of the SUL <sub>peak</sub> in a VOI centered around the most avid point in the lesion
Calculation method	Sum of all lesions	Sum of all lesions	Sum of up to 5 target lesions
CR	Disappearance of all known disease, confirmed at $\geq 4$ weeks	Complete disappearance of FDG uptake in all lesions	Visual disappearance of all metabolic active tumors
PR	>50% decrease from baseline, confirmed at $\geq 4$ weeks	Reduction in SUV > 25%	Reduction of > 30% and at least 0,8 unit decline in SUL <sub>peak</sub>
SD	Any cases that do not qualify for either CR, PR or PD	Any cases that do not qualify for either CR, PR or PD	Any cases that do not qualify for either CR, PR or PD
PD	> 25% increase of one or more lesions or appearance of new lesions	New FDG uptake in a metastatic lesion or SUV increase of > 25% or visible increase in extent of FDG uptake (20% in LD)	> 30% increase and at least 0,8 unit increase in SUL <sub>peak</sub> or new metabolic active tumors or > 75% increase in TLG
Modality	(Contrast enhanced) CT or MRI	<sup>18</sup> F-DG-PET/CT	<sup>18</sup> F-DG-PET/CT
Contrast phase	Possible on all	-	-



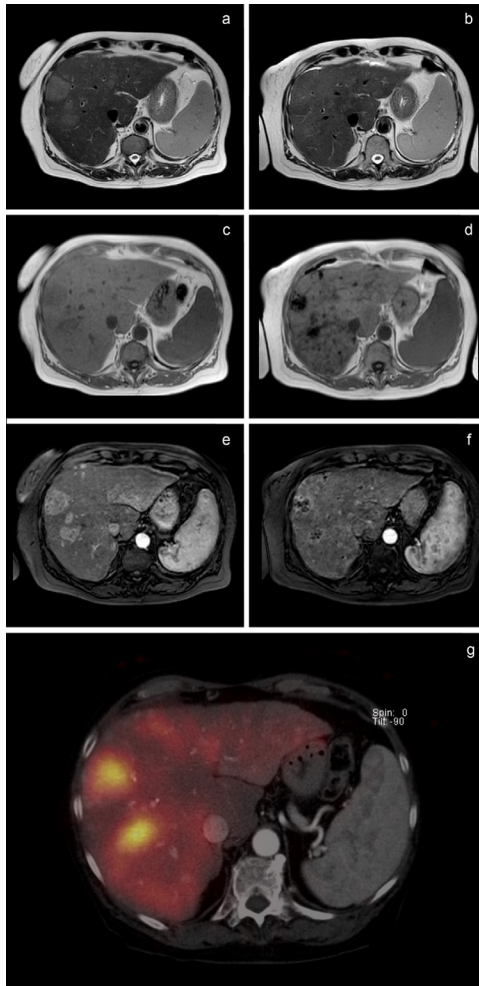


**Figure 1.** 82-years-old female with cirrhosis due to alcohol abuse (Child-Pugh A) and a multifocal HCC in both lobes. In the multidisciplinary tumor board whole liver  $^{166}\text{Ho}$  radioembolization was advised. In the work-up for radioembolization an MRI was performed; displayed are a T2 weighted image (a), T1 in-phase (c) and post-contrast T1 with fat-saturation (arterial phase) (e). Multiple slightly T2 hyperintense, hypervascular lesions were seen with two dominant HCC lesions in segment eight. After treatment a  $^{166}\text{Ho}$  SPECT/CT was acquired (g); with excellent targeting of the HCC lesions in segment eight. Three months after treatment a new MRI was acquired for response assessment (b, d, f). On both the T1 in-phase and post-contrast T1 apparent susceptibility artefacts were present, consistent with the well-targeted lesions and regions in the liver. Both lesions in segment eight show clear signs of response, however, in the dorsal lesion it is difficult to distinguish a partial from a complete response.

at one month after resin  $^{90}\text{Y}$  radioembolization was associated with overall survival (93). Response according to RECIST 1.1 on MRI at three months was also associated with overall survival.

Objective response rates at one month are 39% for TLG and 11% for RECIST1.1, with new extrahepatic lesions being the main cause of progressive disease. Similar results were found for CRLM at 2-4 months after glass  $^{90}\text{Y}$  and  $^{166}\text{Ho}$  radioembolization (8, 10). In the study by Shady et al. the liver progression-free survival was 4.0 months for responders on  $^{18}\text{F}$ FDG-PET/CT performed seven weeks after resin  $^{90}\text{Y}$  radioembolization (using the EORTC criteria) vs. 1.9 months for non-responders ( $p < 0.001$ ) (82). RECIST 1.1 response evaluation at seven weeks was not associated with liver progression-free survival. Based on these findings, the response to radioembolization treatment of CRLM is preferably evaluated by the use of  $^{18}\text{F}$ FDG-PET/CT after 1-3 months, applying either the EORTC criteria or PERCIST criteria (Table 5).

**Table 5.** Follow-up strategy after radioembolization for the most commonly treated malignancies.

	Colorectal liver metastases	Neuroendocrine liver metastases	Hepatocellular carcinoma
<b>Preferred</b>			
Imaging modality	$^{18}\text{F}$ FDG PET/CT	Multiphase CT	MRI
Timing of first follow-up	1 month	6 months	3 months
Response criteria	EORTC or PERCIST	mRECIST	mRECIST*
<b>Alternative**</b>			
Imaging modality	Multiphase CT	$^{68}\text{Ga}$ -somatostatin receptor PET/CT	Multiphase CT
Timing of follow-up	3 months	3 months	3 months
Response criteria	Choi or RECIST 1.1	N.A.	mRECIST (or Choi)

\* additional features, such as ADC increase, should be taken into account. \*\* for colorectal liver metastases the alternative strategy is not preferable, for HCC multiphase CT can be considered as follow-up modality

In NELM, overall survival after radioembolization is longer and significantly influenced by extrahepatic disease, with an approximately twice as long overall survival without extrahepatic disease (34, 86). In the study by Memon et al. a median time to response for NELM after glass <sup>90</sup>Y radioembolization was reported to be 4.9 months on a patient-basis using the WHO criteria (95). Other studies used RECIST 1.1 for CT-based response evaluation after three, six or twelve months with partial response rates up to 33% at six months and 25% at twelve months (34, 35, 86, 96). Corresponding patient-based disease control rates at 6-12 months varied between 67% and 92%. Given the longer overall survival and high disease control rates (though based on suboptimal response criteria), NELM response to radioembolization is preferably assessed after six months. Which modality we should use in daily practice and the ideal response criteria are still unclear. Response evaluation using <sup>68</sup>Ga-somatostatin receptor PET/CT in combination with PET/CT-based criteria or contrast-enhanced CT in combination with the Choi criteria could be interesting to explore.

For HCC, MRI is the recommended follow-up modality after radiological interventions, including radioembolization (97). By contrast, most studies used multiphase CT, probably related to the reduced availability of MRI (6, 7, 27, 87). mRECIST and RECIST are mostly used for response assessment (6, 26, 27, 87), though only response according to mRECIST at one and three months was associated with overall survival and time-to-progression (6, 87). In the LEGACY study by Salem et al., analyzing 162 HCC patients undergoing glass <sup>90</sup>Y radioembolization the median duration of response was 10.6 months according to mRECIST with most patients reaching a complete response between 6 weeks – 6 months (median progression-free survival: 41 months) (85). This population consisted of patients with a solitary HCC < 8 cm in size without macrovascular invasion (40% BCLC C, only based on an Eastern Cooperative Oncology Group (ECOG) performance score of 1). In contrast, the median time to progression in the SIRveNIB trial (<sup>90</sup>Y resin radioembolization vs. sorafenib) was 6.4 months. This trial, similar to the SARAH and SORAMIC trial, consisted of patients with a higher tumor burden and often macrovascular invasion (31%, 43% and 63% in the SIRveNIB trial, SORAMIC trial and SARAH trial, respectively) (27, 57, 85). Median progression-free survival in the SIRveNIB trial (based on RECIST 1.1) was 6.3 months, with a similar progression-free survival for intrahepatic and extrahepatic tumor locations (26).

Based on these findings, response assessment in case of HCC should be performed using mRECIST (or the Choi criteria) at an interval of 3-6 months (**Table 5**). The choice of the imaging modality and interval (three vs. six months) will also depend on the tumor load and presence of macrovascular invasion (BCLC stage). A patient with a higher BCLC stage (based on tumor extension, not ECOG performance score) is more amendable to early intrahepatic progression and/or extrahepatic progression (98). The latter is not analyzed using MRI (99).

A word of caution, progression on all modalities and response criteria should be called with care, since regularly small lesions become visible on CT due to the decrease in density after treatment or even radiation-associated pseudo-lesions can appear. Small liver metastases are difficult to discern if the tumor density (measured in HU) is similar to the density of the normal parenchyma. For example, in patients with CRLM the normal parenchyma density will often be decreased after multiple lines of chemotherapy due to the development of steatosis (especially, after 5-fluorouracil/leucovorin and irinotecan) (100, 101). The density of the hypovascular CRLM will resemble the decreased density of the normal parenchyma, and small lesions can become inappreciable (**Figure 2**).

In response to radioembolization the density of the metastases will further decrease (a parameter used in the Choi criteria) (82, 84, 87). The metastases will become visible, yet should not be interpreted as new metastases. In case of doubt, re-evaluation of the lesions at the next follow-up will allow for a distinction between (durable) response of pre-existing metastases or progressive disease due to new metastases.

Conversely, pseudo-lesions can appear in case of a focal deposition of a large number of microspheres in the normal parenchyma. This will result in a focally high absorbed dose and necrosis of the normal parenchyma (**Figure 3**).

In summary, in the currently published literature RECIST 1.1 is still the preferred and most used method for response evaluation, though it was found to be inferior for all tumor types. Additional morphologic signs of response or preferably more suitable response criteria (such as the Choi criteria) need to be implemented to meaningfully assess response (correlated with progression-free and overall survival) in primary liver tumors and liver metastases.

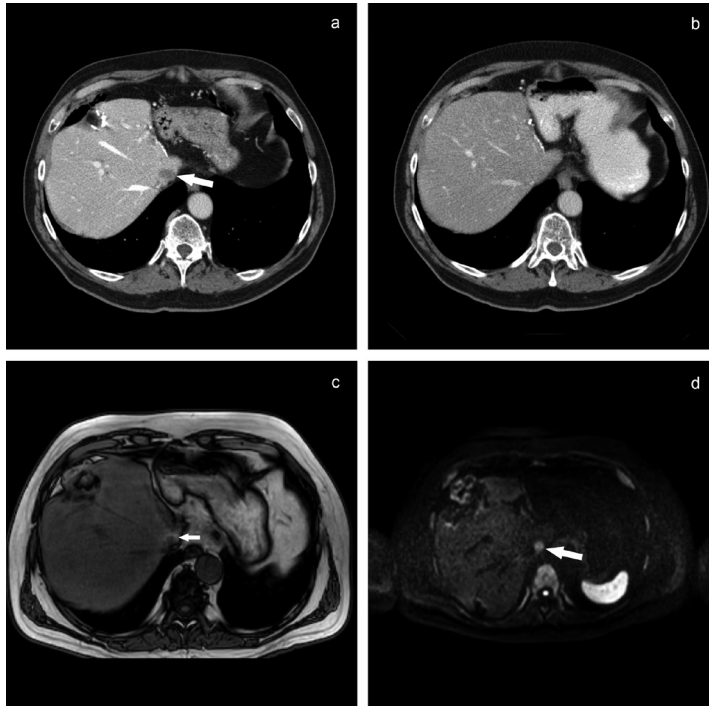


**Figure 2.** 56-years-old male with metachronous colorectal liver metastases. In the recent past a left hemihepatectomy and several metastasectomies (involving segment four, five and six/seven) were performed. During follow-up a new hypodense lesion appeared in the cranial part of the caudate lobe (arrow in a). Subsequently, treatment with a chemotherapeutic regimen of capecitabine, oxaliplatin and bevacizumab (=CAPOX-B) was initiated. After 2,5 months the CT (in portal venous phase) was repeated to evaluate the response (b). The initial report said that the lesion had fully regressed and no new metastases were present. Careful examination showed persistence of a faint lesion in the caudate lobe, similar in size to the CT of 2,5 months earlier. However, the normal liver parenchyma has decreased in density from ~130 HU to ~90 HU in the portal venous phase, consistent with (chemotherapy induced) steatosis. An MRI was performed to confirm the persistence of the liver metastasis; a T1 out-of-phase (c) and B1000 diffusion-weighted image (d) are displayed. The liver parenchyma has a low signal on the T1 out-of-phase with a rim of perilesional non-steatosis (arrow in c) and the persistence of the metastasis is confirmed on the B1000 (arrow in d), with high signal intensity in the lesion (i.e. restricted diffusion).

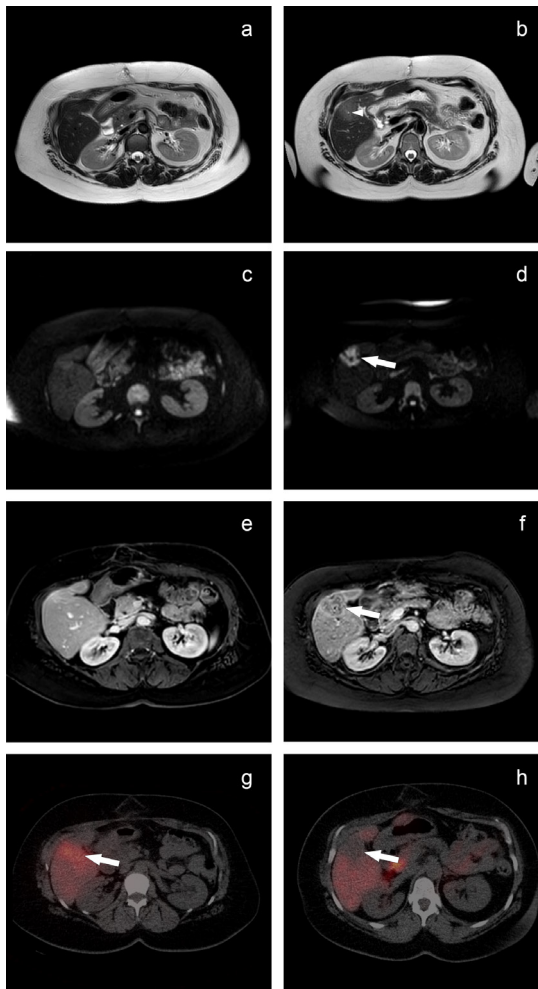


**Figure 3.** 46-years-old female with colorectal liver metastases, previously treated with multiple lines of chemotherapy and radiofrequency ablation of a metastasis in segment four and segment eight. During the last follow-up a recurrence was visible near the ablation zone in segment four and segment eight (images not displayed). Images of the MRI are displayed at another level (segment five and six); including a T2 weighted image (b), a diffusion weighted image (B1000) (d), and a post-contrast T1 with fat-saturation (portal venous phase) (f). Subsequently, a radiation lobectomy of segment 4-8 with  $^{166}\text{Ho}$  microspheres was planned to treat the recurrence in segment four and eight. Three months later a follow-up MRI was performed; including a T2 weighted image (b), a diffusion weighted image (B1000) (d), and a post-contrast T1 with fat-saturation (portal venous phase) (f) at the same level. In segment five a new lesion with restricted diffusion has appeared (arrow in d). The lesion was faintly T2-hyperintense with rim enhancement and a hypovascular aspect on the postcontrast T1 (arrow in f). However, centrally an intact bile duct is seen (arrowhead in b). On the post-treatment  $^{166}\text{Ho}$  SPECT/CT intense  $^{166}\text{Ho}$  accumulation was seen in segment five, corresponding to the location of the new lesion (arrow in g). The new lesion is consistent with focal normal parenchyma necrosis due to non-target  $^{166}\text{Ho}$  radioembolization. Six months later a  $^{99\text{m}}\text{Tc}$ -mebrofenin hepatobiliary scintigraphy was performed (prior to the intended extended right hemihepatectomy) (h), showing the decreased uptake of  $^{99\text{m}}\text{Tc}$ -mebrofenin at the location of the non-target radioembolization (arrow in h).

## Future directions

Only in recent decades developments led to a better understanding of radioembolization with regard to the dose-response relationships and the effect of the different characteristics of the available microspheres, resulting in improved treatment results and a decrease in toxicity (2). And though much advancements have been made, much is still to be improved.

An important improvement is the increasing use of personalized dosimetry, especially in larger injected volumes (2, 11). In personalized dosimetry, the prescribed absorbed dose to the tumor and the non-tumorous liver parenchyma is separately taken into account (using the multi-compartment method). The information gathered during the  $^{99m}\text{Tc}$ -MAA scintigraphy or  $^{166}\text{Ho}$  scout scintigraphy is used to calculate the tumor-to-non-tumor ratio, the lung shunt fraction and determine the volume of both non-tumorous liver and tumor (102, 103). In larger injected volumes, the development of relevant hepatotoxicity is more likely, considering that more of the non-tumorous liver parenchyma is subjected to the influx of the radio-active microspheres (resulting in a higher absorbed dose to the injected parenchyma). The extent to which the injected non-tumorous parenchyma will be subjected depends on the tumor-to-non-tumor ratio. In larger treatment volumes, the use of multicompartment modelling can result in an as high as possible absorbed dose to the tumor, while maintaining the absorbed dose to the non-tumorous liver parenchyma lower than the tolerable dose. The non-tumorous liver absorbed dose should be calculated for the entire liver and not only the treated part, as the whole non-tumorous volume determines the residual liver function after therapy. In small treated volumes (radiation segmentectomy and superselective treatments) the prescribed target volume dose is not limited in patients without an underlying liver disease or in patients with a compensated Child-Pugh A cirrhosis (11); the non-treated volume will counterbalance the functional loss in the treated volume, similar to the volumetric criteria in liver resections. Thus, personalized dosimetry also allows for a choice: one can calculate the prescribed activity based on 1) the estimated tumor absorbed dose or 2) the estimated non-tumorous liver absorbed dose. The first being useful in small injected volumes and livers without underlying liver disease, the second being useful in larger injected volumes and cirrhotic patients (20).

As discussed earlier, the commercially available microspheres have different properties. Also in personalized dosimetry, these differences have to be taken into account, especially the prescribed absorbed dose to the target volume (102).

In the study of Garin et al. the use of personalized dosimetry increased the objective response rate in HCC treatments in patients with cirrhosis (Child-Pugh A: 79-81%) (2). To ensure a safer treatment, only patients with a hepatic reserve (i.e. untreated liver fraction) of >30% were included. In the light of the discrepancy between liver volume and function, especially in underlying liver disease, this volume cut-off value seems inadequate (18, 63). A potentially more reliable method could be the use of hepatobiliary scintigraphy to evaluate the function of the non-treated lobe instead of the volume, similar to its use prior to surgical resection. However, as mentioned above, the added value of hepatobiliary scintigraphy to routine clinical and biochemical screening of patients prior to radioembolization still has to be proven. A promising method to improve patient selection could be to investigate whether tolerable non-tumorous liver absorbed doses can be identified for the different ALBI grades, given the strong predictive value of the ALBI score for hepatotoxicity in patients with cirrhosis (31, 32).

Another potential interesting strategy could be to boost the tumor-to-non-tumor ratio, by either increasing the lesion perfusion or decreasing the non-tumorous liver arterial perfusion (104). Increased lesion perfusion might be established by the use of low-intensity ultrasound in combination with microbubbles (105). Microbubbles, exposed to low-intensity ultrasound, oscillate causing shear stress on the vascular endothelium. In preclinical animal studies this resulted in an increase of small arteriole diameter and perfusion (105, 106). In contrast, decreased perfusion in ultrasound with microbubbles is also reported. Eisenberg et al. used ultrasound-triggered microbubble destruction (at a high mechanical index) to temporarily disrupt HCC vascularization in 28 patients undergoing sublobar <sup>90</sup>Y glass radioembolization; a technique known to improve radiosensitivity in mouse models (104). Their preliminary data showed that the addition of ultrasound-triggered microbubble destruction lead to more complete and partial responses (p=0.02).



Besides boosting the tumor-to-non-tumor ratio, ratio might be the inhibition of local vasodilator production in the liver, including nitric oxide and adenosine, or by blocking their vasodilative effect (64). This could decrease the non-tumorous liver arterial perfusion and improve tumor targeting. The hepatic microcirculation and its mediators are, however, much more complex (64, 67, 107). An early study by Sasaki et al. showed an increased tumor-to-non-tumor ratio after infusion of the vasoconstrictor angiotensin II in the hepatic artery with a peak at approximately 100 seconds (107). Thereafter the arterial blood flow to the non-tumorous liver parenchyma increased again and the tumor-to-non-tumor ratio gradually declined. Unfortunately, this time window is insufficient for injection of a whole target dose. The recovery of the arterial perfusion to the non-tumorous liver parenchyma is most likely due to the adenosine wash-out hypothesis. If the sinusoidal flow is reduced, adenosine accumulation occurs in the periportal space (space of Mall) and re-dilatation of the terminal artery occurs (i.e. mechanism of the arterial buffer response) (67, 108). Hence, sinusoidal flow must be maintained for a longer period of time, while the arterial flow is diminished, as to create sufficient time for microsphere injection during optimized tumor-to-non-tumor ratios. This could be realized by establishing a prolonged state of increased portal venous flow during radioembolization treatment. For example, by the use of the physiological post-prandial increase in portal venous flow or by use of a mesenteric-specific vasodilator, such as dopexamine (108). The portal venous flow increases by a factor 1.6 during meal digestion with a concurrent decrease in hepatic arterial flow, lasting approximately 30 minutes (from 15 to 45 minutes post-prandial) (108-110). This creates a sufficient time window, though implementation in daily practice might be challenging.

Lastly, the safety and efficacy of radioembolization and immunotherapy combination therapy should be further explored. Preclinical studies using mouse models have suggested potential synergistic effects for the combination of external beam radiotherapy and immunotherapy in various solid tumor types (111). Clinical studies using this combination therapy in humans are limited, and a lot is still unclear regarding the optimal timing and sequence of the combination therapy as well as the interfering role of the tumor environment (111). Few studies have explored the safety of radioembolization plus immunotherapy (112, 113). Zhan et al. retrospectively analyzed 26 patients with HCC

treated with radioembolization and nivolumab and/or ipilimumab at a maximum interval of 90 days (113). No additional toxicity related to radioembolization was observed. The efficacy still has to be investigated.

In conclusion, hepatotoxicity is an often encountered side-effect of radioembolization treatment, yet most often clinically acceptable. Standardization of the definition of REILD and/or radioembolization-related hepatotoxicity is necessary to adequately assess its incidence. The most important risk factor for hepatotoxicity is the absorbed dose to the whole non-tumorous liver volume.

The fast-developing improvements in the field of radioembolization, including personalized dosimetry and better patient selection, have led to improved patient outcomes and a better understanding of hepatotoxicity, with a decline of severe REILD as the intended result. Nevertheless, more focus should be given to dose-response relationships with regard to both tumor absorbed dose and non-tumorous liver absorbed dose.

## References

1. Reinders MTM, Mees E, Powerski MJ, Bruijnen RCG, van den Bosch MAAJ, Lam MGEH, et al. Radioembolisation in Europe: A Survey Amongst CIRSE Members. *Cardiovasc Intervent Radiol.* 2018;41(10):1579-89.
2. Garin E, Tselikas L, Guiu B, Chalaye J, Edeline J, de Baere T, et al. Personalised versus standard dosimetry approach of selective internal radiation therapy in patients with locally advanced hepatocellular carcinoma (DOSISPHERE-01): a randomised, multicentre, open-label phase 2 trial. *Lancet Gastroenterol Hepatol.* 2021;6(1):17-29.
3. Powerski MJ, Scheurig-Münkler C, Banzer J, Schnapauff D, Hamm B, Gebauer B. Clinical practice in radioembolization of hepatic malignancies: a survey among interventional centers in Europe. *Eur J Radiol.* 2012;81(7):e804-11.
4. Piana PM, Bar V, Doyle L, Anne R, Sato T, Eschelmann DJ, et al. Early arterial stasis during resin-based yttrium-90 radioembolization: incidence and preliminary outcomes. *HPB (Oxford).* 2014;16(4):336-41.
5. Walrand S, Hesse M, Jamar F, Lhommel R. A hepatic dose-toxicity model opening the way toward individualized radioembolization planning. *J Nucl Med.* 2014;55(8):1317-22.
6. Lee JS, Choi HJ, Kim BK, Park JY, Kim DY, Ahn SH, et al. The Modified Response Evaluation Criteria in Solid Tumors (RECIST) Yield a More Accurate Prognoses Than the RECIST 1.1 in Hepatocellular Carcinoma Treated with Transarterial Radioembolization. *Gut Liver.* 2020;14(6):765-74.
7. Bargellini I, Crocetti L, Turini FM, Lorenzoni G, Boni G, Traino AC, et al. Response Assessment by Volumetric Iodine Uptake Measurement: Preliminary Experience in Patients with Intermediate-Advanced Hepatocellular Carcinoma Treated with Yttrium-90 Radioembolization. *Cardiovasc Intervent Radiol.* 2018;41(9):1373-83.
8. Alsultan AA, van Roekel C, Barentsz MW, Smits MLJ, Kunnen B, Koopman M, et al. Dose-response and dose-toxicity relationships for yttrium-90 glass radioembolization in patients with colorectal cancer liver metastases. *J Nucl Med.* 2021.
9. van den Hoven AF, Rosenbaum CE, Elias SG, de Jong HW, Koopman M, Verkooijen HM, et al. Insights into the Dose-Response Relationship of Radioembolization with Resin 90Y-Microspheres: A Prospective Cohort Study in Patients with Colorectal Cancer Liver Metastases. *J Nucl Med.* 2016;57(7):1014-9.
10. van Roekel C, Bastiaannet R, Smits MLJ, Bruijnen RC, Braat AJAT, de Jong HWAM, et al. Dose-effect relationships of holmium-166 radioembolization in colorectal cancer. *J Nucl Med.* 2020.
11. Chiesa C, Mira M, Bhoori S, Bormolini G, Maccauro M, Spreafico C, et al. Radioembolization of hepatocarcinoma with. *Eur J Nucl Med Mol Imaging.* 2020;47(13):3018-32.
12. Levillain H, Bagni O, Deroose CM, Dieudonné A, Gnesin S, Grosser OS, et al. International recommendations for personalised selective internal radiation therapy of primary and metastatic liver diseases with yttrium-90 resin microspheres. *Eur J Nucl Med Mol Imaging.* 2021;48(5):1570-84.
13. Weber M, Lam M, Chiesa C, Konijnenberg M, Cremonesi M, Flamen P, et al. EANM procedure guideline for the treatment of liver cancer and liver metastases with intra-arterial radioactive compounds. *Eur J Nucl Med Mol Imaging.* 2022;49(5):1682-99.
14. Bilbao JI, de Martino A, de Luis E, Diaz-Dorransoro L, Alonso-Burgos A, Martinez de la Cuesta A, et al. Biocompatibility, inflammatory response, and recanalization characteristics of nonradioactive resin microspheres: histological findings. *Cardiovasc Intervent Radiol.* 2009;32(4):727-36.

15. Pasciak AS, Abiola G, Liddell RP, Crookston N, Besharati S, Donahue D, et al. The number of microspheres in Y90 radioembolization directly affects normal tissue radiation exposure. *Eur J Nucl Med Mol Imaging*. 2020;47(4):816-27.
16. Pasciak AS, Bourgeois AC, Bradley YC. A Microdosimetric Analysis of Absorbed Dose to Tumor as a Function of Number of Microspheres per Unit Volume in 90Y Radioembolization. *J Nucl Med*. 2016;57(7):1020-6.
17. Sato K, Lewandowski RJ, Bui JT, Omary R, Hunter RD, Kulik L, et al. Treatment of unresectable primary and metastatic liver cancer with yttrium-90 microspheres (TheraSphere): assessment of hepatic arterial embolization. *Cardiovasc Intervent Radiol*. 2006;29(4):522-9.
18. de Graaf W, van Lienden KP, Dinant S, Roelofs JJ, Busch OR, Gouma DJ, et al. Assessment of future remnant liver function using hepatobiliary scintigraphy in patients undergoing major liver resection. *J Gastrointest Surg*. 2010;14(2):369-78.
19. Dinant S, de Graaf W, Verwer BJ, Bennink RJ, van Lienden KP, Gouma DJ, et al. Risk assessment of posthepatectomy liver failure using hepatobiliary scintigraphy and CT volumetry. *J Nucl Med*. 2007;48(5):685-92.
20. Chiesa C, Mira M, Maccauro M, Romito R, Spreafico C, Sposito C, et al. A dosimetric treatment planning strategy in radioembolization of hepatocarcinoma with 90Y glass microspheres. *Q J Nucl Med Mol Imaging*. 2012;56(6):503-8.
21. Sangro B, Gil-Alzugaray B, Rodriguez J, Sola I, Martinez-Cuesta A, Viudez A, et al. Liver disease induced by radioembolization of liver tumors: description and possible risk factors. *Cancer*. 2008;112(7):1538-46.
22. Kennedy AS, Nutting C, Coldwell D, Gaiser J, Drachenberg C. Pathologic response and microdosimetry of (90)Y microspheres in man: review of four explanted whole livers. *Int J Radiat Oncol Biol Phys*. 2004;60(5):1552-63.
23. Piana PM, Gonsalves CF, Sato T, Anne PR, McCann JW, Bar Ad V, et al. Toxicities after radioembolization with yttrium-90 SIR-spheres: incidence and contributing risk factors at a single center. *J Vasc Interv Radiol*. 2011;22(10):1373-9.
24. Kennedy AS, McNeillie P, Dezarn WA, Nutting C, Sangro B, Wertman D, et al. Treatment parameters and outcome in 680 treatments of internal radiation with resin 90Y-microspheres for unresectable hepatic tumors. *Int J Radiat Oncol Biol Phys*. 2009;74(5):1494-500.
25. Rahbari NN, Garden OJ, Padbury R, Brooke-Smith M, Crawford M, Adam R, et al. Posthepatectomy liver failure: a definition and grading by the International Study Group of Liver Surgery (ISGLS). *Surgery*. 2011;149(5):713-24.
26. Chow PKH, Gandhi M, Tan SB, Khin MW, Khasbazar A, Ong J, et al. SIRveNIB: Selective Internal Radiation Therapy Versus Sorafenib in Asia-Pacific Patients With Hepatocellular Carcinoma. *J Clin Oncol*. 2018;36(19):1913-21.
27. Vilgrain V, Pereira H, Assenat E, Guiu B, Ilonca AD, Pageaux GP, et al. Efficacy and safety of selective internal radiotherapy with yttrium-90 resin microspheres compared with sorafenib in locally advanced and inoperable hepatocellular carcinoma (SARAH): an open-label randomised controlled phase 3 trial. *Lancet Oncol*. 2017;18(12):1624-36.
28. Wasan HS, Gibbs P, Sharma NK, Taieb J, Heinemann V, Ricke J, et al. First-line selective internal radiotherapy plus chemotherapy versus chemotherapy alone in patients with liver metastases from colorectal cancer (FOXFIRE, SIRFLOX, and FOXFIRE-Global): a combined analysis of three multicentre, randomised, phase 3 trials. *Lancet Oncol*. 2017;18(9):1159-71.

29. Mulcahy MF, Mahvash A, Pracht M, Montazeri AH, Bandula S, Martin RCG, et al. Radioembolization With Chemotherapy for Colorectal Liver Metastases: A Randomized, Open-Label, International, Multicenter, Phase III Trial. *J Clin Oncol*. 2021;39(35):3897-907.
30. Fajardo LF. The pathology of ionizing radiation as defined by morphologic patterns. *Acta Oncol*. 2005;44(1):13-22.
31. Lescure C, Estrade F, Pedrono M, Campillo-Gimenez B, Le Sourd S, Pracht M, et al. ALBI Score Is a Strong Predictor of Toxicity Following SIRT for Hepatocellular Carcinoma. *Cancers (Basel)*. 2021;13(15).
32. van Doorn DJ, Hendriks P, Burgmans MC, Rietbergen DDD, Coenraad MJ, van Delden OM, et al. Liver Decompensation as Late Complication in HCC Patients with Long-Term Response following Selective Internal Radiation Therapy. *Cancers (Basel)*. 2021;13(21).
33. Dignan FL, Wynn RF, Hadzic N, Karani J, Quaglia A, Pagliuca A, et al. BCSH/BSBMT guideline: diagnosis and management of veno-occlusive disease (sinusoidal obstruction syndrome) following haematopoietic stem cell transplantation. *Br J Haematol*. 2013;163(4):444-57.
34. Tomozawa Y, Jahangiri Y, Pathak P, Kolbeck KJ, Schenning RC, Kaufman JA, et al. Long-Term Toxicity after Transarterial Radioembolization with Yttrium-90 Using Resin Microspheres for Neuroendocrine Tumor Liver Metastases. *J Vasc Interv Radiol*. 2018;29(6):858-65.
35. Wong TY, Zhang KS, Gandhi RT, Collins ZS, O'Hara R, Wang EA, et al. Long-term outcomes following 90Y Radioembolization of neuroendocrine liver metastases: evaluation of the radiation-emitting SIR-spheres in non-resectable liver tumor (RESiN) registry. *BMC Cancer*. 2022;22(1):224.
36. Orman ES, Roberts A, Ghabril M, Nephew L, Desai AP, Patidar K, et al. Trends in Characteristics, Mortality, and Other Outcomes of Patients With Newly Diagnosed Cirrhosis. *JAMA Netw Open*. 2019;2(6):e196412.
37. D'Amico G, Morabito A, D'Amico M, Pasta L, Malizia G, Rebora P, et al. Clinical states of cirrhosis and competing risks. *J Hepatol*. 2018;68(3):563-76.
38. Ginés P, Quintero E, Arroyo V, Terés J, Bruguera M, Rimola A, et al. Compensated cirrhosis: natural history and prognostic factors. *Hepatology*. 1987;7(1):122-8.
39. Botta F, Giannini E, Romagnoli P, Fasoli A, Malfatti F, Chiarbonello B, et al. MELD scoring system is useful for predicting prognosis in patients with liver cirrhosis and is correlated with residual liver function: a European study. *Gut*. 2003;52(1):134-9.
40. Johnson PJ, Berhane S, Kagebayashi C, Satomura S, Teng M, Reeves HL, et al. Assessment of liver function in patients with hepatocellular carcinoma: a new evidence-based approach-the ALBI grade. *J Clin Oncol*. 2015;33(6):550-8.
41. Hermann AL, Dieudonné A, Ronot M, Sanchez M, Pereira H, Chatellier G, et al. Relationship of Tumor Radiation-absorbed Dose to Survival and Response in Hepatocellular Carcinoma Treated with Transarterial Radioembolization with. *Radiology*. 2020;296(3):673-84.
42. Jakobs TF, Saleem S, Atassi B, Reda E, Lewandowski RJ, Yaghmai V, et al. Fibrosis, portal hypertension, and hepatic volume changes induced by intra-arterial radiotherapy with 90yttrium microspheres. *Dig Dis Sci*. 2008;53(9):2556-63.
43. Fernandez-Ros N, Inarrairaegui M, Paramo JA, Berasain C, Avila MA, Chopitea A, et al. Radioembolization of hepatocellular carcinoma activates liver regeneration, induces inflammation and endothelial stress and activates coagulation. *Liver Int*. 2015;35(5):1590-6.
44. Seidensticker M, Fabritius MP, Beller J, Seidensticker R, Todica A, Ilhan H, et al. Impact of Pharmaceutical Prophylaxis on Radiation-Induced Liver Disease Following Radioembolization. *Cancers (Basel)*. 2021;13(9).

45. Fan CQ, Crawford JM. Sinusoidal obstruction syndrome (hepatic veno-occlusive disease). *J Clin Exp Hepatol*. 2014;4(4):332-46.
46. Emmons EC, Bishay S, Du L, Krebs H, Gandhi RT, Collins ZS, et al. Survival and Toxicities after. *Radiology*. 2022;305(1):228-36.
47. Braat A, Ahmadzadehfar H, Kappadath SC, Stothers CL, Frilling A, Deroose CM, et al. Radioembolization with (90)Y Resin Microspheres of Neuroendocrine Liver Metastases After Initial Peptide Receptor Radionuclide Therapy. *Cardiovasc Intervent Radiol*. 2020;43(2):246-53.
48. Gil-Alzugaray B, Chopitea A, Inarrairaegui M, Bilbao JI, Rodriguez-Fraile M, Rodriguez J, et al. Prognostic factors and prevention of radioembolization-induced liver disease. *Hepatology*. 2013;57(3):1078-87.
49. van Meer S, van Erpecum KJ, Sprengers D, Coenraad MJ, Klumpen HJ, Jansen PL, et al. Hepatocellular carcinoma in cirrhotic versus noncirrhotic livers: results from a large cohort in the Netherlands. *Eur J Gastroenterol Hepatol*. 2016;28(3):352-9.
50. easloffice@easloffice.eu EAftSotLEa, Liver EAftSot. EASL Clinical Practice Guidelines: Management of hepatocellular carcinoma. *J Hepatol*. 2018;69(1):182-236.
51. Ricke J, Schinner R, Seidensticker M, Gasbarrini A, van Delden OM, Amthauer H, et al. Liver function after combined selective internal radiation therapy or sorafenib monotherapy in advanced hepatocellular carcinoma. *J Hepatol*. 2021;75(6):1387-96.
52. Finn RS, Qin S, Ikeda M, Galle PR, Ducreux M, Kim TY, et al. Atezolizumab plus Bevacizumab in Unresectable Hepatocellular Carcinoma. *N Engl J Med*. 2020;382(20):1894-905.
53. Cheng AL, Qin S, Ikeda M, Galle PR, Ducreux M, Kim TY, et al. Updated efficacy and safety data from IMbrave150: Atezolizumab plus bevacizumab vs. sorafenib for unresectable hepatocellular carcinoma. *J Hepatol*. 2022;76(4):862-73.
54. Chiesa C, Mira M, Maccauro M, Spreafico C, Romito R, Morosi C, et al. Radioembolization of hepatocarcinoma with (90)Y glass microspheres: development of an individualized treatment planning strategy based on dosimetry and radiobiology. *Eur J Nucl Med Mol Imaging*. 2015;42(11):1718-38.
55. Venerito M, Pech M, Canbay A, Donghia R, Guerra V, Chatellier G, et al. NEMESIS: Noninferiority, Individual-Patient Metaanalysis of Selective Internal Radiation Therapy with. *J Nucl Med*. 2020;61(12):1736-42.
56. Garin E, Lenoir L, Edeline J, Laffont S, Mesbah H, Porée P, et al. Boosted selective internal radiation therapy with 90Y-loaded glass microspheres (B-SIRT) for hepatocellular carcinoma patients: a new personalized promising concept. *Eur J Nucl Med Mol Imaging*. 2013;40(7):1057-68.
57. Ricke J, Klumpen HJ, Amthauer H, Bargellini I, Bartenstein P, de Toni EN, et al. Impact of combined selective internal radiation therapy and sorafenib on survival in advanced hepatocellular carcinoma. *J Hepatol*. 2019;71(6):1164-74.
58. Jeyarajah DR, Doyle MBM, Espot NJ, Hansen PD, Iannitti DA, Kim J, et al. Role of yttrium-90 selective internal radiation therapy in the treatment of liver-dominant metastatic colorectal cancer: an evidence-based expert consensus algorithm. *J Gastrointest Oncol*. 2020;11(2):443-60.
59. Garlipp B, Gibbs P, Van Hazel GA, Jeyarajah R, Martin RCG, Bruns CJ, et al. Secondary technical resectability of colorectal cancer liver metastases after chemotherapy with or without selective internal radiotherapy in the randomized SIRFLOX trial. *Br J Surg*. 2019;106(13):1837-46.

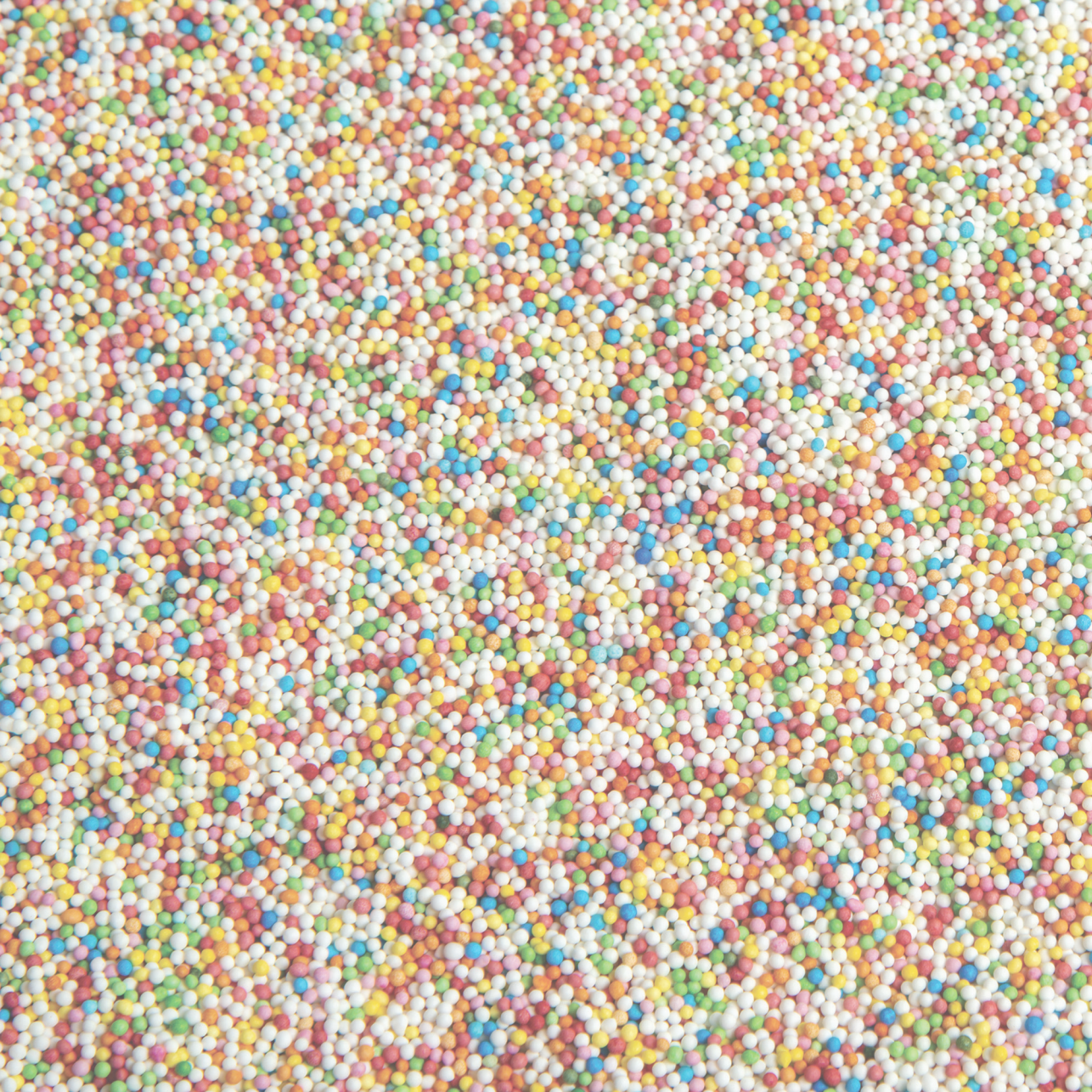
60. Seidensticker R, Seidensticker M, Damm R, Mohnike K, Schutte K, Malfertheiner P, et al. Hepatic toxicity after radioembolization of the liver using (90)Y-microspheres: sequential lobar versus whole liver approach. *Cardiovasc Intervent Radiol.* 2012;35(5):1109-18.
61. Coskun N, Yildirim A, Yuksel AO, Canyigit M, Ozdemir E. The Radiation Dose Absorbed by Healthy Parenchyma Is a Predictor for the Rate of Contralateral Hypertrophy After Unilobar Radioembolization of the Right Liver. *Nucl Med Mol Imaging.* 2022;56(6):291-8.
62. Labeur TA, Cieslak KP, Van Gulik TM, Takkenberg RB, van der Velden S, Lam MGEH, et al. The utility of 99mTc-mebrofenin hepatobiliary scintigraphy with SPECT/CT for selective internal radiation therapy in hepatocellular carcinoma. *Nucl Med Commun.* 2020;41(8):740-9.
63. Allimant C, Deshayes E, Kafrouni M, Santoro L, de Verbizier D, Fourcade M, et al. Hepatobiliary Scintigraphy and Glass. *Diagnostics (Basel).* 2021;11(6).
64. Zipprich A. Hemodynamics in the isolated cirrhotic liver. *J Clin Gastroenterol.* 2007;41 Suppl 3:S254-8.
65. Lake-Bakaar G, Ahmed M, Evenson A, Bonder A, Faintuch S, Sundaram V. Management of Hepatocellular Carcinoma in Cirrhotic Patients with Portal Hypertension: Relevance of Hagen-Poiseuille's Law. *Liver Cancer.* 2014;3(3-4):428-38.
66. Boktor RR, Walker G, Stacey R, Gledhill S, Pitman AG. Reference range for inpatient variability in blood-pool and liver SUV for 18F-FDG PET. *J Nucl Med.* 2013;54(5):677-82.
67. Vollmar B, Menger MD. The hepatic microcirculation: mechanistic contributions and therapeutic targets in liver injury and repair. *Physiol Rev.* 2009;89(4):1269-339.
68. Lam MG, Banerjee A, Louie JD, Sze DY. Splenomegaly-associated thrombocytopenia after hepatic yttrium-90 radioembolization. *Cardiovasc Intervent Radiol.* 2014;37(4):1009-17.
69. Fernández-Ros N, Silva N, Bilbao JI, Iñarrairaegui M, Benito A, D'Avola D, et al. Partial liver volume radioembolization induces hypertrophy in the spared hemiliver and no major signs of portal hypertension. *HPB (Oxford).* 2014;16(3):243-9.
70. Møller S, la Cour Sibbesen E, Madsen JL, Bendtsen F. Indocyanine green retention test in cirrhosis and portal hypertension: Accuracy and relation to severity of disease. *J Gastroenterol Hepatol.* 2019;34(6):1093-9.
71. Krishnamurthy GT, Krishnamurthy S. Cholescintigraphic measurement of liver function: how is it different from other methods? *Eur J Nucl Med Mol Imaging.* 2006;33(10):1103-6.
72. Hoekstra LT, de Graaf W, Nibourg GA, Heger M, Bennink RJ, Stieger B, et al. Physiological and biochemical basis of clinical liver function tests: a review. *Ann Surg.* 2013;257(1):27-36.
73. Smits ML, van den Hoven AF, Rosenbaum CE, Zonnenberg BA, Lam MG, Nijsen JF, et al. Clinical and laboratory toxicity after intra-arterial radioembolization with (90)Y-microspheres for unresectable liver metastases. *PLoS One.* 8. United States 2013. p. e69448.
74. Rassam F, Uz Z, van Lienden KP, Ince C, Bennink RJ, van Gulik TM. Quantitative assessment of liver function using hepatobiliary scintigraphy: the effect of microcirculatory alterations after portal vein embolization. *Nucl Med Commun.* 2019;40(7):720-6.
75. Garlipp B, de Baere T, Damm R, Irsmscher R, van Buskirk M, Stubs P, et al. Left-liver hypertrophy after therapeutic right-liver radioembolization is substantial but less than after portal vein embolization. *Hepatology.* 2014;59(5):1864-73.

76. Bennink RJ, Dinant S, Erdogan D, Heijnen BH, Straatsburg IH, van Vliet AK, et al. Preoperative assessment of postoperative remnant liver function using hepatobiliary scintigraphy. *J Nucl Med.* 2004;45(6):965-71.
77. de Graaf W, van Lienden KP, van den Esschert JW, Bennink RJ, van Gulik TM. Increase in future remnant liver function after preoperative portal vein embolization. *Br J Surg.* 2011;98(6):825-34.
78. Rassam F, Olthof PB, van Lienden KP, Bennink RJ, Erdmann JI, Swijnenburg RJ, et al. Comparison of functional and volumetric increase of the future remnant liver and postoperative outcomes after portal vein embolization and complete or partial associating liver partition and portal vein ligation for staged hepatectomy (ALPPS). *Ann Transl Med.* 2020;8(7):436.
79. Theysohn JM, Ertle J, Muller S, Schlaak JF, Nensa F, Sipilae S, et al. Hepatic volume changes after lobar selective internal radiation therapy (SIRT) of hepatocellular carcinoma. *Clin Radiol.* 2014;69(2):172-8.
80. de Graaf W, van Lienden KP, van Gulik TM, Bennink RJ. (99m)Tc-mebrofenin hepatobiliary scintigraphy with SPECT for the assessment of hepatic function and liver functional volume before partial hepatectomy. *J Nucl Med.* 2010;51(2):229-36.
81. Fendler WP, Philippe Tiega DB, Ilhan H, Paprottka PM, Heinemann V, Jakobs TF, et al. Validation of several SUV-based parameters derived from 18F-FDG PET for prediction of survival after SIRT of hepatic metastases from colorectal cancer. *J Nucl Med.* 2013;54(8):1202-8.
82. Shady W, Sotirchos VS, Do RK, Pandit-Taskar N, Carrasquillo JA, Gonen M, et al. Surrogate Imaging Biomarkers of Response of Colorectal Liver Metastases After Salvage Radioembolization Using 90Y-Loaded Resin Microspheres. *AJR Am J Roentgenol.* 2016;207(3):661-70.
83. Zerizer I, Al-Nahhas A, Towey D, Tait P, Ariff B, Wasan H, et al. The role of early <sup>18</sup>F-FDG PET/CT in prediction of progression-free survival after <sup>90</sup>Y radioembolization: comparison with RECIST and tumour density criteria. *Eur J Nucl Med Mol Imaging.* 2012;39(9):1391-9.
84. Beuzit L, Edeline J, Brun V, Ronot M, Guillygomarc'h A, Boudjema K, et al. Comparison of Choi criteria and Response Evaluation Criteria in Solid Tumors (RECIST) for intrahepatic cholangiocarcinoma treated with glass-microspheres Yttrium-90 selective internal radiation therapy (SIRT). *Eur J Radiol.* 2016;85(8):1445-52.
85. Salem R, Johnson GE, Kim E, Riaz A, Bishay V, Boucher E, et al. Yttrium-90 Radioembolization for the Treatment of Solitary, Unresectable HCC: The LEGACY Study. *Hepatology.* 2021;74(5):2342-52.
86. Braat AJAT, Kappadath SC, Ahmadzadehfar H, Stothers CL, Frilling A, Deroose CM, et al. Radioembolization with Cardiovasc Intervent Radiol. 2019;42(3):413-25.
87. Weng Z, Ertle J, Zheng S, Lauenstein T, Mueller S, Bockisch A, et al. Choi criteria are superior in evaluating tumor response in patients treated with transarterial radioembolization for hepatocellular carcinoma. *Oncol Lett.* 2013;6(6):1707-12.
88. Morsbach F, Sah BR, Spring L, Puipe G, Gordic S, Seifert B, et al. Perfusion CT best predicts outcome after radioembolization of liver metastases: a comparison of radionuclide and CT imaging techniques. *Eur Radiol.* 2014;24(7):1455-65.
89. Choi H, Charnsangavej C, Faria SC, Macapinlac HA, Burgess MA, Patel SR, et al. Correlation of computed tomography and positron emission tomography in patients with metastatic gastrointestinal stromal tumor treated at a single institution with imatinib mesylate: proposal of new computed tomography response criteria. *J Clin Oncol.* 2007;25(13):1753-9.



90. Schmeel FC, Simon B, Sabet A, Luetkens JA, Träber F, Schmeel LC, et al. Diffusion-weighted magnetic resonance imaging predicts survival in patients with liver-predominant metastatic colorectal cancer shortly after selective internal radiation therapy. *Eur Radiol.* 2017;27(3):966-75.
91. Bult W, Vente MA, Zonnenberg BA, Van Het Schip AD, Nijsen JF. Microsphere radioembolization of liver malignancies: current developments. *Q J Nucl Med Mol Imaging.* 2009;53(3):325-35.
92. van de Maat GH, Seevinck PR, Elschot M, Smits ML, de Leeuw H, van Het Schip AD, et al. MRI-based biodistribution assessment of holmium-166 poly(L-lactic acid) microspheres after radioembolisation. *Eur Radiol.* 2013;23(3):827-35.
93. Jongen MJM, Rosenbaum CENM, Braat MNGJ, van den Bosch MAAJ, Sze DY, Kranenburg O, et al. Anatomic versus Metabolic Tumor Response Assessment after Radioembolization Treatment. *J Vasc Interv Radiol.* 2018;29(2):244-53.e2.
94. Deipolyi AR, England RW, Ridouani F, Riedl CC, Kunin HS, Boas FE, et al. PET/CT Imaging Characteristics After Radioembolization of Hepatic Metastasis from Breast Cancer. *Cardiovasc Intervent Radiol.* 2020;43(3):488-94.
95. Memon K, Lewandowski RJ, Mulcahy MF, Riaz A, Ryu RK, Sato KT, et al. Radioembolization for neuroendocrine liver metastases: safety, imaging, and long-term outcomes. *Int J Radiat Oncol Biol Phys.* 2012;83(3):887-94.
96. Braat AJAT, Buijnen RCG, van Rooij R, Braat MNGJ, Wessels FJ, van Leeuwaarde RS, et al. Additional holmium-166 radioembolisation after lutetium-177-dotatate in patients with neuroendocrine tumour liver metastases (HEPAR PLuS): a single-centre, single-arm, open-label, phase 2 study. *Lancet Oncol.* 2020;21(4):561-70.
97. Maas M, Beets-Tan R, Gaubert JY, Gomez Munoz F, Habert P, Klompenhouwer LG, et al. Follow-up after radiological intervention in oncology: ECIO-ESOI evidence and consensus-based recommendations for clinical practice. *Insights Imaging.* 2020;11(1):83.
98. Yeom A, Chi SA, Song KD. Added Value of Pelvic CT after Treatment of HCC. *Radiology.* 2023;307(3):e222314.
99. Moctezuma-Velazquez C, Montano-Loza AJ, Meza-Junco J, Burak K, Ma M, Bain VG, et al. Selective Internal Radiation Therapy for Hepatocellular Carcinoma Across the Barcelona Clinic Liver Cancer Stages. *Dig Dis Sci.* 2021;66(3):899-911.
100. Bethke A, Kühne K, Platzek I, Stroszczyński C. Neoadjuvant treatment of colorectal liver metastases is associated with altered contrast enhancement on computed tomography. *Cancer Imaging.* 2011;11(1):91-9.
101. Miyake K, Hayakawa K, Nishino M, Morimoto T, Mukaihara S. Effects of oral 5-fluorouracil drugs on hepatic fat content in patients with colon cancer. *Acad Radiol.* 2005;12(6):722-7.
102. Bastiaannet R, Kappadath SC, Kunnen B, Braat AJAT, Lam MGEH, de Jong HWAM. The physics of radioembolization. *EJNMMI Phys.* 2018;5(1):22.
103. Braat AJ, Smits ML, Braat MN, van den Hoven AF, Prince JF, de Jong HW, et al. Yttrium-90 hepatic radioembolization: an update on current practice and recent developments. *J Nucl Med.* 2015.
104. Eisenbrey JR, Forsberg F, Wessner CE, Delaney LJ, Bradigan K, Gummedi S, et al. US-triggered Microbubble Destruction for Augmenting Hepatocellular Carcinoma Response to Transarterial Radioembolization: A Randomized Pilot Clinical Trial. *Radiology.* 2021;298(2):450-7.
105. de Maar JS, Zandvliet MMJM, Veraa S, Tobón Restrepo M, Moonen CTW, Deckers R. Ultrasound and Microbubbles Mediated Bleomycin Delivery in Feline Oral Squamous Cell Carcinoma-An In Vivo Veterinary Study. *Pharmaceutics.* 2023;15(4).

106. Bertuglia S. Increase in capillary perfusion following low-intensity ultrasound and microbubbles during postischemic reperfusion. *Crit Care Med.* 2005;33(9):2061-7.
107. Sasaki Y, Imaoka S, Hasegawa Y, Nakano S, Ishikawa O, Ohigashi H, et al. Changes in distribution of hepatic blood flow induced by intra-arterial infusion of angiotensin II in human hepatic cancer. *Cancer.* 1985;55(2):311-6.
108. Walrand S, Hesse M, d'Abadie P, Jamar F. Hepatic Arterial Buffer Response in Liver Radioembolization and Potential Use for Improved Cancer Therapy. *Cancers (Basel).* 2021;13(7).
109. Dauzat M, Lafortune M, Patriquin H, Pomier-Layrargues G. Meal induced changes in hepatic and splanchnic circulation: a noninvasive Doppler study in normal humans. *Eur J Appl Physiol Occup Physiol.* 1994;68(5):373-80.
110. Fisher AJ, Paulson EK, Kliewer MA, DeLong DM, Nelson RC. Doppler sonography of the portal vein and hepatic artery: measurement of a prandial effect in healthy subjects. *Radiology.* 1998;207(3):711-5.
111. Ngwa W, Irabor OC, Schoenfeld JD, Hesser J, Demaria S, Formenti SC. Using immunotherapy to boost the abscopal effect. *Nat Rev Cancer.* 2018;18(5):313-22.
112. Ruohoniemi DM, Zhan C, Wei J, Kulkarni K, Aaltonen ET, Horn JC, et al. Safety and Effectiveness of Yttrium-90 Radioembolization around the Time of Immune Checkpoint Inhibitors for Unresectable Hepatic Metastases. *J Vasc Interv Radiol.* 2020;31(8):1233-41.
113. Zhan C, Ruohoniemi D, Shanbhogue KP, Wei J, Welling TH, Gu P, et al. Safety of Combined Yttrium-90 Radioembolization and Immune Checkpoint Inhibitor Immunotherapy for Hepatocellular Carcinoma. *J Vasc Interv Radiol.* 2020;31(1):25-34.





CHAPTER  
TWELVE

Summary

In the last decades radioembolization has evolved to an established treatment for both primary liver tumors and liver metastases. Currently, colorectal liver metastases and hepatocellular carcinoma are the only reimbursed treatment indications in the Netherlands. Undoubtedly other indications will follow, such as cholangiocarcinoma and neuroendocrine liver metastases, given the promising treatment results in several studies.

Though radioembolization is still mainly performed in the palliative setting, treatments with curative intent (e.g., downstaging to surgery or liver transplantation) are increasingly being performed. As overall survival of patients after radioembolization improves, due to a different treatment intent and/or improved treatment results, more emphasis should be put on clinically relevant treatment-related toxicity and ways to prevent it.

This thesis focused on radioembolization-induced clinical and biochemical hepatotoxicity and potential imaging-based methods for improved patient selection.

### **Clinical perspectives on radioembolization**

In **Chapter 2** the existing literature on radioembolization-induced liver disease (REILD) is systematically reviewed (search date: 10/29/2015). The definitions, reporting and incidence of REILD vary greatly, but lethal REILD is rare (0-5%). However, liver biochemistry test abnormalities occur in up to 100% of patients. In an effort to improve consistent reporting of REILD an updated definition and five-point scoring system of REILD is proposed.

In **Chapter 3** the toxicity profile of radioembolization treatments with  $^{90}\text{Y}$  glass microspheres and  $^{90}\text{Y}$  resin microspheres and their potential differences are investigated. The three-month follow-up of 85 patients is retrospectively analyzed. The clinical, hematological and biochemical toxicity of both  $^{90}\text{Y}$  microspheres is comparable, apart from the post-embolization syndrome related complaints on day one, which are more common in  $^{90}\text{Y}$  resin treatments. A relationship is observed between the non-tumorous liver absorbed dose and REILD grade  $\geq 3$  (i.e. REILD necessitating medical intervention) for resin treatments ( $p=0.050$ ). A similar trend is also seen for glass treatments ( $p=0.144$ ).

Many physicians prescribe periprocedural prophylactic medication to minimize treatment-related toxicity. Yet, no international guidelines exist for its use. Prednisolone and

ursodeoxycholic acid are commonly used to minimize hepatotoxicity. In **Chapter 4** the prophylactic use of prednisolone and ursodeoxycholic acid is studied. Treatment-related toxicity is evaluated in 70 patients (51 with prophylaxis and 19 without). Clinical toxicity, biochemical toxicity and hepatotoxicity were not correlated with the use of prophylactic medication. Only the non-tumorous liver absorbed dose was significantly associated with biochemical toxicity.

### **Nuclear medicine perspectives on radioembolization**

Hepatobiliary scintigraphy using  $^{99m}\text{Tc}$ -mebrofenin is increasingly used to quantify total and regional liver function, specifically prior to major liver resections. Conversely, in radioembolization treatments patient selection is based on clinical, biochemical, hematological and imaging parameters. Liver function is estimated using biochemical markers and clinically derived scores (e.g. Child-Pugh score), together with the volumetric assessment of the liver. In **Chapter 5** and **6** the use of hepatobiliary scintigraphy in patient selection is evaluated.

In **Chapter 5** a case-series of three patients with a hepatocellular carcinoma and underlying cirrhosis is described. All three patients show a considerable decline of the total and regional liver function after lobar treatment (as measured on hepatobiliary scintigraphy). Two patients develop REILD, despite their acceptable clinical and biochemical status prior to treatment.

**Chapter 6** reports the results of 13 patients, who underwent a hepatobiliary scintigraphy prior to and after  $^{90}\text{Y}$  glass right lobar radioembolization. Liver function and volume declined in the treated lobes, while both increased in the contralateral lobe after treatment. However, the limits of agreement between function and volume changes are wide, showing large individual differences. Therefore, hepatobiliary scintigraphy can be a useful adjunct to volumetry in patient work-up.

In **Chapter 7** the effect of  $^{90}\text{Y}$  resin radioembolization treatment on the  $^{18}\text{F}$ -fluorodeoxyglucose ( $^{18}\text{FDG}$ ) activity concentration of the non-tumorous liver parenchyma is analyzed.  $^{18}\text{FDG}$  positron emission tomography/computed tomography (PET/CT) is regularly performed

for response evaluation after radioembolization, especially in colorectal liver metastases. For response assessment, it is paramount to have a constant reference for  $^{18}\text{F}$ FDG activity concentration. The  $^{18}\text{F}$ FDG activity concentration of the non-tumorous liver parenchyma changes mildly, yet significantly after radioembolization, whereas the blood pool  $^{18}\text{F}$ FDG activity concentration remains stable. Knowledge of this mild change can help avoid occasional misinterpretation of therapy-response.

### **Radiological perspectives on radioembolization**

**Chapter 8** focuses on the special anatomy of the caudate lobe and its role in radioembolization treatments. Though only 39% of patients has caudate lobe tumor involvement, 80% of patients shows activity in the caudate lobe post-treatment. Untreated lobes show a significant volume increase (median 33%). Caudate lobe arteries are seldomly visualized on pre-treatment computed tomography (CT) (12-17%), however significantly more are visualized in caudate lobes with tumor involvement. Intentional treatment or bypassing of the caudate lobe is advisable to improve tumor coverage or enhance the functional liver remnant.

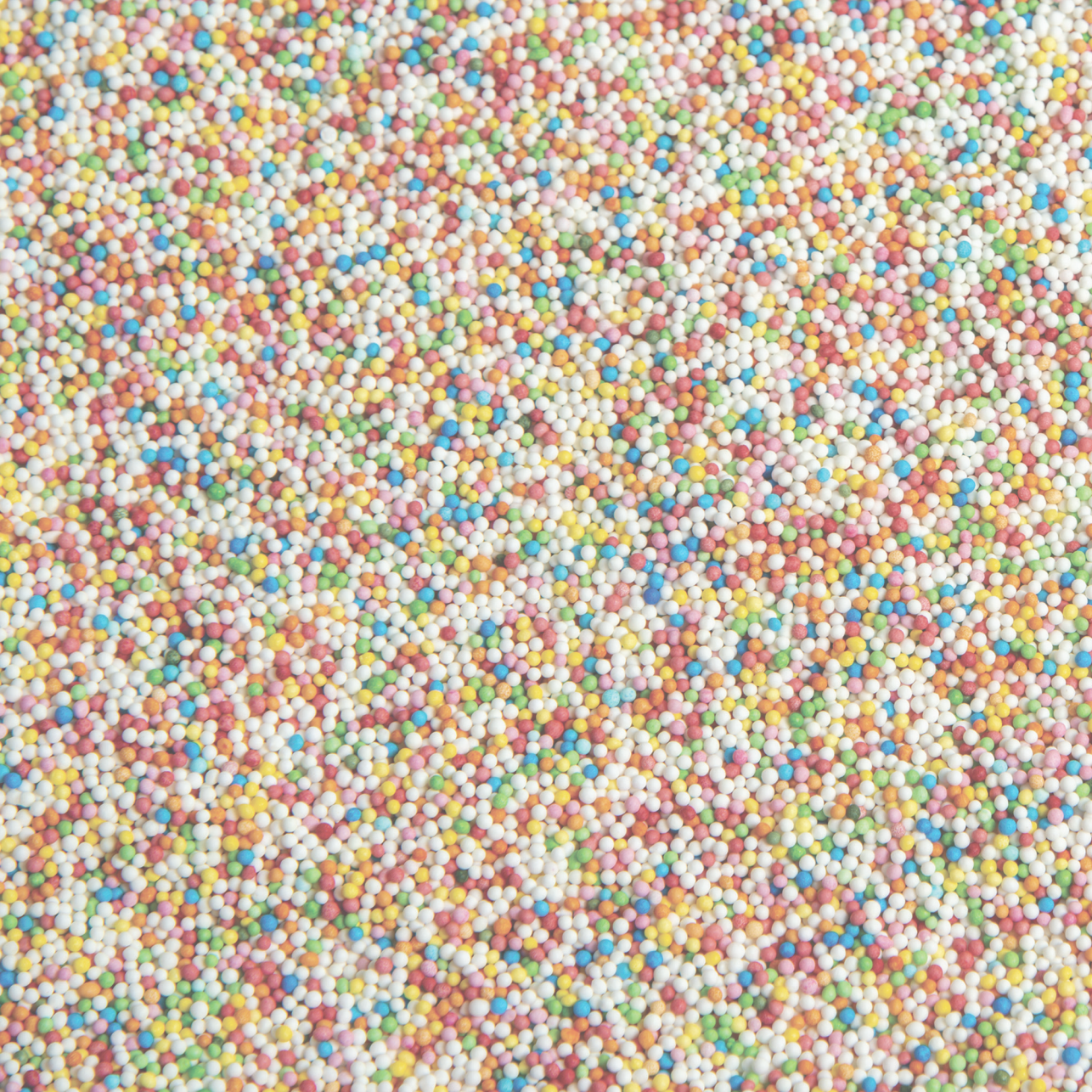
In **Chapter 9** two arterial liver CT protocols are compared with regard to the visibility of small branches from the hepatic artery, such as the right gastric artery and segment four artery. Identification of these arterial branches allows for the establishment of a treatment strategy prior to angiography. Though the contrast-to-noise ratio of the hepatic artery compared to the portal vein was higher in the early arterial phase protocol, the origin detection rates of both arteries were comparable for the early and late arterial phase (post-threshold delay of 10 s and 20 s, respectively), with good inter-rater agreement.

In **Chapter 10** a dual arterial phase protocol is introduced for patients with hypervascular liver metastases (a combination of the arterial phases reported in **Chapter 9**) in order to optimize both small arterial branch detection and lesion enhancement.

No significant difference was observed in the origin detection rates between both arterial phases for the right gastric artery, segment four artery, cystic artery and caudate lobe arteries. Inter-observer agreement on the origin was substantial at best (in case of the

cystic artery). Agreement between arterial phase CT and digital subtraction angiography for the origin detection was moderate at best. Secondly, the influence of the tumor enhancement on the treatment outcome was analyzed. Responding lesions (i.e. complete or partial response according to the Response Evaluation Criteria In Solid Tumors (RECIST 1.1)) had significantly higher Hounsfield unit values in all contrast phases compared to non-responding lesions.







CHAPTER  
THIRTEEN

Nederlandse samenvatting

Radioembolisatie is een lever-gerichte, antitumorale behandeling, waarbij radioactieve bolletjes in de leverslagader worden geïnjecteerd. In Nederland wordt deze behandeling op dit moment alleen nog vergoed bij lever-uitzaaiingen van darmkanker en bij een vorm van leverkanker (hepatocellulair carcinoom).

Levertumoren worden vaak voornamelijk gevoed door de leverslagader, in tegenstelling tot het normale leverweefsel. Dit wordt voornamelijk gevoed door de poortader (die het bloed vanuit het darmpakket via de lever terug naar de grote circulatie vervoert). Dit biedt de unieke kans om de levertumoren selectief te behandelen via de leverslagader, zonder dat het normale leverweefsel hierdoor (te) veel straling absorbeert. Desondanks zal een deel van de bolletjes ook terecht komen in het normale leverweefsel en daar lokale stralingsschade aanrichten. De mate waarin dit problemen oplevert, is afhankelijk van de hoeveelheid bolletjes/straling die in het normale leverweefsel belandt en of er een onderliggende leverziekte is.

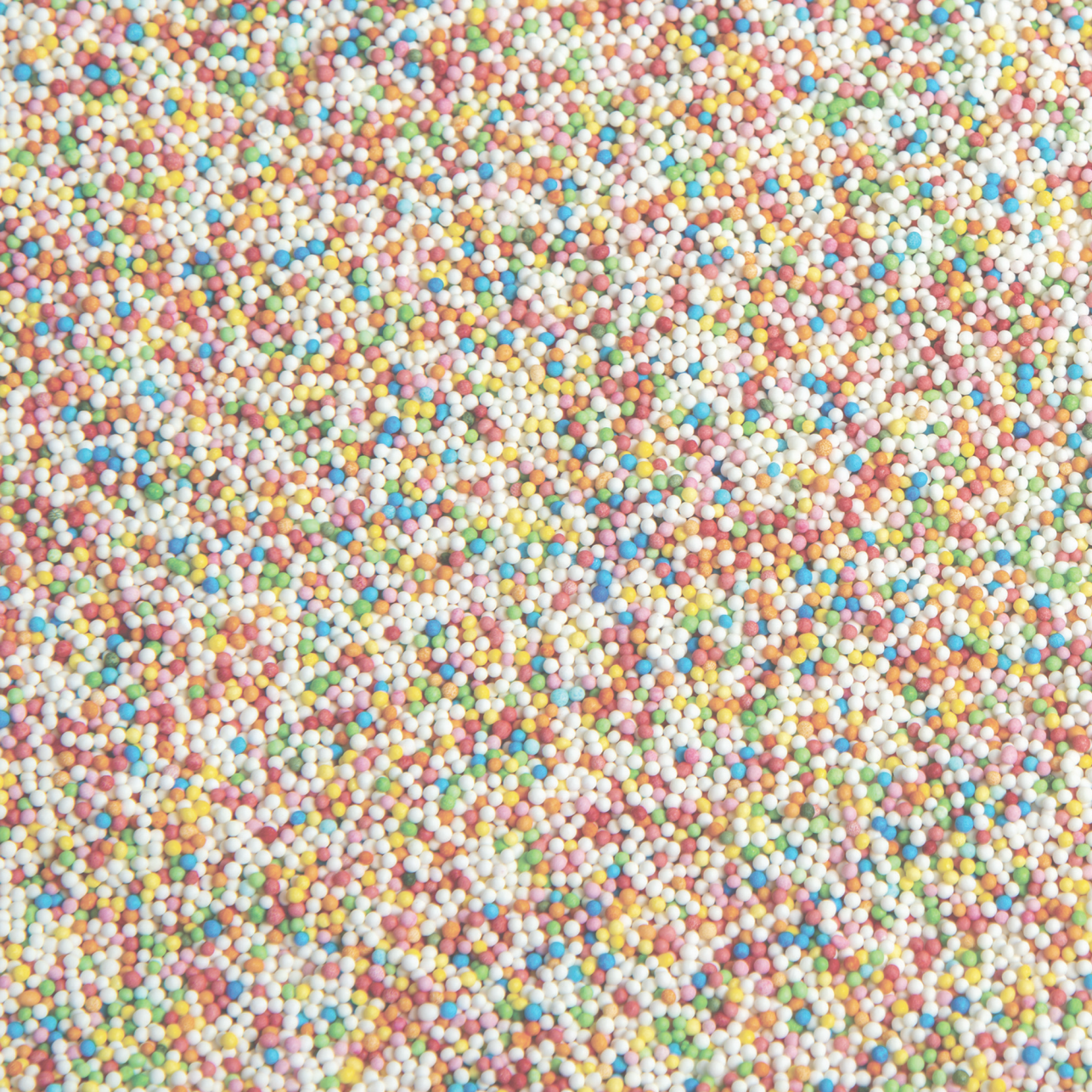
In het eerste deel van dit proefschrift worden enkele klinische aspecten van radioembolisatie-geïnduceerde leverziekte belicht, zoals de manier waarop radioembolisatie-geïnduceerde leverziekte nu is gedefinieerd en wordt gerapporteerd. Verder worden de verschillen in lever-gerelateerde bijwerkingen tussen de commercieel verkrijgbare radioactieve bolletjes met het isotoop Yttrium-90 bekeken en het nut van profylactische medicatie voor het voorkomen van radioembolisatie-geïnduceerde leverziekte. Uit deze studies blijkt dat de belangrijkste factor voor lever-gerelateerde bijwerkingen en dus radioembolisatie-geïnduceerde leverziekte de stralingsdosis op het normale leverweefsel is. Ook is er geen hard bewijs dat profylactische medicatie zinvol is om deze lever-gerelateerde bijwerkingen te voorkomen.

In het tweede deel wordt de aanvullende waarde van 2 verschillende nucleaire onderzoeken, namelijk hepatobiliaire scintigrafie en FDG-PET/CT, op de huidige standaard voorbereiding en evaluatie van de radioembolisatie behandeling geëxploreerd. Met een hepatobiliaire scintigrafie wordt de functie van de lever in kaart gebracht en kunnen regionale verschillen binnen de lever zichtbaar gemaakt worden. Na radioembolisatie treedt een daling van de leverfunctie op in de behandelde delen van de lever (door de lokale stralingsschade). Na

verloop van tijd treedt ook een toename van de leverfunctie op in de niet-behandelde leverdelen; een vorm van compensatie. Op FDG-PET/CT is na behandeling de opname van FDG in de lever minimaal verhoogd, waarschijnlijk zonder veel gevolg voor de normale beoordeling van de FDG-PET/CT scans.

In het derde, radiologische deel wordt een aantal facetten van de CT-scan in de planningsfase van de behandeling onder de loep genomen. Twee scanprotocollen worden vergeleken; een vroege scanfase met aankleuring van alleen de leverslagaders en een latere scanfase met aankleuring van de leverslagaders en beginnende aankleuring van de poortader. De zichtbaarheid van de kleinere leverslagader-aftakkingen is vergelijkbaar voor de beide protocollen, zelfs bij patiënten met sterk doorbloede leveruitzaaiingen. In deze patiëntengroep blijkt ook dat de respons op radioembolisatie beter is, wanneer de uitzaaiingen meer aankleuren op de CT-scan voorafgaand aan de behandeling (ongeacht welke scanfase).

Als laatste worden in **hoofdstuk 11** de bevindingen van dit proefschrift bediscussieerd.





CHAPTER  
THIRTEEN

List of publications

**Towards Response ADaptive Radiotherapy for organ preservation for intermediate-risk rectal cancer (preRADAR): protocol of a phase I dose-escalation trial.**

Verweij ME, Tanaka MD, Kensen CM, van der Heide UA, Marijnen CAM, Janssen T, Vijlbrief T, van Grevenstein WMU, Moons LMG, Koopman M, Lacle MM, **Braat MNGJA**, Chalabi M, Maas M, Huibregtse IL, Snaebjornsson P, Grotenhuis BA, Fijneman R, Consten E, Pronk A, Smits AB, Heikens JT, Eijkelenkamp H, Elias SG, Verkooijen HM, Schoenmakers MMC, Meijer GJ, Intven M, Peters FP.

*BMJ Open. 2023 Jun 15;13(6):e065010.*

**Focused ultrasound and radiotherapy for non-invasive palliative pain treatment in patients with bone metastasis: A study protocol for the three-armed randomized controlled FURTHER trial.**

Slotman DJ, Bartels MMTJ, Ferrer CJ, Bos C, Bartels LW, Boomsma MF, Phernambucq ECJ, Nijholt IM, Morganti AG, Siepe G, Buwenge M, Grüll H, Bratke G, Yeo SY, Blanco Sequeiros R, Minn H, Huhtala M, Napoli A, De Felice F, Catalano C, Bazzocchi A, Gasperini C, Campanacci L, Simões Corrêa Galendi J, Müller D, **Braat MNGJA**, Moonen C, Verkooijen HM; FURTHER consortium.

*Trials. 2022 Dec 29;23(1):1061.*

**Radioembolization-induced changes in hepatic [<sup>18</sup>F]FDG metabolism in non-tumorous liver parenchyma.**

**Braat MN**, van Roekel C, Lam MG, Braat AJ.

*Diagnostics (Basel). 2022 Oct 17;12(10):2518.*

**Toxicity comparison of yttrium-90 resin and glass microspheres radioembolization.**

**Braat MN**, Braat AJ, Lam MG.

*Q J Nucl Med Mol Imaging. 2022 Jun 28.*

**Dose-response relationship after yttrium-90-radioembolization with glass microspheres in patients with neuroendocrine tumor liver metastases.**

Ebbers SC, van Roekel C, **Braat MNGJA**, Barentsz MW, Lam MGEH, Braat AJAT.

*Eur J Nucl Med Mol Imaging. 2022 Apr;49(5):1700-1710.*

**Inflammatory markers and long term hematotoxicity of holmium-166-radioembolization in liver-dominant metastatic neuroendocrine tumors after initial peptide receptor radionuclide therapy.**

Ebbers SC, Brabander T, Tesselaar MET, Hofland J, **Braat MNGJA**, Wessels FJ, Barentsz MW, Lam MGEH, Braat AJAT.

*EJNMMI Res. 2022 Feb 2;12(1):7.*

**Combining radiotherapy and focused ultrasound for pain palliation of cancer induced bone pain; a stage I/IIa study according to the IDEAL framework.**

Bartels MMTJ, Verpalen IM, Ferrer CJ, Slotman DJ, Phernambucq ECJ, Verhoeff JJC, Eppinga WSC, **Braat MNGJA**, van den Hoed RD, van 't Veer-Ten Kate M, de Boer E, Naber HR, Nijholt IM, Bartels LW, Bos C, Moonen CTW, Boomsma MF, Verkooijen HM.

*Clin Transl Radiat Oncol. 2021 Jan 15;27:57-63.*

**A phase I feasibility study of magnetic resonance guided high intensity focused ultrasound-induced hyperthermia, lyso-thermosensitive liposomal doxorubicin and cyclophosphamide in de novo stage IV breast cancer patients: study protocol of the i-GO study.**

de Maar JS, Suelmann BBM, **Braat MNGJA**, van Diest PJ, Vaessen HHB, Witkamp AJ, Linn SC, Moonen CTW, van der Wall E, Deckers R.

*BMJ Open. 2020 Nov 26;10(11):e040162.*



**The focused ultrasound myoma outcome study (FUMOS); a retrospective cohort study on long-term outcomes of MR-HIFU therapy.**

Verpalen IM, de Boer JP, Linstra M, Pol RLI, Nijholt IM, Moonen CTW, Bartels LW, Franx A, Boomsma MF, **Braat MNG**.

*Eur Radiol. 2020 May;30(5):2473-2482.*

**Additional holmium-166 radioembolization after lutetium-177-dotatate in patients with neuroendocrine tumor metastases (HEPAR PLuS): A single centre, single-arm, open-label, phase 2 study.**

Braat AJAT, Buijnen RCG, van Rooij R, **Braat MNGJA**, Wessels FJ, van Leeuwen RS, van Treijen MJC, de Herder WW, Hofland J, Tesselaar MET, de Jong HWAM, Lam MGEH.

*Lancet Oncol. 2020 Apr;21(4):561-570.*

**Personalized dosimetry: The way to limit hepatotoxicity.**

**Braat MNGJA**, Braat AJAT, Lam MGEH.

*J Vasc Interv Radiol. 2020 Mar;31(3):515-516.*

**A pilot study on hepatobiliary scintigraphy to monitor regional liver function in <sup>90</sup>Y radioembolization.**

van der Velden S, **Braat MNGJA**, Labeur TA, Scholten MV, van Delden OM, Bennink RJ, de Jong HWAM, Lam MGEH.

*J Nucl Med. 2019 Oct;60(10):1430-1436.*

**Hepatobiliary imaging in liver-directed treatments.**

van Roekel C, Reinders MTM, van der Velden S, Lam MGEH, **Braat MNGJA**.

*Semin Nucl Med. 2019 May;49(3):227-236.*

**Magnetic resonance imaging-guided high-intensity focused ultrasound is a noninvasive treatment modality for patients with abdominal wall endometriosis.**

Stehouwer BL, Braat MNG, Veersema S.

*J Minim Invasive Gynecol.* 2018 Nov-Dec;25(7):1300-1304.

**Efficacy of radioembolization with <sup>166</sup>Ho-microspheres in salvage patients with liver metastases: A phase 2 study.**

Prince JF, van den Bosch MAAJ, Nijsen JFW, Smits MLJ, van den Hoven AF, Nikolakopoulos S, Wessels FJ, Bruijnen RCG, Braat MNGJA, Zonnenberg BA, Lam MGEH.

*J Nucl Med.* 2018 Apr;59(4):582-588.

**Anatomic versus metabolic tumor response assessment after radioembolization treatment.**

Jongen JMJ, Rosenbaum CENM, Braat MNGJA, van den Bosch MAAJ, Sze DY, Kranenburg O, Borel Rinkes IHM, Lam MGEH, van den Hoven AF.

*J Vasc Interv Radiol.* 2018 Feb;29(2):244-253.e2.

**Hepatobiliary scintigraphy may improve radioembolization planning in HCC patients.**

Braat MNGJA, de Jong HW, Seinstra BA, Scholten MV, van den Bosch MAAJ, Lam MGEH.

*EJNMMI Res.* 2017 Dec;7(1):2.

**Recommendations for radioembolization after liver surgery using yttrium-90 resin microspheres based on a survey of an international expert panel.**

Samim M, van Veenendaal LM, Braat MNGJA, van den Hoven AF, Van Hillegersberg R, Sangro B, Kao YH, Liu D, Louie JD, Sze DY, Rose SC, Brown DB, Ahmadzadehfar H, Kim E, van den Bosch MAAJ, Lam MGEH.

*Eur Radiol.* 2017 Dec;27(12):4923-4930.

## **Colorectal Cancer Staging Atlas**

**MNG Braat**, WB Veldhuis

*ISBN: 978-90-827495-0-2*

### **Portal vein ligation versus portal vein embolization for induction of hypertrophy of the future liver remnant: A systematic review and meta-analysis.**

Isfordink CJ, Samim M, **Braat MNGJA**, Almalki AM, Hagendoorn J, Borel Rinkes IHM, Molenaar IQ.

*Surg Oncol. 2017 Sep;26(3):257-267.*

### **Radioembolization-induced liver disease: a systematic review.**

**Braat MN**, van Erpecum KJ, Zonnenberg BA, van den Bosch MA, Lam MG.

*Eur J Gastroenterol Hepatol. 2017 Feb;29(2):144-152.*

### **The peri-esophageal connective tissue layers and related compartments: visualization by histology and magnetic resonance imaging.**

Weijs TJ, Goense L, van Rossum PSN, Meijer GJ, van Lier AL, Wessels FJ, **Braat MN**, Lips IM, Ruurda JP, Cuesta MA, van Hillegersberg R, Bleys RL

*J Anat. 2017 Feb;230(2):262-271.*

### **Liver CT for vascular mapping during radioembolization workup: Comparison of an early and late arterial phase protocol.**

van den Hoven AF, **Braat MN**, Prince JF, van Doormaal PJ, van Leeuwen MS, Lam MG, van den Bosch MA.

*Eur Radiol. 2017 Jan;27(1):61-69.*

### **The role of <sup>90</sup>Y-radioembolization in downstaging primary and secondary hepatic malignancies: a systematic review.**

**Braat MN**, Samim M, van den Bosch MA, Lam MG.

*Clin Transl Imaging. 2016;4:283-295.*

**The caudate lobe: The blind spot in radioembolization or an overlooked opportunity?**

**Braat MN**, van den Hoven AF, van Doormaal PJ, Bruijnen RC, Lam MG, van den Bosch MA.  
*Cardiovasc Intervent Radiol.* 2016 Jun;39(6):847-54.

**Radioembolization following liver resection: A call for dosimetry.**

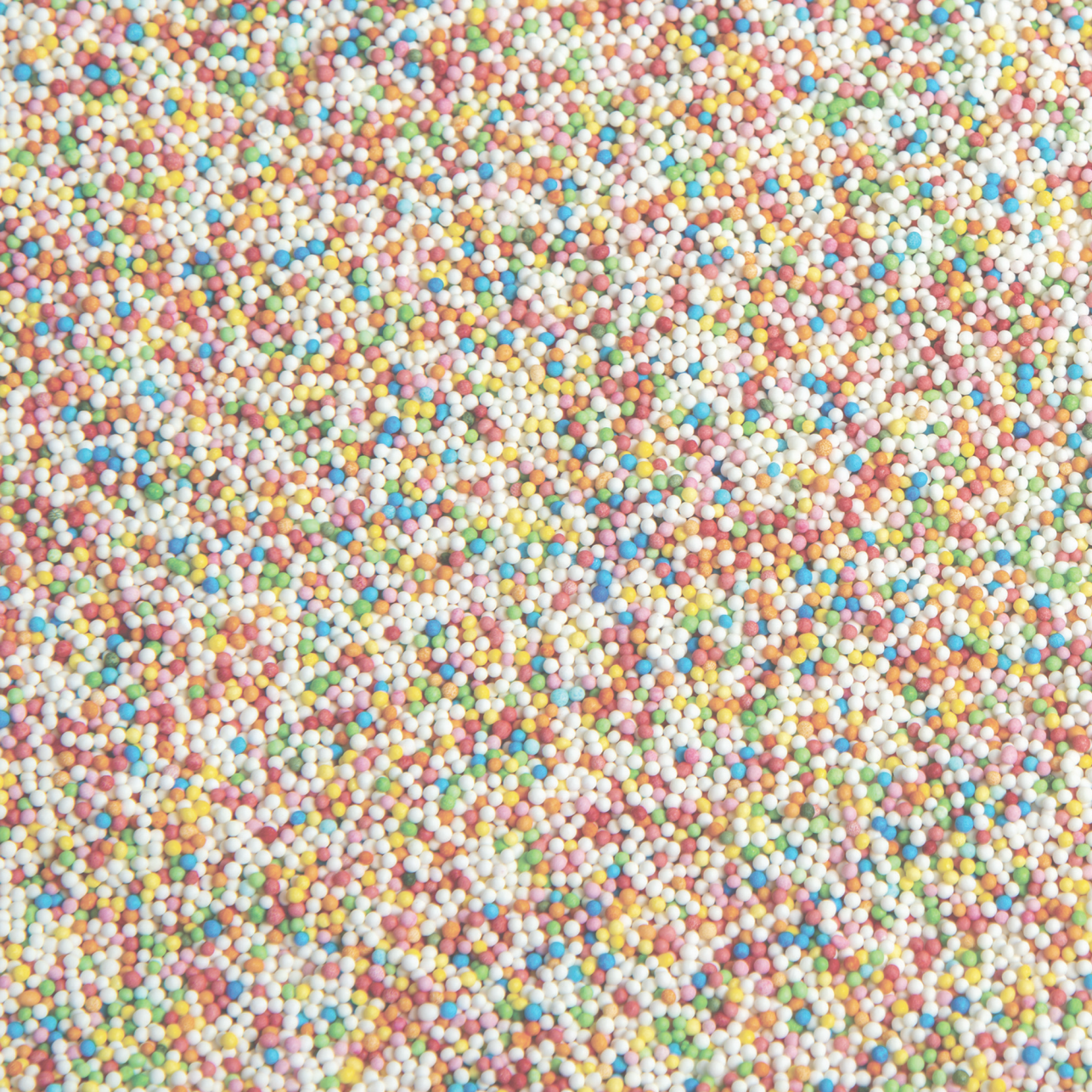
Samim M, **Braat MN**, Lam MG.  
*J Vasc Interv Radiol.* 2016 Apr;27(4):612-3.

**Staging atlas of gynecologic cancer**

**MNG Braat**, WB Veldhuis  
*ISBN: 978-90-818819-6-8*

**<sup>90</sup>Y Hepatic radioembolization: An update on current practice and recent developments.**

Braat AJ, Smits ML, **Braat MN**, van den Hoven AF, Prince JF, de Jong HW, van den Bosch MA, Lam MG.  
*J Nucl Med.* 2015 Jul;56(7):1079-87.





CHAPTER  
THIRTEEN

Curriculum vitae auctoris



Maria Nicole Gerardine Johanna Aleida was born on November 13, 1982, in Breda, the Netherlands. She graduated with honors from the Stedelijk Gymnasium Breda in 2000. Subsequently, she attended medical school at the University of Utrecht. In 2005, she suspended her medical education for four months to learn the Italian language, while living in Rome, Italy.

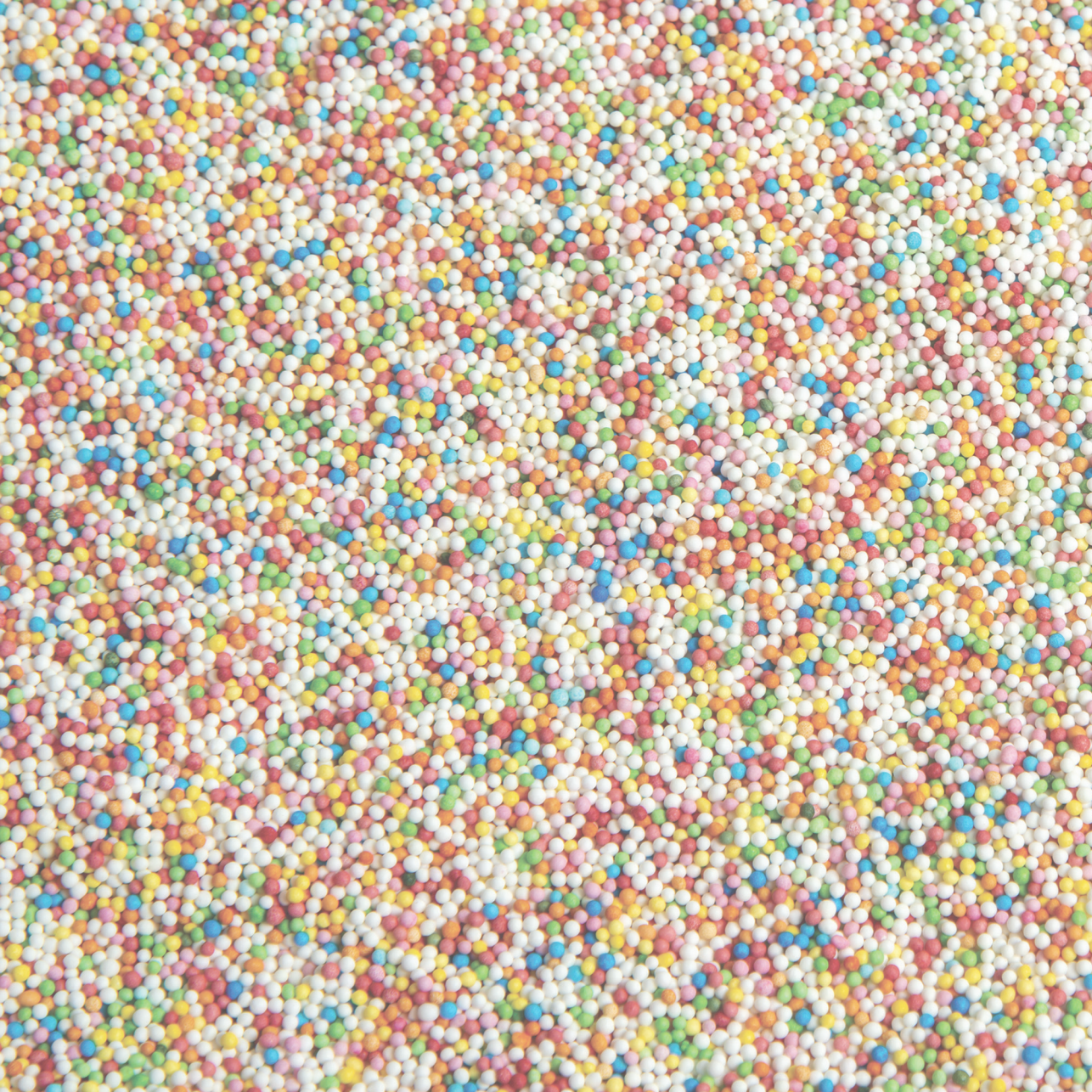
After obtaining her medical degree in 2007, she worked as a surgical resident (ANIOS) in Breda and in the University Medical Center Utrecht (UMCU). After a change of heart, she applied for a radiological residency in 2009. A few months later she started her five-years of radiological residency in the UMCU and St. Antonius Hospital Nieuwegein, with a special interest in abdominal radiology. The following years she worked in the UMCU as a fellow in abdominal, oncological and breast radiology. In 2013, she also became a part of the high-intensity focused ultrasound research group in the UMCU.

In 2016, she became a staff member of the abdominal and breast imaging faculty of the UMCU. Meanwhile, she remained the treating clinician of the HIFU group. Since 2013, she has treated over one hundred patients with MR-guided HIFU and focused part of her research and interest on HIFU treatments of patients with varying conditions. MR-guided HIFU will remain part of her clinical and research interest for years to come.

In 2014, she also started this PhD on radioembolization under the supervision of prof. Marnix Lam and prof. Maurice van den Bosch.

On March 13, 2022 she became mother of her son, Duco.







CHAPTER  
THIRTEEN

Postscriptum

## “All is well that ends well”

Het heeft even geduurd, maar na 9 jaar is dit proefschrift eindelijk afgerond! Soms schoot het lekker op (tegen het einde) en soms was er wat vertraging...

Gedurende de jaren heb ik met velen mogen samenwerken en veel mogen leren van eenieder over het doen van onderzoek, zowel op het inhoudelijke vlak als op het sociale vlak. Ik ben dus ook velen daarvoor dank verschuldigd. Niet alleen aan degenen die hebben bijgedragen aan de verschillende manuscripten, maar vooral ook aan degenen die mij op andere manieren hebben bijgestaan en gesteund. Een aantal mensen wil ik graag in het bijzonder bedanken.

Eerste promotor, prof. dr. M.G.E.H. Lam. Beste Marnix,

Dank je wel voor de begeleiding over de jaren en het vertrouwen dat dit proefschrift tot een goed einde zou komen. In onze overleggen heb je me geholpen de hoofdlijnen te bewaren en de tijdslijn te bewaken. Ik ben je ook erg dankbaar voor de vrijheid die je me hebt gegeven bij de tijdsindeling en de invulling van dit proefschrift.

Tweede promotor, prof. dr. M.A.A.J. van den Bosch. Beste Maurice,

Dank je wel voor het vertrouwen om als vast stafflid aan te mogen treden en dit promotietraject te starten. Jouw gave om mogelijkheden en kansen te zien is benijdenswaardig. Ik probeer nu minder aandacht te hebben voor de mogelijke “beren op de weg” en ook meer vanuit dat perspectief te werken. Veel dank hiervoor!

Co-promotor, dr. J. de Bruijne. Beste Joep,

Dank je wel voor je hulp in de laatste fase van dit proefschrift. Je klinische blik is een welkome afwisseling van mijn radiologische denken. Ik hoop dat we onze samenwerking in de kliniek en op het wetenschappelijk vlak in de komende jaren op dezelfde fijne manier kunnen voortzetten.

Leden van de leescommissie. Prof. dr. P.J. van Diest, prof. dr. R.J. Bennink, prof. dr. I.H.M. Borel Rinkes, prof. dr. H.W.A.M. de Jong en prof. dr. M. Koopman.

Veel dank voor jullie kritische blik op dit proefschrift en voor de fijne samenwerking in de kliniek en op andere fronten in de afgelopen jaren.

Stafleden radiologie en nucleaire geneeskunde van het UMCU. Beste collegae,  
Dank jullie wel voor de fijne samenwerking en de open sfeer! Ik hoop nog lang deel uit te kunnen maken van ons team.

Natuurlijk extra veel dank aan mijn collegae van de interventie en nucleaire geneeskunde, in het bijzonder Rutger Bruijnen, Maarten Smits, alle interventie-fellows in de afgelopen 10 jaar en Bart de Keizer, voor het uitvoeren van de procedures die in dit proefschrift beschreven zijn.

Beste Wouter, Frank, Jeanette en Jip. Dank jullie wel voor de leuke en constructieve samenwerking binnen onze abdomen groep. Ik ben blij dat we nu met zijn vijven een sterk team vormen, waarin we veel van elkaar kunnen leren en overleg heel laagdrempelig is. Dank jullie wel voor de ruimte die jullie me begin 2023 hebben gegeven voor de eindsprint. Jip, als laatste abdomen staflid, ook erg bedankt voor je hulp en adviezen aan het begin van mijn promotie-traject.

Lieve Jan Willem, sinds onze AIOS-tijd zijn we al collegae en nu inmiddels ook jaren kamergenoten en vrienden. Dank je wel voor je luisterend oor op de momenten dat ik er doorheen zat/zit!

Beste Clemens, Roel, en Chrit,

Dank jullie wel voor de fijne research-samenwerking buiten dit proefschrift om. Ik kan veel van jullie leren, en dat brengt me vaak op nieuwe ideeën. Veel dank met name ook voor de ruimte die jullie me hebben gegeven om dit proefschrift te kunnen schrijven naast onze samenwerking op HIFU-gebied. Ik hoop voor dat laatste nu meer tijd te hebben.

Natuurlijk ook dank aan alle HIFU-promovendi (Marjolein, Josanne, Mirjam, Anne-Rose en Stefanie), waar ik in de afgelopen jaren veel mee samen heb mogen werken en soms onderzoeksprikelen mee heb mogen delen.

En veel dank aan Niels, Greet, Jorgen, Laura en Esther voor jullie expertise en gezelligheid op de woensdag ochtend. Dat maakt mijn werkweken leuker.

Veel dank aan alle co-auteurs! Zonder jullie bijdrages en feedback was het niet gelukt. Enkele co-auteurs wil ik ook in het bijzonder bedanken.

Beste Andor, dank je wel voor de fijne samenwerking in het begin van dit traject. Ik kon altijd bij jou en Jip terecht om te scoren, maar ook voor adviezen over statistiek.

Beste Karel, dank je wel voor je onmisbare correcties in mijn eerste manuscript. Jij hebt me o.a. veel geleerd over de gewenste schrijfstijl, met de hulp van vele papieren versies en potlood-correcties.

Beste Roy en Chris, dank jullie wel voor jullie hulp bij de lay-out en het design van dit boekje. De disco-dip zal nog wel even te vinden zijn in jullie werkkamer....

Lieve Stefanie, Anouk en PJ,

Dank jullie wel voor de oneindige gezelligheid, wijn en oesters in de afgelopen jaren! Dat hielp mij altijd enorm het werk en leven te relativieren. Helaas kunnen we dit niet meer zo vaak doen als in die beginjaren zonder kinderen. Hopelijk wordt dat op niet al te lange termijn weer mogelijk (waar dan ook in Europa)!

Lieve Frederique, Elvin en Ilse,

De opleiding is alweer eeuwen geleden. Dank jullie wel voor de gezellige etentjes de afgelopen jaren. Moeilijk te plannen, maar altijd de moeite waard!

Lieve Emma,

Jij weet als geen ander hoe het is om 9 jaar over een promotie-traject te doen. Dank je wel voor de gezellige lunches en je luisterende oor gedurende al die jaren!

Lieve Nicky,

Tijdens deze jaren hebben we samen de mooiste delen van de wereld bezocht en bewonderd. En daar mocht ik onder het genot van goede cocktails af en toe even klagen over dit traject. Dank je wel voor je adviezen en bovenal de gezelligheid op die reizen en tijdens onze luxe diners. Ik hoop dat we ooit nog een keer Jordanië vanuit de luchtballon kunnen zien, zoals we gepland hadden...

Lieve Inger,

Dank je wel voor je langdurige vriendschap! Sinds onze co-schappen is er veel veranderd, maar wij kunnen nog altijd gezellig sparren over het werk en aanverwante zaken onder het genot van een glas wijn. Dank je wel hiervoor! Lieve Ron, ook jij bedankt voor de gezellige avonden en heerlijke diners in de afgelopen jaren!

Lieve Sanne (Snoes),

Dank je wel voor je goede vriendschap en de enorme gezelligheid en warmte die jij altijd met je meebrengt. Het leven is een feest! En dat draag jij iedere dag uit, ook als we samen opgesloten zitten in een kast voor 48 uur.... Wat zouden we hebben gedaan zonder Britney?!? Nu dit boekje af is, heb ik hopelijk meer tijd om samen op het leven te proosten.

Lieve Maartje,

Al meer dan 28 jaar zijn we maatjes. Onwaarschijnlijk was eigenlijk de dag dat we elkaar weer zagen lopen op de Nobelstraat na jaren schrijfstilte. Wat ben ik nog steeds blij dat dat gebeurd is! Dank je wel voor je langdurige en goede vriendschap! Of we nu bijna naast elkaar wonen of letterlijk mijlenver uiteen, ik weet dat je er altijd bent als dat nodig is.

Lieve Wouter,

Het was nooit gelukt zonder jouw steun en gezelschap al die jaren! Dank je wel voor je liefde in het begin en onze hechte vriendschap nu. Eén woord is genoeg, weinig mensen kennen mij zo goed. GMTA.

Lieve Yvonne,

Hoewel we altijd andere dingen kiezen, lijken we toch ook veel op elkaar. Dank je wel voor je steun en je liefde! Ik kan me geen betere zus wensen.

Lieve paranimfen,

Lieve An(neke),

Wie had ooit gedacht na onze eerste epische ontmoeting lang geleden, dat we dit ook nog samen zouden kunnen doen? Niet als chirurg, maar beiden als radioloog. Hadden we af en toe nog maar eens tijd voor wielrennen, cappuccino's, winkelen en wijn op zaterdag, zoals in die beginjaren. Of tonijnsalade.... Wat kan ik daarvan genieten! Dank je wel voor alle gezelligheid, je eindeloze support bij lastige beslissingen en je nuchtere blik! You're always on top!

Lieve Arthur,

Als ik iemand dank verschuldigd ben voor dit proefschrift, dan ben jij het. Dank je wel voor je goede raad, hulp, tijd en expertise die je hebt bijgedragen aan dit proefschrift. Je bent onmisbaar voor mij als broer en collega.

Ik kan alleen maar hopen dat ik in de beginjaren van ons leven en/of ons werkzame leven jou ooit ook zoveel heb geleerd en geholpen als jij mij in deze 9 jaar! Ik hoop dat we kunnen blijven leren (van elkaar). En anders "geen gehoor, goed bericht".

Lieve Steffie, Juul en Ward,

Dank je wel voor de kleine momenten, waarin jullie Duco hebben opgevangen, zodat ik nog een paar pagina's kon schrijven. Voortaan komen we weer samen en alleen voor plezier!

Lieve mama en papa,

Zonder jullie hulp had dit proefschrift nooit het licht gezien. Dank jullie wel voor jullie onvoorwaardelijke liefde, jullie adviezen, en jullie onmisbare hulp in ons leven! Ik (en Duco) genieten van alle momenten met jullie samen.

Allerliefste Duco,

Dit traject is lang voor jou begonnen, maar gelukkig voor ons beiden nu ten einde. Jij bent mijn zonnestraal! Weinig dingen maken mij vrolijker dan jouw lachende gezicht in de vroege ochtend. Iedere dag ga jij met een brede lach en veel enthousiasme tegemoet. Jij maakt mijn leven zoveel mooier! Boks.



